(2)

Bulletin 53
(Part 1 of 4 Parts)

THE SHOCK AND VIBRATION BULLETIN

Part 1
Welcome, Keynote Address,
Invited Papers, Pyrotechnic Shock, and
Shock Testing and Analysis

MAY 1983

A Publication of
THE SHOCK AND VIBRATION
INFORMATION CENTER
Naval Research Laboratory, Washington, D.C.

Office of
The Under Secretary of Defense
for Research and Engineering

SYMPOSIUM MANAGEMENT

THE SHOCK AND VIBRATION INFORMATION CENTER

Henry C. Pusey, Director
Rudolph H. Volin
J. Gordan Showalter
Jessica Hileman
Elizabeth A. McLaughlin
Mary K. Gobbett

Bulletin Production

Publications Branch, Technical Information Division,
Naval Research Laboratory

Bulletin 53
(Part 1 of 4 Parts)

THE SHOCK AND VIBRATION BULLETIN

MAY 1983

A Publication of
THE SHOCK AND VIBRATION
INFORMATION CENTER
Naval Research Laboratory, Washington, D.C.

The 53rd Symposium on Shock and Vibration was held at the Radisson Ferncroft Hotel, Danvers, MA on October 26-28, 1982. The U.S. Army Materials and Mechanics Research Center, Watertowr MA, was the host.

Office of
The Under Secretary of Defense
for Research and Engineering

CONTENTS

PAPERS APPEARING IN PART 1

PAPERS APPEARING IN PART 2

Fluid Structure Dynamics

Dynamic Analysis

PAPERS APPEARING IN PART 3

PAPERS APPEARING IN PART 4

TITLES AND AUTHORS OF PAPERS PRESENTED IN THE
SHORT DISCUSSION TOPICS SESSION

NOTE: These papers were only presented at the Symposium. They are not published in the Bulletin and are only listed here as a convenience.

THE DEVELOPMENT OF A VISCOELASTIC AEROSPACE STRUCTURES TECHNOLOGY DAMPING DESIGN GUIDE
J. Soovere, Lockheed-California Co., Burbank, CA, M. Drake, University of Dayton Research Institute, Dayton, OH, L. Rogers and V. Miller, Air Force Wright Aeronautical Laboratories, Wright Patterson AFB, OH

APPROXIMATE RELAXATION MODULUS FROM THE FRACTIONAL REPRESENTATION OF COMPLEX MODULUS
L. Rogers, Air Force Wright Aeronautical Laboratories, Wright Patterson AFB, OH

DEVELOPMENT OF HIGH FREQUENCY ISOLATION SYSTEM
F. J. Andrews, Barry Controls, Watertown, MA

A RECENT APPLICATION EMPLOYING ELASTOMERIC TECHNOLOGY TO ISOLATE A HIGH RESOLUTION AERIAL RECONNAISSANCE CAMERA
D. F. Reynolds, Barry Controls, Watertown, MA

MERCURY ISOLATION SYSTEM/DESIGN, DEVELOPMENT MANUFACTURE AND TEST
M. Peretti, Barry Controls, Watertown, MA

LOOSENING OF BOLTED JOINTS DURING VIBRATION TESTING
J. J. Kerley, Jr., Goddard Space Flight Center, Greenbelt, MD

BOLTS AND FASTENER TIGHTENING TO BROCHURE IDEALNESS THROUGH VIBRATION SIGNATURES
A. S. R. Murty, Indian Institute of Technology, Kharagpur, India

DEVELOPMENT OF A MATERIAL TESTING MACHINE CAPABLE OF HIGH CYCLE LOADINGS SUPERIMPOSED ONTO LOW CYCLE LOADINGS
R. C. Goodman, University of Dayton Research Institute, Dayton, OH

PREDICTION OF STRUCTURAL RELIABILITY FROM VIBRATION MEASUREMENTS
P. Mlakar, U.S. Army Engineer Waterways Experiment Station, Vicksburg, MS

PROGRESS REPORT ON U.S. STATE OF THE ART ASSESSMENT OF MOBILITY MEASUREMENTS PROGRAM
D. J. Ewins, Imperial College of Science and Technology, London, England

UNDERWATER SHOCK ANALYSIS OF A MISSILE LAUNCH TUBE
K. C. Kiddy, Naval Surface Weapons Center, Silver Spring, MD

THE VIBRATION OF SLIGHTLY CURVED RECTANGULAR PLATES UNDER COMPRESSION
S. M. Dickinson and S. Ilanko, University of Western Ontario, London, Ontario, Canada and S. C. Tillman, University of Manchester, Manchester, England

SHOCK ANALYSIS OF DICED DISK TRANSDUCER USING ANSYS
A. Haecker and H. Mitson, Gould, Inc., Cleveland, OH

SESSION CHAIRMEN AND COCHAIRMEN

Date	Session Title	Chairmen	Cochairmen
Tuesday, 26 Oct. A.M.	Opening Session	Mr. Richard Shea, U.S. Army Materials and Mechanics Research Center, Watertown, MA	Mr. Henry C. Pusey, Shock and Vibration Information Center, Naval Research Laboratory, Washington, DC
Tuesday, 26 Oct. P.M.	Elias Klein Memorial Lecture Plenary A	Mr. Henry C. Pusey, Shock and Vibration Information Center, Naval Research Laboratory, Washington, DC	
Tuesday, 26 Oct. P.M.	Machinery Dynamics	Dr. Ronald L. Eshleman, The Vibration Institute, Clarendon Hills, IL	Mr. Samuel Feldman, NKF Engineering Associates, Inc., Vienna, VA
Tuesday, 26 Oct. P.M.	Pyrotechnic Shock-Measurement/ Simulation	Mr. C. Douglas Hinckley, TRW Systems, Ogden, UT	Mr. Peter Bouelin, Naval Weapons Center, China Lake, CA
Tuesday, 26 Oct. P.M.	MIL-STD-810D Panel Session	Mr. Preston Scott Hall, Air Force Wright Aeronautical Laboratories, Wright Patterson Air Force Base, OH	Mr. Rudolph H. Volin, Shock and Vibration Information Center, Naval Research Laboratory, Washington, DC
Wednesday, 27 Oct. A.M.	Maurice Biot 50th Anniversary Lecture Plenary B	Mr. George J. O'Hara, Naval Research Laboratory, Washington, DC	
Wednesday, 27 Oct. A.M.	Vibration: Test and Criteria	Mr. John Wafford, Aeronautical Systems Division, Wright Patterson Air Force Base, OH	Mr. Howard D. Camp, Jr., U.S. Army Electronic Research and Development Command, Ft. Monmouth, NJ
Wednesday, 27 Oct. A.M.	Shock Testing and Analysis	Mr. Edwin Rzepka, Naval Surface Weapons Center, Silver Spring, MD	Mr. Ami Frydman, Harry Diamond Laboratories, Adelphi, MD
Wednesday, 27 Oct. P.M.	Damping	Dr. Frederick C. Nelson, Tufts University, Medford, MA	Dr. Lynn Rogers, Air Force Wright Aeronautical Laboratories, Wright Patterson Air Force Base, OH
Wednesday, 27 Oct. P.M.	Fluid-Structure Dynamics	Dr. Anthony J. Kalinowski, Naval Underwater Systems Center, New London, CT	Dr. Martin W. Wambsganss, Argonne National Laboratory, Argonne, IL
Thursday, 28 Oct. A.M.	Plenary C	Mr. Richard Shea, U.S. Army Materials and Mechanics Research Center, Watertown, MA	
Thursday, 28 Oct. A.M.	Dynamic Analysis I	Lt. Col. John J. Allen, Air Force Office of Scientific Research, Washington, DC	Dr. Robert L. Sierakowski, University of Florida, Gainesville, FL
Thursday, 28 Oct. A.M.	Vehicle Dynamics	Dr. Richard A. Lee, U.S. Army Tank-Automotive Command, Warren, MI	Dr. Grant R. Gerhart, U.S. Army Tank-Automotive Command, Warren, MI
Thursday, 28 Oct. P.M.	Dynamic Analysis II	Dr. James J. Richardson, U.S. Army Missile Command, Redstone Arsenal, AL	Mr. Brantley R. Hanks, NASA Langley Research Center, Hampton, VA
Thursday, 28 Oct. P.M.	Short Discussion Topics	Mr. R. E. Seely, Naval Weapons Handling Center, Earle, Colts Neck, NJ	Mr. E. Kenneth Stewart, U.S. Army Armament, Research and Development Command, Dover, NJ

WELCOME

Dr. Edward S. Wright -
Director
U.S. Army Materials and Mechanics Research Center
Watertown, MA

I would like to officially welcome all of you to the 53rd Shock and Vibration Symposium. Just the fact that there have been 53 of them speaks very well for the history and stature of the symposium. It obviously has been held at the highest level of standards in the past, and a review of the program for this one indicates that it is certainly no exception. It appears to be outstanding. The symposium offers a key mechanism for the interchange of information in the shock and vibration field between government, industry and universities, and we feel it is extremely valuable.

Since many of you will be visiting the Army Materials and Mechanics Research Center later in the week, either to attend the classified sessions that will be held there, or to tour our laboratories, I would like to tell you a little bit about our Center while you are here. It also gives me the opportunity to do a little propagandizing or P.R. work. As I have been asked several times, "What's an AMMRC?"; I will tell you a little bit about that.

Basically, we are a corporate lab of DARCOM, the Army Materiel Development and Readiness Command; this is the part of the Army that is responsible for developing, procuring, and supplying to the field, all of the military equipment for the Army. We are responsible for research and development in the areas of materials and mechanics for the total DARCOM community.

We are located about six miles due west of Boston. We are in the center of a number of very well-known universities; we are also located near some other government agencies, such as the Air Force Electronics Systems Division at Hanscom Field, and the Department of Transportation's Research Center. We are on the site of the old historic Watertown Arsenal. The Arsenal, as such, was one of the many arsenals closed during the 1960's, and a portion of what was the Arsenal evolved into the Army Materials and Mechanics Research Center.

We are one of the three labs, out of about 20 DARCOM labs, that report directly to the Headquarters. So basically, we are a corporate lab, and as such, we work for all of the systems development commands. We do not have a specific system development responsibility ourselves, but we are responsible for supporting all of the other commands. That means I have many bosses, one of whom is sitting on my right and will be giving your Keynote Address: General Stevens, who commands AVRADCOM, the Army Aviation Research and Development Command.

We work not only for the development commands, but also for the readiness commands, which actually procure and supply the equipment to the field forces. We also work for the project managers who are responsible for the development and the production of major systems such as the Abrams tank, the Bradley Fighting Vehicle and the Apache attack helicopter. We have a research and development mission of our own, but one of our greatest reasons for being is the support that we give, not only to these Army organizations, but to their contractors as well. Quite often it is the contractors that first see the materials problems either in development or production.

I mentioned that we have a research and development mission. Basically, we are the lead lab, as designated by DARCOM, in the areas of materials, solid mechanics, and materials testing technology. In this context, testing technology refers to testing for the purposes of accepting materials and components for use in systems, rather than testing associated with our research and development mission.

Current emphasis includes materials processing, and the characterization of materials to ensure reliability and reduce costs in future systems. I will not discuss our various areas of interest at this time, since you will see examples of this work when you visit us.

In addition to our basic R&D mission we perform many other functions, and foremost among them is the support we provide to the systems developers. I would like to point out one other item; that is the management of information and analysis centers. These are portions of the DOD Information and Analysis Center Program that are

paid for out of DLA funds but administered by the three services. We are responsible for three information analysis centers: Metals and Ceramics Information Center which is located at Battelle, Thermo-Physical and Electronic Property Center, and the Non-Destructive Testing Information and Analysis Center (NTIAC). NTIAC is somewhat similar to the Shock and Vibration Information Center (SVIC). We ran NTIAC in-house at the Army Materials and Mechanics Research Center for a long time, just as the Naval Research Laboratory still runs SVIC. I can well appreciate some of the trials and tribulations that Mr. Psey and his staff must endure, based upon our own similar experience. I do feel that SVIC is doing an out-standing job. We help support the SVIC, and we certainly benefit from what it does. We hope to continue our close relationship with the Center.

I feel shock and vibration is very important to AMMRC. Many aspects of the work that we do for the Army involves shock and vibration. We are responsible for research on armor and penetrator materials and for the development and evaluation of armor materials and penetrator materials for Army systems. In the mechanics area we are concerned with the interaction of armor and penetrators, and I think that this is the epitome of the shock regime. We also get involved in vibration problems. For example, we do quite a lot of work on that "flying fatigue machine" known as the helicopter. So we are deeply interested in the shock and vibration business, and appreciative of the efforts of SVIC.

I would like to preview some of the facilities and activities that you will see during your visit to AMMRC. For example, we have set up a new range within the last few years to work on quarter-scale modeling of both long rod, high density penetrators, and armors designed to defeat such penetrators. The full scale penetrators are fired out of 120 millimeter or 155 millimeter tank cannons. We can launch quarter-scale projectiles up to about 6,000 ft/sec in the firing range, and study the penetrator-armor interaction process. Going to higher shock regimes, you will also see our slap facility. It is part of our Ballistic Missile Defense Materials Characterization activity and here we are talking about pressures up in the megabar regime.

We are more than just a basic research laboratory, we also have production capabilities. An example of this is our metal-working activity. I feel it very important to our materials development mission that we are able to produce and fabricate materials, not just in small lab quantities, but in quantitits up to those approaching pilot scale so that the production processes then can be scaled up by industry. These prototyping capabilities include machining facilities. We get deeply involved in the manufacture of prototypes for various parts of the Army including most of the Development Commands, but in particular for the Armament Command, for whom we have made most of the prototypes of nuclear artillery projectiles in past years.

We are also active in the polymer and composite material processing technologies. For example, we have film stretching equipment for making stretched film armor materials such as XP polymer, injection molding equipment, and equipment for compounding and blending rubber. In fact, we are initiating a new coordinated program pulling together all of the scattered research and development work within DARCOM on rubber, and we will be using the compounding and blending operation in this effort.

A final example includes our filament winding, pultrusion, autoclaving and braiding facilities. These represent processing areas in the composites and polymers area which we feel will become more and more important in future Army systems. With the emphasis on weight saving, higher performance, survivability, and ballistic damage tolerance, I predict that composites will be the wave of the future in many Army systems. We are putting a substantial part of our program into this area, since we feel that this is the current growth area.

Again, welcome to the Boston area. We look forward to seeing you at AMMRC.

KEYNOTE ADDRESS

AVRADCOM RESEARCH IN HELICOPTER VIBRATIONS

Major General Story C. Stevens
Commander, U.S. Army Aviation
Research and Development Command
St. Louis, Missouri

Since the maiden flight in 1940 of the first Army helicopter pictured in Figure 1, the Army helicopter has encountered a multitude of vibration problems. These problems have decreased system productivity and increased life cycle costs. The following is a progress report on reducing helicopter vibrations.

Over the past 40 years, there has been significant progress in vibration reduction as indicated by Figure 2. This reduction was partly the result of innovative industry and government-sponsored research, and partly because of increasingly stringent Army specifications. Initial reductions were accomplished by gradual improvements in vibration design approaches along with trial-and-error airframe detuning.

Over the past two decades, improvements were achieved, for the most part, by add-on vibration control devices designed to reduce rotor vibratory loads and airframe vibrations. However, the weight of these devices has increased from approximately 2% of the payload to approximately 10% of the payload. As a result, mission payloads have been reduced.

Even though vibration levels have been lowered, numerous vibration-related problems still persist in the design of the modern helicopter. Today's vibration problems are more critical due to changes in overall mission requirements which include: nap-of-the earth and high speed flight, advanced weapons delivery, survivability, transportability, high reliability, and low maintenance. The problems that had to be overcome during recent development programs provided impetus to develop advanced vibration reduction methods. About five years ago, AVRADCOM's Research and Technology Laboratories responded to this need by emphasizing research efforts directed towards vibration analysis, vibration control and vibration testing.

Fig. 1 — First Army helicopter, Sikorsky R-4

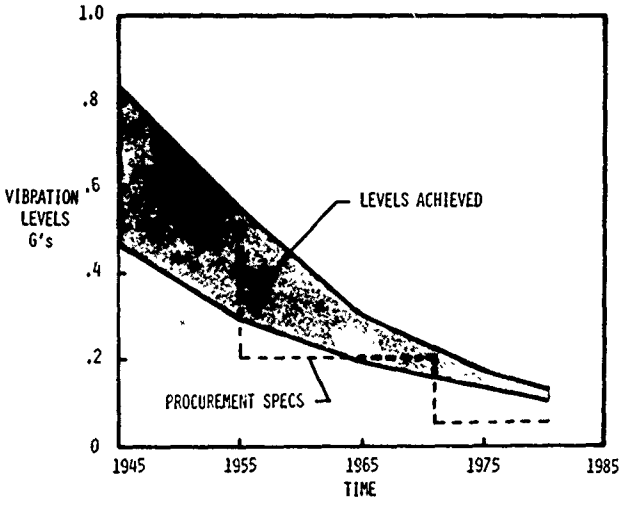

Fig. 2 — Trend of helicopter vibration levels

To put this research in perspective, we will consider: *first*, reviewing vibration design considerations which impact the modern Army helicopter; *second*, assessing vibration technology to establish research priorities; and *finally*, highlighting specific Army research programs which address major technology deficiencies.

The impact of high vibrations on helicopter design can best be described by recounting problems experienced during initial flight testing of the Army's newest helicopters. These helicopters are the UH-60 or Blackhawk, which is a utility helicopter, and the AH-64 or Apache, which is an attack helicopter, both of which are shown in Figure 3. The problems on these helicopters included higher than expected rotor vibratory loads, rotor/airframe interactions, airframe reasonances near excitation frequencies, high empennage vibrations and ineffective vibration control devices. As a result, vibration levels measured on the prototype aircraft were significantly above Army specifications throughout the flight regime. These first flight vibration levels for the Blackhawk, shown in Figure 4, are typical for recent development aircraft. For the Blackhawk and Apache, these vibrations were reduced, as indicated in Figure 5, after making numerous configuration changes which included raised rotors, aerodynamic fuselage fairings, modified hub absorbers, installed airframe aborbers, local stiffness changes, crew seat modifications, and isolated stabilators. Although these changes reduced vibration levels to within Army specifications, they still required substantial amounts of flight, ground and wind tunnel testing.

The configuration changes which were necessary to solve Blackhawk and Apache vibration problems impacted both system acquisition and productivity. The cost required to solve vibration problems during the development cycle is illustrated in Figure 6 in terms of engineering effort. During the design phase, effort increases gradually until first flight. At this point, an abrupt increase occurs that extends well into the development cycle. This increase can significantly delay helicopter delivery schedules. The payoffs for minimizing engineering effort and resulting schedule overruns are significant. In addition, operational costs have also increased due to higher weight penalties required to reduce vibrations.

SIKORSKY BLACK HAWK
UTILITY TACTICAL TRANSPORT
AIRCRAFT SYSTEM
(UTTAS)

HUGHES APACHE
ADVANCED ATTACK HELICOPTER
(AAH)

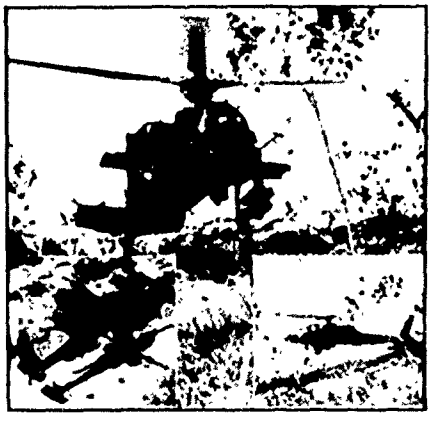

Fig. 3 — Modern Army helicopters

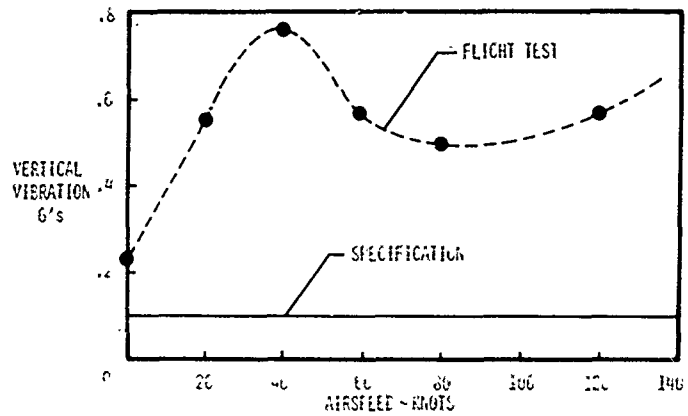

Fig. 4 — UTTAS prototype vibration levels

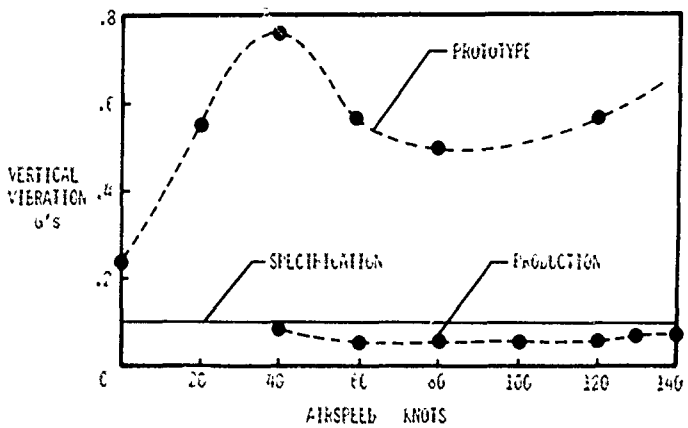

Fig. 5 — UTTAS prototype and production vibrations

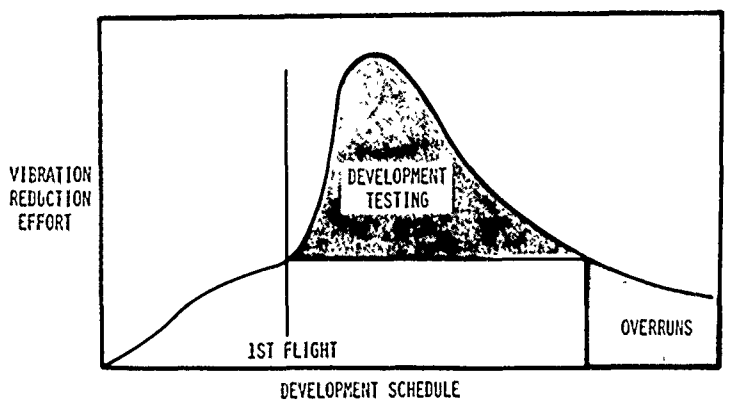

Fig. 6 — Vibrations impact system acquisition

Besides increasing costs during the development cycle, high vibrations can degrade overall helicopter productivity in several major areas. These areas include flight envelopes, human factors, structural integrity, reliability and maintainability, and transportability. A brief discussion of each of these areas follows.

In absolute terms, flight envelope limitations can be the most severe vibration penalties. The significance of forward speed on vibrations is shown in Figure 7. Vibration levels typically increased in the transition region around 30 to 40 knots followed by a decrease in the 80 to 90 knot region and rapidly increased for higher airspeeds. In aircraft developed in the 1950's, high vibrations sometimes limited forward speeds and degraded maneuverability. However, the Blackhawk and Apache were successfully designed to achieve mission profiles which were power rather than vibration limited. Nevertheless, even if power is available, helicopter forward speed and maneuverability are ultimately vibration limited as indicated in Figure 8.

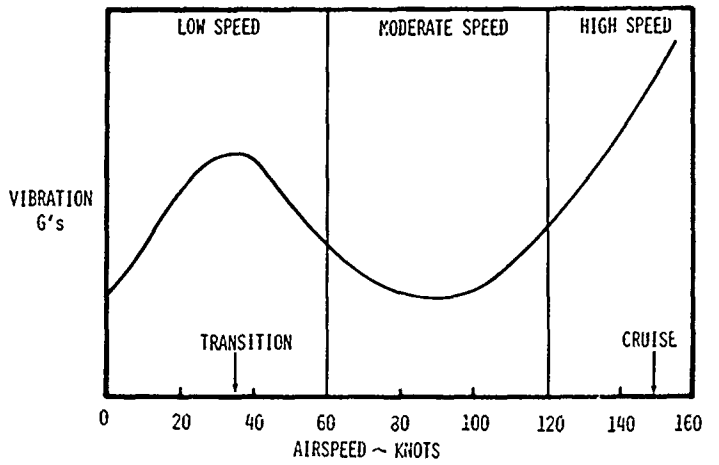

Fig. 7 — Vibration versus airspeed

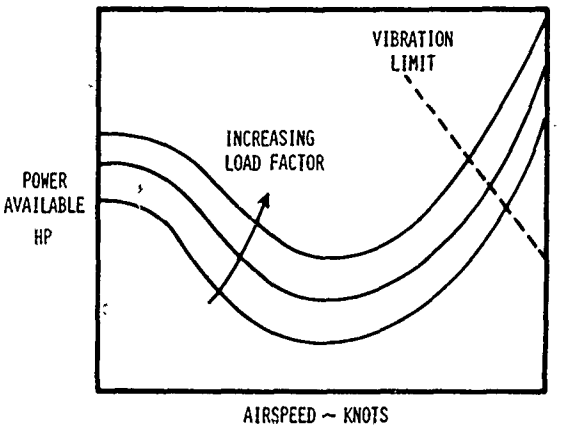

Fig. 8 — Vibrations limit flight envelopes

In the human factor area, adverse vibration and noise elements affect sensor perceptions (see Figure 9). Much of the human dynamic response data relates vibration amplitude and frequency to comfort and proficiency limits. These data show that high vibrations reduce performance and the ability to carry out complicated mental, tactile and visual acruity-related tasks. The trend towards complex displays and target designation systems places increased demands on these skills. Consequently, high vibrations degrade weapons delivery, especially in marginal weather and nap-of-the-earth operations. Over the years, lower vibration levels have increased human comfort and proficiency which improves crew mission effectiveness as noted in Figure 10.

High vibrations, or more specifically high vibratory stresses, affect the fatigue life and hence the structural integrity of both primary and secondary helicopter components. In fact, component fatigue margins have, in many cases, been reduced by high vibrations encountered during prototype flight testing. Of course, vibrations sustained in normal operations further reduce fatigue life margins. As a result, the operational life of helicopter components can be increased, as shown in Figure 11, by reducing vibrations.

In addition to reducing operational life, excessive vibrations also reduce reliability and increase maintenance of airborne equipment. In Figure 12 you can see that there

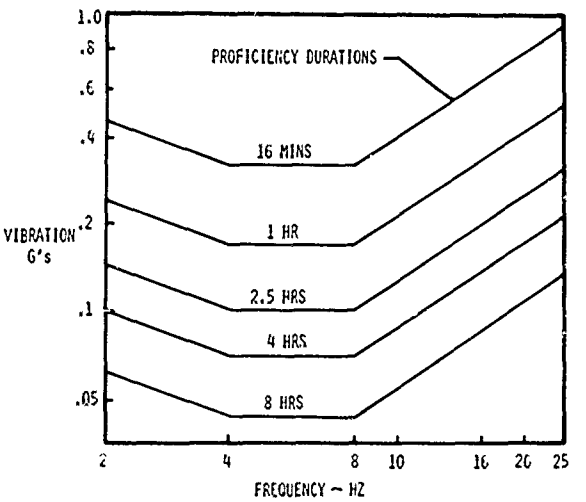

Fig. 9 — Human factors requirements

is a direct correlation between reduced failure rate and maintenance with reduced vibration levels. Failure rates associated with hydraulics, power trains, structures and

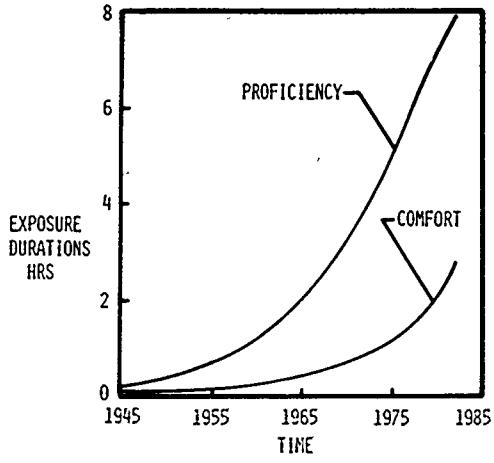

Fig. 10 — Human factors improvements

flight controls are related to frequency, amplitude and duration of the vibration environment. For example, Figure 13 shows that actuator failure rates are much lower in fixed-wing applications. The greater failure rate in helicopters can be attributed to higher vibration levels as well as high cycle usage. Although the connection may not be immediately obvious, vibrations and other factors affect helicopter transportability. For example, the Blackhawk and Apache procurement specifications required helicopter dimensions to be compatible with cargo compartments of military transport aircraft. The transportability requirement initially resulted in the main rotors being located close to the airframe. However, in this configuration rotor downwash caused higher than expected empennage vibrations and canopy drumming. These vibrations were so severe that they limited aircraft speed. Subsequently, main rotor to airframe separations were increased, as noted in Figure 14, to reduce vibrations at the expense of transportability.

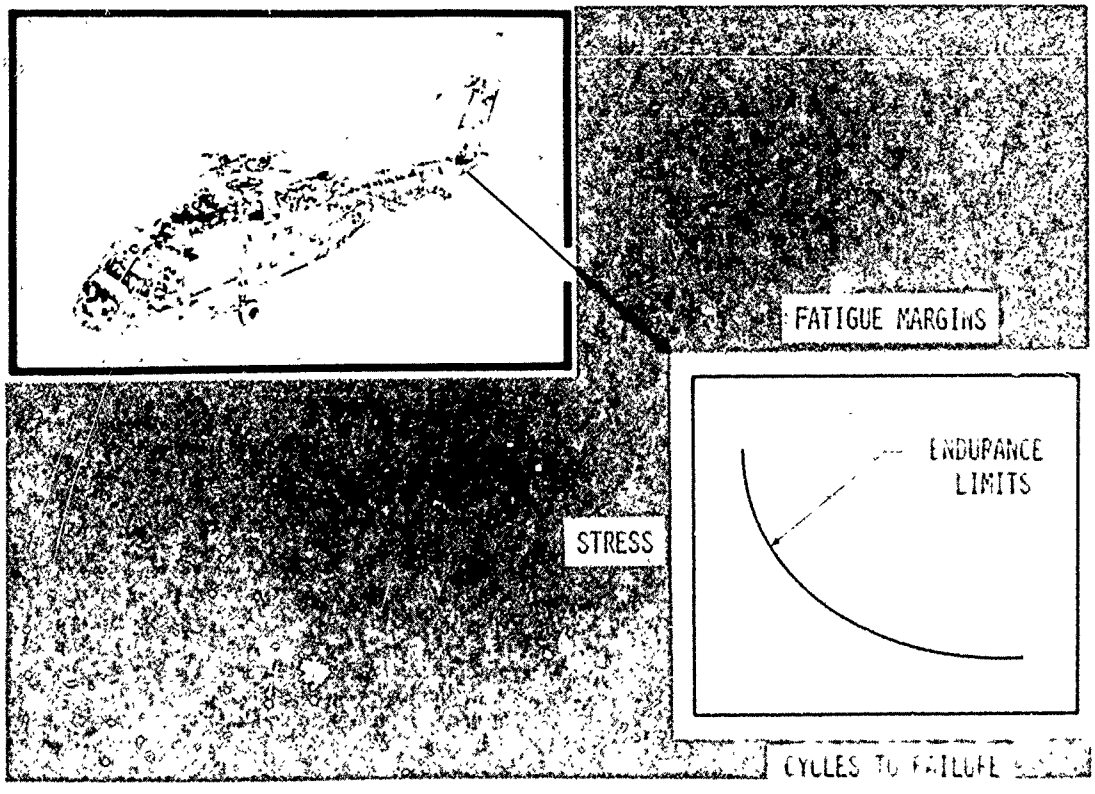

Fig. 11 — Structural integrity

The previous illustrations gave a perspective on the significance of vibrations during helicopter development. They underscored that high vibration levels affect a wide variety of helicopter design and operational features. Now, I would like to give you an assessment of where vibration technology stands.

Advanced vibration design technology has the potential to improve helicopter mission capabilities as well as eliminate costly trial-and-error development testing. To focus research on high payoff areas, AVRADCOM's Research and Technology Laboratories prepared a comprehensive Vibration Research Development Plan. This document reviewed past, current, and planned Army research programs; assessed the state of the art; identified significant vibration technology voids; and recommended areas for future research.

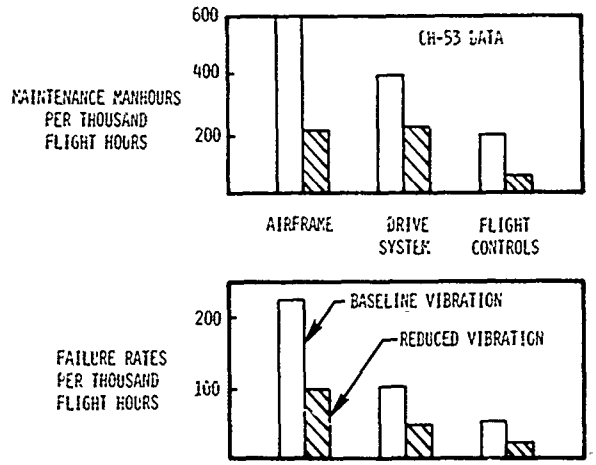

Fig. 12 — Vibrations versus R&M

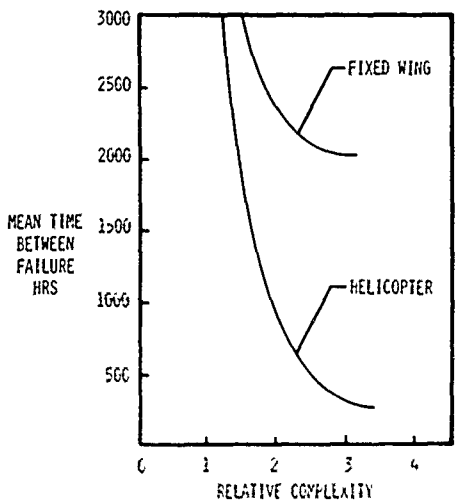

Fig. 13. — Fixed wing vs helicopter actuator failure rates

To put these findings in perspective, let us briefly review vibration design considerations. There are several exitation sources of helicopter vibrations that must be considered. The primary sources, as noted in Figure 15, are periodic loads transmitted by main and tail rotors as well as rotor downwash impingements. In addition, gust loadings, weapon recoil excitations, and engine exhaust interactions are likely sources of high vibrations. To minimize these vibrations, rotor and airframe configurations need to be designed as indicated in Figure 16. These configurations will yield low inherent vibrations. Then a variety of vibration control devices is available to further minimize vibrations at critical points. Consequently, the practical vibration solution usually combines passive vibration design and vibration control devices. Furthermore, vibration design strongly depends on an integrated testing methodology. The role of vibration testing is twofold. First, as noted in Figure 17, it provides a basis for verifying the vibration environment, and second, it supplements voids in existing analytical capabilities.

Based on the foregoing design considerations, five major categories of helicopter vibration research can be identified.

1. Rotor vibratory loads
2. Airframe structural dynamics
3. Rotor/Airframe coupling
4. Vibration control devices
5. Vibration testing

Each of these categories will be discussed in terms of technology deficiencies.

The first category, rotor vibratory loads, can be seen in Figure 18. Considerable research has concentrated on developing sophisticated rotor vibratory loads analyses. However, most of this research has focused on the basic disciplines of rotor aerodynamics and structural dynamics rather than on loads analyses. Hence, aerodynamic and structural phenomena intrinsic to rotor vibratory laods are still not completely understood and improvements in loads analyses have lagged those in these basic disciplines. Consequently, vibratory loads analyses are forced to rely on empiricisms and approximations. As a result, rotor loads predictions have not been very effective for detail design. In fact, these analytical deficiencies have required the designers to depend heavily on vibration control devices and trial-and-error testing.

In Figure 19 we see the next category, which is an airframe structural dynamic assessment. Helicopter airframes are complicated structures characterized by multiple cutouts, abrupt discontinuities and numerous dynamic components. Airframe analyses have evolved into applications of large-scale finite element models. Even with this advanced capability, helicopter designers have achieved only limited success in designing airframes with acceptable resonance placements. A significant deficiency has been an incomplete understanding of modeling requirements for complex helicopter structures. There has also been inadequate consideration of more design-respective finite element analysis programs. Thus, as with the rotor analyses, these sophisticated airframe analyses have not been very effective in the design process. Again, these deficiencies have led to a reliance of relatively heavy vibration control devices instead of passive design concepts.

Rotor/Airframe coupling is addressed in Figure 20. Coupling analyses depend on both structural dynamic and aerodynamic interfaces. Effective analysis and understanding of helicopter vibrations require sophisticated rotor/airframe coupling procedures. Applications of these coupling procedures have been limited by deficiencies in rotor and airframe analyses as well as computional limitations. In the past two or three years, the research community has increased analytical efforts in rotor/airframe coupling. This research has primarily addressed structural dynamic coupling aspects. Aerodynamic interactional vibration problems experienced during recent development programs provide ample evidence of existing voids in this area.

The fourth category of helicopter vibration research, as noted in Figure 21, is vibration control devices. The development of vibration control devices has been the dominant factor in reducing helicopter vibrations. These devices include main rotor hub absorbers, airframe absorbers, and transmission isolators. Local isolators have

also been applied to crew seats, instrument panels, cabin floors and fuel tanks. There is a substantial level of effort within the Army and industry that focuses on minimum weight vibration control devices. More recently, active control concepts are being considered as alternatives to minimize rotor vibratory loads and reduce helicopter vibrations. The significant progress in vibration control warrants continued development of advanced concepts.

In the last research category, vibration testing, three major areas—ground and flight testing, wind tunnel testing, and human factors testing—have been assessed. These tests are frequently used to quantify flight loads and vibrations, to correlate and supplement analysis and to establish human vibration exposure criteria.

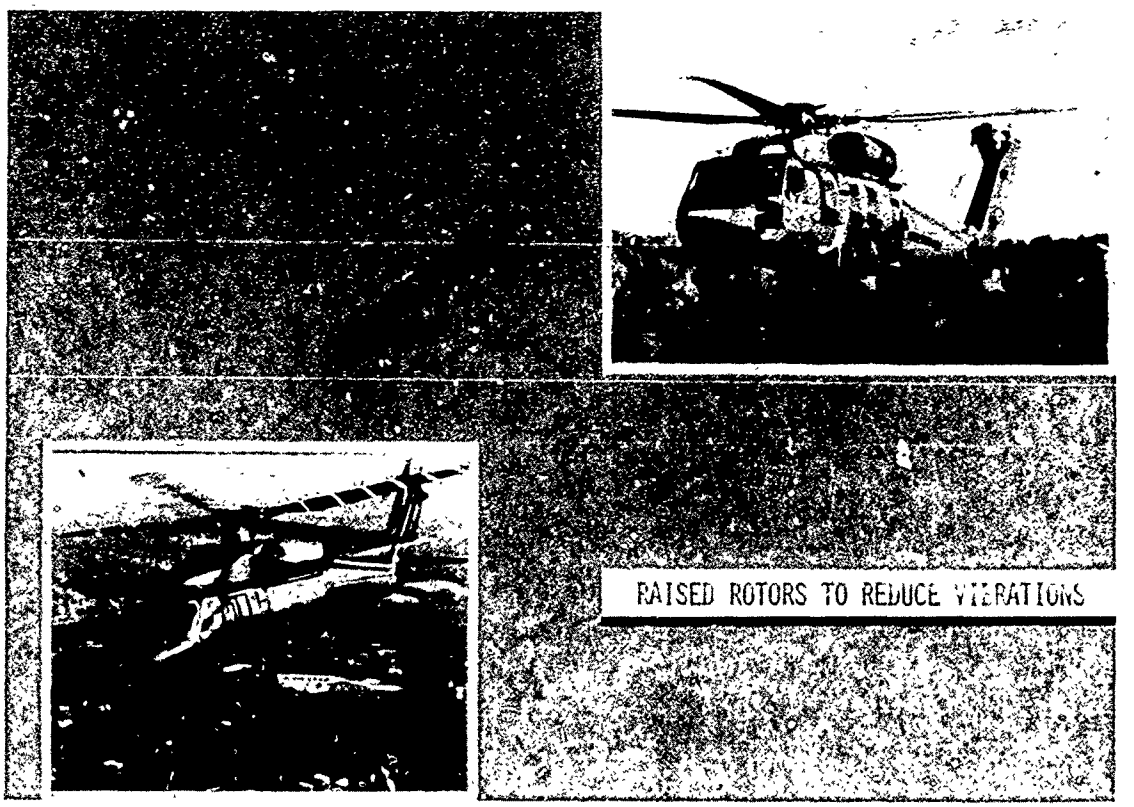

Fig. 14 — Transportability requirement

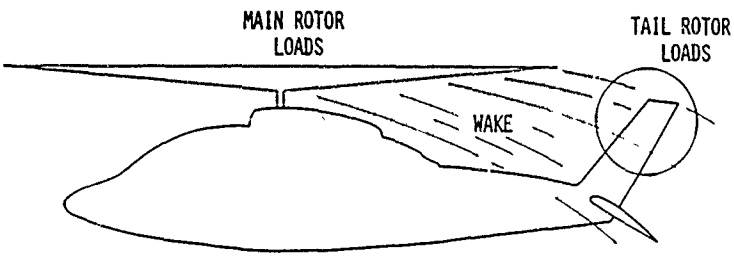

Fig. 15 — Sources of high vibration

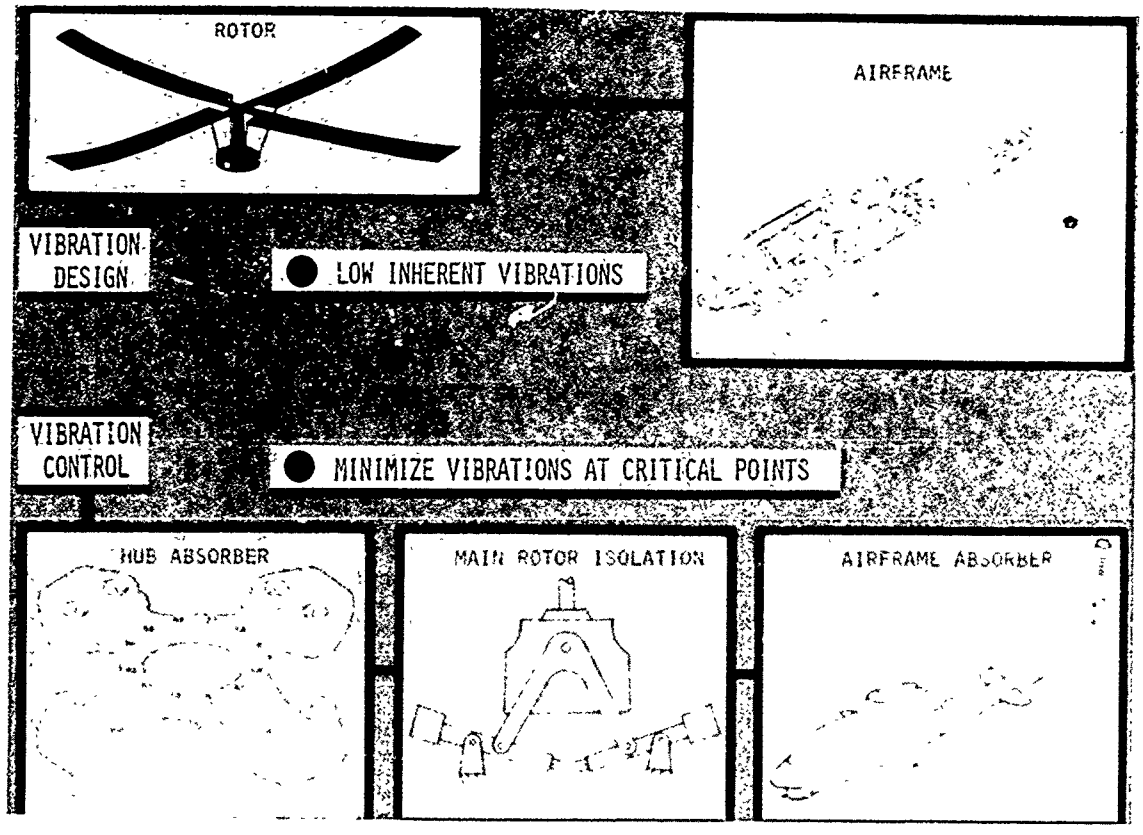

Fig. 16 — Vibration design considerations

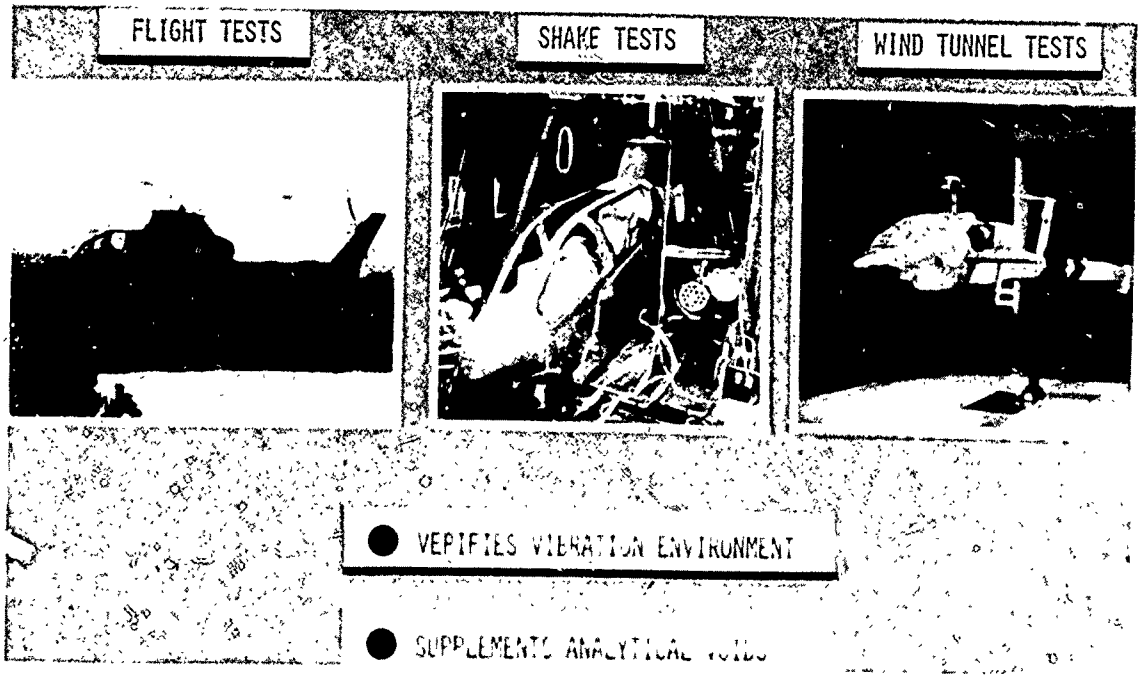

Fig. 17 — Role of vibration testing in design

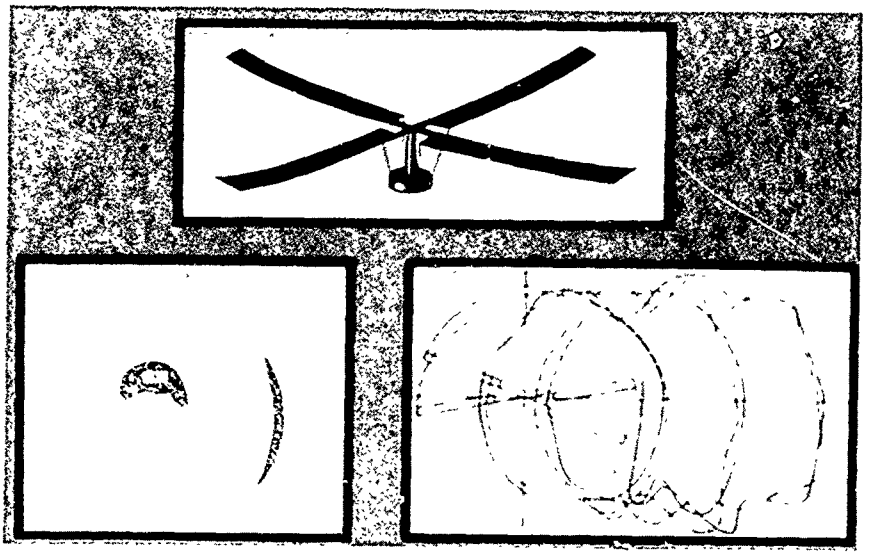

- RESEARCH FOCUSSED ON BASIC DISCIPLINES
- CURRENT METHODS RELY ON EMPIRICISM
- ROTOR LOADS DESIGN METHODOLOGY NOT VERY EFFECTIVE
- TOO MUCH RELIANCE ON VIBRATION CONTROL DEVICES

Fig. 18 — Rotor vibratory loads assessment

- FINITE ELEMENT MODELS MAJOR TOOL
- COMPLEX MODELING REQUIREMENTS
- RESONANCE PLACEMENT HARD TO ACHIEVE
- AIRFRAME DYNAMICS METHODOLOGY NOT VERY EFFECTIVE
- TOO MUCH RELIANCE ON VIBRATION CONTROL DEVICES

Fig. 19 — Airframe structural dynamics assessment

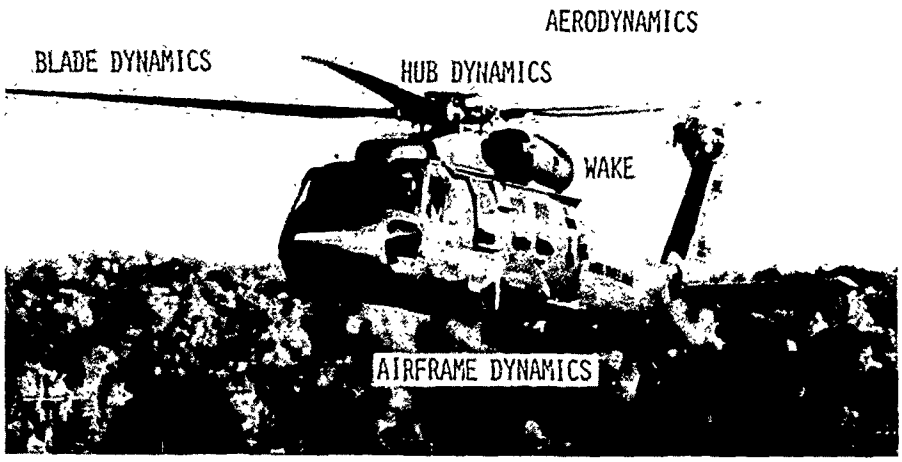

- ROTOR/AIRFRAME INTERACTIONS CAUSE MAJOR VIBRATION PROBLEMS
- CURRENT RESEARCH EMPHASIZES STRUCTURAL DYNAMIC COUPLING
- VIBRATION EFFECTS OF AERODYNAMIC COUPLING NOT WELL DEFINED

Fig. 20 — Rotor/airframe coupling assessment

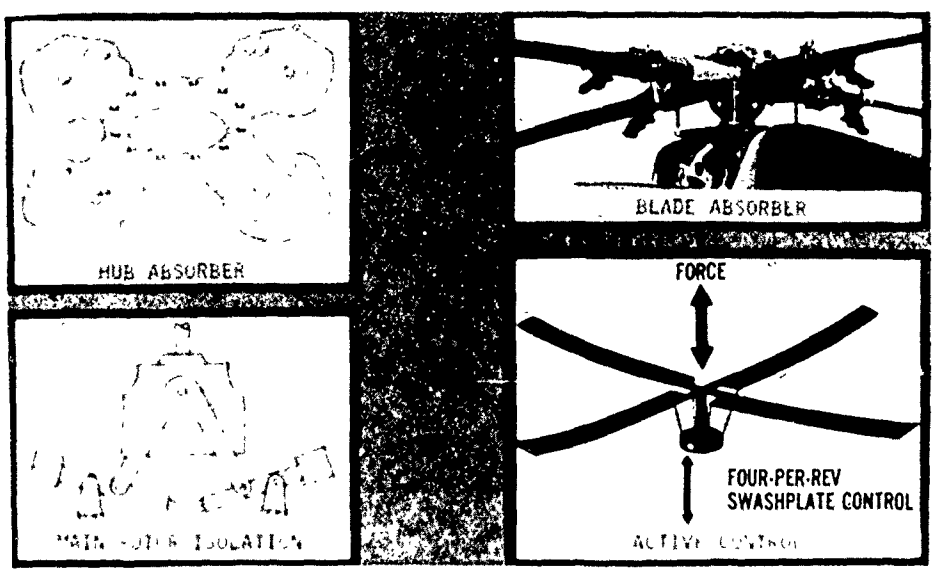

- MAJOR CONTRIBUTOR TO REDUCED VIBRATIONS
- MANY DIVERSE APPLICATIONS
- ACTIVE CONTROL LIMITED TO ROTOR

Fig. 21 — Vibration control devices assessment

There has been considerable Army research in ground and flight vibration testing to develop methods for measuring rotor vibration loads, improving airframe math models, correlating analytical predictions and optimizing flight vibrations as noted in Figure 22. These efforts will ultimately provide standardized methods or testing, correlating and evaluating helicopter vibrations. In fact, advances in ground and flight vibration testing are critical to reduce or eliminate trial-and-error development testing.

ELIMINATE
TRIAL-AND-ERROR
TESTING

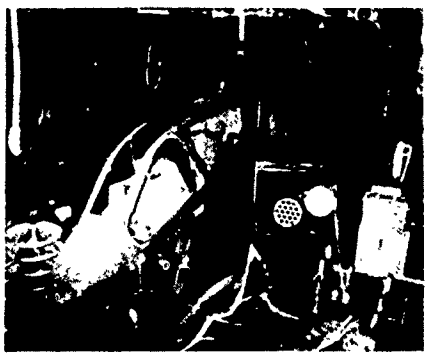

COMBINE TEST AND ANALYSIS TO

- MEASURE VIBRATORY LOADS
- IMPROVE MATH MODELS
- CORRELATE ANALYSIS
- OPTIMIZE VIBRATIONS

Fig. 22 — Ground and flight testing assessment

The Army has conducted numerous wind tunnel tests like the one pictured in Figure 23. These tests were to investigate vibratory rotor loads. From a vibrations viewpoint, current wind tunnel testing is addressing specific rotor concepts and active controls such as passive, aeroelastic tailoring and higher harmonic control investigations. These tests usually focused on problems that deal with limited parametric test variations for specific rotor types and operating conditions. Therefore, existing results are difficult to synthesize since a comprehensive wind tunnel data base has not been developed. Wind tunnel investigations are important for solving specific problems and for improving our understanding of the physical mechanisms. This understanding is essential to develop effective analytical methodology.

Human factors testing has been conducted to evaluate the effects of vibrations on comfort and proficiency. These subjective evaluations have identified fundamental relationships which govern human response. For example, human factors data are currently being used by the Army to relate vibration amplitudes, frequencies, and durations of exposure to specified tolerance limits. Present studies indicate that when combined with audio and visual environments, even acceptable vibration levels degrade human performance. Consequently, more comprehensive human vibration exposure criteria should include vibration, noise and visual effects.

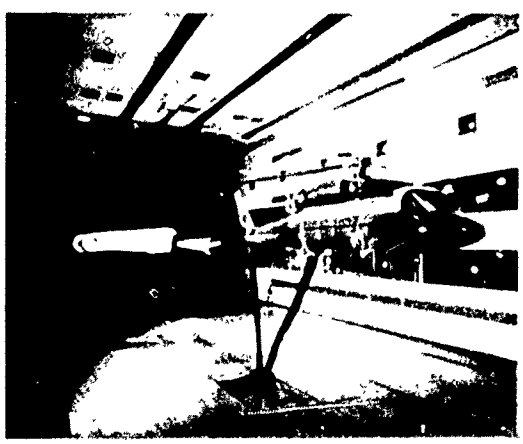

VIBRATORY ROTOR LOADS DATA BASE IS EXTENSIVE
BUT DIFFICULT TO SYNTHESIZE

CURRENT TESTS FOCUS ON SPECIFIC ROTOR CONCEPTS
AND ACTIVE CONTROLS

Fig. 23 — Wind tunnel testing assessment

The technology deficiencies which I have discussed can be summarized into three major areas of concern relative to helicopter vibrations. First, the inability of present design methodology to accurately predict rotor vibratory loads and coupled rotor/airframe vibrations; second, too much reliance on vibration control devices rather than passive design concepts; and third, a lack of definitive procedures to make maximum use of vibration test data, instead of trial-and error testing, for solving vibration problems. Now, I would like to describe some current Army research programs which are addressing these concerns.

As the assessment of vibration technology indicates, there is much to be done in developing technology to reduce helicopter vibrations. Several approaches are currently being addressed that should provide both near-term and far-term solutions. The near term efforts include the development of advanced vibration control systems with minimum weight penalties. Also, advanced vibration testing techniques are being evaluated and implemented. Far-term efforts are addressing passive design and aeroelastic tailoring methodologies.

In the vibration control area, passive and active systems are being developed for near-term applications. For example, in Figure 24 we see that predesign studies for passive total main rotor isolation show the concept is feasible with a weight penalty approaching one percent or less of aircraft design gross weight. To demonstrate the concept, a program has recently been initiated for detail design and bench testing of a total main rotor isolation system. If the system performs as promised, a flight test demonstration program may follow. In addition to main rotor isolation, a program to design and bench test a monofilar hub vibration absorber is in progress. This advanced rotating hub absorber, shown in Figure 25, produces force cancellation at two frequencies using a single active mass. Current hub absorbers require two active masses for this purpose. Consequently, the monofilar absorber has the potential to reduce weight penalties and provide a higher degree of vibration reduction. Again, if the ground tests are successful, a flight test demonstration may follow. Besides passive design approaches, an active method to vibration control is the Army's higher harmonic control program. For this approach, the main rotor swashplate is oscillated at the blade passage frequency with the inputs being computer controlled. The control algorithm was evaluated in the NASA/Langley Transonic Dynamics Tunnel and, as Figure 26 shows, vibration levels were reduced. Higher harmonic control has also been installed on an OH-6A helicopter pictured in Figure 27. Initial open-loop flight test results show significantly reduced vibration levels, and computer controlled closed-loop testing is planned in the near future.

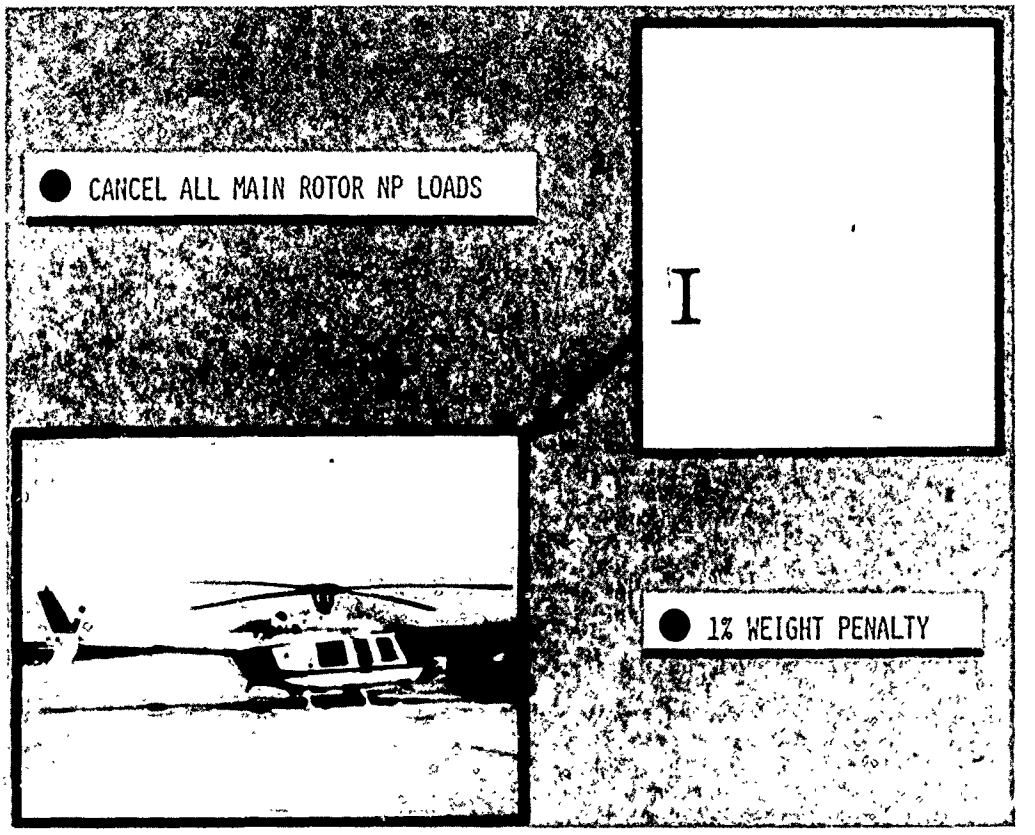

Fig. 24 — Total main rotor isolation

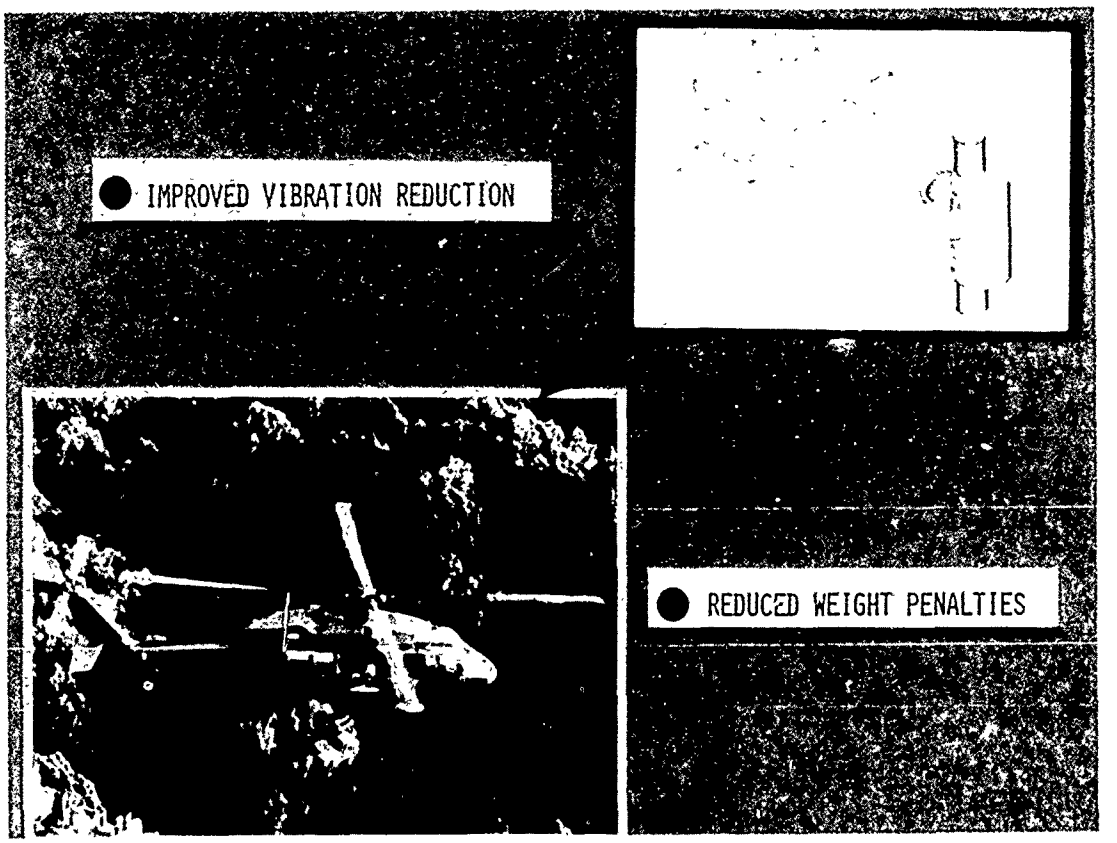

Fig. 25 — Monofilar hub absorber

In the vibration testing area, methodology is being developed for using ground vibration test data to upgrade math models, combining ground and flight vibration data to determine rotor hub vibratory loads, and combining ground and flight vibration data to optimize structural design changes and to design vibration control devices (see Figure 28). As a result, these techniques should provide systematic methods for resolving helicopter vibration problems during development flight testing.

Far-term and potentially higher payoff solutions are also being pursued. To improve passive design methodology, a coupled rotor/airframe vibration analysis has been developed. The capabilities of this analysis are shown in Figure 29. They include unsteady rotor aerodynamics, aeroelastic rotors, wake/empennage interactions, elastic airframes, rotor and airframe absorbers, rotor isolation systems and higher harmonic control. The analysis is intended to be a preliminary design tool for evaluating various approaches to reduce vibrations. Army research is also addressing technology deficiencies in airframe structural dynamic modeling methodology. More design-responsive finite element programs are being considered to evaluate airframe dynamics and flight vibration optimization. In addition, modeling requirements for composite structures are being analyzed and correlated.

Besides analytical developments, current research is focusing on vibration load control through aeroelastic blade tailoring, as indicated in Figure 30. The effects of tip geometry on blade dynamics response is being pursued through wind tunnel and flight tests. Wind tunnel investigations of aerodynamic interactions have also been conducted with results shown in Figure 31. This effort was the first comprehensive attempt to measure flow anomalies and interactional forces acting on a helicopter configuration. The results of this program should lead to a better understanding of the flow enviornment. Furthermore, this understanding will guide the analyst in developing realistic theories for evaluating interactional effects on vibrations.

All of these programs are major efforts to resolve deficiencies in helicopter vibration technology. There are many other research programs underway which are concentrating on the basic disciplines of aerodynamics and structural dynamics.

Now that current Army research has been discussed, you can get some impressions of our future needs by studying Figure 32. As shown, there are numerous technology voids in the area of helicopter vibration design. Many of these deficiencies are being addressed by current Army research. However, much remains to be accomplished to reach our goal of designing helicopters with low inherent vibrations. Additional research efforts are needed in vibration analysis, vibrations testing and vibration control.

Designing rotors with low inherent vibratory loads requires a long-range commitment to examine aerodynamic and structural dynamic modeling approaches and solutions, and to apply this advanced methodology in conjunction with passive aeroelastic tailoring. In addition, future wind tunnel testing should establish comprehensive data bases to validate and synthesize improved analytical capabilities.

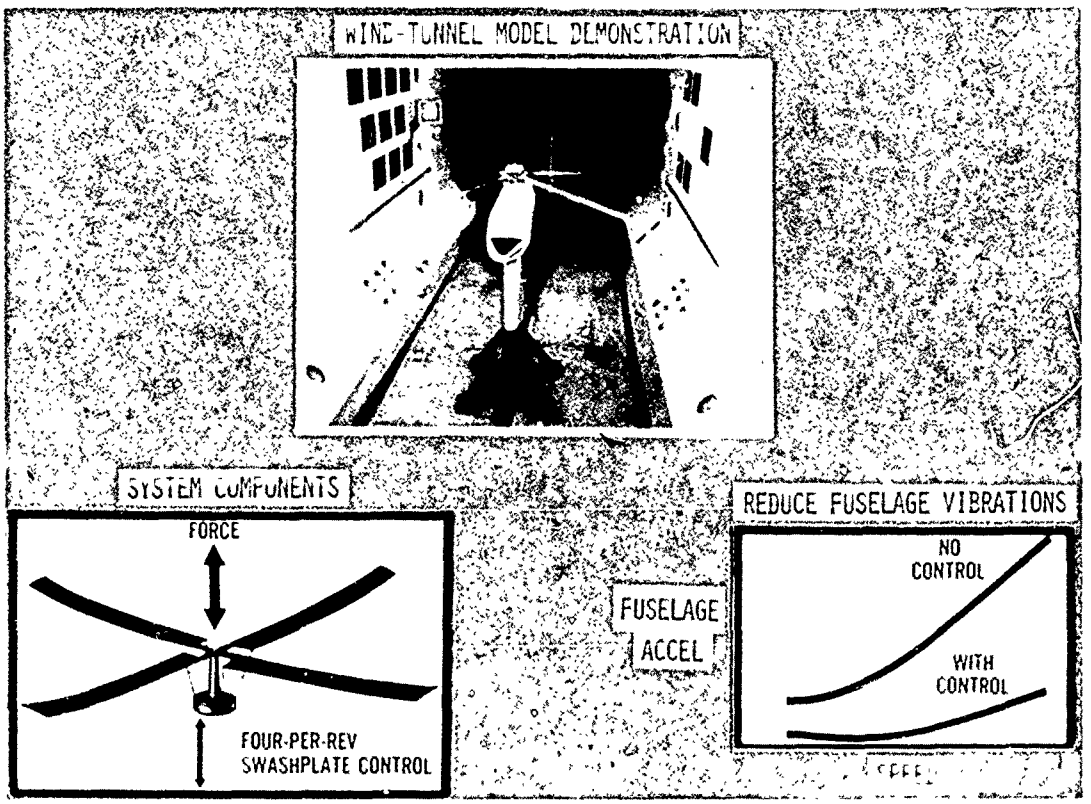

Fig. 26 — Higher harmonic control

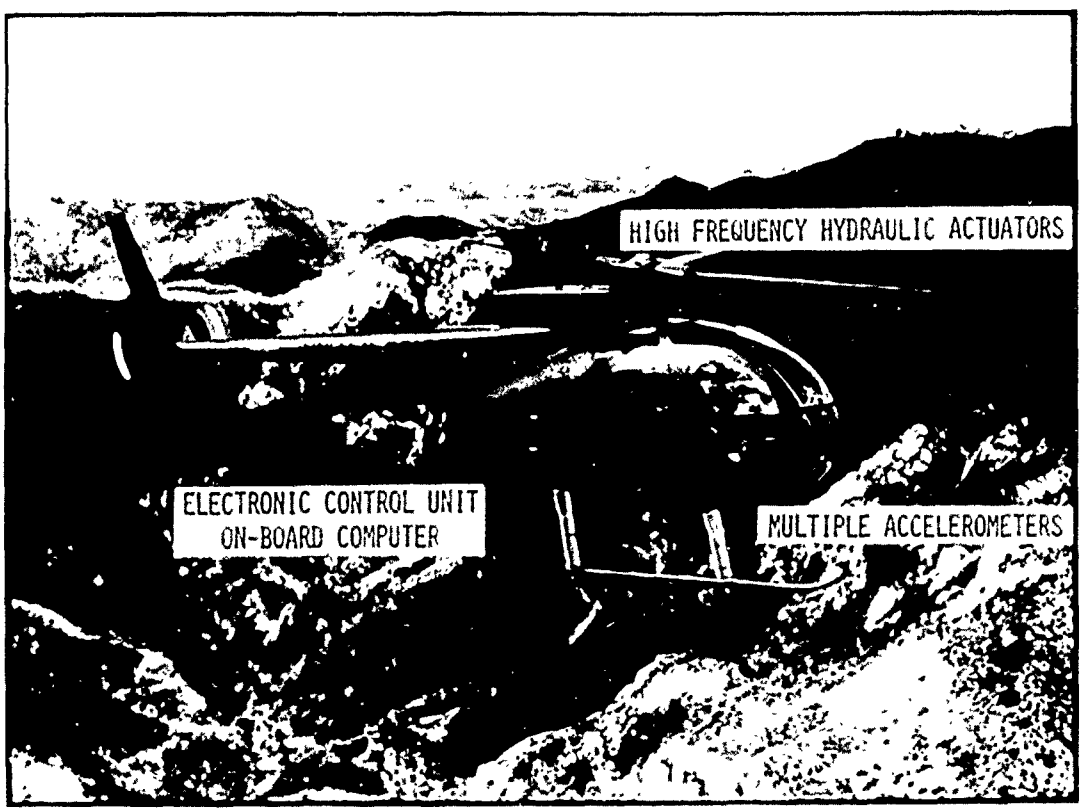

Fig. 27 — OH-6A HHC demonstration

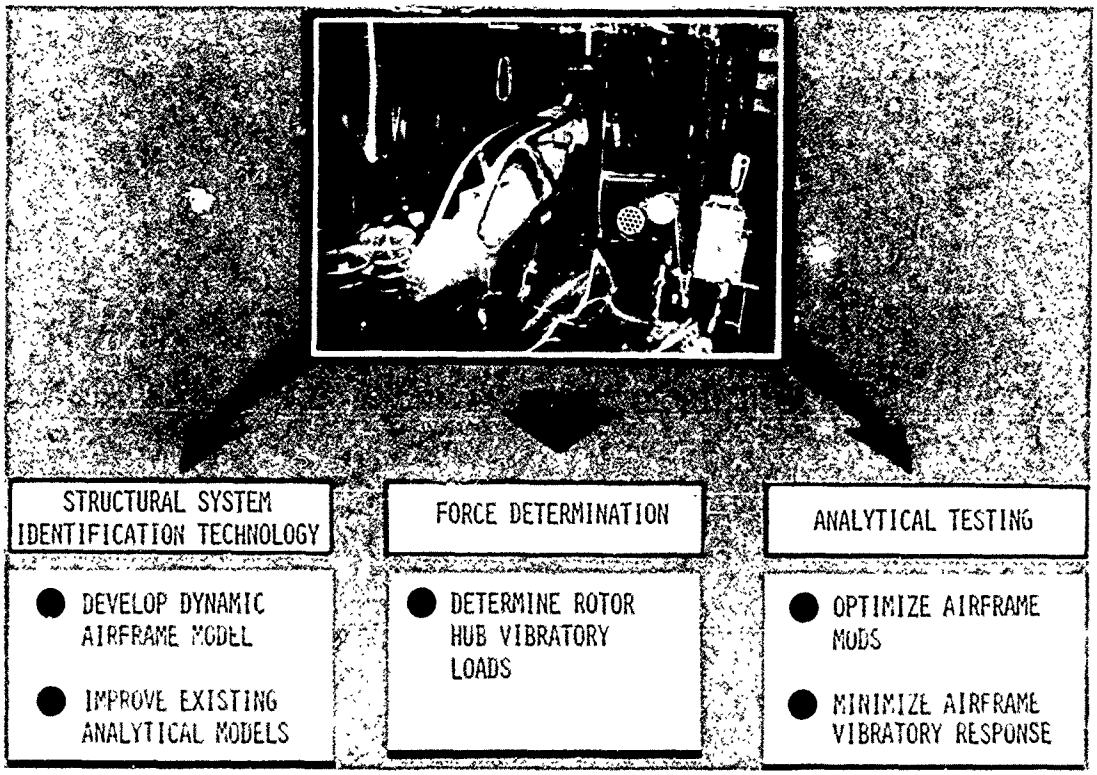

Fig. 28 — Advanced ground and flight vibration testing

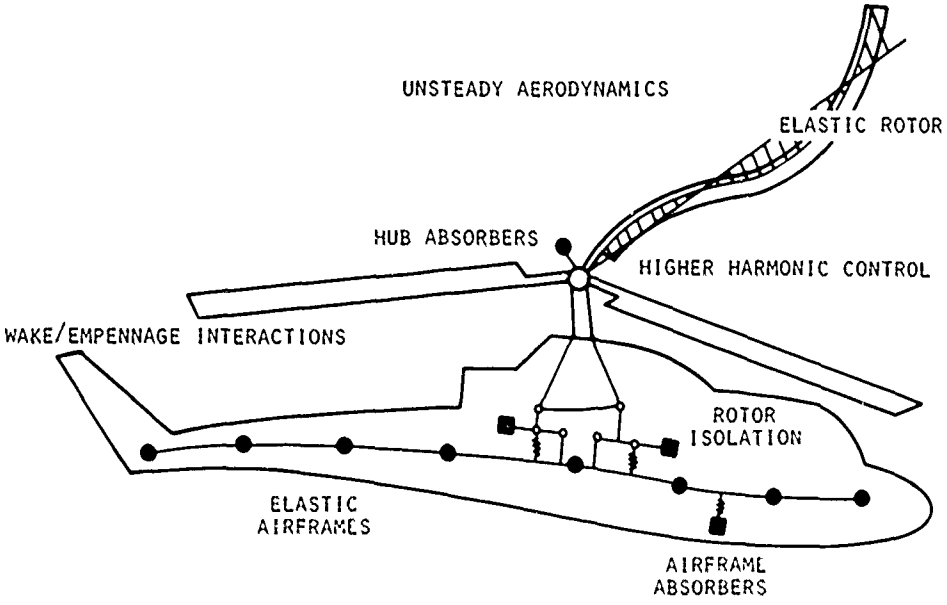

Fig. 29 — Coupled rotor/airframe vibration analysis

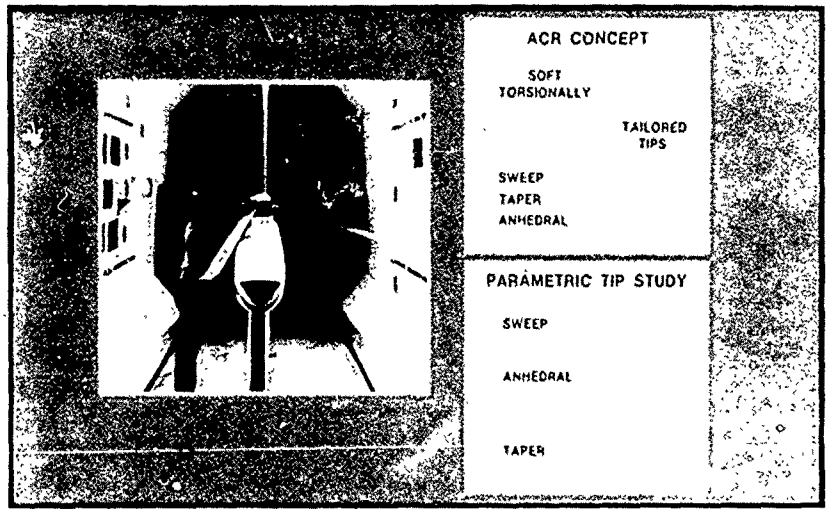

- REDUCE BLADE VIBRATORY LOADS
- ASSESS TIP EFFECTS ON BLADE DYNAMICS

Fig. 30 — Aeroelastic tailoring of rotors

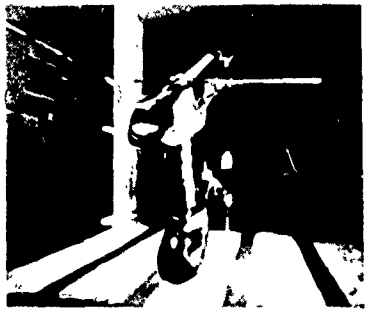

- UNDERSTAND FLOW INTERACTIONS
- IMPROVE EMPENNAGE DESIGN
- GUIDE ANALYTICAL DEVELOPMENT
- REDUCE VIBRATIONS AND A/C FATIGUE LOADS

Fig. 31 — Aerodynamic interaction studies

FUTURE NEEDS

- **ROTOR VIBRATORY LOADS**
  - Improve aerodynamic and structural dynamic analyses
  - Demonstrate rotor aeroelastic tailoring
  - Validate capabilities through wind tunnel testing
- **AIRFRAME STRUCTURAL DYNAMICS**
  - Correlate and improve finite element modeling
  - Improve vibration optimization techniques
  - Demonstrate current ground and flight vibration testing methodology
- **ROTOR/AIRFRAME COUPLING**
  - Validate present coupling analyses
  - Experimental investigations to define aerodynamic coupling effects
  - Improve analytical capabilities
- **VIBRATION CONTROL DEVICES**
  - Provide multi-frequency capabilities at lower weight
  - Improve R&M
  - Reduce system integration problems
- **HUMAN FACTORS TESTING**
  - Develop more comprehensive tolerance criteria
  - Simulate multi-axis and multi-frequency excitations including noise effects

Fig. 32 — Future needs

Improved helicopter airframe design requires a similar long-range commitment. If airframe dynamics are to be passively designed, finite element models need to be correlated with data to quantify modeling deficiencies. These correlated models can then be used to demonstrate vibration optimization. To supplement improved analysis capabilities for solving vibration problems, current ground and flight vibration testing methodology also needs to be demonstrated.

Advancements in rotor and airframe analyses can directly improve rotor/airframe coupling design. Additional research is required to determine the accuracy and limitations of present coupling analyses. Moreover, aerodynamic coupling is a major issue which demands a substantial experimental effort to further define and evaluate interactional effects on vibrations.

Besides improved analysis methodology, refinements in vibration control devices are needed. These refinements should include lower weight, multi-frequency capabilities, improved reliability and maintainability and earlier integration into the overall aircraft system. Based on the recent success with higher harmonic control of the rotor, future active control concepts need to be considered for airframe control surface and rotor/airframe interfaces.

Finally, in the area of human factors testing, a human factors simulator should be established to develop more comprehensive tolerance criteria. The facility should be capable of simulating multi-axis and multi-frequency excitations as well as noise and visual effects.

The Army hopes to implement programs which address these higher priority needs. Furthermore, as Figure 33 indicates, the technology developed in these areas need to be periodically merged into technology demonstrators. For example, the Rotor Systems Research Aircraft, the Tilt Rotor Aircraft and the Advancing Blade Concept Aircraft have helped in transferring technology to engineering development and production.

I would like to conclude this presentation by reiterating that, through research, vibration problems have been minimized for the Army's modern operational helicopters. However, reducing prototype vibration levels to meet Army needs has typically been a lengthy and costly process. And yet, there is still potential for significant improvements.

These improvements will be discovered through vibration research, and Army programs are underway in many areas. As shown in Figure 34, these areas include vibration analysis of coupled rotor/airframe vibrations, aeroelastic tailoring of rotors, advanced vibration control devices and innovative vibration testing techniques. Future programs will also be needed in the human factors area.

The potential payoffs to Army aviation by reducing the impact of vibrations on helicopter design are tremendous motivators to continue the course we have set. Reducing costs and enhancing overall mission capabilities can be achieved through advancements in vibration technology. Those who have struggled to satisfy Army vibration requirements for this unique flying machine are to be commended for their efforts, but much remains to be done.

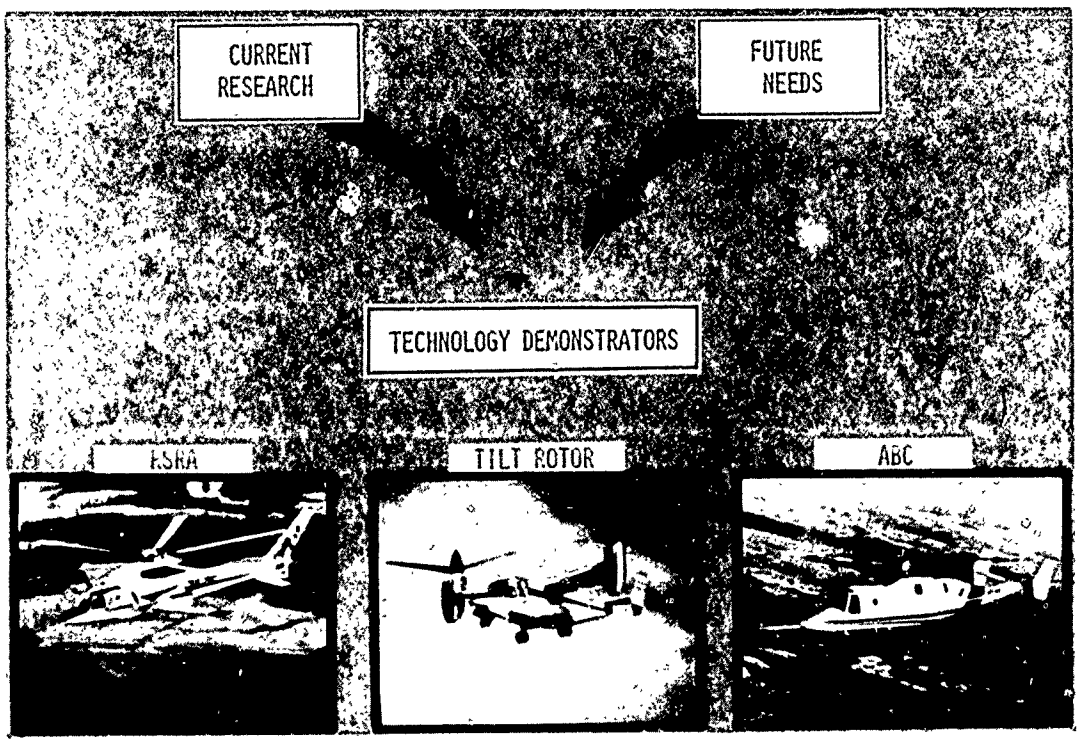

Fig. 33 — Vibration technology enhancements

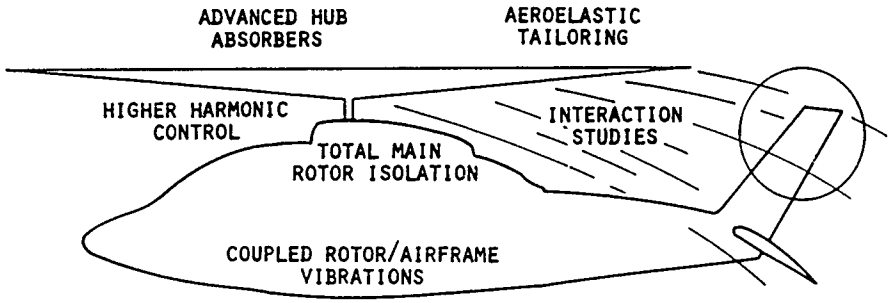

Fig. 34 — Progress in vibration research

INVITED PAPERS

TECHNICAL INFORMATION SUPPORT FOR SURVIVABILITY

H. C. Pusey, R. H. Volin and J. G. Showalter
Shock and Vibration Information Center
Naval Research Laboratory
Washington, D.C.

DOD policy requires that system survivability be a major consideration in the systems acquisition process. The need for an effective DoD survivability/vulnerability information service is established. The technology sources and the user community are examined and options are discussed for the organization of the information service. Recommendations are offered on the steps to take for the establishment of such a service.

INTRODUCTION

The readiness of our combat forces to engage the enemy in the event of war has always been the principal concern of those responsible for implementing our defense strategy. The combat systems used in our defense must be operational at all times. We need the assurance that, no matter from what quarter or in what form an attack comes, we have the capability to respond to the extent that our freedom, indeed our very existence, is not jeopardized. What does this tell us about the requirements for our combat systems? Very simply, the design of these systems must be such that they are guaranteed to survive and have retaliatory capability under any and all combat threats. To make this happen, we must understand all potential threats and the effects produced by those threats. We must incorporate this understanding into the design of our systems, at least to the extent that we remain in the game until all the cards are played. Obviously, this does not mean that we will sustain no losses or damage. What it does mean is that our total force response capability will be intact at all times. Accomplishing this goal involves a combination of military tactics, evasion, and system hardness. This paper is concerned with the systems survivability considerations that are a major part of this effort.

Evolving DOD Policy

Although military strategists have always been concerned with enemy threats, it wasn't until the 1960's that the Department of Defense (DoD) began considering this problem in an organized way. The effort began with the Joint Technical Coordinating Group for Munitions Effectiveness (JTCG/ME). Although one might infer that this Tri-service Group was principally made up of weaponeers, the implications related to the survivability of our own systems were clear from the outset. In 1971, the Joint Technical Coordinating Group for Aircraft Survivability (JTCG/AS) was officially chartered. Destined to lead the way in establishing survivability as a design discipline, the JTCG/AS supported and inspired work in survivability/vulnerability from a systems-oriented standpoint. Analytical assessment tools were developed; Standards, Handbooks and Guides began to be published. Workshops, conferences and symposia were organized to meet the need for informative exchange and feedback. Meanwhile, in 1975 Admiral Kidd issued NAVMAT Instruction 3920.4A directing a vigorous Naval Combat Survivability Program for each weapon system. In effect, this Instruction brought together the Navy elements which were to be concerned with survivability programs and helped to put these programs in place in the Naval Systems Commands. Similar activities were going on in the Army and Air Force. It was indeed clear that survivability had officially become a major consideration in the acquisition of Defense Systems.

Implementing Documentation

The principal documents implementing DOD policy on survivability are DODINST 5000.2, "Major System Acquisition Procedures," and DODINST 5000.3, "test and Evaluation." In these documents, the concern and the requirements are clear. In DODINST 5000.2, for example, survivability is counted as one of four major factors in mission analysis. Furthermore, the directive stresses that "The effectiveness of a proposed weapon system in its intended threat environment is a fundamental concern of the acquisition effort and shall be considered by the program manager from the outset." DODINST 5000.2 also requires that system-threat interaction be studied early in the program and that the results be specifically updated throughout the development stages. Throughout DODINST 5000.3 on Test and Evaluation it is mandated that operational suitability and effectiveness be examined by testing "as early as possible in the acquisition cycle." Furthermore, in the Development Test and Evaluation Phase, testing must ensure that survivability/vulnerability and other engineering considerations are reasonably complete. Since these two Instructions drive the RDT&E process for Defense Systems Acquisitions, it follows that each Military Department must implement the requirements in its own way. As an example, consider the Navy requirements now in place.

The current operative Navy document is NAVMATINST 3900.16, "Combat Survivability of Naval Weapon Systems." This directive requires that research and development efforts to support combat survivability be planned and funded. The

survivability R&D efforts are to develop concepts, procedures, materials and designs for hardware and software to enhance survivability of mission-essential weapon systems. All applicable threats are to be considered, not only for new systems, but for all modernization, improvement and retrofit programs. The Instruction specifies that no program will be initiated unless survivability considerations are addressed at the outset and that such considerations will become increasingly specific as the system development program proceeds. Test and evaluation matter plans (TEMPS) must identify survivability requirements and develop plans to verify that the system meets these requirements. Beyond the broad requirement that all weapons effects be considered in survivability design, there are a number of more specific documents from OPNAV, NAVMAT and the SYSCOMS which address threat definition and hardness requirements for different threat effects produced by conventional or nuclear attack.

What all of this means is that every systems development program, every project office, and every responsible official must pay heed to survivability requirements through all stages of development and, indeed, into the fielding of the systems. This raises a few questions. Where can the program manager, the project officer, or the working engineer go to learn about the latest available technology to support survivability requirements? Are the sources for such information easily identified and, if so, are they accessible? Finally, is there a single office to which one can go to get assistance with survivability information problems? In brief, the answers are that there are many sources for survivability-related information, some better known than others, but there is no single clearirghouse for this information. The rest of this paper is devoted to an assessment of the survivability/vulnerability information support requirements, along with some thoughts on how to meet them.

SURVIVABILITY/VULNERABILITY INFORMATION NEED

As a result of the strong positive DOD policy on combat systems survivability, the three Military Departments support extensive research and development efforts which generate large quantities of useful information and data to support the development of new, more survivable weapons systems. The JTCG/ME and JTCG/AS have led the way in this research on a Tri-Service basis. Separately, the Army, Navy and Air Force Program Offices, Commands and Laboratories support literally thousands of RDT&E tasks, either as a part of major programs or as a part of the 6.1 and 6.2 R&D effort. The volume of technical information generated is tremendous. Much of this information, when made available and properly applied, can be brought to bear on some aspect of the survivability design problem. To show why this is true, it is necessary to examine combat survivability as a design discipline in terms of what is required to support the design.

In the simplest terms, system survivability involves a threat or combination of threats with the system as a target for those threats. The idea is that somehow the system must be designed to survive those threats. For each threat, then, we must have a complete description of the threat characteristics and effects. If it is a missile, for example, we must know its range, velocity and expected trajectory. How can we detect its approach? How much reaction time do we have? What are the warhead characteristics? Is it conventional or nuclear; fragmenting or penetrating? Now, let us assume that the missile is attacking a ship and that the ship is unable to evade the attack by the use of appropriate countermeasures. Let us further assume that the ship's weapons are unable to destroy the missile before it reaches the ship. Assuming a hit, then, how should the ship be designed to that its probability of survival is high?

To answer the last question, we must first have detailed information about the effects of the missile warhead. Will it be a proximity external explosion producing fragments and blast? At what distance? What is the expected blast overpressure? What size fragments at what velocities can be expected? Perhaps the missile warhead has a shaped charge to penetrate the hull and explode inside the ship. Appropriate parameters must be defined for that situation. Secondly, we must have a full description of all the ship's systems in both functional and structural terms. Using this information, we are able to model the ship and/or its systems and use appropriate algorithms to assess vulnerability to the threat. We can combine the results of this vulenrability analysis with assessments of vulnerability to other threats to provide a more complete picture. The process of vulnerability assessment allows us to examine options to increase survivability. For example, changes in materials or structural characteristics can be examined for effectiveness. Options for redundancy can be studied. And we can look at ways to minimize secondary effects such as fire or flooding. Finally, we can confirm the results of our analysis and design by appropriate tests.

Even for this simple example, it is obvious that a lot of details have been omitted. When one considers all possible threat effects, it becomes clear that a broad range of technical disciplines and associated methodologies are involved in designing for survivability. It is also clear that the technology evolving from all of these disciplines is applicable in one way or another to the design of defense systems, whether they be for land, sea, air or space operations. Table 1 provides an incomplete listing of technologies and areas of expertise that are employed in survivability design.

Present and Proposed Sources for Survivability/Vulnerability Information and Data

The ultimate source for S/V information are the results of DOD R&D programs that directly or indirectly support survivability enhancement efforts. Direct R&D support may come from the well-coordinated Tri-service programs such as the JTCG/ME and JTCG/AS, or from single service survivability programs managed by an appropriate Command or Laboratory. A single Code in NAVSEA, for example, manages survivability R&D programs to support individual ship designs and total fleet survivability concepts. The Ballistics Research Laboratory at the Aberdeen Proving Ground controls programs which support the survivability of the Army's ground vehicles and other systems. The USAF Ballistic Missile Office provides survivability R&D support for some of our major offensive weapons, such as MX. The list goes on.

Indirect R&D support is provided as required from the extensive programs on materials, structures, electronics and other areas which produce new technology applicable to the solution of some facet of the survivability problems. In short, the information support scenario for survivability is complex. It requires information resources in specific technological areas with analysis and screening capabilities to match their new technology to specific survivability problems. Once the problems are clearly defined, there are a number of information organizations that can do this; they can serve as valuable

TABLE 1
Multidisciplinary Nature of Survivability

Threat-Related Technologies	Survivability Design	Secondary Effects and Other Factors
Air Blast	Design Methodology	Damage Repair
Shock	Threat Definition	Fire Protection
Vibration	Target Modeling	Fire Fighting
EMP(EMI)	Computer Programs	Flood Control
Fragments/Penetrators	Analysis Methods	Human Factors
Thermal Radiation	Materials	Collective Protection
Chemical/Biological	Structural Analysis	Individual Protection
Directed Energy	Combat Data	Biodynamics
Signatures	Countermeasures	Psychological Response
RF Optical RCS	Failure Analysis	Visual Activity
IR EM	Damage Analysis	Man-Machine Interface
Acoustic Magnetic	Trade-off Analysis	Medical

resources. To be completely effective, it is also necessary that information organizations understand survivability as a design discipline and be familiar with the survivability community to the extent that they can direct new information to those requiring it on a timely basis. There are a few information organizations that can do this. We will now examine a few of these resources.

Combat Data Information Center (CDIC)

CDIC was established at Wright-Patterson AFB, Ohio, in April, 1970. It grew out of the need to handle data collected in the Battle Damage Assessment and Reporting Program which began in 1968. It is now the central repository and data dissemination center for combat and combat-related data, as well as operational and test data. Such information can be used in aircraft, ground vehicle and ship survivability, vulnerability, maintenance, logistics and military operations studies. CDIC has collected more than 12,000 incidents of combat and operational loss and damage data from the Southeast Asia conflict. Data is available on ground vehicle damage from the 1973 Arab-Israeli war and from several other sources.

CDIC maintains five data bases. The Combat Data on Weapon Systems includes the tri-service fixed-wing and rotary-wing data bases, the Army ground vehicle data base, the Yom Kippur data base, and the Rapid Area Maintenance Team data base. The Aircraft Component Test Data Bases are generated from five specialized data bases, which are used in the early stages of survivability engineering development. These are for Fuel System, Wing Damage, Engineer Testing, Blast Fragmentation, and Continuous Rod Testing. The Reference Library Data Base contains reports that are pertinent to the combat laser and component test data bases. The Southeast Asia Transmittal Sheet Data Base inventories Army Southeast Asia records. The remaining data base, LASERDAB, is rapidly expanding. Sponsored by the JTCG/AS, CDIC will provide a central repository for laser test data relating to the terminal effects of laser radiation as a potential weapon, the response characteristics of aerospace materials and components to laser radiation, and the investigation of countermeasures to the laser threat.

In support of their basic service, CDIC maintains an extensive reference library of publications useful in survivability design studies of military vehicles. Staffed with professionals who are competent in the field, this Center is an extremely valuable resource for the survivability community.

DASIAC

Originally the Defense Atomic Support Information Analysis Center, DASIAC is now the Defense Nuclear Agency's repository for nuclear-related information. Some of the subjects covered are as follows.

- Nuclear weapon explosion phenomena.
- Nuclear weapons damage effects on military strategic and tactical systems/components.
- Military systems hardening design procedures.
- Survivability/vulnerability analysis.
- Nuclear weapon safety and physical security.
- Military tactics and doctrine.
- Nuclear weapons effects testing.

Through its holdings and the expertise of its professional staff, DASIAC has extensive capability to provide information and consultative services relative to survivability under nuclear threats.

Shock and Vibration Information Center (SVIC)

This Center was established at the Naval Research Laboratory as the Centralizing Activity for Shock and Vibration. Under the leadership of Dr. Élias Klein, the Activity was to be the mechamism for "a coordinated attack on Navy shock and vibration problems." The first principal service effort began with a symposium held in January 1947. This series of meetings continues as the Shock and Vibration Symposia, the present meeting is the 53rd Symposium. By 1949 the Army and Air Force had also become sponsors and the Activity began to serve all of the DOD. In 1962, the National Aeronautics and Space Administration formally became the fourth sponsor. Over the years the mission and services expanded and, in 1964, SVIC assumed its present name and became an official DOD Information Analysis Center.

To give boundaries to the technology covered by SVIC, consider the various phases in the research, development, test and evaluation of any system. The nature of the full life mission of the system, including combat requirements, must be established so that the criteria for its design and development can be defined. To do this the environments must be assessed, the performance specifications written, methods of analysis and design selected and applied, computer programs selected or written, materials of construction evaluated, components isolated or protected, the system tested, its response measured and the measured data analyzed. It is in all these

areas that SVIC collects, reviews, analyzes and disseminates the information generated by the evolving technology.

Over the years a major part of the dynamics effects information handled by SVIC has been applicable to the survivability problem. In fact, the Center was originally created as a mechanism for interchange of information on methodology to enhance the survivability of ships subjected to underwater explosion phenomena. More recently, because no other resource was available, SVIC has served NAVSEA in particular with information on threat effects extending far beyond the dynamic effects currently covered by its scope. At the request of the Survivability Code at NAVSEA, SVIC is preparing a proposal to formalize this effort by establishing a parallel information activity for survivability/vulnerability. As will be shown later, it is important that this effort move forward. But, considering only its current mission, SVIC is a major information resource for the survivability community.

Computerized S/V Models

The JTCG/AS recently established a Survivability/Vulnerability Model Repository at Battelle Memorial Institute. Computerized models are an essential part of vulnerability assessment. The first models in this repository relate to aircraft survivability during attack by surface-to-air missiles. Whether this repository will ultimately include models relating to ground systems and ships is not yet clear. It is clear that a central source for this kind of information would be extremely useful.

The SURVIAC Proposal

Recognizing that survivability/vulnerability is a crucial element in the development and fielding of military systems, the JTCG/AS has proposed the creation of a Survivability/Vulnerability Information and Analysis Center (SURVIAC). The mission statement that follows is quoted from the JTCG/AS proposal.

"SURVIAC's mission is to perform the functions of a full service Department of Defense (DOD) Information and Analysis Center (IAC) as described in DOD Instruction 5100.45, "Centers for Analysis of Scientific and Technical Information." It will provide scientific and technical information and support activities to organizations within DOD and to their contractors. SURVIAC's principal field of interest will be the vital technical area of nonnuclear survivability/vulnerability as it relates to US/Foreign aircraft and missile systems.

"SURVIAC's data bases will consist of those identifiable existing data bases of the nonnuclear survivability/vulnerability community and those under development. It will be able to refer to constantly updated computerized bibliographical information on various relevant documents. It will update, review, and expand to incorporate current relevant research results. It will analyze, appraise, and summarize information and disseminate such through bulletins, directories, bibliographies, and reports.

"SURVIAC will also serve as a repository and ultimately perform configuration management control for survivability methodologies.

"SURVIAC will provide a single focal point within DOD for nonnuclear survivability/vulnerability information."

The results of a survey conducted by the JTCG/AS overwhelmingly support the need for a survivability information analysis center. Ninety-two percent of the responders indicated there was a need and 89% indicated they would use it. On this basis, a new information activity is certainly required. Whether its operations be based upon the SURVIAC proposal or the SVIC proposal, or both, is not important. It is only important that the survivability/vulnerability information requirements be met in the most effective way.

Other Information Analysis Centers

Considering the information presented in Table 1, there are a number of information analysis centers not yet mentioned that are potentially useful sources for survivability programs. In the materials area there are centers on metals and ceramics, metal matrix composites, and plastics, to name only a few. The usefulness of centers on infrared technology and aerospace structures are obvious by their names, as are those on tactical weapons guidance and control, and tactical technology. There are a number of other IACs that can provide information and support in specialized areas.

Other Resources

The excellent newsletters, personnel directories, handbooks and other publications of the JTCG's and others are valuable sources of information. The American Defense Preparedness Association has sponsored six symposia in as many years on survivability and vulnerability of weapons systems. There have been a number of other symposia related to various aspects of survivability. Other professional societies provide grist for the technology mill. Short courses on survivability are available on a regular basis, notably by the Naval Postgraduate School and MIT. Information about these and similar activities must be made a part of the survivability information network.

The Missing Links

From the foregoing discussion it is evident that there are a number of information resources available to support the complex survivability program efforts. Unfortunately, these resources are rarely used to their fullest capacity and often not for survivability. There are many possible reasons for this, but for the most part, one or more of the following will apply.

- The user is not aware that the resource exists.
- The user does not know how to access the resource.
- The information activity is not aware of all its potential users.

In other words, the basic problem is communication. There is a breakdown in the line between the source and the user. To solve this problem, it is suggested that a communication link be established in the form of a gatekeeper organization to coordinate the flow of information between users and sources. Such an organization would, in effect, be the core of a survivability/vulnerability information network with the principal mission to provide rapid response to user needs. With the capability to assess and understand the user's problem and with full knowledge of all available resources, this activity could quickly bring the user face-to-face with the proper source. Or it could act as an information broker

with direct online access to the major sources. Since the users are also the generators of new technology, the information flow would be in two directions, assuring that the latest information is placed in the proper repository in a timely manner.

It is also evident that another missing link is the survivability/vulnerability information analysis center as proposed by the JTCG/AS and SVIC. There is presently no information activity available that can control and rapidly disseminate information related to all threat effects on all defense systems. Furthermore, there is no center that can deal effectively with the special information related to survivability as a design discipline. Although it is clear that such a resource is sorely needed, it is instructive to pose a few questions about the form it will take.

- Should there be only one analysis center to handle information relative to all systems?
- Should there be more than one analysis center, each oriented to specific systems?
- Should the coordination function mentioned earlier be a part of the analysis center function?
- What should be the organizational structure of the Center(s)?

Although more discussion on these points will be given later, it may be said as a point of departure that proposals tend to reflect the interest of the source. The SURVIAC proposal, for example, offers a broad scope, but implies emphasis on aircraft survivability. Similarly, the SVIC proposal, as first contemplated, would lean toward the interests of the Fleet. Any proposal from organizations concerned with mobile or fixed ground systems would likely be similarly weighted. Yet, the SVIC experience has clearly shown that technology developed for Army and Air Force systems is applicable to the design of survivable ships and there is little doubt that the reverse is true. No matter how the job is done, it is therefore important that we capitalize on this potential cross-fertilization.

TECHNOLOGY SOURCES AND USERS

An essential element in planning an information activity is to identify the fundamental sources of technology that will feed the information system. For survivability-related information it is useful to examine DOD organizations which support RDT&E efforts in threat-related technologies. For this purpose, a search was conducted on the Work Unit Summary Reports (DD-1498's) at the Defense Technical Information Center. Key words for the search were selected based upon potential relevancy to survivability and all files for the Army, Navy and Air Force were examined. The results were overwhelming, indicating many varied sources for the survivability technology base. Furthermore, since the sources of new technology are often also the users, it was possible to couple the DD-1498 examination with major program interests and identify the principal users. Of course, it must be kept in mind that these results are preliminary and that the user community extends beyond the in-house activities to include the contractors that support them.

Army

The results of the Army search are given in Table 2. It should be noted that only seventeen principal Army organizations are listed and that the interests of all subordinate organizations are reflected in the Table. For examples, the Chief of Engineers has three field activities which are very active in this area. They are the Corps of Engineers, Huntsville Division, the Construction Engineering Research Laboratory and the Waterways Experiment Station. Three of the Army commodity commands have several laboratories and/or field activities. ARRADCOM and AVRADCOM each have five such organizations and ERADCOM has six. DARCOM, which has oversight over all commodity commands, is the Army's representative on the Joint Logistics Commanders, the sponsor of the Joint Technical Coordinating Groups.

Navy

The nineteen principal Navy organizations are listed in Table 3, along with their indicated potential as sources or users of threat-related technology. All Naval Systems Commands report to the Naval Material Command (NAVMAT) which corresponds to the Army's DARCOM. As with the Army, several of the Navy organizations listed reflect the results of subordinate activities. Two project managers with particular concern with survivability are listed. As a matter of fact, all program offices are or should be users of survivability information.

Air Force

Table 4 gives the Air Force results. The list of eighteen principal Air Force organizations includes the Air Force Logistics Command and the Air Force Systems Command, both of which are represented on the Joint Logistics Commanders. The principal R&D laboratories are under the administration of the Air Force Systems Command.

Other DOD

Although no specific search was conducted, it is evident that the Defense Nuclear Agency (DNA) and the Defense Advance Research Projects Agency (DARPA) are both sources and users of survivability technology. DNA's interests are, in fact, a mirror image of the interests of the three Military Departments, at least as far as nuclear effects technology is concerned. The intelligence agencies are key sources for threat information in support of all systems.

Summary

In considering the results of this preliminary study, it should be noted that an organization has been cited as a source of threat-related technology only when a relevant project was revealed in the DD-1498 search. Undoubtedly, a more complete search would reveal additional sources. Such a search should be conducted as a part of the planning process for a survivability center. Other useful information can be gleaned from a DD-1498 search as well, such as a list of principal investigators to be included in a technology-oriented who's who.

The process of designating organizations as users made use of information taken in part from the DD-1498 search and in part from a first-hand knowledge of the nature of the major program of the organizations listed. Since judgment is involved the results may be questioned. A more detailed study is in order to verify or add to these results. In any event, it is felt that this preliminary study indicates the breadth, if not the depth, of sources and users of threat-related technology.

TABLE 2
Sources and Users of Survivabilitv-Related Infomation

U. S. Army	Thread-Related Technologies																						
	Vibration	Structural Analysis	Materials Sciences	Human Factors	Impact Shock	Ground Shock	Underwater Expl., Shock	Air Blast Conventional	Air Blast (Nuclear)	Armor (Fragments)	Thermal Radiation	Nuclear Radiation	CBW	EMP, EMC, EMI	Signatures: Acoustic	Signatures: EM	Signatures: Magnetic	Signatures: Radar (RCS)	Signatures: IR	Damage Control & Fires	Directed Energy
Ballistic Missile Defense Sys. Cmd. (BMDSCOM)	X	X	X		X	X		X	X	X	X	X	X	X		X		X	X	X	
Chief of Engineering		■	■			■		X	X		X	X		X						X	
Development and Readiness Command (DARCOM)	X	X	■	■	X	X		X	X	X	X	X	X	X	X	X		X	X	X	X
Army Mat. & Mech. Research Center (AMMRC)	■	■	■		X					X	X	X		X				X	■		X
Human Engineering Laboratory (HEL)	X			■	X			X	X	X	X	X	X						X		
Natick Research & Development Command (NARADCOM)	X		■	■	■								■					X	X	X	
Armament Readiness Command (ARRCOM)		X	X		■		■	X											X		
Armament Research & Development Com. (ARRADCOM)	X	■	■	■	■					■	X	X	O		■					■	X
Aviation Research & Development Com. (AVRADCOM)	■	■	■	■	X			X	X	X	X	X	X	■	■	■		X	X	■	■
Communications Electronics Command (CECOM)	X		■		X					X		■		■		X	■				
Missile Command (MICOM)	■	■	■	X	■			X	X	X	X	X		X	X	X		■	■		■
Tank-Automotive Command (TACOM)	X	■	■	■	X	X	O	X	■	X		X	X		X	X	X	X	X	X	
Test & Evaluation Com. (TECOM)	X		X	X	■			■	X	■	X	X	X	X							
Electronics Research & Devel. Com. (ERADCOM)	X		X		■					X	X	■		■		■		■	■		X
Mobility Equipment R&D Command (MERADCOM)	X	X	X		X								X		■	■	■	■	■	X	X
Army Research Office (ARO)		X	X	X	X	X		X	X	X	X	X	X	X		O					X
Army Materiel Systems Analysis Activity (AMSAA)		■			■	■		■	X	■	X	X	X	X					X	X	

O indicates SOURCE
X indicates USER

TABLE 3
Sources and Users of Survivability-Related Information

U.S. Navy	Threat-Related Technologies																						
	Vibration	Structural Analysis	Materials Sciences	Human Factors	Impact Shock	Ground Shock	Underwater Expl. Shock	Air Blast Conventional	Air Blast (Nuclear)	Armor (Fragments)	Thermal Radiation	Nuclear Radiation	CBW	EMP, EMC, EMI	Signatures: Acoustic	Signatures: EM	Signatures: Magnetic	Signatures: Radar (RCS)	Signatures: IR	Damage Control & Fires	Directed Energy
Office of Naval Research (ONR)		X	X	X			X	X	X	X	X	X		X	X	X	X	X	X		X
Naval Research Laboratory (NRL)	[illegible]	[illegible]	[illegible]	O			[illegible]	X	X	[illegible]	X	[illegible]	O	[illegible]	[illegible]	[illegible]	[illegible]	[illegible]	[illegible]	[illegible]	[illegible]
Naval Oceanographic R&D Activity (NORDA)			O												[illegible]		X				
Chief of Naval Operations (CNO)	X	X	X	X	X		X	X	X	X	X	X	X	X	X	X	X	X	X	X	X
Naval Biodynamics Laboratory (NBL)			[illegible]	X			X	X	X		X	X	X		X						
Naval Material Command (NAVMAT)	X	X	X	X	X		X	X	X	X	X	X	X	X	X	X	X	X	X	X	X
Naval Air Systems Command (NAVAIR)	X	X	X	X			X	X	X	X	X	X		X	X	X		X	X	X	X
Naval Electronics Systems Command (NAVELEX)	X	X	X	X	X		X	X	X	X		X		X	X	X	X	X	X		X
Naval Sea Systems Command (NAVSEA)	X	X	X	X	X		[illegible]	[illegible]	[illegible]	[illegible]	[illegible]	[illegible]	[illegible]	[illegible]	X	X	X	X	X	X	[illegible]
Theater Nuclear Warfare Project Office (PM-23)		X	X				X		X		X	X		X	X					X	X
Strategic Systems Project Office (SSPO) (PM-1)	X	X	X	X	X		X	X	X	X	X	X	X	X	X	X	X	X	X	X	X
Naval Air Development Center (NADC)	[illegible]	X	X	[illegible]	X			X	X	X		X		X	X	X		[illegible]	[illegible]	X	
Naval Ocean Systems Center (NOSC)	[illegible]	X	[illegible]	X			[illegible]	O	O	O	O	[illegible]		[illegible]	[illegible]	[illegible]	[illegible]	O	X	O	[illegible]
Naval Weapons Center (NWC)	[illegible]	[illegible]	[illegible]		[illegible]		X	[illegible]	[illegible]	[illegible]	[illegible]	[illegible]		[illegible]	O	[illegible]		[illegible]	[illegible]	O	[illegible]
David Taylor Naval Ship R&D Center (DTNSRDC)	[illegible]	[illegible]	[illegible]	[illegible]	[illegible]		[illegible]	[illegible]	[illegible]	[illegible]	[illegible]	[illegible]	[illegible]		[illegible]	X	X	X	X	[illegible]	
Naval Surface Weapons Center (NSWC)	[illegible]	[illegible]	[illegible]	X	[illegible]	X	[illegible]	[illegible]	O	[illegible]	[illegible]	[illegible]	[illegible]	[illegible]	[illegible]	[illegible]	[illegible]	[illegible]	[illegible]	O	X
Naval Underwater Systems Center (NUSC)	X	[illegible]	[illegible]	X	O		[illegible]		O			X		[illegible]	[illegible]	[illegible]	X				
Naval Coastal Systems Center (NCSL)	X	X	X			X	X	X	X		X	X			[illegible]	X	[illegible]				
Naval Facilities Engr. Command (NAVFAC)	[illegible]	[illegible]	[illegible]	X	X	[illegible]		X	X	X			X	X						X	

O indicates SOURCE
X indicates USER

TABLE 4
Sources and Users of Survivability-Related Information

U.S. Air Force	Threat-Related Technologies																				Damage Control & Fires	Directed Energy
	Vibration	Structural Analysis	Materials Sciences	Human Factors	Impact Shock	Ground Shock	Underwater Expl. Shock	Air Blast Conventional	Air Blast (Nuclear)	Armor (Fragments)	Thermal Radiation	Nuclear Radiation	CBW	EMP, EMC, EMI	Signatures							
															Acoustic	EM	Magnetic	Radar (RCS)	IR		
Air Force Test and Evaluation Command (AFTE)	X	X		X		X		X	X		X	X		X		X		X	X	X	
Air Force Systems Command (AFSC)	X	X	X	X	X	X		X	X	X	X	X	X	X	X	X		X	X		X
Armament Division (AD)	■	■	■		■	X		■	X	■		X			■	■		■	■		
Aeronautical Systems Division (ASD)	■	■	X	X	O			X	X	X	X	X	■	X	X	X		X	X	X	X
Electronic Systems Division (ESD)	■	■	■					X	X	X	X	X		■	■	■	■	■	■	■	
Space Division (SD)	X	■	■							X	X	■		X				■	■		■
Air Force Office of Scientific Res. (AFOSR)	■	■	■	■	X	■	■	■	■	X	■	■	■	■	■	■		X	■		■
Aero Propulsion Laboratory (APL)	■	■	■					X	X	X	■	■		■	■			■	■	■	■
Avionics Laboratory (AL)	X	■	■							X		X		X		■		■	■		
Flight Dynamics Laboratory (FDL)	■	■	■	■	■			■	X	■		X		■	■	■	■	■	■	■	■
Materials Laboratory (ML)	■	■	■		■					X	X	X		X		■			■		■
Geophysics Laboratory (AFGL)	■					■								O	■	■	■		■		■
Weapons Laboratory (AFWL)	■	■	■			■		X	X	X	■	■		■		X					■
Ballistic Missiles Office (BMO)	X	■	X			X		X	X	X	X	X		X		X		X	X		X
Engineering Services Center (AFESC)		■	■	■	■	■		■	■		■	■		■						■	
Arnold Engineering Development Center (AEDC)	■	■	X					X	X						■				■		
Rocket Propulsion Laboratory (RPL)	■	■	■					X	X						■				■		
Air Force Logistics Command (AFLC)		X	X	X		X		X	X	X	X	X	X	X						X	

O indicates SOURCE
X indicates USER

INFORMATION ANALYSIS CENTER FOR SURVIVABILITY

From the earlier discussion and from some additional consideration of the need, an effective information analysis center for survivability/vulnerability will now be conceptualized. The need dictates that such center be *the focal point* for all information bearing on the complex multidisciplinary areas of system survivability and vulnerability. The center must serve as the instrument for satisfying every conceivable information requirement that would support the enhancement of survivability for all systems whether they be for land, sea, air or space. Furthermore, the center must collect, analyze, store, retrieve and disseminate information bearing on all threats, including primary and secondary effects. By using its own devices or working with a coordination center, the survivability center must establish rapid and effective lines of communication with all technology sources and information resources that can either directly or indirectly provide support for its mission. The new center must serve the information needs of users at all levels, from the Program Manager to the bench engineer.

Services of the Center

For convenience, the description of services to be provided by the survivability center is placed in three categories as shown in Table 5. Each of these categories will be discussed in turn.

Publications

Although there may be other special publications not included in the list of examples in Table 5, it is felt that those mentioned are representative of the need. A short description of each potential type of publication follows.

- Current awareness publications, issued monthly or quarterly would contain abstracts from the current literature, literature reviews, previews and reviews of technical conferences, book reviews, short course announcements and other items of current interest. The review articles would include appropriate highlights on technical "gaps," those critical areas in special need of research attention.
- As implied by the name, state-of-the-art monographs are critical assessments of our present capabilities in specific technological areas. Each monograph is to be written by an expert in the area treated.
- Special bibliographies with commentary covering well-defined technical areas may be prepared on request or other evidence of need. Such bibliographies may also be a part of the state-of-the-art monographs.
- Users may register their field of interest with the survivability center and automatically receive notification of new publications or activities in that field. Of course, they may register in several fields if they wish.
- Design handbooks, data books and "how to" documents should be prepared and issued as required.
- Guidance documents dealing, for example, with the interpretation of directives or specifications could be made available when needed. Special indexes also fall in this category.
- Directories of key personnel, test facilities, computer programs and the like should be prepared on a regular basis.
- The Center should be heavily involved in the preparation and coordination of standards relating to survivability/functions of a Secretariat.
- The annual report should include a compendium of all R&D activities during the year, with a prognosis for the year to come.
- Proceedings of conferences and symposia sponsored by the Center should be published.

TABLE 5
Services of DoD Survivability Vulnerability Center

Publications	Direct Response to Users	Training
Current Awareness*	Search	Symposia
State-of-the-Art Monographs	Analysis	Seminars
Annotated Bibliographies	Consultation	Workshops
Field of Interest	Guidance	Short Courses
Surveys	Interpretation	
Handbooks	Referral	
Guidance Documents	Special Teams**	
Directories	Access Data Bases	
Standards (Coordination)		
Annual R&D Compendiums*		
Proceedings		
Newsletters		

*Identifies technical "gaps"
**Capability to organize an ad hoc team of experts for quick response to an urgent problem

- One or more newsletters may be required to highlight current events. In some cases, this may be a part of the current awareness publication.

Direct Response to Users

An information analysis center is unique primarily because the majority of the center's staff consists of professionals in the technical community that it serves. The center also has indepth access to other experts in its field on an "as required" basis. The IAC staff therefore has the ability to understand a user's problem and to provide him with a rapid and relevant answer. In other words, the IAC staff can "communicate" with the user on the user's technical level. Using this ability, the staff responds to routine user queries by performing one or more of the first six functions listed in the second column of Table 5. The key to a rapid and effective response is the interaction between the IAC and the user.

Another advantage of an IAC is flexibility, the capability to modify its method of operation to respond to user needs, because of the complex multidisciplinary nature of the survivability effort, it is suggested that an IAC in this area must provide at least two additional services.

- Special Teams—A current Who's Who of experts in all disciplines related to survivability/vulnerability should be maintained by the center. A selected number of these experts should be "on tap" for assignment to special teams as required to consider difficult and urgent problems. The team members may be from one or from several technical areas, depending upon the nature of the problem. Their job would be to quickly provide a solution or recommended course of action on the problem at hand.

- Access Data Bases—Since there are a number of potentially useful information and data bases in a number of different organizations, it would be the job of the survivability IAC to assist the user in accessing bases which might contain information bearing on his survivability-related problem.

Training

As can be inferred from Table 5, "Training" includes both information interchange and educational activities. In the case of the survivability IAC, it is anticipated that such activities would be extensive, involving a number of conferences and courses in the different technical areas of concern to the survivability community.

Organizational Structure

The organizational concept proposed in Figure 1 is suggested on the assumption that the center will be *the focal point* for survivability for all of DOD. It is further assumed that the Center will also perform the required function of coordination with other information resources. No assumption is made as to whether the IAC would be operated in-house, under contract, or both. If the concept works at all, it would work under any of these methods of operation.

The concept is based on the fact that the Center must handle survivability design and vulnerability assessment information related to all systems. The nature of this information is reflected in the listing of subject areas under the three boxes on "Targets." A more specific listing might be as follows.

- Mission area definition
- Operational capability
- Combat readiness criteria
- Threat assessment
- Threat projection
- Threat exploitation
- Threat lethality assessment
- Damage phenomena
- Damage effects
- Damage and failure modes
- System response
- Vital components definition
- Vital functions definition
- Functional/inactivation diagrams
- Operational impairment criteria
- Survivability enhancement options
- Signatures (detectability)
- Active defense
- Design for survivability
- Susceptibility assessment
- Vulnerability assessment
- Survivability enhancement trade-offs
- Susceptibility data
- Vulnerability data

The fact that each of the above subject areas can be broken down into more specific areas leads one rapidly to the conclusion that a single center for all systems may not be the best option. However, the concept is also valid for system-oriented centers. The boxes on "Targets" would only more specifically reflect the nature of the systems for air, land or sea.

The box on "Technology Analysis and Utilization" is to indicate that a large technology base is available to support survivability design and that the Center should be able to access and suggest application of that technology. The "Program Management Liasion Office" is to have the Center stand ready to provide advice and assistance at the highest levels and to receive and pass along policy changes to the users. The dotted lines to other organizations are there to indicate that the Center would perform the coordination function. The rest of the boxes in Figure 1 are self-explanatory.

THE COORDINATION FUNCTION

It was shown earlier that survivability-related information resides in a number of organizations and suggested that a coordination activity (CA) is essential to tie the survivability information network together. This activity could be a separate organization and probably should be if the decision is made to create only one survivability IAC. If, on the other hand, two or more systems-oriented survivability IACs are established, the coordinating activity (CA) could well be tied to one of them. In either case, the functions of the coordination activity would be separate and specifically defined. From Table 5, for example, the CA would pick up the box on "Technology Analysis and Utilization," leaving the survivability center(s) with only system-related responsibility. The CA would establish communication links with all network information activities, including the survivability center(s). The CA would be an information broker for the users and a technology broker for the survivability center(s). Most important, the CA must serve to expedite, not impede, the flow of information.

SUMMARY

Firm DOD policy dictates that survivability is a major consideration in system acquisition. Survivability programs have been established by the Army, Navy and Air Force, both jointly and separately. These programs involve the consideration of a number of threats and theri effects and, consequently, a complex multidisciplinary effort. It is considered essential that a viable survivability/vulnerability information service be established to support these programs.

Several primary and secondary sources for survivability-related information have been identified and proposals have been made for survivability centers to fill the gaps. It has been suggested that we have the option of creating a single *focal point* for survivability information centers. It was also suggested that a coordination activity be established as the core of the survivability information network. Some options for the organizational structure of a survivability center(s) have been examined and the functions of the coordination activity have been discussed. In general, the need for a survivability/vulnerability information service has been clearly established. The organizational aspects are yet to be defined.

RECOMMENDATIONS

Since it is important that we move forward as quickly as possible, it is recommended that the establishment of the DOD Survivability/Vulnerability Information Service proceed as follows.

1. The proposal for SURVIAC should be accepted on an interim basis to handle information related to aircraft survivability/targets.

2. SVIC should proceed to establish an interim Fleet Survivability Information Analysis Center and to develop a proposed structure for the Coordination Activity.

3. A workshop should be conducted at an early date to develop specific recommendations on all aspects of the survivability information problem. Workshop participants should be key survivability personnel from the Army, Navy and Air Force and representatives of information activities that are potential members of the survivability information network. The recommendations from this workshop should be submitted to DOD for appropriate action.

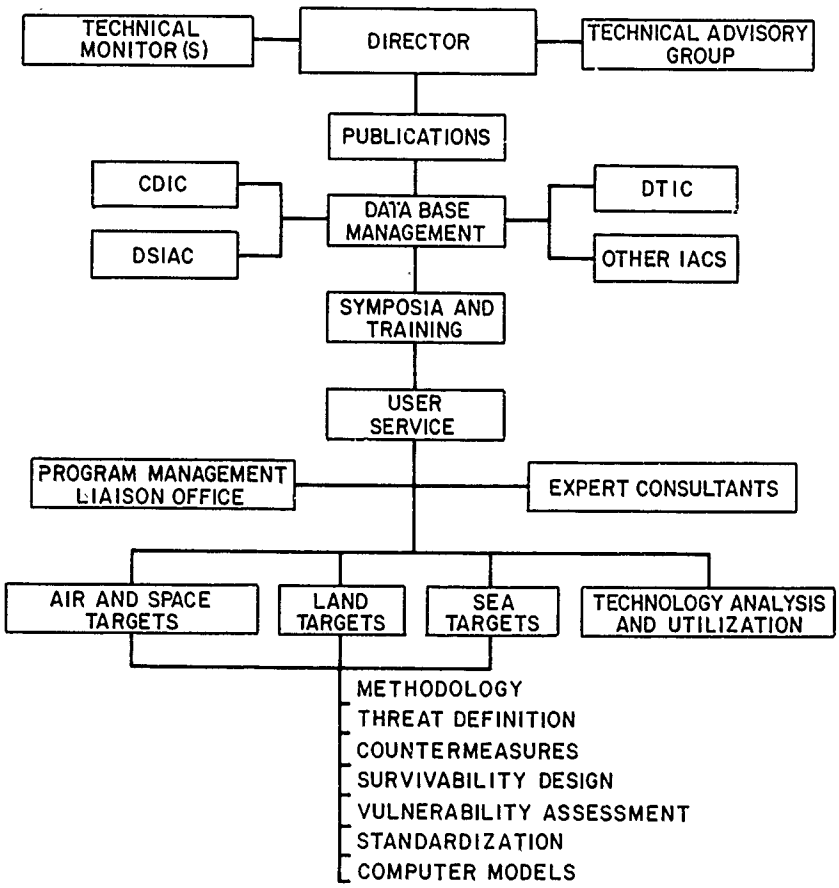

Fig. 1 — Organizational concept for DoD survivability/vulnerability center

AIRCRAFT SURVIVABILITY

Mr. Dale B. Atkinson
Chairman, Joint Technical Coordinating Group on
Aircraft Survivability (JTCG/AS)
Naval Air Systems Command
Washington, D.C.

This paper gives an overview of the Naval Air Combat Survivability Program and selected activities of the Tri-Service Joint Technical Coordinating Group on Aircraft Survivability (JTCG/AS).

Survivability is defined by the NAVMAT Combat Survivability Instruction (NAVMATINST 3900.16) as the capability of a weapon system to continue to carry out its mission in a hostile threat environment and is a function of both susceptibility and vulnerability. Susceptibility takes into account those factors that determine whether the aircraft is hit by a threat and vulnerability takes into account those factors that determine whether the aircraft is killed by the threat mechanisms if it is hit.

Figure 1 shows a simplified probability of survival equation that illustrates how the two areas are tied together. Susceptibility includes the probability of being detected and the probability of being hit if detected; it is a function of aircraft signature levels, countermeasures employed, tactics, such as nap of the earth (NOE) flying for helicopters, and other factors. Vulnerability is the probability of being killed if hit; it is a function of the design of the subsystems of the aircraft, how they are integrated into the total aircraft, and what vulnerability reduction features, such as fuel system fire and explosion suppression, are incorporated into the aircraft's design.

DOD survivability policies are stated in DODINST 5000.2 and DOD Directive 5000.3. DODINST 5000.2 includes a requirement for survivability goals and thresholds in the decision coordinating paper (DCP) and a description of the survivability program in the integrated program summary (IPS). DOD Directive 5000.3 requires that survivability be assured through test and evaluation early in the program. Navy survivability directives implement DOD policy. NAVMAT Instruction 3900.16 establishes combat survivability policies for all naval weapon systems, including ships and aircraft. NAVAIR Instruction 3920.1 established the Naval Air Combat Survivability Program.

The objective of the overall Naval Air Combat Survivability Program is to ensure that our naval weapon systems can survive in sufficient numbers to carry out their missions in a hostile threat environment. A second objective requires a 6.3 R & D program to provide the survivability technology, hardware, and design and analysis tools necessary to meet the first objective.

I will briefly discuss the functions and responsibilities of two organizations, the NAVAIR Combat Survivability Branch and the Tri-Service Joint Technical Coordinating Group on Aircraft Survivability.

NAVAIR Instruction 3920.1 establishes the Combat Survivability Branch (AIR-5164) as the survivability focal point within NAVAIR with responsibilities for establishing NAVAIR survivability policies and procedures, developing survivability technology and hardware, developing required standardization documents, and for providing systems

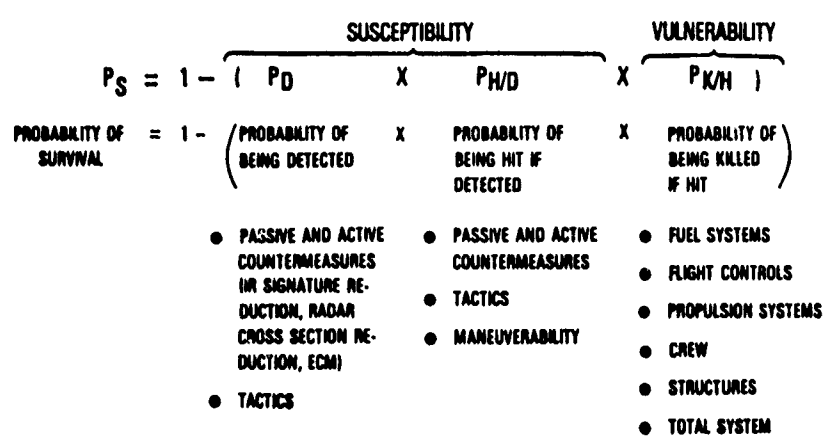

Fig. 1 — The Survivability Equation

survivability support to the aircraft project managers (PMA's).

The mission of the Joint Technical Coordinating Group on Aircraft Survivability (JTCG/AS) is to coordinate the Services survivability R & D programs and to carry out the Joint Survivability Program with funding provided by the three Services.

The JTCG/AS is chartered under the Joint Logistic Commanders (JLC) and organized as shown in Figure 2. The activities of the JTCG/AS are directed by a four member Executive Board composed of one principal member from each of the four Commands (NMC, AFSC, DARCOM, AFLC). The day-by-day management of JTCG/AS programs is carried out by the JTCG/AS Central Office Staff which is located at the Naval Air Systems Command. Each Command provides one representative to the JTCG/AS Central Office. Each of the Command representatives serves as director for one of the four functional subgroups. The two committees shown provide advisory services. The JTCG/AS involves over 150 project engineers and coordinators from 30 Army, Navy and Air Force Laboratories and Commands.

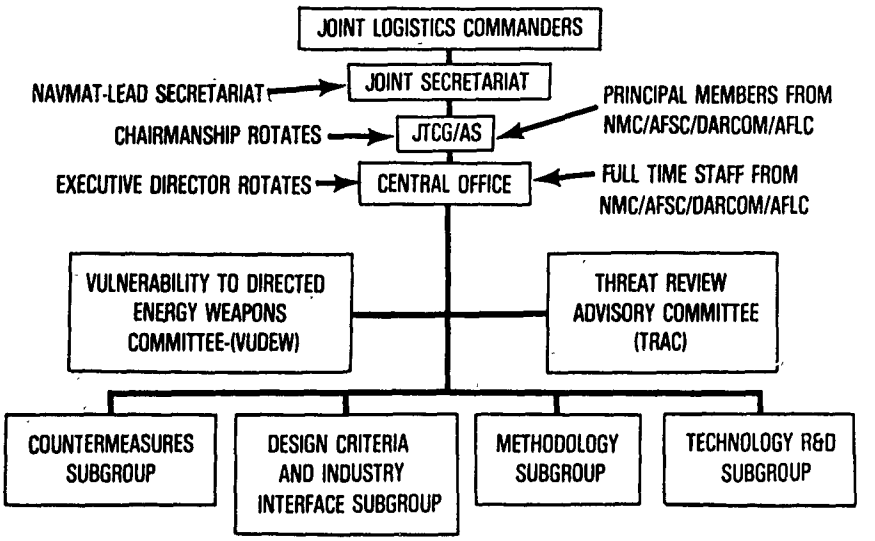

Fig. 2 — Organization of the JTCG/AS

Aircraft Survivability R & D is carried out under PE63262N which includes four major projects (see Figure 3). The purpose of Project W0591 is to develop survivability enhancement hardware and techniques for application to Navy and Marine Corps aircraft under the Weapons System Survivability Program. Project W0592 addresses a related problem area, that of aircraft and ordnance hazards in aircraft carrier deck fires. Project W1088 provides the Navy portion of the funding for the Joint Survivability Program. Project W1277 is currently our only nuclear survivability program and addresses only the electromagnetic pulse (EMP) aspects of nuclear weapon effects.

The type of R & D conducted is shown in Figure 4. Vulnerability testing is conducted at the Naval Weapons Center's (NWC) Aircraft Survivability Test Facility to determine subsystem and total aircraft damage and kill modes. Vulnerability reduction technology, hardware and design criteria are developed for all the major subsystems and for their integration into the total aircraft. Aircraft signature measurement is conducted, as well as the development of methods for reducing the major detectable signatures of the aircraft. Electronic countermeasures are not developed under this program element but are handled under other program elements managed by PMA-253, with which we work closely.

Most of the past and current efforts under PE63262N have addressed aircraft survivability against conventional threat systems. Major new areas we are now beginning to

PE 63262N - AIRCRAFT SURVIVABILITY/VULNERABILITY

- PROJECT W0591-SL - AIRCRAFT SURVIVABILITY
- PROJECT W0592-SL - AIRCRAFT AND ORDNANCE SAFETY
- PROJECT W1088-SL - JOINT TECHNICAL COORDINATING GROUP ON AIRCRAFT SURVIVABILITY (JTCG/AS) - NAVY
- PROJECT W1277-SW - NUCLEAR EMP SURVIVABILITY OF AIRCRAFT (FAANTAEL)

Fig. 3 — Aircraft Survivability R&D

address include laser, nuclear (non EMP effects), and chemical/biological/radiological (CBR) threat effects.

The next area I will discuss is that of specifying survivability requirements and the procedures we use in carrying out weapon systems survivability programs. The survivability military standards are shown in Figure 5. The Navy published MIL-STD-2072(AS), "Establishment and Conduct of Programs for Aircraft Survivability" in 1977. Using the Navy MIL standard as the starting point, the JTCG/AS developed

- VULNERABILITY TESTING AND DEVELOPMENT OF VULNERABILITY REDUCTION TECHNOLOGY/HARDWARE/DESIGN CRITERIA FOR:
  - AIRCRAFT/SUBSYSTEM DAMAGE/KILL MODES (FIRE/EXPLOSION/HYDRAULIC RAM/FUEL INGESTION)
  - PK/H INPUTS TO VULNERABILITY EVALUATION
  - FUEL SYSTEMS
  - PROPULSION SYSTEMS
  - FLIGHT CONTROLS
  - HYDRAULIC SYSTEMS
  - STRUCTURES
  - CREW STATIONS
  - OTHER SUBSYSTEMS
  - TOTAL AIRCRAFT INTEGRATION
- SIGNATURE TESTING AND DEVELOPMENT OF SUSCEPTIBILITY REDUCTION TECHNOLOGY/HARDWARE/DESIGN CRITERIA FOR:
  - CONFIGURATION/SUBSYSTEM CONTRIBUTION TO TOTAL SIGNATURE
  - PD/PH/D INPUTS TO SUSCEPTIBILITY EVALUATION
  - VISIBLE/EO SIGNATURE
  - IR SIGNATURE
  - RADAR CROSS SECTION (RCS)
  - ACOUSTIC SIGNATURE
  - NO COUNTERMEASURES HARDWARE DEVELOPMENT
- DEVELOPMENT OF SURVIVABILITY EVALUATION/DESIGN INTEGRATION METHODS FOR:
  - MISSION/THREAT ANALYSIS
  - SIGNATURE REDUCTION/COUNTERMEASURES INTEGRATION
  - VULNERABILITY EVALUATION
  - VULNERABILITY/SUSCEPTIBILITY REDUCTION INTEGRATION
  - SURVIVABILITY DESIGN/TRADE OFF STUDIES
  - SUSCEPTIBILITY EVALUATION
  - SYSTEM SURVIVABILITY EVALUATION

Fig. 4 — Naval Aircraft Survivability R&D Programs

MIL-STD-2072(AS) – ESTABLISHMENT AND CONDUCT OF PROGRAMS FOR AIRCRAFT SURVIVABILITY – 25 AUG 77

MIL-STD-2069 – REQUIREMENTS FOR AIRCRAFT NONNUCLEAR SURVIVABILITY PROGRAM –24 AUG 81

MIL-STD-2072A(AS) – REQUIREMENTS FOR AIRCRAFT NUCLEAR SURVIVABILITY PROGRAM

MIL-STD-2089 – AIRCRAFT NONNUCLEAR SURVIVABILITY TERMS – 21 JUL 81

MIL-STD-1629A – PROCEDURES FOR PERFORMING A FAILURE MODE, EFFECTS AND CRITICALITY ANALYSIS (SURVIVABILITY FMEA/DMEA) – 24 NOV 80

Fig. 5 — Standards for Survivability

DOD MIL-STD-2069, "Requirements for Aircraft Nonnuclear Survivability Program" which was approved in 1981. The Navy is currently developing MIL-STD-2072A(AS), "Requirements for Aircraft Nuclear Survivability Program" to cover this area for the Navy. This MIL standard will also be coordinated as a DOD MIL standard in the future, through the JTCG/AS Nuclear/Nonnuclear Survivability Interface Committee.

MIL-STD-2069 provides uniform requirements and criteria for establishing and conducting a survivability program. It provides the structure for a classified detailed survivability specification which is developed for each aircraft. The procedures for applying this MIL standard is as follows. MIL-STD-2069 is called out in the weapons system RFP and detail specification. A classified survivability addendum tailored to the specific aircraft's mission, threat and acquisition phase is written for each new aircraft and becomes part of the RFP and aircraft detail specification. For existing systems, we conduct an in-house survivability evaluation and trade-off study to identify the high payoff items for potential incorporation during modification programs.

The five major steps in the survivability evaluation process are shown in Figure 6. A baseline survivability evaluation is conducted for each weapon system which becomes the basis for the trade-off studies as shown in Figure 7. Following the baseline survivability evaluation, alternative survivability design concepts are reviewed to select those that are feasible for potential incorporation on the particular aircraft or helicopter under study. Those concepts selected are then used in iterations of the baseline survivability evaluation, taking into account any weight or cost penalties, to determine and rank the high payoff items. These are then recommended to the PMA for incorporation. We have a wide array of both susceptibility and vulnerability

reduction techniques currently available, and are continuing to develop lighterweight, more effective techniques and hardware as given in Figure 8.

Figure 9 summarizes the overall process for the Naval Air Combat Survivability Program. The Combat Survivability Branch (AIR-5164), in conjunction with the other organizations shown, develops the necessary survivability technology, hardware, design and evaluation methods, and standardization documents required to do the job. The Combat Survivability Branch then provides engineering support and technically manages the systems survivability programs for the PMA's to develop combat survivable and effective weapons systems.

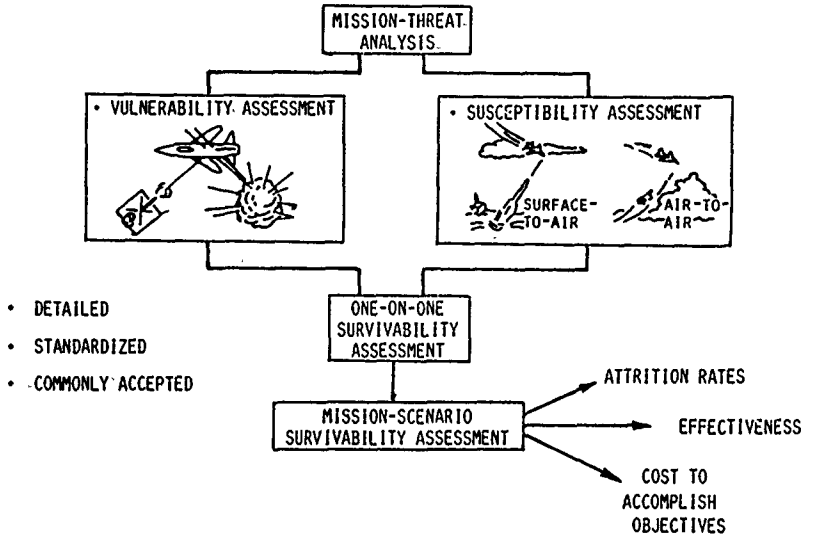

Fig. 6 — Survivability Assessment Process

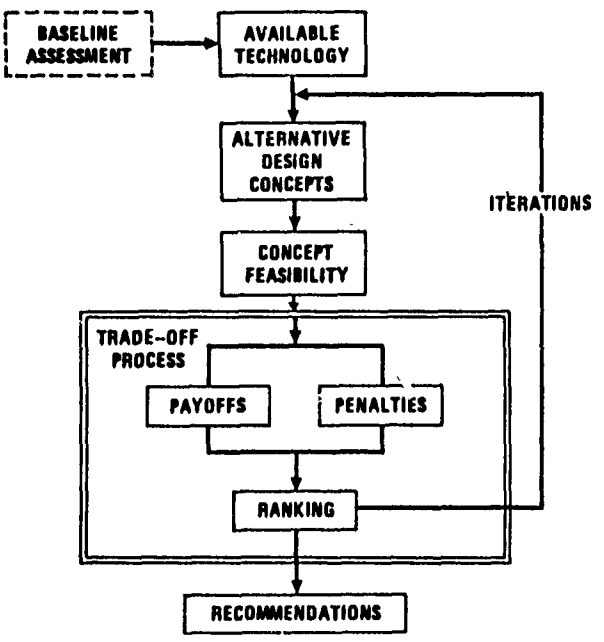

Fig. 7 — Trade-off Study Approach

SUSCEPTIBILITY REDUCTION			VULNERABILITY REDUCTION
THREAT SUPPRESSION	DETECTION AVOIDANCE	DAMAGE MECHANISM AVOIDANCE	
• Anti-radiation missiles • Armament • Flash blinding	• Minimum exposure weapon delivery (stand-off weapons, adverse weather capability)	• Radar acquisition and SAM/AAA warning receiver • IR missile launch warning sensors • Aircraft performance	• Component redundancy • Component location • Component shielding • Active damage suppression (fire detection/extinguishing)
	COMMON • Electronic noise jammers and deceivers • Signature reduction (radar, IR, visual, aural, UV) • Expendables (chaff, decoys, flares) • Tactics • Optical/electro-optical countermeasures • Crew skill and experience		• Passive damage suppression (damage tolerance, delayed failure, leakage suppression, fire and explosion suppression, fail-safe response) • Elimination of vulnerable components

Fig. 8 — Examples of Available Techniques for Susceptibility and Vulnerability Reduction

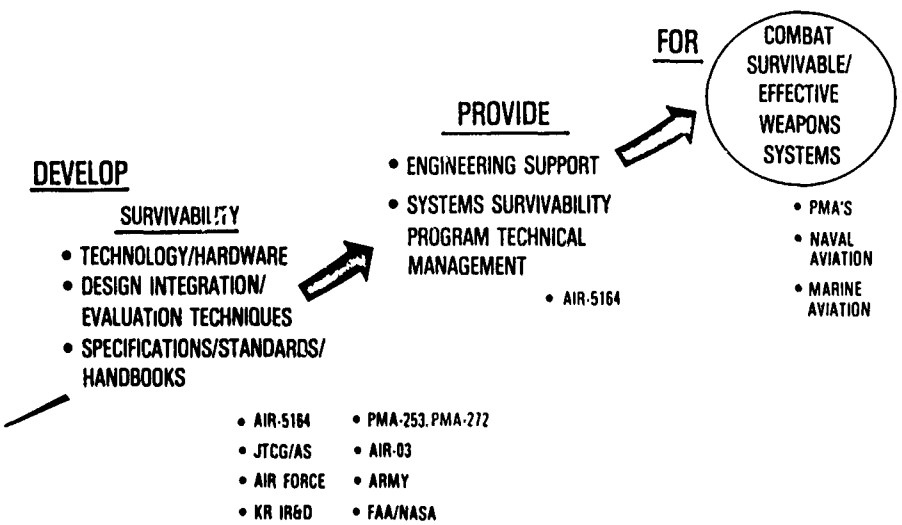

Fig. 9 — Weapon Systems Combat Survivability Process

We have established systems survivability programs for all the major Navy and Marine Corps aircraft and helicopters as listed in Figure 10. With that overview of the Naval Air Combat Survivability Program, I will now briefly discuss some of the JTCG/AS activities in information dissemination. Key methods of information dissemination are through publications, training, workshops and information repositories. Since 1981, five standardization documents have been completed, or are nearing completion. One example is MIL-STD-2069, previously discussed, for use by program managers to incorporate survivability requirements into their acquisition programs. Another is the four volume military handbook on "Aircraft Nonnuclear Survivability Design". Forth seven technical reports were published over the last two years and distributed to both government and industry. A quarterly newsletter is published and distributed to over 3,000 government and industry personnel. A directory of survivability experts in DOD and Industry, as well as a bibliography of survivability technical reports, are published periodically. The final draft of a text book for use in Service schools and universities is nearing completion. MIL-HDBK-336, "Aircraft Nonnuclear Survivability Design" is to be published in four volumes. Volume 1 has been published and the other three volumes will be published in the near future.

Both graduate level and short courses in survivability are offered or planned by the Naval Post Graduate School and the Air Force Institute of Technology. The Naval Post

FIXED WING		HELICOPTERS	MISSILES
F/A-18	C-2A	CH-53E/MCM	IIR MAVERICK
AV-8B	S-3A	SH-60B (LAMPS MK III)	
EA-6B	F-14A	AH-1T	
P-3C	A-6E	CH-46E	
E-2C	A-6F	SH-3	
RF/A-18	ECX	JVX	
	VFMX		

PROPOSED

	A-4M	F-8
OV-10	A-7E	F-4
	AV-8C	

Fig. 10 — Current Aircraft Systems with Established Survivability Program

Graduate School's four day short course has been offered six times to date, to personnel from both government and industry.

Two survivability and computer-aided design workshops have been conducted. As a result, both industry and DOD designers have placed greater emphasis on integrating survivability modules with their computer-aided design programs. These workshops advance the development of interservice cooperation and help insure the full integration of survivability considerations in the conceptual and preliminary design phases for aircraft.

There are two existing data and information repositories. The Combat Data Information Center located at Wright-Patterson AFB, is a joint operation with the JTCG for Munitions Effectiveness (JTCG/ME) and contains a number of essential data bases, primarily combat damage, loss, and repair data. A survivability model repository is funded by the JTCG/AS and managed by the Air Force Wright Aeronautical Laboratories.

We have developed a joint proposal in conjunction with the JTCG/ME, to establish a survivability/vulnerability information and analysis center to be called SURVIAC. The Combat Data Information Center and the Model Repository will be combined to form the core of the SURVIAC, which will then be expanded to provide the broader services of an information and analysis center (IAC). A central focal point, through data collection and analysis, and quick response user services, will ensure the availability of up-to-date methods, models, and test data to both government and industry users. SURVIAC is being proposed as a DLA funded and administered IAC, with the JTCG/AS and JTCG/ME providing technical management.

The JTCG/AS briefed the Joint Logistic Commanders (JLC) on the SURVIAC proposal on 22 Sept 1982. The JLC endorsed the proposal and directed the JTCG/AS to accelerate the SURVIAC schedule. The JLC also directed the JTCG/AS to prepare a letter to Dr. DeLauer, Under Secretary of Defense for Research and Engineering (USDR&E), recommending that USDR&E approve the establishment of the SURVIAC. The JLC signed the letter forwarding the proposal to Dr. DeLauer on 25 Oct 1982. The SURVIAC proposal is now being staffed throughout OSD.

UNITED STATES FLEET SURVIVABILITY OF U.S. NAVAL COMBATANT SHIPS

Captain F. S. Hering, USN
Naval Sea Systems Command
Washington, D.C.

Good morning, ladies and gentlemen. I am Director of the Ship Survivability and Readiness Division Sub-Group of the Naval Sea Systems Command. It is a pleasure to speak to a captive and presumably non-hostile audience this morning, instead of defending my position in the daily wars we fight with the Pentagon and within our own Command. Most everything we want to do to a ship makes it bigger, heavier, and more costly, yet there is unremitting pressure on ship designers to make them smaller, cheaper, and lighter. I want to talk to you today about the state of naval ship survivability -- past, present, and future.

At this symposium, we are focusing on shock, a weapons effect which can wreak havoc on ships, with damage ranges out to many miles. In fact, shock is the principal weapons effect which threatens our submarines. This morning, I am going to expand our perspective to look at the whole spectrum of threats and what the Navy is doing to survive against them. First, we will look at the background, which provides the framework within which this vital matter is best appreciated. Then, I will discuss several topics which will provide you with a broad perspective of the problems we face in bringing a new ship into the Fleet, ready to fight and survive, and ready to go back and fight again. Now for some background information.

During World War II, battle damage received by ships taught the U.S. Navy the importance of (1) good watertight subdivision in ships, (2) the overriding importance of magazine protection, and (3) the retention of combat capability achievable by use of decentralized systems. The first use of the STYX missile against the Israeli destroyer ELATH woke us up to the true damage potential of the anti-ship missile and led directly to development of today's anti-ship missile defense systems -- both active and passive. Damage control and firefighting came in for a lot of scrutiny and improvement as a result of the aircraft carrier fires in the 1960's. The fire susceptibility of aluminum first began to be a concern after the BELKNAP-KENNEDY collision.

During the Vietnam conflict, USS WARRINGTON, a World War II destroyer, received incapacitating shock damage from a mine detonation. The shock intensity was equivalent in severity to that experienced during shock tests, such as our recent ones on USS KIDD and USS ARKANSAS. There was extensive damage to machinery and auxiliaries on the WARRINGTON. The ship was towed to Subic Bay, considered beyond economical repair, and eventually scrapped.

In counterpoint, I should mention that USS HOLT, a KNOX Class destroyer designed in the 1960's, survived a mine detonation nearly identical to that received by the WARRINGTON and was back in action with minimal damage within hours. The expertise of engineers such as yourselves has helped us make great strides in designing shock mitigation techniques for hull, mechanical, and electrical systems in warships following our World War II experience.

Southeast Asia taught us that small weapons can cause big headaches when the USS WORDEN was put out of action at a great repair cost by a very small fragmenting warhead. This incident has led us into an extensive backfit program on 51 ships in seven different classes, designed to protect against this so-called "cheap-kill" threat.

A nuclear weapons effect called the electromagnetic pulse (EMP) is being simulated in low level tests. It is showing itself to be a problem. This phenomenon of EMP can disrupt and damage unprotected electronic circuits thousands of miles away, even when other nuclear effects, such as blast and thermal, are totally absent.

Finally, the Falklands once again pointed out the danger of the anti-ship missile and, even more dramatically, the danger of uncontrolled fire aboard ship, and the susceptibility of aluminum to fire.

The U.S. Public Law on Navy shipbuilding reads, "It is the policy of the United States to modernize the combatant force of the United State Navy through the construction of advanced,

versatile, survivable, and cost effective combatant ships in sufficient numbers and having sufficient combat effectivenes to defend the United States against enemy attack and to carry out such other missions as may be assigned to the Navy by law."

That isn't a speech; it's the law! It is a top-down directive that we make our ships more survivable. Furthermore, the law requires the President to comment on the survivability aspects of any ship acquisition request sent to Congress.

A systematic approach to ship survivability was developed in the 1970's and is being implemented in the design of our new combatants and, selectively, to our operational ships. We have developed survivability technologies, methods, and experimental techniques. We also developed survivability jargon. Let me, before proceeding further, define some of the basic concepts of ship survivability.

Three of the key terms are susceptibility, vulnerability, and survivability. Susceptibility is the probability that the ship and its system will be exposed to weapon effects. The weapons might be conventional or nuclear; they could be missiles, bombs, torpedos, mines, or even particle beam devices. To reduce susceptibility, you must avoid exposure and reduce the probability of being hit. The capability of doing this requires a summation of active defenses such as Close-In-Weapons-Systems (CIWS) and area defense missile systems. It also requires avoiding detection by use of electronic warfare and reducing ship signatures. Typical signatures that might be reduced are radar cross section (RCS), infra-red, acoustic, and magnetic.

Vulnerability is the degree of mission degradation resulting from exposure to the effects of the weapons. It is the probability of being killed, given that you have already been hit. Mission degradation may be in terms of combat capability, mobility, or loss of water tight integrity. Reducing the degree of vulnerability involves the area of passive protection, i.e., building a tough ship, that once hit and damaged, can tolerate the damage and continue fighting, or, when hit, can rapidly recover, control the damage, and continue its mission.

More succinctly, survivability is more than limping home to fight another day. It is the capability of a system to continue to carry out its mission in a combat environment. Therefore, survivability involves both active and passive protection efforts as well as damage recovery techniques. A shipboard missile system contributes to survivability, just as fragmentation protection is a part of the survivability enhancement process.

Now that I have defined these terms, let me say that survivability is a complex issue that involves many factors, and they are all important to a ship in combat. An equation which relates all the factors shown in Figure 1 that permits us to make clear-cut, trade-off decisions, does not exist. Achieving an overall balance will always strongly rely on judgment, experience, and common sense. Nevertheless, they are all related, and, to the best of our ability, we consider them all in developing a survivability strategy for each ship design. this paper, I am going to look principally at the areas shown by the heavy arrows in Figure 1. However, we must not lose sight of the fact to be truly survivable, a Battle Group must ce its susceptibility. That is, they must imize their probability of being hit. This , a key role of the AEGIS combat system being installed in the TICONDEROGA Class cruisers. As you have probably read, TICONDEROGA has recently undergone very successful sea trials and will soon be joining the Fleet.

Before considering modern ships, it can be fun to look back at really ancient threats, and see how they were circumvented by our predecessors. An appropriate example is the Korean "Turtle Ship" shown in Figure 2. This ship was built in the year 1590, almost 400 years ago. The Turtle Ship was carefully designed to withstand contemporary threats, by passive as well as active defenses, as indicated in Figure 3. The passive defenses include a clear, rounded weather deck covered with iron plates. This "citadel" enclosed and protected personnel and equipment. With this type of weather deck, cannonballs and arrows ricocheted off. To neutralize flaming arrows, the sails used for cruising were stowed during combat, and oarsmen were employed to propel the ship. This not only reduced the fire hazard, but provided far greater maneuverability. To neutralize boarders, the deck was equipped with fixed spearheads and spikes. For active defense, this ship not only carried a cannon, but a dragon's head on the bow through which fire and flame were ejected from a furnace down below. Admiral Yee Sun Shin, the inventor and designer of this ship, was usually able to conduct his battles at night, so this dragon head belching fire was a very effective psychological tool indeed.

Today, with our more sophisticated technology, the threats as well as the defenses against them are quite different. To defeat them, we must be at least as innovative and thorough in providing passive and active defense for our ships as Admiral Yee Sun Shin was in 1590. Threats to modern naval ships and their effects are shown in Figure 4. The matrix shows that these weapons cause damage by hull penetration, shock, blast, fragments, and chemical and biological effects. Beyond these effects, nuclear weapons produce damaging thermal and electromagnetic radiation, as well as fallout.

Figures 5 through 9 give the flavor of some effects. Figure 5 shows typical fragment damage to topside antennas and sensors. Damage like

this rendered USS WORDEN ineffective in combat. Figure 6 illustrates how a good ship design and good damage control can save a ship. Torpedos carry very large charges, yet the USS KEARNY survived this nasty hit in World War II. Figure 7 shows the devastating effect of an internal burst weapon. This is HARPOON, our U.S. Navy Sea Skimmer. Very similar results would occur with a weapon such as EXOCET, which hit HMS SHEFFIELD in the Falklands. Figure 8 is Operation SAILOR HAT, simulating nuclear air blast effects. It shows, among other things, the importance of hardening superstructures against blast. Figure 9 is a picture of the USS FORRESTAL off Vietnam. This terrible fire caused great loss of life and property.

Yet, we have learned many lessons. We have gone a long way to make our ships more survivable. Our new design, the DDG 51, is a highly survivable ship. Survivability design features incorporated into this new design have been introduced early in the design phases and provide for well-balanced survivability design throughout the ship. Figure 10 offers a closer look at this ship. Preliminary design is complete and contract design has begun. The Fleet will get the lead ship late in this decade. Some of the survivability features being incorporated in the DDG 51 are (going clockwise from above the stack in Figure 10):

- Improved blast protection from a nuclear weapon burst at optimum altitude will result in a higher blast overpressure protection level than has ever been seen in a destroyer before and will include comparable thermal level protection.
- Equipment hardening for Electromagnetic Pulse (EMP) protection will require careful quality control during detail design and construction.
- Fragmentation protection of vital spaces and magazines will be provided at well defined levels to withstand kinetic energy and density of fragments.
- Chemical, biological, and radiological defense will be provided by a collective protection system (CPS). This is a full time system which uses internal ship pressurized air to keep the ship free of bugs and drugs inside.
- Location of vital ship elements in the hull will improve survivability by taking advantage of new technology and lessons learned about arrangements. Included in this element is the return to steel superstructures.
- Enhanced fire fighting and damage control will make use of a new systems approach to these matters, looking at the ship as a whole and ensuring a more balanced installation less vulnerable to loss of capability.
- Shock hardening standards have been validated through testing and experience and will be met through analysis and tests of equipment and components as part of the procurement process. We will follow that by full-scale shock testing of the lead ship, and corrective action as necessary.
- Protection from transient radiation effects on electronics, called TREE, is a new feature. TREE is caused by neutron flux and gamma radiation from nuclear weapon bursts. This will require careful attention to electronics design details.
- Reduction of the acoustic signature has, as a goal, matching or bettering the performance of the very quiet DD 963. This is a very important feature in avoiding detection and identity.
- Reduced radar cross section features are provided. This is a relatively new feature which we will touch on shortly.
- Reduced IR signature will reduce both detection and terminal aiming of enemy missiles equipped with infrared seekers.

There is no question but that the DDG 51 will be the most survivable destroyer ever built. A quick look at some of the design features of this ship show how these improvements will be achieved.

- Hull and Deckhouse Structure
- AN/SPY-1D Radar
- Vertical Launching System
- Topside Arrangement
- Sloped Deckhouse
- Vital Spaces
- Magazines
- Waveguides and Cables
- In-Hull Vital Spaces
- Full-Time Systems
- Multiple Zones, All Pressurized
- Controlled Access and Decontamination Stations
- Filters
- Personnel Protection
- Hull Sloped Out from Waterline to Main Deck

- o Deckhouse Sloped
- o No Corner Reflectors
- o Minimum Topside Clutter
- o Use of RAM (Radiation Absorption Material) Where Required

Topside structure, equipment, weapons systems, and arrangements are designed to withstand the blast effects of nuclear weapons to a practical level. All vital spaces are protected to a level capable of defeating expected threats without substantial penalty to ship performance in terms of weight, payload, stability, and margins. Magazines are protected to a higher level of fragment protection than other spaces because of their vulnerability. Waveguide and cables are protected in trunks and are routed through interior structures. Many spaces are located deep within the hull (CIC, COMM, CIC Equipment Room, Magazines, Central Control Stations, and Damage Control Central). The CPS System covers the entire ship. The multiple zones are all pressurized. There are high efficiency filters capable of removing damaging or contaminated particles. The crew will have improved gas masks, better protective clothing, decontamination equipment, and detectors. Substantial R&D testing is required in the radar cross section reduction effort called RCS Reduction. The basic principles of radar cross section reduction have been implemented in the DDG 51.

Ships are limited in space, weight, stability, and services. The operator desires maximum performance, i.e., fire-power, speed, endurance, ease of operation, minimum maintenance, and a tough (survivable) ship. All this he wants at a minimum cost or, a frequently heard term, "affordable cost." These are tall orders levied on the ship designer who is constantly confronted with trade-offs.

Typical trade-offs are shown in Figure 11. Three weapons effects, fragmentation, air blast, and CBR, are on the left-hand side of the equation. In order to achieve a prescribed level of protection, any of the five capabilities (combat capability, survivability, mobility, habitability, or electrical and machinery) which could have been implemented into the design had to be traded off. Therefore, speed and endurance are reduced, or fewer missiles will be carried, one less helicopter, or no sonar, or it will cost more money per ship. One of the designer goals is to enhance survivability through synergistic configuration. An example of the synergistic configuration is shown in Figure 12. The synergistic configuration is a powerful but only a partial solution to the cost and performance problem. The example shows a ship where certain conventional non-survivability design features can enhance the survivability capability of the ship. The Helo landing deck is more efficient with a steel deckhouse; this also provides fragmentation, blast, and fire protection. Mack structure makes it easier to shock and blast harden topside equipment and protect against EMP. A wide waterplane hull allows more flexibility in topside arrangement such as redundancy, rattle space, and ease of maintenance. Rugged equipment and structurally optimized foundations enhance shock, and blast-induced shock resistance capability of the ship, and also reduces maintenance.

For one more look at affordability, see Figure 13. It is interesting to see the fractional cost of various survivability design features as a percentage of unprotected ship cost. You can see that protection against a cruise missile is a substantial expense. These cost fractions are merely for comparison purposes and would vary depending on the ship type.

In order to bring the reader up to date on some of the on-going efforts in ship survivability, a few items of special interest will be discussed.

EMPRESS II: Regardless of the hardening techniques employed, verificaton testing is necessary. At present, the only EMP test facility available for the testing of Navy ships is EMPRESS I (Electromagnetic Pulse Radiation Environmental Simulator for Ships). This facility is located at the Naval Surface Weapons Facility, Solomons, Maryland. Use of this facility is limited to small ships, such as frigates, due to draft limitations and bridge clearance restrictions. There is currently an R&D program for the development of an improved EMP test facility referred to as EMPRESS II. The goal of this project is to develop and acquire a facility capable of testing large ships.

FFG EMP TRIAL: The FFG 7 class is one of the few that can fit into our current EMPRESS facility. One ship of this class (FFG 15) was tested in June '81. A second may be tested in late FY-83 or FY-84. The objective is to verify that the EMI (very similar to EMP) fixes being installed in the class and the EMP fixes proposed in our survivability program are adequate.

SHIP HARDENING PROGRAM: This is a recently approved program which is dedicated to taking fleet-wide corrective action on hardness deficiencies which have been revealed by ship shock tests. Funding for this program is approved for FY-83 at the levels requested, and the program will continue until all necessary follow-up action on these tests has been accomplished.

As a related matter, our shock test data base is basically up-to-date, with the exception that no modern carriers have been tested, and our most recent submarine shock tests were performed in 1962. We intend to fill these data base gaps, and NAVSEA has started to plan the

necessary tests. We are also planning the first shock test of an AEGIS cruiser. YORKTOWN, second ship of the TICONDEROGA class, has been tentatively selected for shock testing in October 1984.

We are not at the end of our efforts. Some might say we have only begun. As new weapons come into our arsenal, we can expect our potential enemies to achieve similar ones. Trends in survivability are dictated by trends in weapons. We need innovative ideas for structural and protective materials. We need improved computer modeling tools to better integrate weapons effects with survivability design features. We must implement survivability design features early in the design process. This is done by integrating two important design tools: the ship synthesis model, a computer program used during feasibility design, and the ship vulnerability model, which determines ship survivability characteristics. We need to sharpen these important tools so that we can have an optimized survivability design with minimum impact on ship performance. We need more emphasis on nuclear hardening and on chemical and biological defense. We need deeper and broader assessments of passive versus active protection, and their interface with reliability. We need to develop more capable design analysis methods, addressing areas such as nuclear blast-induced shock, penetration of ship structure, structural optimization for weight savings, radar cross section modeling, and so forth. Lastly, we need to improve our standards, specifications guidance documents, and our design criteria in the area of ship survivability.

There is no question that ship survivability is getting considerable attention. Although most of this attention has been constructive and positively directed, it remains that the overall effectiveness of our surface forces has been seriously questioned because of the perception that our ships are unduly vulnerable to modern weapons. To say that our ships are vulnerable sitting ducks is patently incorrect, and we should take all possible opportunities to correct this impression. At the same time, it is important that we continue to take every reasonable action to improve the survivability posture of the Fleet as a whole.

Programming and accomplishing SHIPALTS to protect aircraft carrier magazines, backfitting against the cheap kill, and making firefighting improvements will go a long way to enhance survivability of our existing ships. Even greater opportunities for survivability improvements, of course, reside with our future ship designs. Our new DDG 51 provides an example of the major survivability improvements that are now available to our new construction ships.

The DDG 51 design illustrates another important point, and that is that highly-effective levels of ship survivability are, in fact, affordable. It is not impossibly costly to protect our ships. What is difficult, is to find the optimum balance between offensive capability, active defense, and passive protection. In short, the survivability characteristics of our present Fleet ships are being improved but will always be somewhat limited, basically because we designed them that way. Similarly, our future Fleet can be highly survivable, and in fact, it will be — if we design it that way.

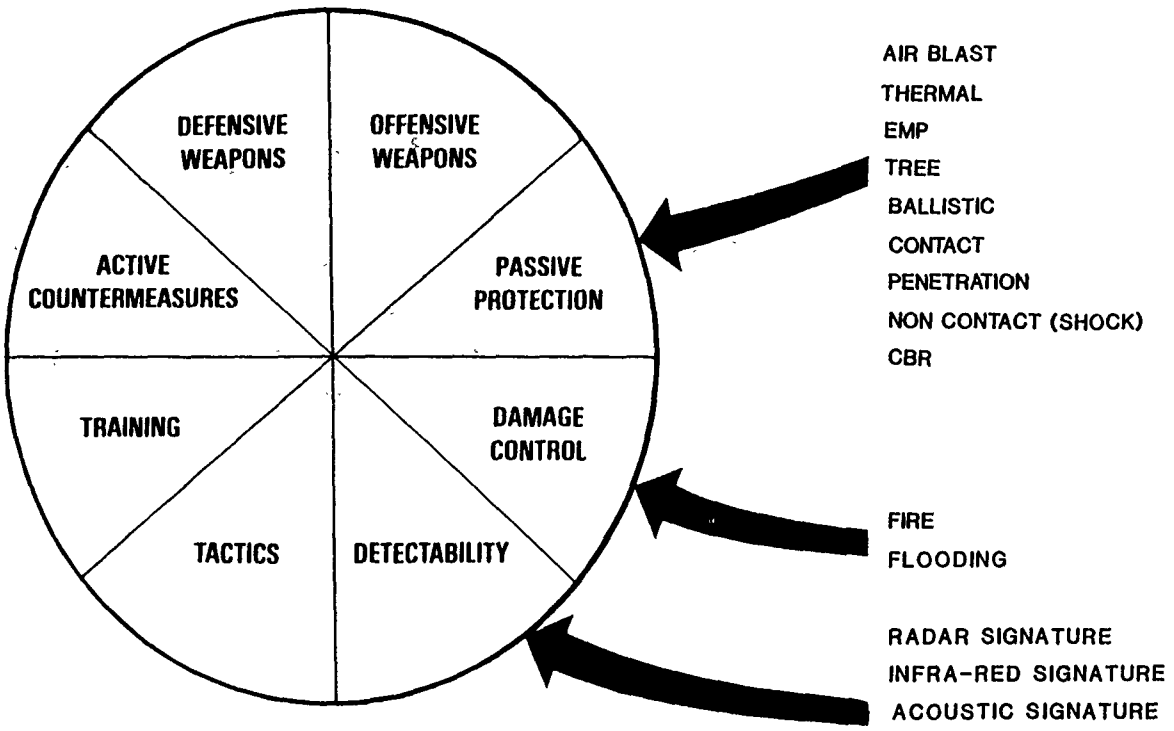

Fig. 1 — Combat survivability factors

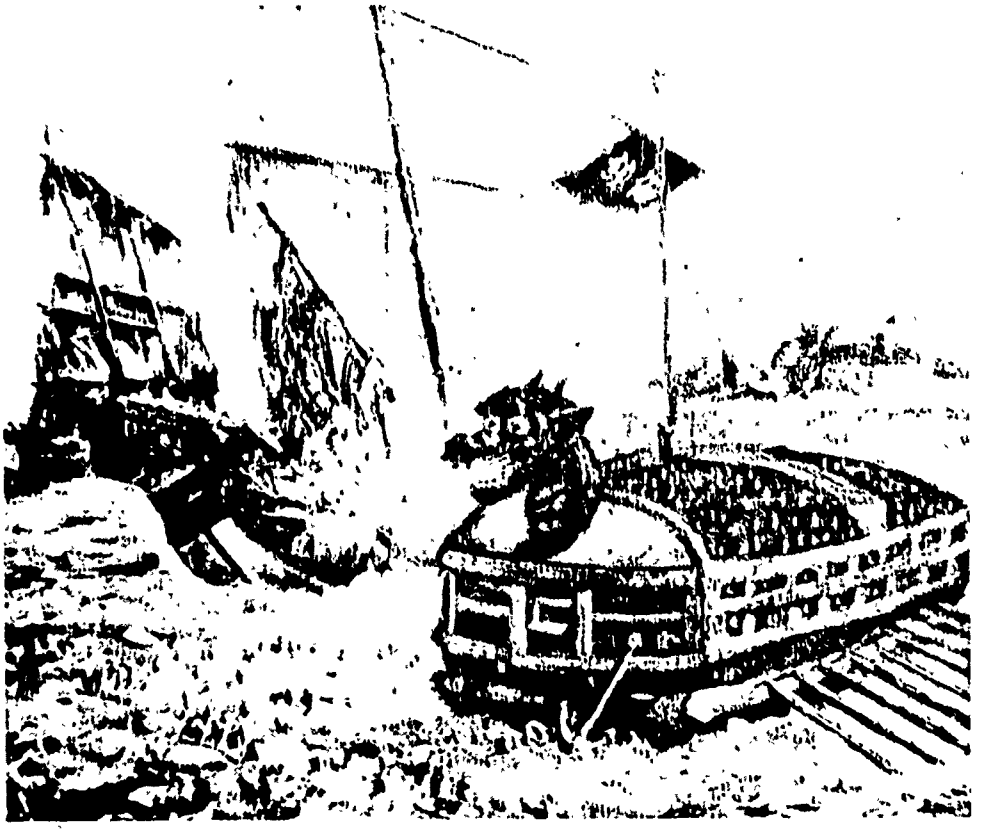

Fig. 2 — Korean Turtle ship defeating Japanese, A.D. 1590

THREAT	EFFECTS							
	SHOCK	BLAST	FLOODING	PENETRATION	FRAGMENTS	EMP/ THERMAL/ RADIATION	PERSONNEL	FIRE
CANNON BALLS			X	X	X		X	X
ARROWS/SPEARS							X	X
BOARDERS							X	

Fig. 3 — Turtle ship's threats, A.D. 1590

THREAT	EFFECTS							
	SHOCK	BLAST	FLOODING	PENETRATION	FRAGMENTS	EMP/ THERMAL/ RADIATION	PERSONNEL	FIRE
CONV. MISSILES/BOMBS	X	X	X	X	X			X
MINES	X	X	X		X			
TORPEDOES	X	X	X		X			
PROJECTILES		X		X	X			X
NUCLEAR WEAPONS	X	X				X	X	X
CB							X	

Fig. 4 — Today's threats

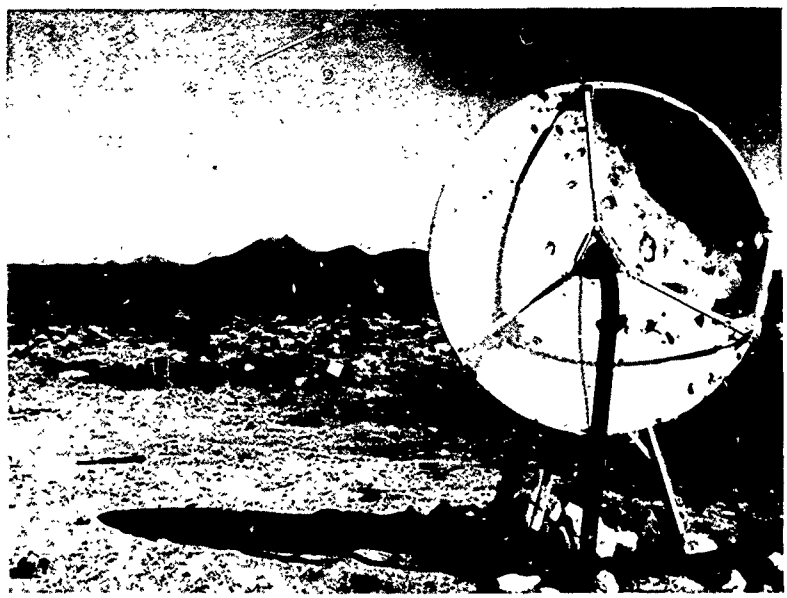

Fig. 5 — Fragment damage to antenna

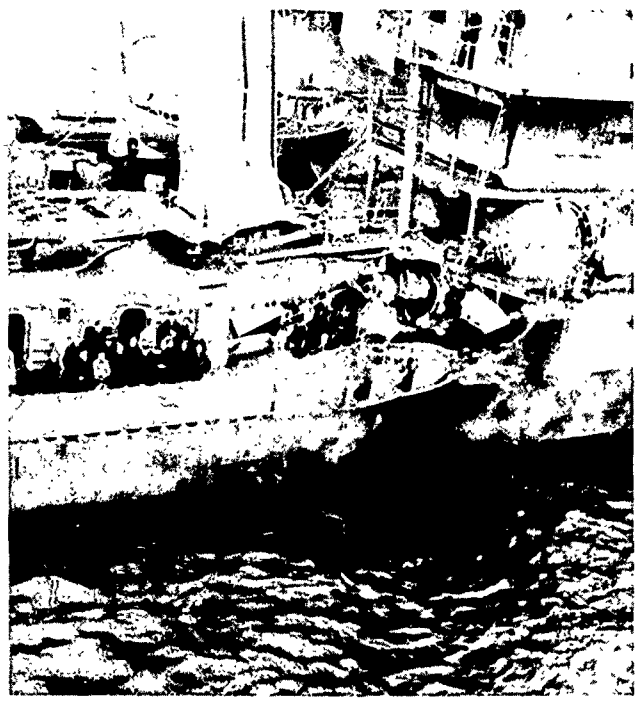

Fig. 6 — This torpedo damage was withstood by USS KEARNY

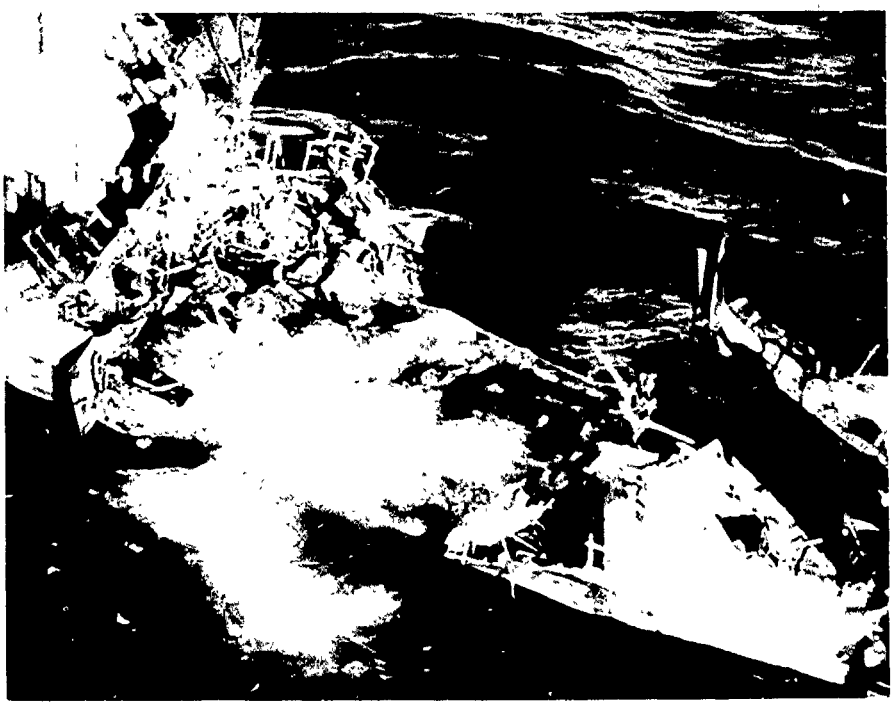

Fig. 7 — Devastating effect of harpoon missile

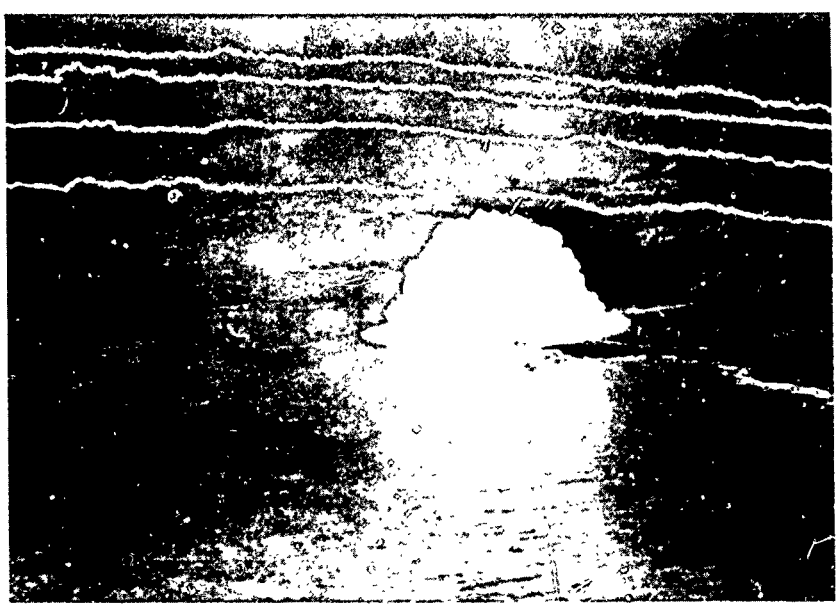

Fig. 8 — Operation SAILOR HAT — simulated nuclear air blast effects

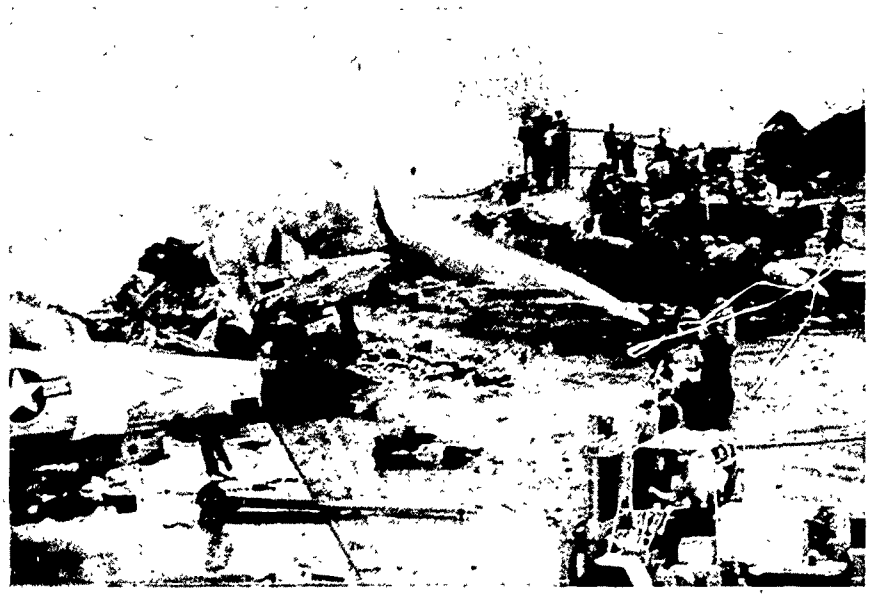

Fig. 9 — Very damaging fire aboard USS FORRESTAL in 1967

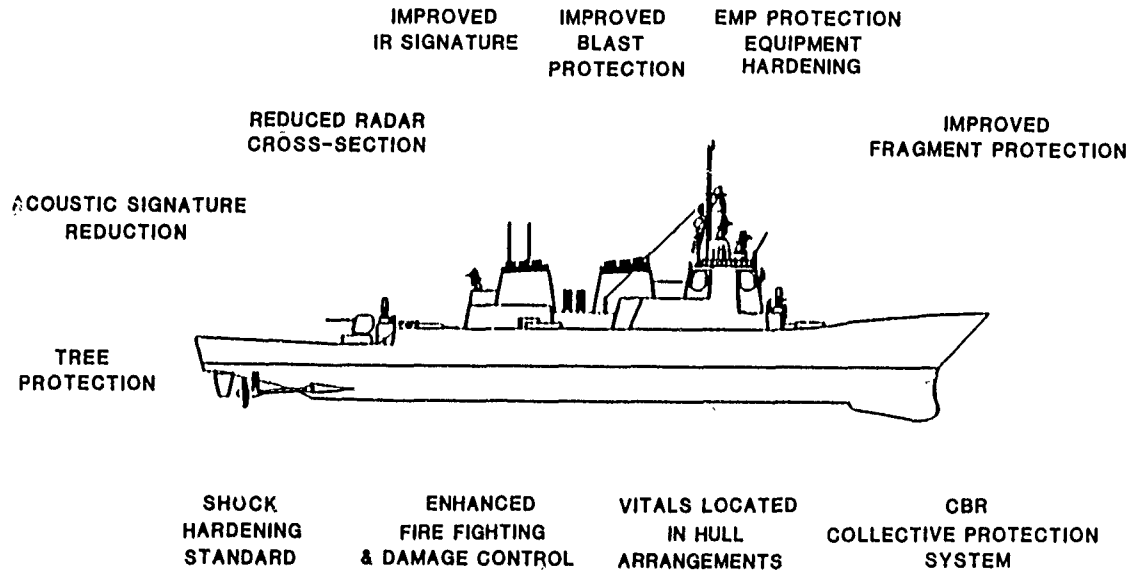

Fig. 10 — DDG 51, survivability features

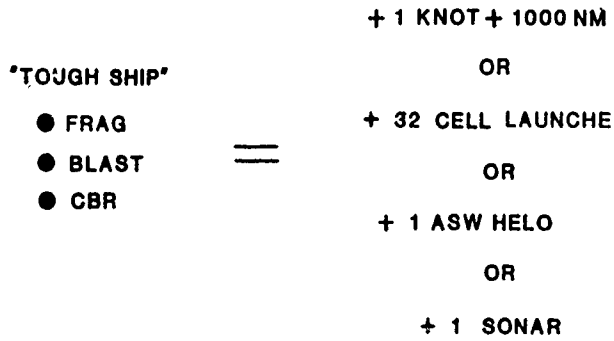

Fig. 11 — Typical design tradeoffs

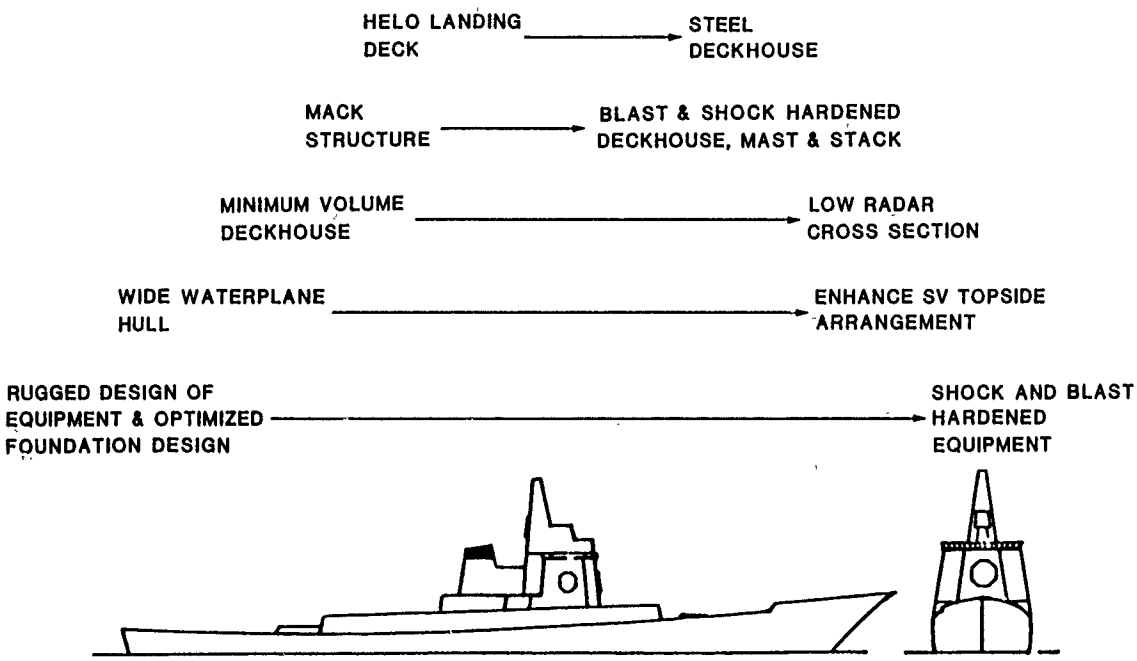

Fig. 12 — Example of synergistic configuration

SHOCK	1/2
NUCLEAR AIR BLAST	1
EMP	1/2
CBR	1–3
FRAGMENTS	1–5
DAMAGE CONTROL	1
CRUISE MISSILE	10–20
*% OF OF UNPROTECTED SHIP COST	20–25

Fig. 13 — Approximate cost of survivability features (expressed as percent of unprotected ship cost)

ELIAS KLEIN MEMORIAL LECTURE

VIBRATION CHALLENGES IN MICROELECTRONICS MANUFACTURING

Eric E. Ungar and Colin G. Gordon
Bolt Beranek and Newman, Inc.

The manufacture of smaller, more tightly packed, integrated circuits requires facilities designed to meet stringent vibration requirements. Vibration control is complicated by the need for extensive process support equipment and some service personnel in the vicinity of the sensitive machines.

Facility criteria that have been developed on the basis of earlier facility experience have tended to be unrealistic and inadequately defined. The present paper delineates the shortcomings of these criteria and indicates how better criteria may be defined.

Information on vibration levels that are permissible for critical items of optical equipment is essential to the development of realistic facilities criteria. The limitations of some of the available data are discussed, together with suggestions for overcoming them and for improving optical equipment items from the standpoint of their structural dynamics.

INTRODUCTION

An integrated circuit "chip" basically consists of a substrate on which there are deposited a series of extremely thin layers of various materials. The patterns and materials of these layers, and the connections between them, are designed to accomplish the desired circuit functions.

There has been a continuing trend toward chips with more and faster data processing capability, implying smaller and more tightly packed circuit elements—and thus establishing a need for greater precision in the patterns in which the material layers are deposited.

The production of these patterns involves a series of steps that are essentially photographic. The image sharpness in these steps and the registration of successive patterns atop each other determine the circuit density that can be obtained. Some limits on the attainable image sharpness are established by the basic properties of the light or other radiation that is used for the photographic exposure; newly developed technology, in fact, makes use of electron beams whose wavelengths are shorter than those of light, in order to capitalize on the resulting reduced diffraction and increased resolution. However, it appears that other limits result from wobbling of the optical systems occurring during the photographic exposures.

An idea of how stable microelectronics manufacturing equipment needs to be may be obtained by noting that current production chips have line widths of 5 to 7 μm, that in the near future production of chips with line widths of 1.5 to 2 μm is expected, that efforts toward production of line widths of 0.5 to 1.0 μm are in progress—and that registration requirements typically are of the order of ten percent of the line width. (Note: 1 μm = 1 micron $\approx 4 \times 10^{-5}$ in $\approx$ 0.04 mils.)

The aforementioned wobbling—or, more precisely, the corresponding motion of the light (or other radiation) beams across the image surface—is associated with vibratory relative deflections of the optical system. It is these vibrations that are the primary concern of the present paper.

This paper represents an attempt to provide a broad overview of the major problem areas, in part from a historical perspective, in order to present some challenges and guidance to vibration specialists. However, delineation of specific problem solutions has been omitted and identification of specific facilities and equipment items has been avoided for three reasons: (1) requirements for different facilities may differ greatly, depending on numerous equipment, usage and environmental factors, (2) rapid change in microelectronics technology leads to continuous changes in equipment and to updating of its performance data, and (3) much of the specific data is proprietary.

FACILITIES

Effects of Process Requirements on Configuration

Facilities for the manufacture or development of integrated circuits tend to be complex, largely because of the many different items of equipment that are required. The photographic processes themselves typically involve multiple stages of chemical treatment—such as coating, baking, developing, etching and stripping—implying the need for extensive piping systems to bring gaseous and liquid chemicals to the areas where they are used. Additional piping is needed to support the rinsing, washing, scrubbing and drying operations, as well as to provide fuel (and oxidants) for various process furnaces. The many chemicals that are used require the installation of hoods for the removal of fumes and the provision of wastewater treatment and waste chemical disposal means.

All of the microcircuit production steps need to be carried out in a clean, controlled atmosphere, requiring not only that temperature and humidity be maintained within tight limits, but also that particulate contamination be kept to an acceptable level. The control of particulate contamin-

ants typically is achieved by means of "clean room" systems that produce controlled uni-directional (non-turbulent) flow of thoroughly filtered air in the working spaces. These systems, as well as the more conventional heating and air conditioning systems, again require extensive ducts and piping serving the processing areas.

Because of all these support requirements, integrated circuit manufacturing facilities tend to be designed as arrays of modular spaces, with each space housing perhaps a dozen major pieces of production-related equipment and about four to six workers. Each work space is surrounded by support equipment areas or "service aisles", in which maintenance of strict particulate contamination control is not required. A typical space configuration is illustrated by the architectural sketch of Fig. 1. The work spaces and support equipment areas communicate with each other via a multitude of conduits, ducts and pipes that provide power and that supply and remove various gases and liquids.

Sources of Vibration

The aforementioned support systems tend to include equipment items that may generate significant vibrations. Typically, the major sources of vibrations consist of the numerous large fans that supply air to the clean rooms, the turbulent air flows within the duct systems, the pumps and chillers that generate and circulate chilled water for air conditioning and process equipment cooling, and the flow of water and of other liquids in pipework.

Some relatively small support equipment items, such as vacuum pumps, tend typically to be located in the service aisles, in close proximity to the areas they serve—and thus may cause appreciable vibrational disturbances in spite of their small size. Traffic of vehicles (e.g., electric or unpowered carts along these aisles transporting heavy compressed-gas cylinders and the like) also may constitute a source of potentially disturbing vibrations in the work area. In many

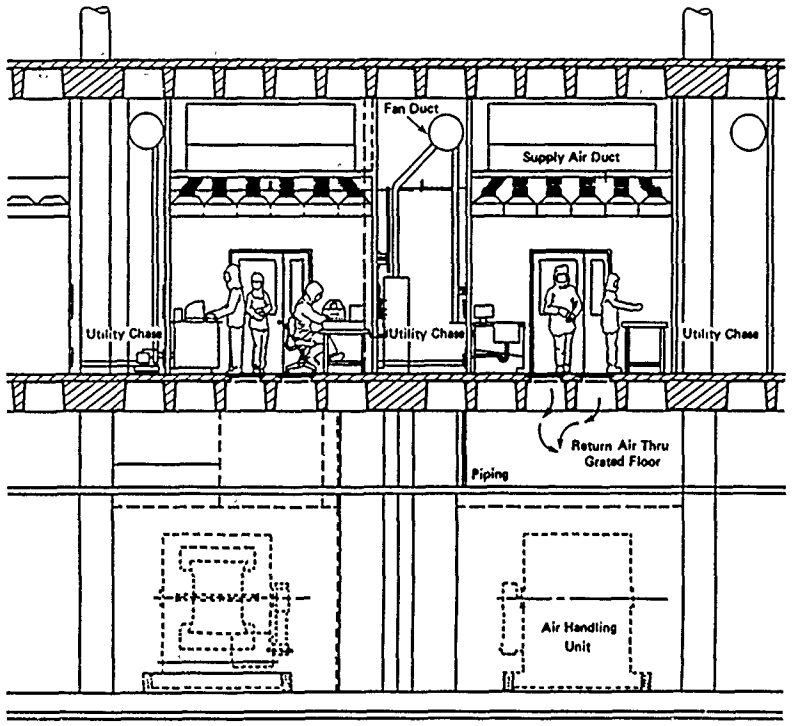

Fig. 1 — Typical "clean room" arrangement for microelectronics manufacture.

instances, however, the activities of personnel—particularly walking—in or near the work areas tend to constitute a major source of problematic vibrations, in addition to the mechanical equipment mentioned earlier, whereas external sources, such as nearby road or rail traffic, typically are of lesser importance at reasonably selected plant sites.

Vibration Criteria Considerations

The floor of a microelectronics manufacturing area must provide a vibration environment that permits the sensitive equipment housed in that area to perform satisfactorily. Manufacturing facilities also need to be flexible, in order to be able to accommodate changes in the technology and advances in the state of the art. Facility users rarely will accept specific areas designed only for specific equipment items, and they tend unhesitatingly to state that they want their facilities to be suitable for tomorrow's equipment, which is not yet invented, but which is bound to have tighter requirements as line widths become smaller.

Because some of the suppliers of microelectronics fabrication equipment have not provided adequate specifications of the maximum floor vibrations to which given items of equipment may be exposed during operation (as discussed later in this paper), facility engineers have been left without much guidance. For some early facilities, they thus have

simply and naively set forth the requirement that the absolute displacement of the facility floor not exceed the desired line width resolution (or image displacement) at all frequencies below a certain value. This sort of criterion is unrealistic, even if one ignores the very low frequencies, where such phenomena as tidal and atmospheric effects make it practically impossible to meet this requirement. It does not take account of the fact that the image movement results from a relative displacement between structural components of the equipment, and that this relative displacement may differ considerably from the absolute displacements of the equipment's support points. At low frequencies, where the equipment behaves dynamically essentially as a rigid body (as one may conclude from basic structural dynamics considerations), the relative displacements may be several orders of magnitude smaller than the absolute input displacements.

Some facility specifications, as illustrated in Fig. 2, have deviated from frequency-independent displacement limits, perhaps on the basis of empirical experience with some specific items of equipment. It is unlikely, however, that the stringent requirements implied by these specifications at the low end of their frequency range ever were met.

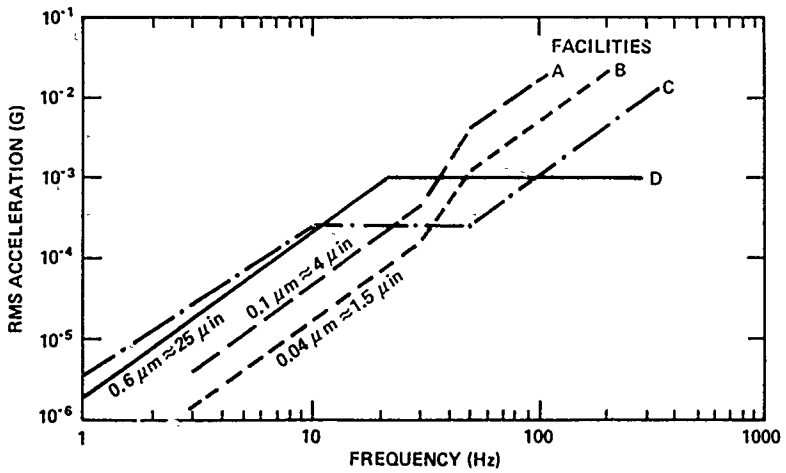

Fig. 2 — Some recent microelectronics facilities floor vibration criteria specified by facility users. (Slanted lines with μm labels are lines of corresponding constant displacement amplitude.)

An approach based entirely on empirical facility vibration data has more recently been taken by facilities engineers. They have simply measured the vibration environments in areas where various equipment items are operating satisfactorily and have set forth the requirement that the vibrations at every frequency in the newly designed facility be less by a given factor than the most severe corresponding vibrations in the areas where measurements were taken. The purpose of the reduction factor was to provide an additional margin of safety and to account for the expected greater vibration sensitivity of newer equipment.

Unfortunately, the bandwidths used for the aforementioned environmental data analyses are rarely indicated, often resulting not only in the unwitting combination of data corresponding to different bandwidths, but also in a lack of definition of the bandwidths applicable to a specification.

However, this empirically based approach has some shortcomings, even if the measurement bandwidths are fully identified. For example, a particular vibration environment, which may be unacceptable because of the effect of only one of its frequency components, in this approach would lead to the setting of restrictive limits on all other frequency components— resulting in potentially costly over-conservatism.

Fully realistic and sensible criteria also must take proper account of the combined effects of different excitation components. For example, if an acceleration a_1 at frequency f_1 is barely acceptable if this vibration component is present by itself, and if an acceleration a_2 at frequency f_2 similarly is barely acceptable, both according to some criterion curve developed on the basis of a series of narrow-band excitations—then, is an environment satisfactory if it contains both of these components? Intuitively, the answer depends on the separation between the two frequencies: components with widely different frequencies are likely to act independently and to affect different equipment modes preferentially, so that their simultaneous presence is likely to be acceptable, whereas components that do not differ much in frequency may have additive effects. Perhaps the best means for coping with this problem consists of defining criteria in tems of bandwidths that are typical of equipment response bandwidths, so that measurement in these bandwidths takes account of the combination of the frequency components present in the environment approximately as does the equipment response.

Furthermore, in the setting criteria it is not sufficient merely to establish boundaries on the vibration levels as a function of frequency, in specified bandwidths. One also needs to delineate the time interval(s) over which measurements are to be carried out, as well as the statistics (amplitude distribution) of the vibration levels. Of course, any given data sample must extend over several periods of the lowest frequency component of interest, so that one can analyze that component adequately.

In addition, however, practical considerations for a manufacturing facility make it necessary to characterize the vibration environment encountered during an entire working day, so that one ideally should measure this environment

over several such days. In establishing a meaningful criterion in relation to long-term environmental vibrations, one needs to consider how significantly microelectronic manufacturing equipment is affected by occasional disturbances. For equipment or processes that must continue without interruption for extended periods, one requires that the environment exceed the disturbing levels only extremely rarely, whereas for others, more frequent disturbances may be acceptable. It often turns out that the equipment items that are most sensitive to vibrations do not operate continuously and that some of the most sensitive items include control systems that prevent photographic exposure if the image is inadequately sharp. It thus often is useful to state criteria in terms of percentile levels—i.e., the vibration levels which are exceeded a given percent of the time during defined periods of the working day.

Design Considerations

In view of the extreme vibration-sensitivity of the equipment, it is important that a relatively vibration-free site be selected for a microelectronics facility. For this purpose, performance of a vibration survey is generally recommended as part of the site evaluation process. such a survey should include measurements during the quietest (most vibration-free) times and during the most active times, and ideally should extend over long enough periods so that meaningful statistical discussion. For example, one may want to evaluate the vibration amplitudes in each one-third octave band that are exceeded 50, 20, 10 and 5 percent of the time, so that one can calculate what percentage of the time the site vibrations meet the facility specifications. Of course, such a detailed site study may not be necessary in cases where vibration levels that are clearly too high or that are very low are observed over a significant period.

As implied in the foregoing paragraph, vibration surveys and the attendant data reduction should not be undertaken blindly, but with facility criteria in mind. Criteria and attenuation possibilities must also be considered, of course, in evaluating sites or selecting one of several alternatives. For example, one generally may more readily isolate equipment against site vibrations that exceed the criteria in some high frequency regions than against others that exceed the criteria at lower frequencies.

Some site vibration reduction may be achievable by controlling external sources. For example, nearby roadways and rail-lines may be smoothed, speed-bumps may be removed, and traffic may be rerouted (or confined to non-operating hours of the day or week) or slowed down.

The most important aspect of a facility design usually consist of providing a suitable structure, particularly for that part of the building that houses the vibration-sensitive equipment. The second most important aspect typically consists of providing a layout that separates the sensitive equipment from vibration sources.

The facility should be configured so as to locate major vibration-producing items (such as pumps, compressors and fans) as far as possible from the critical clean room areas, and careful attention needs to be paid to providing adequate vibration isolation between the sources and the sensitive areas. Some facilities have been designed with all major support equipment housed in a separate building; others have been built with all support equipment located near the sensitive areas, but mounted on entirely separate structural systems. In all cases, the routing and support of the extensive ducting and pipework systems also needs to be considered from the vibration isolation standpoint.

The building structure should be designed so that neither the sensitive areas nor the parts that house vibration-producing equipment have resonance frequencies that match the excitation frequencies associated with the vibration sources. If avoidance of resonances is impossible or uncertain, the use of increased structural damping may be considered; however proven means that provide such damping are not readily available, and one must keep in mind that increased damping broadens the response bandwidth and thus may increase vibrations due to some source components while decreasing those due to others.

Vibration reduction at the source is recommended where possible. This approach may involve the selection of alternatives that inherently produce less vibrations (e.g., using rotating compressors in place of reciprocating pumps; keeping the flow velocities in ducts and pipes low), choosing equipment that is less likely to excite structural resonances or that can be isolated more effectively (e.g., high speed axial flow fans in place of lower speed centrifugal blowers), and specifying better dynamic balancing of equipment.

Primary vibration reduction considerations also involve configurating the entire facility so as to minimize in-plant vehicle and foot traffic near and in the sensitive areas. Where vehicular traffic is unavoidable, care must be taken to avoid surface irregularities, structural joints, and sudden structural stiffness changes along the vehicle paths.

People walking often turn out to constitute a critical source of vibrations about which one can generally do very little that is practical in existing facilities. However, appropriate structural choices can generally be made relatively readily in the process of designing a new facility.

Attention to details is required also not only in the design and specification of isolation systems for all vibrating equipment items so as to obtain adequate performance and to avoid any mechanical short-circuiting, but also in inspecting the final installations. After a facility has been built, measurements may be required to verify that source vibration level and isolation system performance specifications have been met, to determine to what extent the entire facility indeed meets its criteria, and to identify what may need to be done to correct discrepancies.

OPTICAL EQUIPMENT

Typical Configuration

Although many different types of equipment tend to be employed in microcircuit manufacturing, the equipment items that are most sensitive to vibrations fall into the broad class of optical equipment—if one considers this class to include also production and inspection equipment that employs radiation other than light, such as electron beams. For the present discussion, optical equipment thus includes common light microscopes, as well as electron microscopes of all types, in addition to such microcircuit fabrication items as aligners, registration analyzers, pattern generators and wafer steppers.

Although the various specific items of optical equipment may differ considerably in their operational details, they nevertheless share a number of major features from the

viewpoint of their structural dynamics. As shown schematically in Fig. 3, a typical equipment item consists of an optical column and an image stage which must be maintained in a precise position relative to each other (at least during an exposure or observation interval). For the present discussion it does not matter whether radiation coming from the optical column is used to expose an item on the image stage or whether an item on the image stage is viewed (by eye or electronically) via the optical system.

The "optics support frame" in the figure indicates the structure that is intended to provide the desired aforementioned relative positioning. This structure may be relatively complex in some equipment items; it may, for example, enclose the entire optical system, and it may include electro-mechanical arrangements for adjusting (or stepping or rotating) the stage relative to the optical column.

The entire optics support frame typically is supported on a secondary structure, which is labeled "table" in the figure, and that structure—in turn—rests on a support base. The more sensitive items of optical equipment generally are installed on soft springs (often of the air spring type, in which case the table system often is called a "air table") and may include additional vibration isolation mounts, as also sketched schematically in the figure.

Vibration Criteria

If one knows the amount of image motion that is permissible in a given situation, together with the "transfer function" between the image motion and the floor vibration, one may expect to be able to derive appropriate floor vibration criteria—i.e., limits that the floor vibrations must not exceed if a given desired image quality is to be maintained.

The suppliers and users of optical equipment generally tend to have very precise information on the permissible image displacements, but to know little or nothing about the vibration transfer functions. It should be noted that even for a given machine in a given, fixed configuration, obtaining a transfer function is not easy. Although one generally may count on response linearity for the small amplitudes of concern here (so that one need not consider variations with amplitude) and although one can usually neglect the effects of purely rotational motions, one still needs in general to evaluate the magnitudes of optical column displacements relative to the image stage in each of three orthogonal directions—for each of three orthogonal directions of floor motion—and, of course, all as functions of frequency. Obviously, greater complexity results for machines whose configurations can change appreciably, e.g., due to motion of an image stage.

Although a "transfer function" thus in general may be represented by nine curves that indicate the frequency-variation of the ratio of the x, y and z image displacements to the x, y, and z floor displacements (or accelerations), considerable simplification is possible in many instances. For optical systems that have relatively large depths of focus, for example, relative displacements along the optical column axis tend to be less important than the others. In most facility structures, the horizontal floor vibrations tend to be considerably less significant than the vertical ones and can therefore be omitted from consideration.

Under these simplifying circumstances one may need to deal with only two in-plane image displacements in response to vertical floor vibrations. One may then represent these two remaining transfer function curves conveniently by a single one that corresponds to an envelope or a vector sum, resulting in a simply applied, conservative measure of the maximum image displacement occurring in any in-plane direction due to vertical floor motion.

It appears that the vibration criterion problem for optical equipment has for a long time not been addressed adequately. Many equipment suppliers have provided only a "single number" floor vibration criterion, such as a maximum permissible displacement (or velocity or acceleration) without any frequency information or any hint of how the specified value was to be measured (or how it was obtained). The variations of the permissible acceleration magnitudes with frequency implied by a number of these criteria are indicated in Figs. 4 and 5. It is evident that many of these criteria require unrealistically small motions, particularly in the low frequency region—where these magnitudes are practically impossible to achieve, and where also the equipment items are likely to experience relatively little deflection (and concommitant image dis-

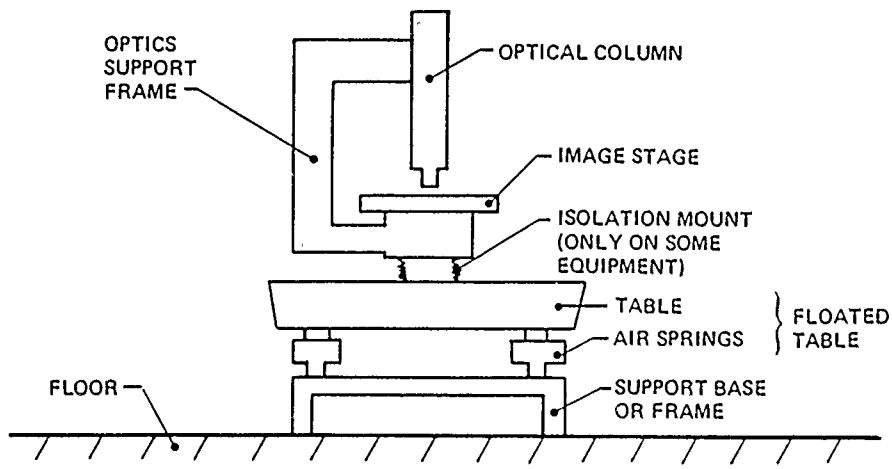

Fig. 3 — Schematic sketch of optical equipment.

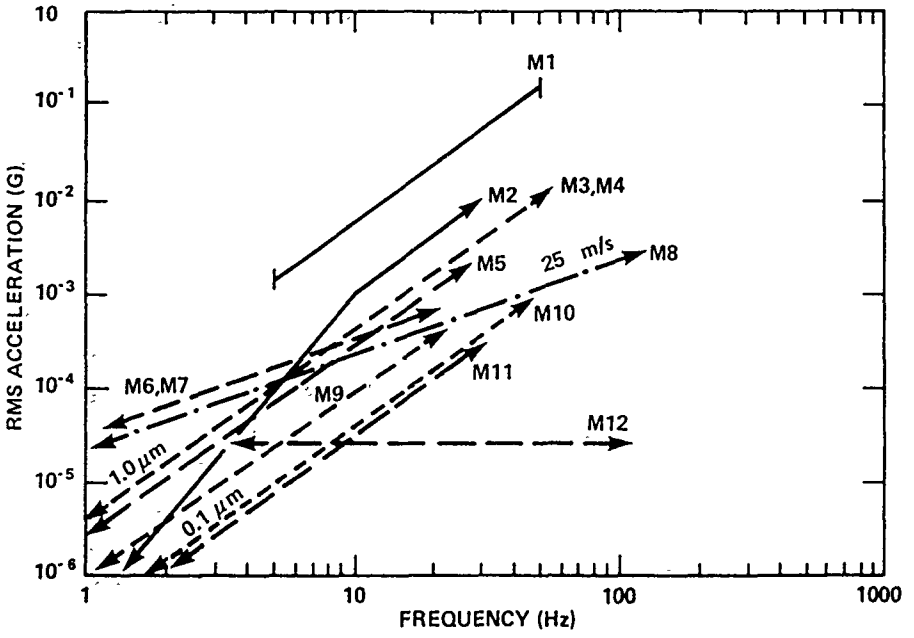

Fig. 4 — Suppliers' floor vibration criteria for twelve different electron microscopes. (Slanted lines with μm and μm/s labels are lines of corresponding constant rms displacement or velocity, respectively. Arrows at ends of lines imply that specified criterion is stated without frequency restriction.)

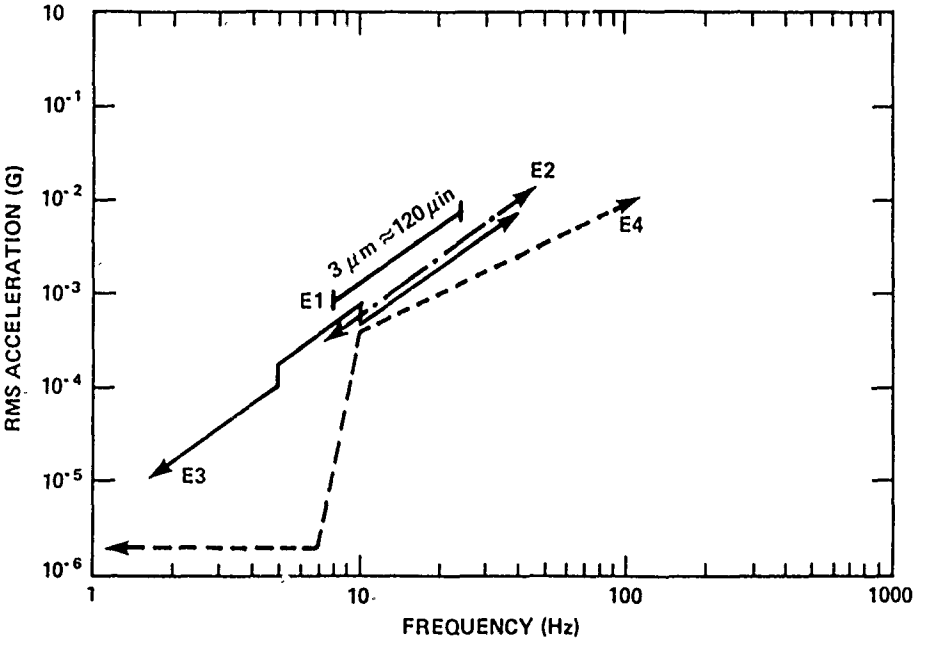

Fig. 5 — Suppliers' floor vibration criteria for four different items of electron-beam microelectronics manufacturing equipment. (Same notes apply here as for Fig. 4.)

placement) for a given amount of floor vibration, as has been mentioned.

Several of the equipment criteria that have been put forth, however, are somewhat more realistic and apparently take account of some of the equipments' structural dynamics aspects. For example, as indicated in Fig. 4, some criteria restrict applicability of the stated single-number values to limited frequency regions, others state different values for two or three different frequency regions, and some indicate more complex frequency-dependencies that may have been based on tests or observations. Again, no background documentation appears to be available.

In view of this dearth of useful criterion information, we have taken some steps toward developing defensible realistic criteria, at least for some equipment that is currently in use. We made floor vibration measurements near operating equipment at several facilities, both under normal ambient conditions and in the presence of several different types and levels of disturbing vibrations (e.g., due to nearby traffic or several people walking), and we obtained the corresponding equipment users' evaluation (based on subjective judgements or optical measurements) concerning the acceptability of these vibrations.

Some of the results of this work are illustrated in Fig. 6, which represents the highest observed floor acceleration spectrum peaks (in one-third octave bands) corresponding to conditions under which satisfactory equipment operation was obtained. Two facts should be noted: (1) The magnitudes of some of these peaks were limited by the floor vibrations that could be obtained in these investigations, and not by the onset of unsatisfactory equipment operation. (2) Since all frequency components acted on the equipment simultaneously, one cannot judge which may limit the equipment's performance; considerably higher magnitudes of some components may be acceptable without adverse effects. Thus, the data presented here correspond to conservative criteria—i.e., the equipment is likely to perform satisfactorily even if the floor vibrations exceed the magnitudes represented by the data points, and the equipment will certainly perform satisfactorily if the vibrations do not exceed those corresponding to the data points.

In order to establish well-defined criteria by this approach, a great deal of data collection and analysis is needed. Ideally, data should be obtained for a wide variety of floor vibration conditions that produce both acceptable and unacceptable equipment performance for each item of equipment, and the data should be analyzed in terms of frequency bands that are relevant to the equipment response, as discussed in the previous section. However, some other approaches, based on more concentrated investigations of specific items of equipment, may be preferable.

One such approach involves determination of the transfer functions between floor accelerations and image displacements that were discussed earlier, and then calculating the maximum floor vibrations that result in acceptable image displacements. Evaluation of these tranfer functions is relatively straightforward, but requires extended availability of the optical equipment for testing, as well as provisions for controlled simulation of the floor vibrations and sensitive means for measuring the small image displacements of concern or the corresponding relative displacements between the image stage and the optical columns.

Another approach to developing precise vibration criteria for a specific item of optical equipment makes use of an analytical model of the equipment, developed on the basis of parameter values deduced from a series of measurements made on the equipment item. Once the item is modeled mathematically, the model can readily be used for determining the desired transfer functions—and these, in turn, can be employed to calculate the permissible floor vibrations as mentioned previously.

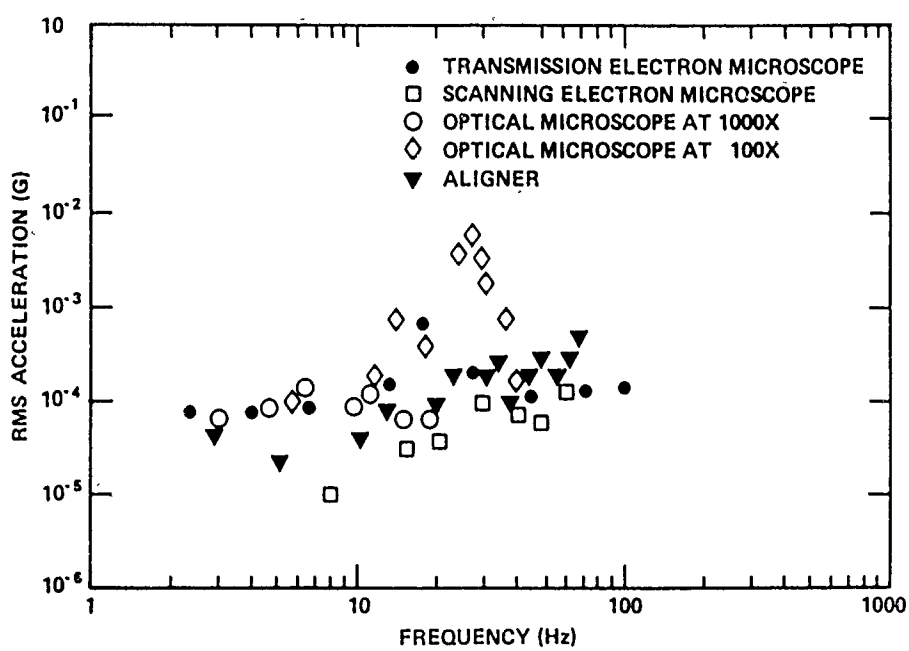

Fig. 6 — Maximum floor vibration spectrum peaks (in one-third octave bands) at which optical equipment items operated satisfactorily.

Because typically only the lowest few modes of each major structural component of a piece of equipment tend to contribute significantly to the dynamic response of the equipment in the low-frequency region of primary concern, the number of parameters needed for the mathematical model generally is not excessive. Often, just a few simple measurements may suffice to evaluate these parameters. For example, observation of the decay of free vibrations produced by an impact or by plucking (deflecting and releasing) a component, with and without disabling the isolation systems, can provide information on the natural frequencies and damping of the structural components and isolation systems. The currently available sophisticated computerized modal analysis systems and system identification (parameter evaluation) codes can, of course, also provide the desired modal and transfer function information.

Figure 7 illustrates criteria for two modern pieces of optical equipment, developed by their manufacturers on the basis of direct transfer function measurements. Also shown is a criterion curve developed by us for one of these same equipment items by use of a two degree of freedom model derived from simple field measurements. One may note that the two corresponding criterion curves agree well with each other, with the differences probably ascribable primarily to the way that the actual information was represented by simple envelope curves.

By comparing Figs. 4, 5 and 7 one may also observe that the more rationally developed criteria of Fig. 7 are less stringent than the older, less defensible, criteria—particularly at the low frequencies. Wider availability of such more rationally derived criteria thus may reduce the severity of the vibration control problems that need to be addressed in the design of microelectronics manufacturing facilities.

CONCLUDING REMARKS

It is apparent that there exists a need for reasonable facilities vibration criteria that neither overstate nor understate the sensitivity of microelectronics manufacturing equipment.

Such facilities criteria can best be developed from corresponding criteria for the equipment. Much of the available equipment criteria information is inadequate; the derivation of realistic specifications from measured transfer functions or analytical models is recommended.

Structural dynamics considerations appear often to have been given inadequate attention in the design of microelectronics manufacturing equipment. Although most sensitive equipment items are furnished with air-spring isolation tables, for many little effort appears to have been made to optimize the isolation systems (e.g., in terms of decoupling of modes and use of two-stage isolation). Many equipment items could also benefit from modifications that increase the dynamic rigidity of the structure interconnecting the optical column and the image stage, that result in greater modal frequency separation, that provide significant increases in structural damping, and that reduce vibrations produced by internal sources such as stepping motors.

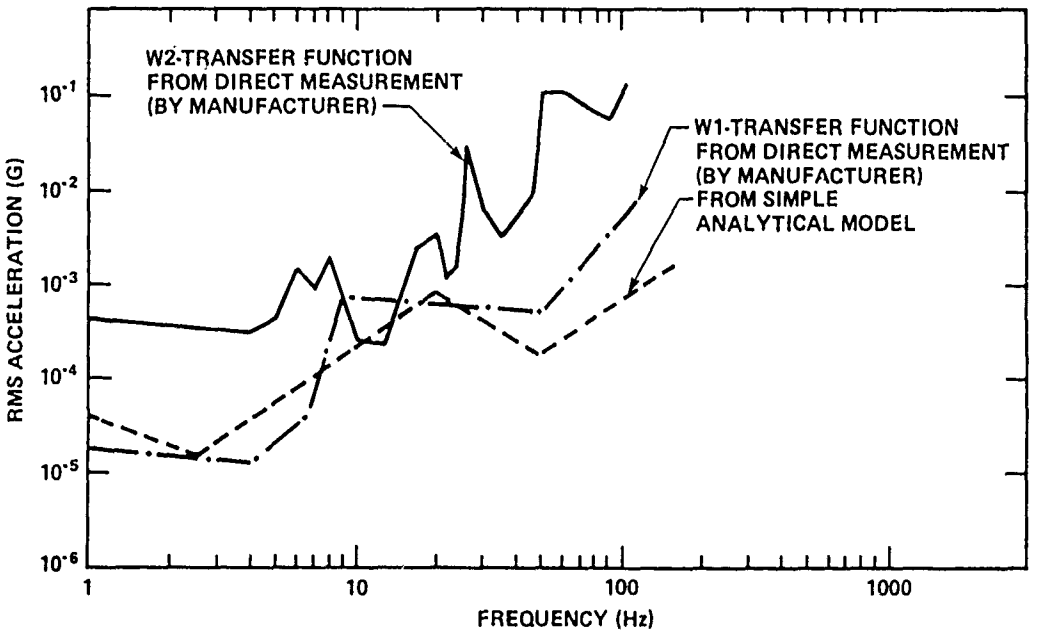

Fig. 7 — Narrow-band vertical floor vibration criteria for 1μm line width, developed from floor-acceleration/-image-displacement transfer functions.

MAURICE BIOT 50th ANNIVERSARY LECTURE
THE EVOLUTION OF SPECTRAL TECHNIQUES IN NAVY SHOCK DESIGN

Gene Remmers
David Taylor Naval Ship Research and Development Center
Bethesda, Maryland

INTRODUCTION

The purpose of this paper is to commemorate the 50th anniversary of Maurice A. Biot's initial development of spectral techniques to calculate stresses in structures which are subjected to dynamic loads from transient motion excitation. The evolution of this basic and very important work to U.S. Navy shock design applications is described in three parts. The first part is principally a historical account of Dr. Biot's contributions covering his Ph.D. thesis in 1932 (1), the mechanical analyzer in 1941 (2), and the application to engineering seismology in 1942 (3). The second part describes the U.S. Navy shock design methods of the 1940's, including the initial application of Biot's approach in 1948. The subsequent discovery by the Navy of the importance of and proper accounting for equipment-ship interaction effects is covered. The third part describes how this application was refined during Navy shock design development from 1959 to the present.

PART I CONTRIBUTIONS OF BIOT

The general problem addressed in Biot's theses is the calculation of the maximum stresses of a building structure which are induced by earthquake motion as shown in Figure 1. A distinctive characteristic of this problem is that neither the location of nor the severity at the excitation source causing the earth motion is known except in general terms. It is necessary to use some manifestation of the excitation source such as motion on or in the vicinity of the building. The most useful manifestation of the excitation source is the motion of the ground at the base of the building. This is shown conceptually in Figure 2 where, for convenience in writing this paper, the dynamical properties of the building are represented as a dynamical chain of three masses and springs, with motion oriented to the vertical. This is not the model used by Biot. He used a three mode shear beam to analyze the building's response to horizontal motion.

BEFORE BIOT

For perspective, the principles of the analytical methods that were known just prior to Biot's thesis are described.* By using normal mode theory the dynamical properties of the building could be represented by a set or series of normal mode oscillators which have the property of independently responding to the base motion. An actual building would have a normal mode for each degree of freedom which are very large in number. Figure 3 shows how the somewhat simplified three degree of freedom building model of Figure 2 is represented by three normal mode oscillators, each having an effective mass and frequency. The response of each informal mode oscillator to the base motion, Z(t), could be calculated separately with the Duhamel integral shown in Figure 3. These normal mode responses could then be superimposed in a complicated relationship, Equation (44) of Reference 4, to go back and compute the response of each mass of the dynamical chain. Next the time history of the relative motion across the springs of the dynamical chain could be examined to find the maximum deflections of the springs from which the maximum stresses could be calculated and compared to the yield stresses of the materials. In this way one could predict if a given building would be damaged by that earthquake. The limited computational aids of the day made this method impractical, if not impossible, to use.

*(NOTE: These are not necessarily the analytical methods for calculating earthquake stresses in actual use at that time. Also, for general clarity, the terminology that resulted from the later Navy developments described in (4) is used throughout this paper.)

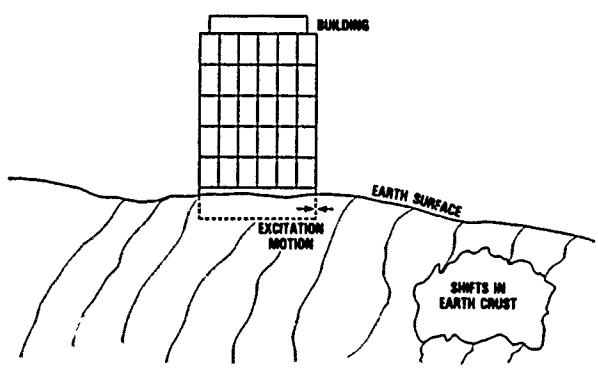

Fig. 1 — Shock design problem for earthquakes

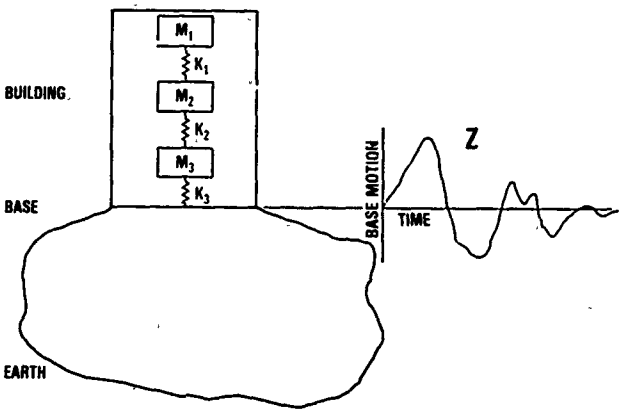

Fig. 2 — Dynamical chain representation of the building responding to base motion

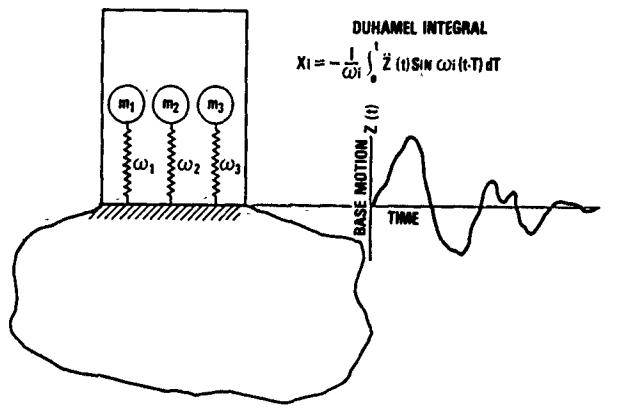

Fig. 3 — Normal mode representation of the building

1932 — BIOT'S THESIS

The engineering science conducted by Biot was to develop the concept of acceleration spectrum (now called shock spectrum) which allowed the calculation of the structural parameters to be separated from the calculation of the base motion response. He also showed how to pick a small number of modes which were adequate for engineering purposes and how to use the response in these modes to calculate an upper bound to the stress induced by earthquake motion.

He defined the acceleration response spectrum (shock spectrum) to consist of the maximum response motion values of each of a set of simple (single-degree-of-freedom) oscillators covering the design frequency range. The definition of shock spectrum is developed in Figure 4 where the equation for response of an oscillator to base motion $\ddot{y}$ is divided by the acceleration of gravity g to give a dimensionless quantity. The result is the maximum absolute acceleration (in number of g's) is equal to the maximum relative displacement across the spring of the simple oscillator, which is the shock spectrum value at frequency ω. Note that this equation shows that the shock spectrum value is independent of the mass of the oscillator so long as it has frequency ω. This very interesting feature will be addressed in a later section on interaction effects.

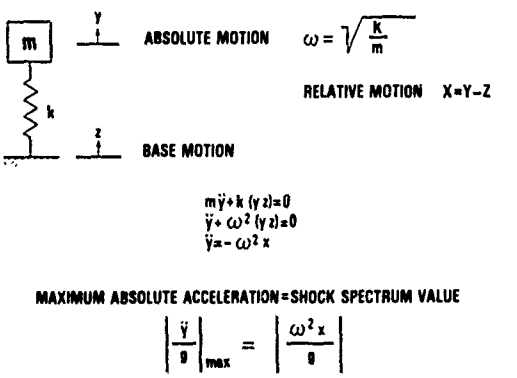

Fig. 4 — Definition of shock spectrum value from response of simple oscillators

Biot observed that each normal mode of the modal representation of a building behaves like a system with a single degree of freedom; therefore, the concept of an input spectrum could be applied to each mode separately. Figure 5 shows how the tedious Duhamel integral calculation was avoided by reading the maximum response directly from the spectrum plot at the frequencies ω of the normal modes.

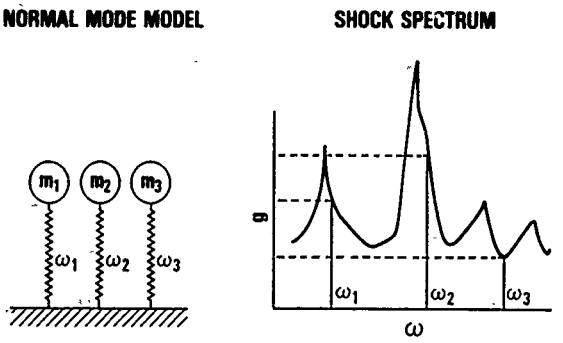

Fig. 5 — Maximum response of normal mode oscillators read directly from shock spectrum

He also showed that the number of modes that need be considered for maximum stress calculations can be rather small in number. The building was modeled as a shear beam responding to horizontal motion (instead of the dynamical chain used in this paper). After calculating the first three frequencies and mode shapes, he showed that the deflection of the top of the building resulting from their sum was 94 percent of the deflection that would result if the building had only one degree of freedom. He concluded that the first three modes were a sufficient number to consider.

In summary, Biot developed the concept of shock spectra which gives a rather good direct characterization of the severity of an earthquake, much more so than the recorded transient motion which gives little indication of severity. Solution of the design problem (involving an infinite set of integrals, each multiplied by a time varying function) was simplified to using the first few terms of the infinite series and replacing the time varying function associated with each term with a single value of each function (i.e., shock spectrum value). This gives a good approximation to the upper bound of the stress in a structure imparted by base motion. The only significant limitation to Biot's work is the traditional assumption in the field of engineering seismology that the motion of the earth is not affected by the dynamic properties of the building. The means of dealing with this limitation and an assessment of its significance will be discussed later. Nevertheless, this approach to calculating shock induced stresses became the basic method which is still used to this day.

1941 -- TORSIONAL PENDULUM ANALYZER

While Biot's thesis showed how the calculation of building stresses were made much easier with the use of shock spectra, the process of computing shock spectra with the Duhamel integral was still a tedious and time consuming process. Biot turned his talents to developing a torsional pendulum analyzer (2) which is a mechanical analog of the Duhamel integral. Understanding the function of this device gives insight to how a shock spectrum represents the damaging potential of earthquake motion.

An isometric view of the torsional pendulum apparatus is shown in Figure 6. An input record is traced on the strip chart of the upper paper drive. A transparent pickup arm with fixed crossline rests above the input record chart and is clamped to the piano wire from which the pendulum is supported by a precision bearing pivot. The natural angular frequency of the pendulum bob shown in the middle of Figure 6 can be adjusted by adding or moving the weights in and out from the center. A bar attached to the underside of the pendulum serves as a recording stylus arm for the lower paper drive.

As the record runs by on the upper paper drive, the operator moves the pickup arm to follow the excursions of the input record tracing with the cross-line. Torque applied to the piano wire in this manner causes the pendulum to undergo angular displacement in response to the waveform of the input record. The response is traced out by the stylus on the paper of the lower recorder.

A sample record from this device is shown at the bottom of Figure 6. The angular displacement response can be seen to build up to a maximum and after the transient motion is complete the displacement settles down to a steady amplitude called residual shock spectrum which will be discussed later. (Note that this response time history is the Duhamel integral response calculation at one frequency.) The maximum displacement of the response shown is the shock spectrum value at this frequency. This maximum displacement characterizes the damaging potential of the input motion at this one frequency. This process is repeated for each frequency chosen and in this manner a plot of shock spectrum values over a frequency range of interest is determined.

Application of the torsional pendulum analyzer to calculation of the shock spectrum of the motion of the side plating in the Flag Cabin of the USS CANBERRA (CA 70) is depicted in Figure 7 which is taken directly from Reference 5. Figure 7a is the recorded shock motion of the plate due to a secondary-battery salvo. Figure 7b is the maximum relative displacement of a simple oscillator driven by the shock motion as calculated by the pendulum analyzer. This involved adjusting it to 31 different frequencies. The bottom curve, Figure 7, is the middle curve scaled by ω^2/g to come up with a pure number ration of shock spectrum g values.

The torsional pendulum analyzer was claimed in its day to be a big time saver over hand calculation of shock spectra. Even so, it took a pair of experienced operators about eight hours to compute one shock spectrum of about 30 frequencies. Nevertheless, enough earthquake shock spectra could be computed to apply Biot's approach to building design.

1942 — APPLICATION TO ENGINEERING SEISMOLOGY

Shock spectra computed from recordings of basement motion of several buildings that were subjected to at least two different earthquakes were studied by Biot and applied to calculation of stresses and building design (4). In doing this, he made several observations that affected his recommendations on the use of spectra in design. First, he found that the damaging potential of a single earthquake varied greatly from one building to the next in the same neighborhood. Second, he found that the frequencies of the peaks in shock spectra are not constants within the same neighborhood when comparing two Ferndale, California earthquakes. (The reason for these observations are discussed later in the Navy developments part of this paper.) From the second of these observations Biot concluded that the individual sharp peaks of the shock spectra were unimportant in design. (Later Navy developments led to the same conclusions but for a different reason.)

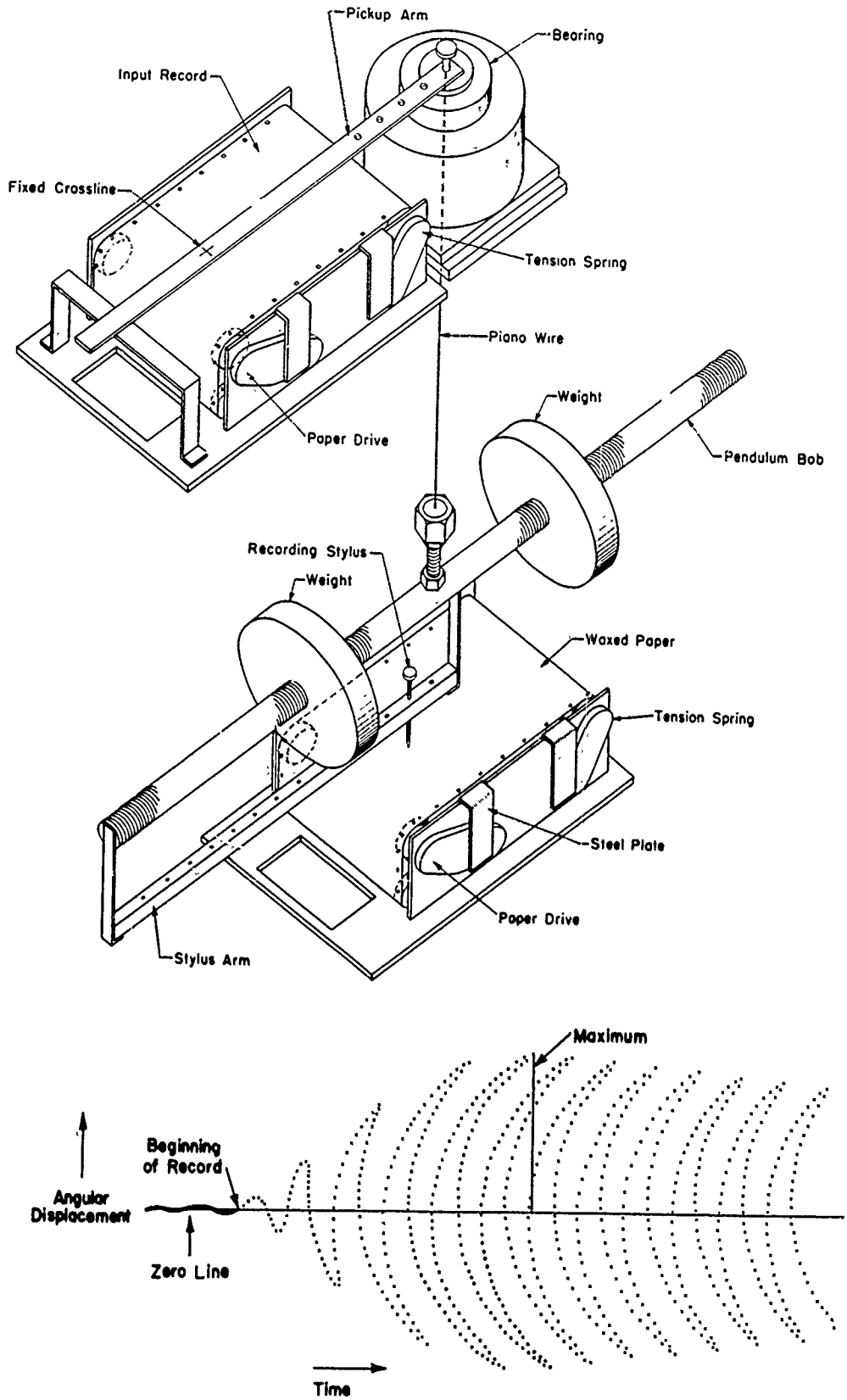

Fig. 6 — Torsional pendulum analyzer and example of response to transient input (from TMB Report 567)

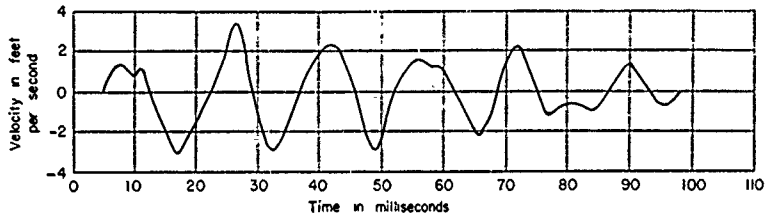

(a) Shock motion due to a secondary-battery salvo, recorded as velocity of panel of side plating in flag cabin of the USS CANBERRA (CA70)

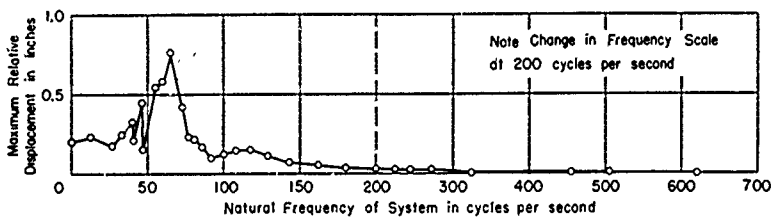

(b) Maximum relative displacement of systems with a single degree of freedom driven by shock motion shown in Fig. 7a

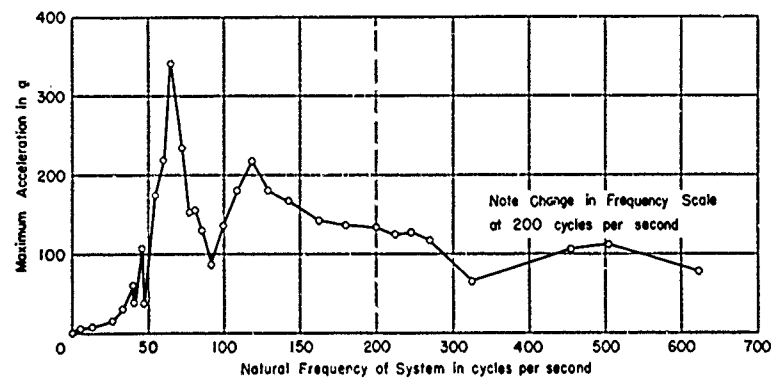

(c) Maximum acceleration of systems with a single degree of freedom driven by shock motion shown in Fig. 7a

Fig. 7 — Shock motion in flag cabin of USS CANBERRA (CA70) and resulting relative displacement and acceleration spectra (from TMB Report 567)

This led Biot to recommend using the envelope of a collection of spectra from the same location as the basic information for design purposes. This conservative approach, illustrated in Figure 8. assured adequate strength for any and all of the recorded earthquakes.

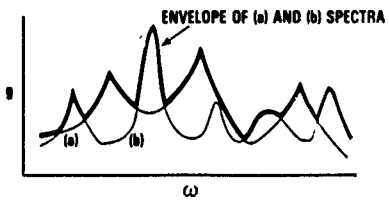

Fig. 8 — Illustration of envelope spectra formed from two shock spectra

However, when this envelope of shock spectra was used to go back and calculate the design stresses in those same buildings, the calculated stresses were much higher than the stresses observed during any one earthquake. He concluded that the envelope of the spectra constituted an upper design limit due to factors that tend to reduce the observed stress. He suggested that these factors might be damping, plastic deformation, variation of period with amplitude and influence of foundation. He stated that influence of foundation consisted of internal friction in nearby soil, radiation of elastic waves into the soil by the building and rotational components. His commendable candor about these observations shows that he was confronted with the fact that building motion might be interacting with the motion of the nearby earth, but he didn't pursue it. This served to make the overall method more conservative as will be seen later.

These accomplishments by Biot described in the first part of this paper formed the basis for Navy development shock design methods described in the rest of this paper.

PART II — NAVY DEVELOPMENTS

Generally speaking the U.S. Navy underwater explosion shock problem consists of two concerns for both ships and submarines which can be seen by referring to Figure 9. One concern is the integrity and watertightness of the hull structure while the other concern is that the integrity of the equipment E (which represents machinery, combat system components, and other items) be as great as the hull integrity when exposed to underwater warhead explosion. This paper addresses the equipment only and does not address the hull response problem.

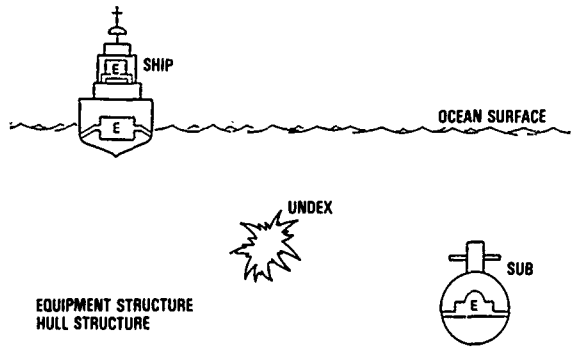

Fig. 9 — Shock design problem for ships

In principle the equipment shock response problem could be dealt with by choosing several worst case charge sizes and locations from which stresses appearing in equipment could be calculated by working from the explosive charge characteristics through the water medium to the response of the wetted hull structure, then through the intervening decks, bulkheads and other items to the response of the equipment. This is a very extended calculation that has not been practical. Fortunately, this problem is greatly simplified if one has recordings of response motion at the base of the equipment support taken during full scale ship shock trials, and uses Biot's method. The analogy to the earthquake design of buildings is shown in Figure 10.

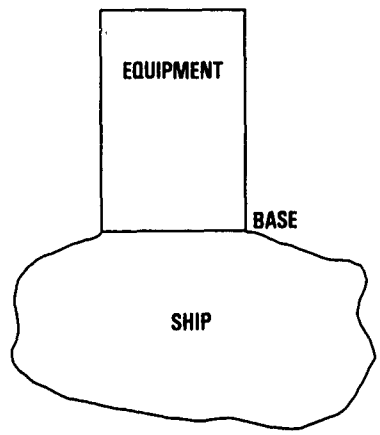

Fig. 10 — Analogy to earthquake design

A chronological description of the use and improvements to Biot's shock spectrum techniques by the Navy follows.

1942 — REED GAGE

An early Navy application of Biot's work was the development of the reed gage in 1942 by Dr. Bernard Miller at DTMB. The reed gage is beautiful for its simplicity because it is a passive mechanical device that directly records the shock spectrum of a transient motion.

It consists of a set of tip mass loaded cantilever beams (reeds), shown in Figure and described in (6), that were tuned to frequencies spanning the range of shock design concern. When mounted at the base of shipboard equipment in need of shock hardening during a full scale shock trial, the maximum response of each reed (oscillator) is recorded by the stylus attached to the tip mass of each reed. This set of maximum responses is the shock spectrum. The same reed gage could be mounted on a shock machine along with the same equipment in need of hardening and be used to establish that the severity of the machine tests duplicated the severity of the full scale shock environment.

Principal limitations to the reed gage were in its crude frequency resolution, the fact that the reeds are not simple oscillators, and the weight of the device, 20 pounds and up depending on the number of reeds. Nevertheless, it was used extensively in hardening equipment by means of shock machine test.

1948 — BIOT ENVELOPE SPECTRA APPLIED TO NAVY EQUIPMENT

The application of envelope spectra to the design of shipboard equipment began in about 1948 (7), again with the finding that this resulted in a considerable overdesign. In some cases, it was not possible to go back and design individual equipment items to be strong enough to survive the levels of the envelope shock spectrum, even though these same equipment items had survived the separate shocks from which the envelope spectrum was formed. Relaxing the envelope spectrum levels by using an envelope of the lower 90 percent of all the points was proposed as shock testing machine levels (8). These were called fiducial limit shock spectra. Again consistent over-design resulted.

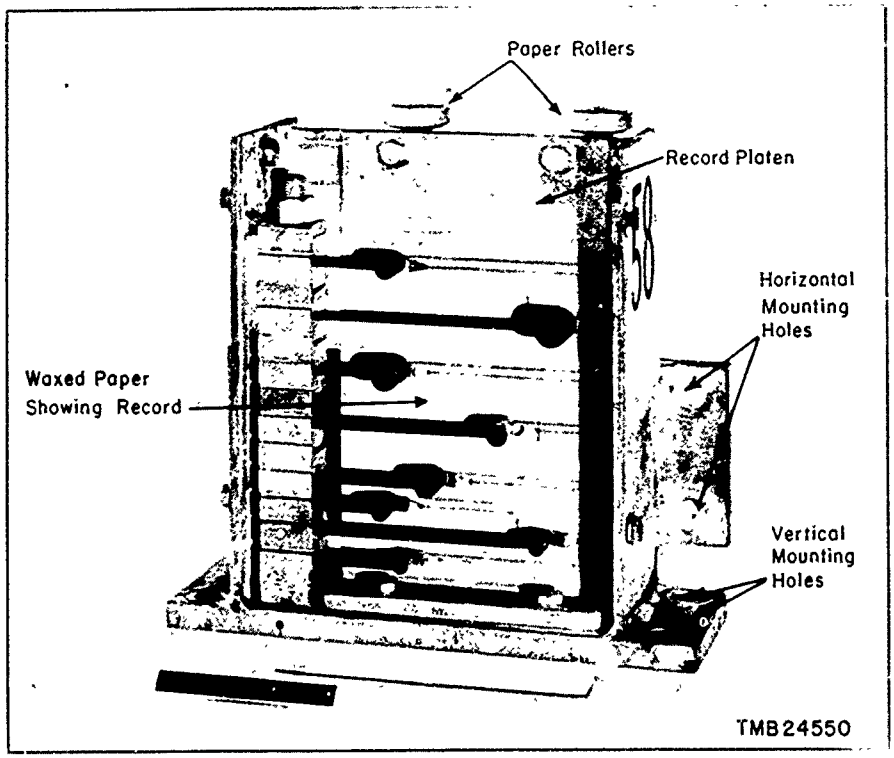

Fig. 11 — Photo of a reed gage (from DTMB Report 613)

1957 -- SERENDIPITY -- SHOCK SPECTRUM DIP

Effects of equipment ship structure interactions had been observed in ship shock trial measurements over the years where heavier equipment responded with lower shock levels than lighter equipment. This is somewhat intuitive and also indicates that equipment items interacted with the ship structure and thereby affected the shock spectrum levels at the base of the equipment. Probably because the equation for shock spectrum values shown in Figure 4 clearly shows that spectrum values depend only on frequency, Navy developments generally didn't pursue interaction effects until strange results in reed gage response were serendipitously found during a full scale shock trial.

For two equipment items, one of the reeds of the reed gage mounted at the equipment base gave unexpectedly low response to the shock motion. Careful analysis of the dynamic response characteristics of these equipment items showed in each case a normal mode natural frequency (also called fixed base natural frequency to be defined later) of the equipment exactly corresponded to the frequency of the reed with very low response. This was called the shock spectrum dip effect and the importance of interaction effects for naval application was recognized (9).

The dynamical chain representation of the building shock problem shown before in Figure 2 (valid for the assumption that the surrounding earth approaches being infinitely massive and rigid with no interaction with the building) becomes the dynamical chain representation shown in Figure 12 where the rest of the ship structure must be considered as part of the dynamical system.

FEATURES OF NORMAL MODE REPRESENTATION OF STRUCTURES

The next Navy development was an important experiment which established the equipment-ship interaction effects. It will be easier to understand this experiment in terms of several features of the normal mode representation of structures, some of which were developed by the Navy after the interaction experiment.

Figure 13 shows three progressively larger portions of the dynamical chain structure of Figure 12 are replaced by normal mode representations. In Figure 13a only the top mass is replaced with the modal mass m_{a1} equal to the structural mass M_1 and the mode frequency γ_{a1} equal to $\sqrt{K_1/M_1}$. In Figure 13b the top two masses and springs are replaced by two normal mode oscillators with masses and frequencies as shown which differ from those of Figure 13a. Similarly, for Figure 13c the three degree of freedom part of the structure is replaced with three normal mode oscillators as shown again with modal masses and frequencies different from those of Figures 13a and 13b. Note that Figure 13c represents the equipment-ship system of Figure 12 with the equipment portion represented by a normal mode modal. The motion of and the forces through M_4 the attachment point of the equipment to the ship, is made identical for all three systems in Figure 13 (which includes the original dynamical chain structure of Figure 12) by setting two conditions which are shown in Figure 14. First condition is that the normal mode frequencies be the fixed base natural frequencies of the equipment structure (i.e., the natural frequencies that would occur if the equipment were attached to an infinitely rigid and immovable base). Notice that these frequencies do not necessarily appear as resonances in the structural

system. Second condition is that the sum of the modal masses equal the mass of the equipment. This second condition can be used as a convenient indication of how many normal modes are required to adequately model a structure in stress calculations. The equation for modal mass in terms of structural mass given in (4) is also shown in Figure 14. Now we can go to the interaction experiments.

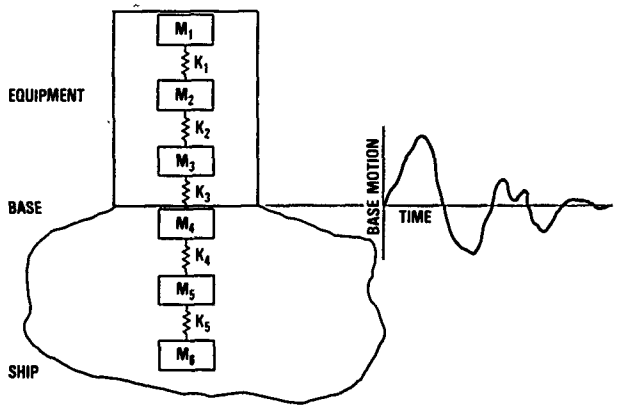

Fig. 12 — Dynamical chain representation of the equipment-ship system

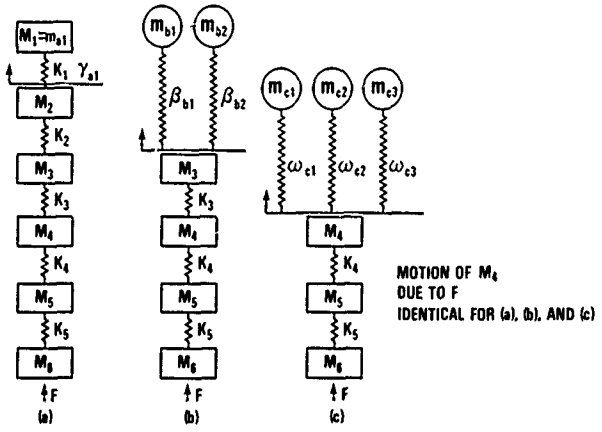

Fig. 13 — Illustration of replacing parts of structures with normal mode models

1958 — STUDY OF EQUIPMENT INTERACTION

Equipment-ship interaction effects were explored in an experiment (10) which studied changes in the mass and stiffness structural parameters of the equipment. Results demonstrated that measured shock spectra are quite sensitive to the natural frequencies of the equipment structure and that the peaks in a shock spectrum are caused by system natural frequencies. The really important aspect of this experiment, however, was discovering that shock spectrum values to be used for design are at the equipment fixed base natural frequencies which tend to be near the valleys or dips, not the peaks of the spectrum. This showed potential extreme overconservatism in design could result from use of either envelope spectra or fiducial limit spectra.

Arrangements of the experiments is shown in Figure 15. Special features of the test structure used to simulate equipment consist of the two parallel rectangular beams separated by spacer blocks shown at B and the adjustable mass attached to the upper beam center. The lower beam was attached to a supporting fixture at D while the supporting fixture was bolted to four mounting points on a shock machine table. Two different stiffness parameters for this test structure could be chosen by having the spacer blocks in either position A or position B between the beams. Stiffness could be varied while keeping the mass constant and vice versa. Base motions were measured by the velocity pickup from which shock spectra were computed.

Variation of stiffness resulted in the shock spectra shown in Figure 16. The stiffer configuration A gave a different peak in the shock spectrum than the less stiff configuration B because the natural frequencies of the entire dynamical system changed. Yet test structure frequencies (equipment fixed base natural frequencies) at which one would normally read shock levels off the spectrum for calculation of stresses are shown to be at the dashed lines just above the frequency scale of Figure 16. They are not anywhere near spectrum peaks.

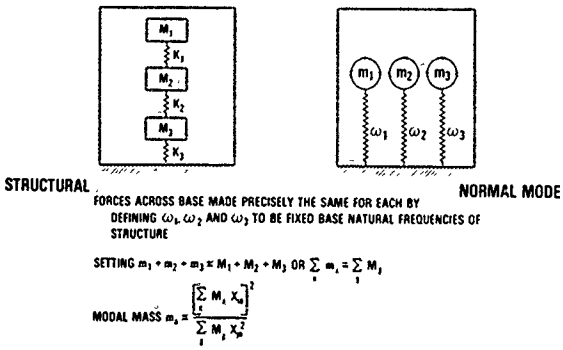

Fig. 14 — Conditions for equating the normal mode model reaction to the equipment structure reaction

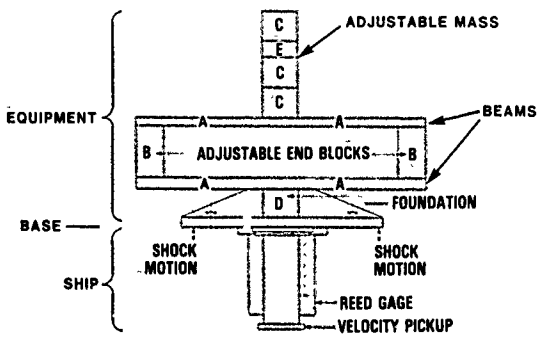

Fig. 15 — Equipment interaction experimental arrangement (from NRL Report 5236)

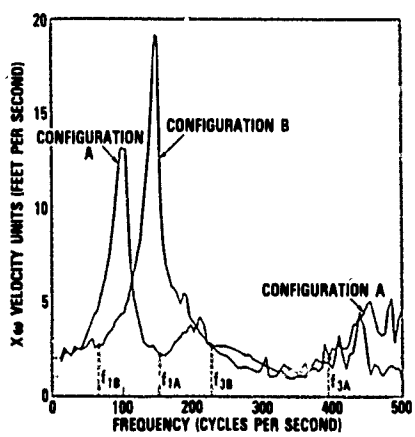

Fig. 16 — Effect of Varying Equipment Stiffness on Shock Spectrum (From NRL Report 5236)

This explains Biot's earlier observation of the variation of shock spectrum peak frequencies. The system frequencies cause the peaks and these system frequencies depend strongly on interaction effects.

Potential for over-design from using peaks or envelope shock spectra is illustrated. Assume the shock-spectrum from configuration B is part of an envelope spectrum that is used to design an equipment with the same mass but the different stiffness, configuration A. One goes to frequency f_{1A} (fixed base frequency of the first normal mode of configuration A) and the spectrum level read would be on the peak of configuration B shock spectrum. Since the correct level for design at f_{1A} is on the configuration A shock spectrum, over-design by a factor of 7 or 8 results.

The envelope of the peaks from all variations of mass and stiffness in this experiment are shown in Fig. 17 along with an envelope of the minimum from the same spectra. The black dots are the shock spectrum levels at all of the fixed base natural frequencies which are the correct levels to use in calculating stress. These correct levels lie much closer to the minimum envelope than to the envelope of the peaks, which was the basic criteria for design prior to this experiment.

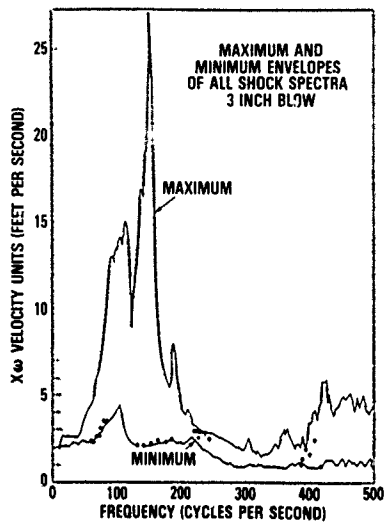

Fig. 17 — Comparison of Shock Spectrum Levels for Design, Shown by Black Dots with Maximum Envelope and Minimum Envelope of Shock Spectra

EFFECT OF EQUIPMENT INTERACTION ON SHOCK SPECTRUM

With the importance of interaction effects established the definition of shock spectrum given in Figure 4 will be examined. Whether or not the assumption that no interaction occurs entered into this definition is not clear. The equation has been taken to show that stress calculations based on a shock spectrum depends only on frequency. The difference between system frequency and fixed base natural frequency was not addressed. Yet the increasing of both the mass and the stiffness by the same large factor can be hypothesized such that an extremely massive and stiff oscillator with the same frequency would result. By intuition this will affect the input motion.

Inspection of the equations of motion of the first two masses of a dynamical chain shown in Figure 18 reveals where the interaction effects appear. The equation of motion for M_1 is seen to depend only on frequency just as the definition of Shock Spectrum Values. The equation of motion for M_2 shows that changes in spring K_1 appears as a modification of the motion of M_2.

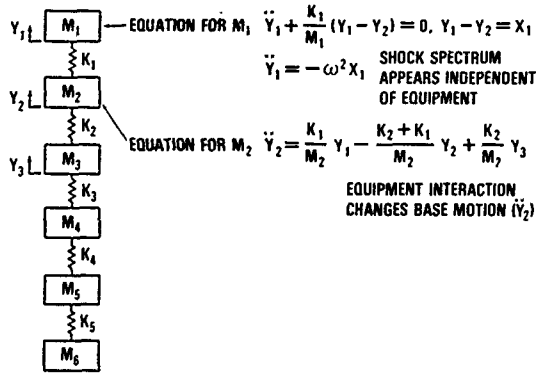

Fig. 18 — Equipment interaction effect on shock spectrum

In other words the definition of shock spectrum does not change. Interaction effects appear as changes to the input or base motion. The original shock spectra remain fully valid for calculation of stresses when interaction effects are accounted for so long as the spectrum values at the fixed natural frequencies of the equipment are used.

1959 — DESIGN SHOCK SPECTRA

A theoretical study of equipment-ship interactions (11) defined a design shock spectrum to be a set of maximum values of the relative displacements of simple oscillators that are functions of both normal mode frequencies (equipment fixed base natural frequencies) and a function of the modal masses. This appears to define a surface depending on mass and frequency which is used for determining shock input design levels. The author of (11) no longer prefers the term "design shock spectrum" as a result of further developments decided in Part III.

PART III — REFINEMENTS AND FURTHER DEVELOPMENTS

Experience from applications of the Navy developments to various shock design problems produced additional insights and refinements described in this part of the paper. Aids and special techniques in measuring and using shock design values for use with Biot's methods are presented along with an examination of limiting factors.

RESIDUAL SHOCK SPECTRUM

Maximum excursion in the response amplitude of a simple undamped oscillator excited by a transient input base motion has been defined as the shock spectrum value at that frequency. The simple oscillator response amplitude that remains after the transient decays in called the residual shock spectrum value. Residual shock spectrum is shown to be mathematically equal to the input motion Fourier spectrum magnitude (12). When a residual shock spectrum is plotted on the same graph as the shock spectrum the dips or valleys in residual shock spectrum indicates the fixed base natural frequencies at which to read the shock design values.

The cause of these dips can be seen by looking at the dynamical chain representation of the equipment ship system in Figure 12. Response levels at the fixed base natural frequencies of the equipment tend to be the nulls in the base motion which in turn appear as minima in the Fourier spectrum magnitude of the base motion. Thus, dips in a residual shock spectrum indicate the equipment fixed base natural frequencies, but not unambiguously. The part of the dynamical chain below the base also can cause nulls in the base motion. Even with this ambiguity, this aid has been useful in determining shock design values.

REVISION OF EARTHQUAKE SPECTRUM SUGGESTED

A paper at the 1960 Earthquake Conference in Tokyo (13) suggested a revision of earthquake specta along the lines of Navy design shock spectra for shock design values. This has not been done so far. Over-conservatism from using envelope spectra is offset somewhat by use of a less conservative method of combining the stresses from each mode. The net conservatism appears to be about a factor of two, unlike the extreme conservatism found in Navy applications, and the original method of Biot has always worked well for building design.

MEASUREMENT OF MODAL FREQUENCIES AND MASSES

Design shock spectra are functions of both mass and stiffness parameters of the equipment. Collection of these shock design values from equipment base response during ship shock trials requires determination of normal mode frequencies (for stiffness parameters) and modal masses.

Determination of equipment normal mode frequencies with a vibration generator was studied analytically (15) with the discovery that the vibration could only be applied at the base of the equipment. The tendency had been to place the vibration generator at the top of buildings of equipment (i.e., top mass of the dynamical chain of Figure 12, apparently because it caused the greatest response of the entire system. Reference (14) showed it is not possible to measure equipment normal mode frequencies fixed base natural frequencies with the shaker at the top. The first experimental measurement of fixed base natural frequencies of an equipment while in a larger dynamical system (equivalent to Figure 12) was made in (15).

The first experimental measurement of the modal masses of an equipment test structure was accomplished in (16). At this point, measurement of both the mass parameters needed to define the design shock spectrum had been established.

EFFECT OF DAMPING ON DESIGN SHOCK VALUES

Presence of damping in equipment-ship systems can affect measured design shock spectrum values. Results of an analytical study of these damping effects (17) on a dynamical chain system is shown in Figure 19. Shock spectra of the motion of M_4 for three levels of system damping are shown. The additional damping has a strong effect on the peaks of the spectra which correspond to the system natural frequencies, however, the effect on shock spectrum levels at the fixed base natural frequencies, shown by the dashed line arrows, are rather small. Thus, design shock values are reduced by a small amount by the presence of damping.

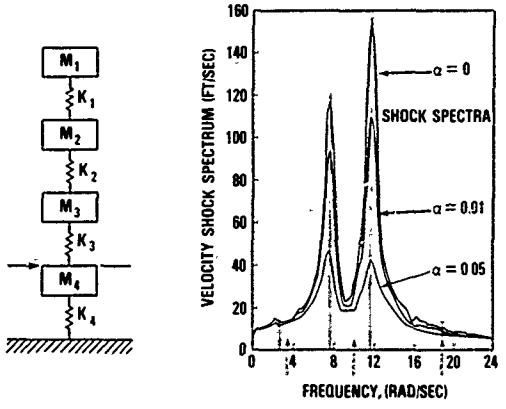

Fig. 19 — Effect of damping on design shock values

EFFECT ON NEARBY STRUCTURE

Presence of a second mode or a nearby structure can affect the level of design shock spectrum values. The significance of this effect was studied in (18) where design shock values for a simple structure by itself were compared with the design shock values for the same simple structure with a roughly comparable structure nearby. Conceptually, the results are shown in Figure 20 where a level of 10 for the lone structure would be reduced roughly to a level of 9 by the presence of the second structure. It was determined that design spectrum values are relatively insensitive to the effects of a second mode of structure nearby.

EFFECT OF YIELDING ON DESIGN SHOCK VALUES

Severe shock motions can cause yielding in either the equipment of the ship. The problem of interpretation of measured shock responses for determining design shock values when yielding occurs has been studied in (19) and (20). Figure 20, also described in (21), illustrates the results of increased amounts of yielding. A design shock level sufficient to produce 90 SKI stress in the foundation was assumed to result from the shock motion. Foundations with yield stresses ranging from 30 KSI to 150 KSI at the fixed base natural frequency were assumed to exist, so long as the foundations remained elastic (i.e., for the 100 KSI and 150 KSI cases) the elastic shock design value would be measured. When yielding occurred, the shock design values are seen to be higher than the elastic case, the highest value for the greatest yielding. Should the shock design values from the tests with equipment foundation yielding be used to design an equipment to elastically survive the shock, the design levels would be more severe than necessary.

On the other hand, when yielding occurs in the ship, the measured shock design values will lie below the elastic value. Equipment designed with these shock design values (yielding in the ship) will be inadequately designed and subject to failure in the shock motion environment.

CONCLUSION

Evolution of the concept of shock spectra to the concept of design shock spectra has been described. Exploration of some limiting effects in Part III has shown that a design shock spectrum covers a small band of values rather than a more defined surface. This band of values is quite adequate for equipment design purposes. Thus, the use of the term shock design value has come to be preferred when referring to shock input information.

The original work of Dr. Biot has endured very well over the past 50 years and has been very important for U.S. Navy applications.

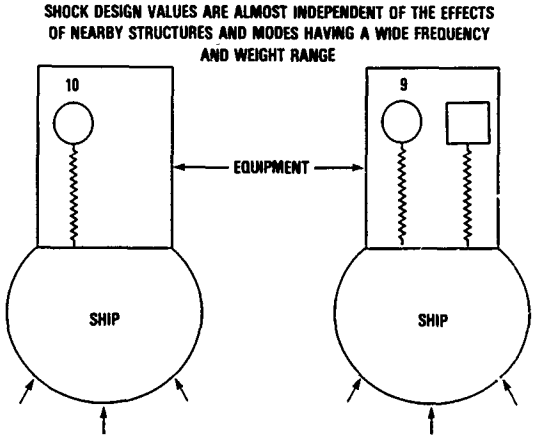

Fig. 20 — Effect of a nearby structure

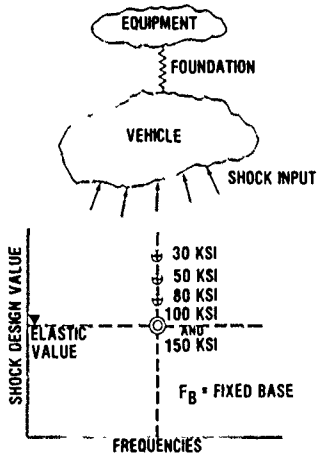

Fig. 21 — Effect of yielding on design shock values

ACKNOWLEDGEMENT

Inspiration for writing this paper was provided by George J. O'Hara of NRL. He also provided valuable guidance and generous assistance in assembling the reference material.

REFERENCES

1. "Transient Oscillations in Elastic Systems," by Maurice A. Biot, Thesis No. 259, Aeronautics Department, California Institute of Technology (1912).

2. "A Mechanical Analyzer for the Prediction of Earthquake Stresses," by M.A. Biot, Bulletin of Seismological Society of America, 31:2 (Apr 1941).

3. "Analytical and Experimental Methods in Engineering Seismology," by M.A. Biot, Proceedings of American Society of Civil Engineers (Jan 1942).

4. "Elements of Normal Mode Theory," by G.J. O'Hara and P.F. Cunniff, NRL Report 6002 (15 Nov 1963).

5. "Response of Systems with a Single Degree of Freedom to Shipboard Shock Motions," by S. Fifer and R.D. Specht, TMB Reprot 567 (Oct 1947).

6. "A Theoretical Study of the Multifrequency Reed Gage for Measuring Shock Motion," by Samuel Davidson and Emily J. Adams, DTMB Report 613 (Jul 1949).

7. "The Equivalent Static Accelerations of Shock Motions," by J.P. Walsh and R.E. Blake, NRL Report F-3302 (21 Jun 1948).

8. "Design Criteria for a Shock Testing Machine for Heavy Weight Submarine Equipment," by R.E. Blake and J.D. Gossett, NRL Memo Report 254 (Jan 1954).

9. "Effect of Equipment Dynamic Reaction on Shock Motions of Foundations," by R.O. Belsheim and R.E. Blake, NRL Reprot 5009 (Oct 1957).

10. "Effect Upon Shock Spectra of the Dynamic Reaction of Structures," by G.J. O'Hara, NRL Report 5236 (16 Dec 1958).

11. "Shock Spectra and Design Shock Spectra," by G.J. O'Hara, NRL Report 55386 (12 Nov 1959).

12. "Impedance and Shock Spectra," by G.J. O'Hara, JASA, 31:10:1300 (Oct 1959).

13. "The Meaning of Spectra of Earthquake Records Obtained In or Near Structures," by Merit P. White, Tokyo Earthquake Conference (Summer 1966).

14. "Resonance Testing in the Determination of Fixed Base Natural Frequencies of Shipboard Equipment," by L.P. Petak and R.E. Kaplan (15 Dec 1964).

15. "Experimental Technique for Determining Fixed-Base Natural Frequencies of Structures on Non-Rigid Attachment Points," by G.M. Remmers and H.C. Mayo, NRL Memo Report 1800 (31 Aug 1967).

16. "Measurement of a Structure's Modal Effective Mass," by G.J. O'Hara and G.M. Remmers, Shock and Vibration Bulletin 39 (Jan 1969).

17. "Structural Interaction Effects on Shock Spectra," by P.F. Cunniff and R.P. Collins, JASA, 43:2:239 (Feb 1968).

18. "The Effect of a Second Mode and Nearby Structures on Shock Design Values," by G.J. O'Hara and L.P. Petak, NRL Report 6676 (5 Apr 1968).

19. "Yielding Effects on Shock Spectra," by W.R. Mentzer, Jr. and P.F. Cunniff, SVIC Bulletin 36 (Part 2) (Jan 1967).

20. "Yielding Effects on Design Shock Spectra," by G.J. O'Hara and H. Huang, NRL Memo Report 3862 (Sep 1978).

21. "Efficient Elastic-Plastic Design of Small Foundations," by G.J. O'Hara and P.F. Cunniff, NRL Report 4918 (22 Sep 1982).

DISCUSSION

Voice: How does the recent work of Kelly and Sackman tie into Dr. Biot's work?

Mr. Remmers: I am not familiar with the work of Kelly and Sackman. I think the essence of the question is do the earthquake people still use envelope spectra, or do they use the Navy approach? I really don't know first-hand if that is the case, but I am told by students of earthquake design that they still use the old envelope spectra of Biot.

MATERIALS IMPLICATIONS OF ADVANCED THERMAL AND KINETIC ENERGY THREATS

Robert Fitzpatrick
John Mescall
Army Materials and Mechanics Research Center
Watertown, MA 02172

INTRODUCTION

Directed energy threats open a new frontier in the area of military research and technology. In general, directed energy refers to Lasers, Microwave Systems, and Particle Beam Devices (Fig. 1). Directed energy systems are capable, at least in theory, of depositing energy onto a target thereby causing damage. The damage is generally a result of very rapid and intense heating which results in structural failure, or failure of sensitive electronic materials due to thermal overload.

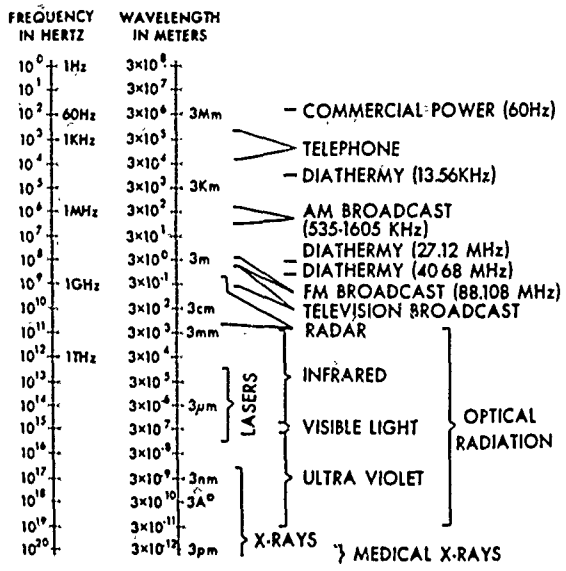

Fig. 1 — The electomagnetic spectrum

For purposes of this discussion, my remarks will be concerned with directed energy as applied to Lasers, because Lasers represent the threat with which we will have to deal in the near term. The discussion will be limited principally to the behavior of materials subjected to laser radiation rather than issues of target acquisition, pointing and tracking, fire control, and damage recognition. These target acquisition and fire control requirements represent extremely difficult technological problems that must be solved if the Laser is ever to be used as a weapon against hard targets. Questions that must be resolved are outlined as follows:

- Can laser beams be propagated over large distances along predictable paths?
- Can available active and passive countermeasures be overcome?
- Is there a place for large scale, high power, high value directed energy weapons on the battlefields?

While these questions are being addressed, the Army materials community is developing a data base on materials and structures vulnerability. This data base will not only serve the hardening community, which has the task of offering protection against directed energy, but also will help the weapon developers determine the effectiveness of their systems.

Laser Technology

The Research and Development Community has produced families of lasers that use various mediums (gas, liquid, and solid) to produce coherent radiation over a wide range of frequencies and powers. These lasers can operate from the ultraviolet to the infrared region of the electromagnetic spectrum, while ranging in power from a few milliwatts to mega-watts of power and operate in continuous or pulsed mode. (Fig. 2)

Not surprisingly low energy lasers have already found their way into the military inventory. Uses include lasers for designating targets, range finders, illuminators, simulators, and training devices.

Military Lasers can be divided into three broad categories: Low energy lasers, which can be hazardous to the eyes and sensitive electro optical devices; medium energy devices which can destroy optical elements, ignite fuel, or destroy highly stressed components; High energy devices capable of vaporizing materials, detonating explosives, and fracturing missile cases.

Low Energy Lasers

Low energy lasers used by the military operate within the band pass of the eye, and therefore, represent a serious threat to personnel. Personnel in combat must be concerned about vulnerability to conventional projectiles as well as intense laser radiation. The soldier's telescope, binoculars, and other optical aids will greatly increase his vulnerability to eye injury from lasers operating in the visible and near infrared region of the spectrum.

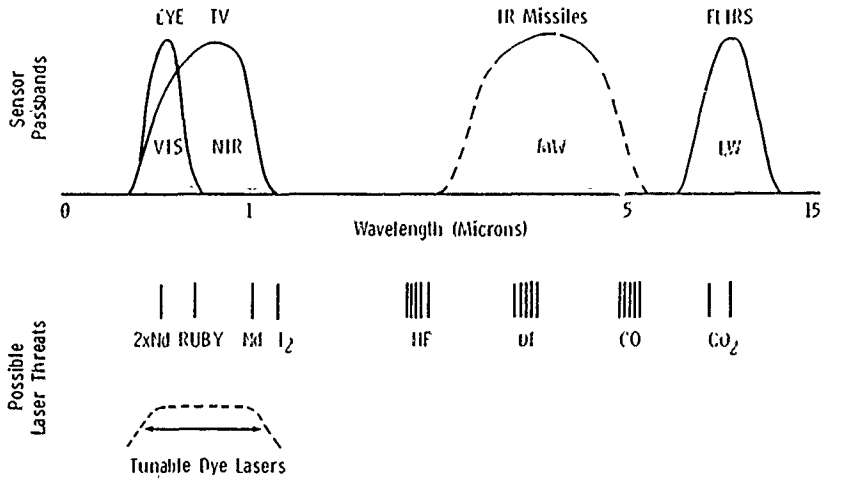

Fig. 2 — The in-band laser threat

The blink response time of the human eye is approximately 0.15 seconds, while a pulse of visible laser light requires only 10 to 20 nanoseconds to cause lesions on the macula which will result in a blind point in the center of the field of vision.

Laser damage to the eye depends on many factors, including laser intensity, optical magnification, angle of incidence day or night adaption of the eye at time of exposure, and the overall health and age of the individual being exposed. In addition, the effects of eye exposure to lasers will be strongly dependent on the tasks being carried out by the effected invididual. Momentary flash blinding of a passenger in a ground vehicle may be of little consequence, while the same exposure to a pilot maneuvering his aircraft could result in a fatality.

Medium/High Energy Lasers

Medium and High Energy Lasers operate in the infra-red region of the electromagnetic spectrum. These lasers are low energy devices also operate in either the pulsed or continuous wave mode.

During the mid-1970's, a number of critics pointed out that it would be difficult to destroy targets of military interest using high energy lasers. Pointing and tracking difficulties, jitter caused by the vibration in the laser platform, and atmospheric effects such as thermal blooming, energy absorption by moisture and dispersion by aerosols all contribute to a reduction in the total energy that can be placed on a target. Clearly these arguments have merit, and one may wonder why the materials community would develop a data base, or be concerned about a threat from a high or medium energy laser. The reason why a data base on materials effects is necessary and is being developed, is that many sub-systems that main battle platforms depend upon are very sensitive to modest amounts of energy that can be accurately delivered. For example, optical materials including glass and plastic absorb virtually 100% of the energy in their thin outer surface layers, thus catastrophically damaging the surface of the optical materials. (Fig. 3) Image intensifiers, T.V. systems and infra-red sensors are designed to act as eyes in the same portion of the electro magnetic spectrum as many lasers operate, Hence, a device that is designed to operate with weak signals in the microwatt range are destroyed when exposed to a few watts of power. Early arguments concerning target vulnerability centered on hole burning as a means of destroying materials, while totally ignoring the stress state of the target being irradiated. (Fig. 4) A stressed aircraft wing or drive train component operating at 80% to 90% of its design load will quickly fail if heated a few hundred degrees above ambient temperature. In some cases failure can occur as a result of the formation of quench cracks that develop upon rapid heating and cooling of metal alloys. Another phenomena that was not appreciated until recently, involves the very large increase in energy absorbed by aluminum targets that are irradiated with lasers powerful enough to form plasmas on the surface of the material. Normally a smooth aluminum surface will reflect 97% to 99% of the 10.6 micron radiation emitted by a CO_2 laser. If one calculates the amount of energy required to melt a hole in a given amount of aluminum, considering that 99% of the energy is reflected, one might conclude that a very large laser would be required. Interestingly enough holes can be produced in aluminum with much less energy on target than was originally thought to be necessary. Laser radiation at sufficient levels to ignite a plasma at the surface will produce large amount of ultra violet (UV) radiation. (Fig. 5) The reflectivity of the aluminum at the UV wave lengths is much lower than that at 10.6 microns and hence the target material absorbs many times as much energy per pulse.

In addition to the enhanced absorption due to the shift in wave length, laser supported combustion (LSC) waves impart stress on the heated metal surface. As the aluminum is heated the temperatures approaching the solidus temperature, the impulses caused by the LSC wave creates holes before actual melting takes place.

Testing of stressed composite structural materials which exhibit high absorptivity and poor thermal conductivity have been tested in wind streams with the result that the amount of energy required to cause tensile failure is lower than expected. The reason for the tensile failures of samples tested in a wind stream is due not only to radiative heating by the laser beam, but also to thermal conduction of energy transferred by debris blown downstream by the wind flowing over the surface of the target.

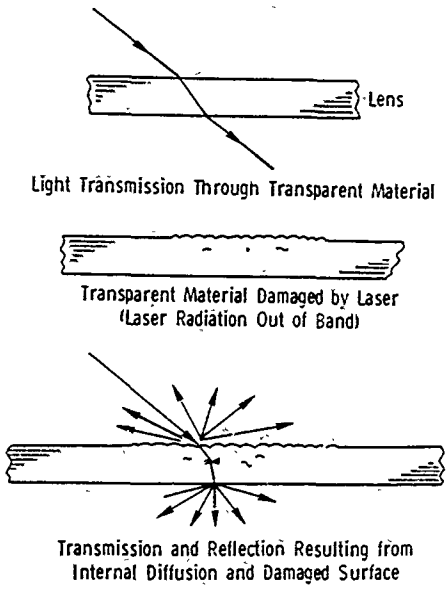

Figure 3

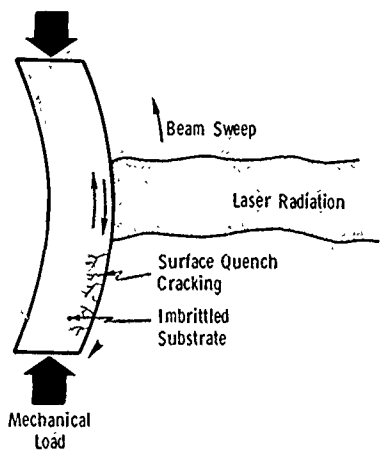

Fig. 4 — Laser irradiation of mechanically loaded materials

Materials Interaction

From the point of view of the weapons developer, a high energy laser must output more than 20 kilowatts of continuous power or a minimum of 30 kilojoules of pulsed power. From the materials scientist's point of view, high energy is defined as that level of energy impinging on a target that will destroy or damage the target. For example, a few tenths of a joule passing into an optical system may not be tolerated while a few kilojoules of energy on a re-entry vehicle surface may be inconsequential to that system.

Powerful CO_2 and chemical lasers can destroy hard targets by hole burning, destroy optical surfaces at distances of many kilometers, and have serious impact or electro-optical system at even greater ranges. Protection from damage due to laser radiation is a formidable task. Eye protection against visible lasers can be achieved using filters; however, tunable lasers cannot be countermeasured using filter technology.

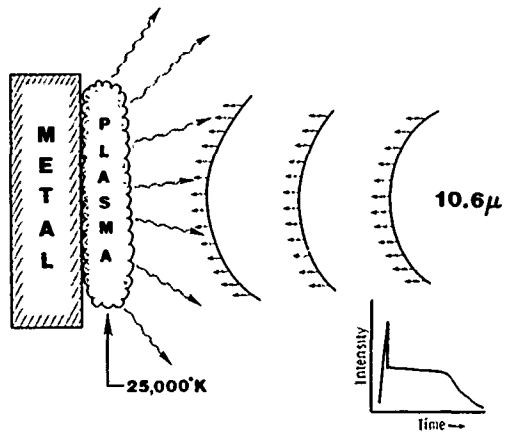

Figure 5

Presently, there is interest in developing fast acting optical switching schemes, which may be used in optical devices. These switching schemes include electro-optical devices using lead, lanthonum, zercoriuum titinate (PLZT),. (Fig 6); Self-destructing thin organic films, (Fig 7); and highly stressed metalic films, (Fig 8).

Survivability and vulnerability issues concerning laser irradiated mechanically loaded structures are truly challenging.

Modeling laser effects must account for wavelength, beam profile, beam power, pulse width, absorption coefficients, and angles of incidence. Experimental verification of computer codes on structural elements subjected to radiation from large high power lasers is very expensive. Given that every large high power laser has its own peculiar beam characteristics, it is difficult and expensive to gather large amounts of statistically significant information to be used as a data base. As laser technology matures, the amount of energy that can be precisely and instantaneously put on target will increase. The need for dealing with this threat is now becoming apparent. Within a few years many military systems will require that laser hardening protection be built into the system in the design stage of engineering development.

This morning I have raised some questions and hopefully made you aware of some of the technically challenging survivability and vulnerability issues associated with the directed energy threat. Dealing with the radiation from these new systems will be a challenge to the analysts, the design engineers, the planners, and management.

Kinetic Energy Threats

We turn next to the class of kinetic energy devices of interest to the Army. For this class of problems, energy levels are much higher than those discussed in the earlier portions of this paper. In larger calibre anti-tank weapons, for example, it is common to delivery up to 5 Megajoules of energy at the target. Clearly not all of this energy is used with one hundred percent efficiency, and this brings us to the central question of just what are the events which occur when a projectile strikes a piece of armor plate, or when a cylinder is filled with high-explosive and the latter is detonated.

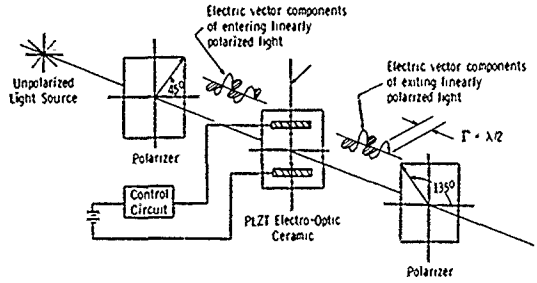

Figure 6

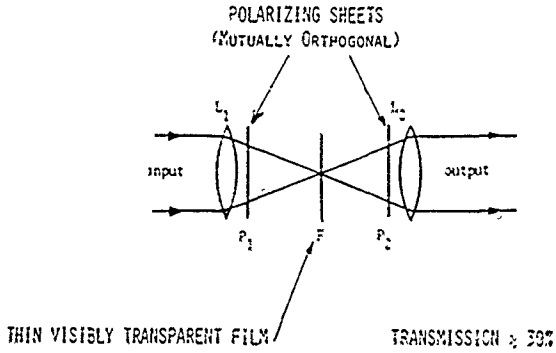

Fig. 7 — Dynamic eye protector

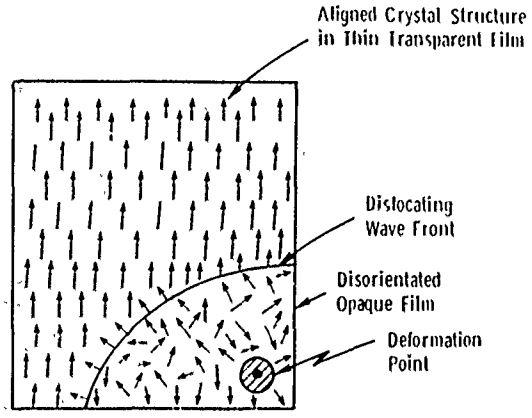

Fig. 8 — Ferroic fast-acting switch

Our SPECIFIC interest in these problems, all of which involve the development and propagation of shock waves in solids is to uncover the role played by material properties in these scenarios. By material properties we mean not only the mechanical strength (i.e., yield strength and flow stress) of a material but, more to the point, the nature of the fracture process (tensile or shear) and the quantitative details of states of stress and deformation leading to fracture under these highly dynamic conditions. Such conditions include peak stress levels of several hundreds of thousands of pounds per square inch, strain levels of fifty to one hundred percent and very short time duration—tens of microseconds.

We approach this stated problem by a combined theoretical and experimental program which I'd like to outline for you today, along with a few representative examples of progress.

The principal theoretical tool we employ is the HEMP code (1), a two dimensional finite difference computer program which solves the conservation laws (mass, momentum and energy) in two spatial dimensions and time. We are therefore able to treat problems of plane strain or ones with rotational symmetry.

As an illustration of the type of result obtainable with this approach, Figure 9 shows some details of the penetration process when a high density long-rod penetrator strikes a steel plate at an impact velocity of 5000 feet/sec. The details shown in Figure 9 are at 22 microseconds after impact. The mechanism of penetration occurring is primarily that of erosion; the projectile tip generates a cavity whose diameter is roughly twice that of the projectile. As the material at the projectile tip is compressed, it relieves the pressure by flowing backward out along the border of the cavity. Similarly, target material in front of the penetrator tends to flow in this general direction. If the target is deep enough (relative to projectile length and velocity), this process will continue until the entire length of the projectile is consumed. If on the other hand the projectile is long enough not to be consumed by the erosion process, then as the projectile tip nears the target's rear surface other penetration modes such as plugging and tensile cracking will begin to enter the picture.

Some of this type of detail can be gleaned from dynamic experimental observations and from cross-sections of the post-mortem targets. Computer simulations are able to provide additional insight by detailing the states of stress and strain within the interior of the projectile-target regions. Figure 9b shows isobars of constant pressure at 22 microseconds. By studying a sequence of such contours, we can infer a great deal about the stress states associated with the erosion process. It turns out that there are essentially three phases associated with such impact conditions. There is an initial shockphase characterized by very high states of stress (in this case 400 kilobars) and very short duration (in this example three microseconds). The second phase is characterized by a quasi steady state condition in which moderate compressive stresses persist in a non-oscillatory manner for a much longer period of time (in this example fifty kilobars and fifty-plus microseconds). Figure 9b shows conditions at 22 microseconds, but plots from 10 to 40 microseconds look very similar, with the principal difference being the movement of the projectile-target interface.

A key observation is that the intense stress waves set up during this second stage do not propagate away from the region of the interface; they remain within what we term a processing zone. This concept has several interesting characteristics which have important ramifications for both kinematic and material property issues. We note that the third

stage of the penetration process does not begin until some new element is introduced such as the process zone nearing the target rear surface or the projectile tail entering the process zone. This final stage is characterized by an oscillatory low amplitude stress state representative of those associated with structural vibration.

Some of the characteristics of the processing zone are as follows: It is fairly small in spatial extent—its diameter is roughly twice that of the penetrator. Its center is at the projectile-target interface and it moves with that point in time. Duration of the second stage is controlled by target thickness, projectile length and velocity.

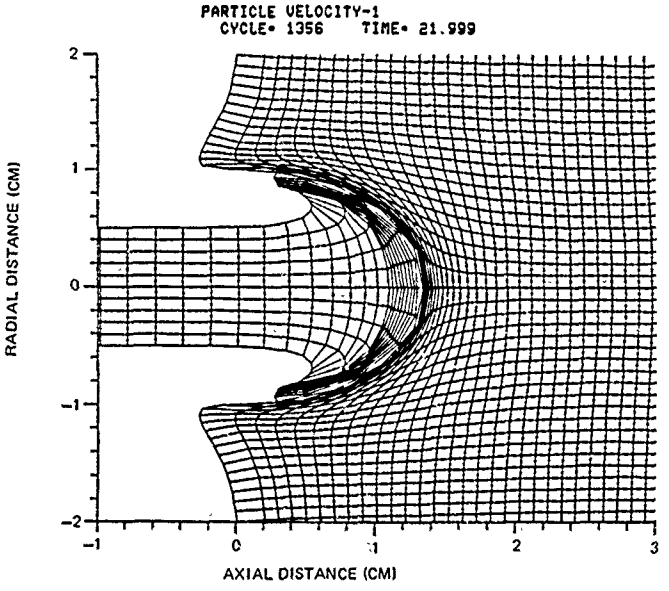

Fig. 9a — Computer simulation of penetration of steel target by DU long rod. Impact velocity was 5000 ft/sec.

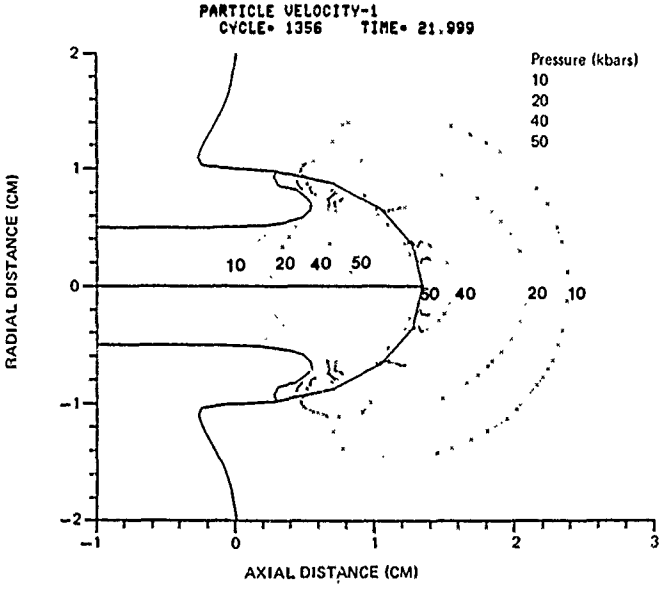

Fig. 9b — Pressure contours shown are in kilobars. They outline the active process zone of the problem.

Nearly everything of physical interest happens within the processing zone. Projectile material is decelerated only when it enters the zone, target material is accelerated only when the zone reaches it. This theoretical statement has been verified by experimental observations of the tail of the projectile entering the target. These kinematic characteristics further are consistent with and indeed help to explain several anomalies observed in ballistic testing. These include the shape of residual velocity versus impact velocity curves and depth of penetration versus impact velocity curves.

This fact that the dominant second stage of deep penetration is controlled by a steady compressive field of stress has important implications so far as mechanical characterization of materials for such applications is concerned. In particular it means we should know a great deal more about the compressive behavior of ordnance materials than we currently do. The natural tendency when evaluating a new alloy or a new processing procedure is to perform tensile tests to measure tensile yield or ultimate tensile strength, or to measure fracture toughness, mode I. The HEMP results displayed earlier and the process zone concept imply that we should expect little direct correlation between such tests and most ballistic environments.

One reason the compressive (or upset) test is so little used is that very little is known about the complex states of stress which result after barreling occurs. Note that to glean useful data from the upset test for ballistic applications, it is necessary to impose large strains and induce large triaxial stress fields. It turns out that there are a fair number of similarities between those states prevailing in the process zone and those in the upset test. In this context the HEMP code is very useful in providing information on the internal states of stress and deformation even for the static upset test. Figure 10 shows a comparison of a cross section of a 4340 steel specimen which has been reduced in height by roughly fifty percent along with the HEMP simulation of the same experiment. A careful study shows the agreement between the two is excellent.

Failure in such tests can occur in one of two competitive modes. The most commonly observed mode is initiated on the outer surface near the equator. Figure 11 shows an example for a high strength 4340 steel specimen which was reduced in height by seventy percent.

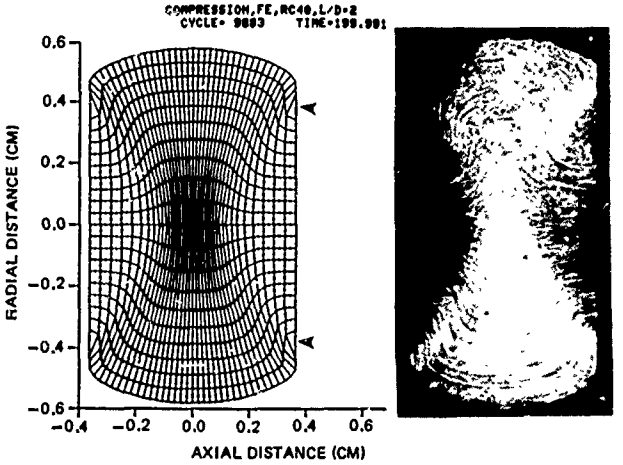

Fig. 10 — Comparison of experimental cross-section of compressed steel specimen with computer simulation of same test. 4340 steel specimen had been reduced-in-height by fifty percent. Arrows give location in deformed specimen of the material originally located on the specimen top surface. Material outside arrows was originally on curved cylindrical surface.

Fig. 11 — Cracked outer surface of upset steel cylinder after approximately 70 percent reduction-in-height

HEMP simulations reveal that the state of stress which produced such fracture pattern is one of biaxial tension, despite the nominally compression load. It is intuitively clear that as barreling of the cylindrical specimen proceeds a circumferential tensile stress develops along the equatorial outer surface. What is far less obvious is that the axial stress at this location gradually loses its compressive flavor and indeed becomes tensile prior to fracture. The intensity of the axial tension stress at the equator depends strongly upon the material and its heat treatment (2,3). The utility of the HEMP code in this context rests in its ability to determine the character and magnitude of stress and deformation fields under such complex stress states and associated large plastic strains.

The failure mode discussed so far in connection with the upset test is a tensile failure. There is another mode associated with shear which is also observed in the upset test, but which is far more pervasive. In fact it is observed to a greater or lesser extent in nearly every ordnance event.

In the upset test the shear mode of failure tends to be an internal one. It can occur in some materials along the boundary between a relatively undeformed zone (a "dead" zone) and the heavily deformed zone immediately adjacent to it. The contour labeled "d" in Figure 12 locates the region in which shear fractures sometimes occur, as shown in Figure 13.

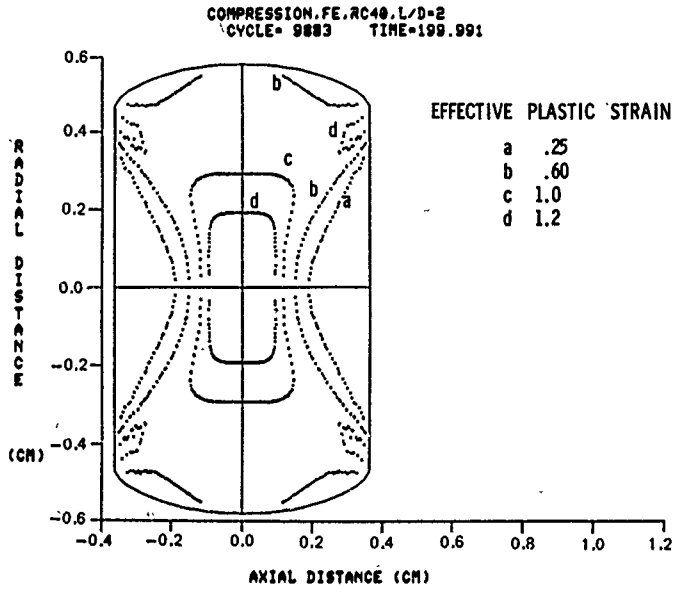

Fig. 12 — Contours of effective plastic strain within upset cylinder shown in Figure 10.

Fig. 13 — Interior fracture pattern in upset DU specimen. Of particular interest are cracks at 45 degree angle to compressed ends and their connection to maximum strain contours of Figure 12.

The shear mode of fracture is presently poorly understood. It generally consists of the sudden localization of a shear deformation field which has been proceeding in a relatively uniform manner. It is sometimes thought that this localization is precipitated by a thermal softening of the material which overwhelms the tendency of most materials to strain-harden. The temperature which produces softening arises from the deformation process itself. It has been observed in dynamic torsion tests that some materials exhibit a maximum in their stress-strain curve, which is suggestive that the thermal effects are beginning to dominate and to produce a so-called plastic instability.

To examine some of the implied consequences of a material having such an instability in its constitutive law, we studied numerically (using HEMP) the problem of a slab of material being deformed in pure shear under plane strain conditions.

Consider the deformation of a rectangular block of material whose upper edge is held fixed while its lower edge is given a uniform velocity; the other two edges are free. Figure 14 shows that the deformation proceeds fairly uniformly until about 70 microseconds, after which a localization of deformation sets in and is well established by 100 microseconds. Most of the imposed deformation taking place after 70 microseconds is absorbed in the localized band.

It is important to note that this localization process does not occur in this numerical simulation if the material is represented by a conventional stress-strain curve with work hardening but without the plastic instability.

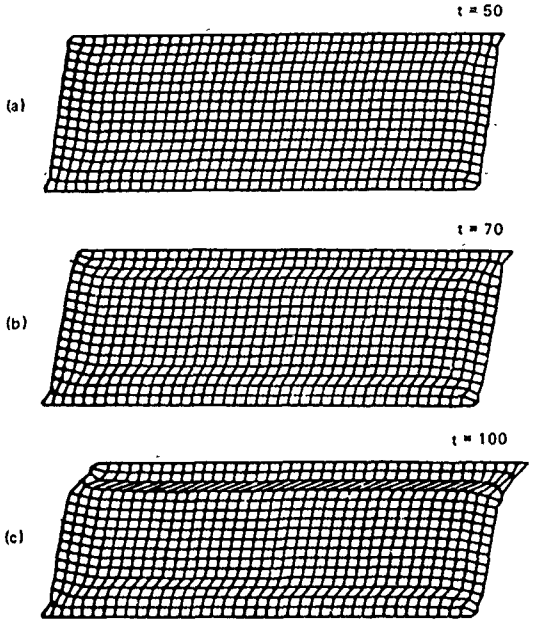

Fig. 14 — Computer simulation of the development of a localized shear band for a material with an instability in its stress-strain curve. Lower edge is moved relative to upper edge at 4000 cm/sec. Time is in microseconds.

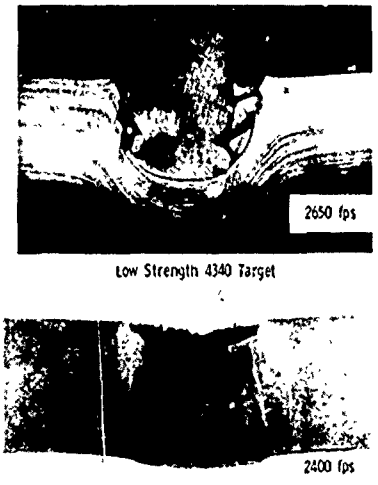

Fig. 15 — Differences in failure mode in steel targets. Adiabatic shear band present in high-strength target, not in softer target.

The consequences of the adiabatic shear band process (the plastic instability) in a ballistic sense can be seen in Figure 15, in which two steel targets were impacted by similar projectiles. The softer steel failed after massive plastic deformation by having a plug sheared out. It was expected that the impact velocity required to perforate the harder target would be higher than that required for perforation of the softer target. However, it may be seen that a new mode of fracture intervened and the perforation velocity was considerably less than might be expected. This new mode of fracture is clearly associated with an extreme localization of the shear deformation developing within the target.

We have attempted to illustrate some of the difficulties encountered in describing the role of material properties in kinetic energy devices employed by the Army and other DoD agencies. We have also shown how a combined theoretical/experimental approach is essential in the resolution of these difficulties. Clearly, much more work is needed in both approaches.

DISCUSSION

Mr. Lee (U.S. Army Tank Automotive Command). How do you get away with assuming the conservation of energy? It would seem like there would be a great deal of heat generated during the impact.

Mr. Mescall: There is, but we take that into account. In fact, we compute the heat generated, and we allow it to soften either the penetrator or the target. We take the plastic deformation which is generated, convert that into a temperature rise, assuming that all of the plastic deformation goes into heat, and allow that to soften. In fact, that is the thing that triggers the adiabatic instability, or the adiabatic shear instability.

REFERENCES:

1. Wilkins, M. L., Calculation of Elastic-Plastic Flow, Lawrence Radiation Lab., Livermore, CA, Rep. No. UCRL-7322, Rev. 1 (1969).

2. Mescall, J., Papirno, R., and McLaughlin, J., Stress and Deformation States Associated with Upset Tests in Metals, ASTM STP 808 (1983).

3. Papirno, R., Mescall, J., and Hansen, A., Fracture in Axial Compression Tests of Cylinders, ASTM STP 808 (1983).

Summary of MIL-STD-810D Panel Session

26 October 1982

Moderator: Mr. Preston Scott Hall, Air Force Wright Aeronautical Laboratories, Wright-Patterson Air Force Base, OH

Co-Moderator: Mr. Rudolph H. Volin, Shock and Vibration Information Center, Naval Research Laboratory, Washington, DC

Panelists: Mr. Preston Scott Hall, Air Force Wright Aeronautical Laboratories, Wright-Patterson Air Force Base, OH
Mr. Jack Robinson, U.S. Army Test and Evaluation Command, Aberdeen Proving Ground, MD
Mr. Robert Nichols, U.S Army Test and Evaluation Command, White Sands Missile Range, NM
Mr. Steven Strong, U.S. Naval Avionics Center, Indianapolis, IN

The purpose of this panel session was to receive user reaction to the changes in MIL-STD-810C. New test methods were added, and some of the existing test methods were extensively revised. The discussion was confined to the revisions in Method 514, Vibration, because the changes were the most extensive, they generated most of the comments, and many of the changes were controversial.

The most significant change is the requirement to tailor test schedules to the environmental conditions on the intended vehicle, using measured data. Other major changes in the vibration test procedures are an increased emphasis on the use of random vibration, the division of vibration test procedures into those that simulate transportation and those that simulate vehicle application, tests for engineering development, tests for flight worthiness, and tests for minimum structural integrity.

Jack Robinson reviewed the changes in the ground transportation vibration test schedules, and he provided the background and the rationale behind these schedules. The most significant change is the replacement of sinusoidal vibration with random vibration for simulating all transportation environments, including common carrier trucks and tactical wheeled and tracked vehicles. The test times and the default test schedules in this version of the standard were derived from data collected during their test methodology studies on a two wheeled trailer, a tactical wheeled vehicle and a tracked vehicle. Specific test schedules have not been developed for ground vehicle installed equipment, therefore, test requirements should be based on measured environmental data for the intended vehicle.

Robert Nichols described how Appendix 1 to Method 514.3 can be used to develop laboratory vibration tests from field data. He also discussed changes in testing procedures for simulating the helicopter vibration environment. Appendix 1 to method 514.3 contains a flow chart that provides an overview of all of the necessary steps for setting laboratory test requirements, and he used this flow chart to describe some of the more important steps for tailoring laboratory test schedules for simulating vehicle dynamic environments. He strongly emphasized the need to collect field data, and to use it to tailor the test specification to the intended vehicle.

Two important changes have been made to the test procedures for simulating the helicopter vibration environment. The first change is related to the test spectrum; it consists of a series of discrete frequency spikes, at the rotor passage frequency and its harmonics, superimposed on low level broad band random vibration. The second change is the division of the helicopter into several zones according to the source of vibration.

Steven Strong described the changes to vibration tests for shipboard equipment. Two tests will appear in MIL-STD-810D. One will be a default .001g2/Hz, 1-50Hz, white noise random vibration test. Several studies were examined, and their results showed that this test spectrum would cover most of the requirements to simulate shipboard random vibration. A sinusoidal vibration test in accordance with MIL-STD-167 (SHIPS) will also be required. The recommendation was made to continue testing shipboard equipment in accordance with MIL-STD-167 at the present time because there is nothing better. The existing levels in MIL-STD-167 envelope most of the measured data, MIL-STD-167 includes a search for equipment resonances to ensure that they don't coincide with shipboard excitation, and many report good experience with its use. However, fleet conditions could be different than those in MIL-STD-167 or the default random vibration test requirement,

therefore tests should be tailored by using measured data. Further, the Navy should examine MIL-STD-167 to consider the possibility of future modification.

Scott Hall described changes in test methods for equipment in propeller aircraft. The major source of vibration is a combination of aerodynamic low level broad band random vibration and complex periodic vibration due to propeller blade passage. As in the case of the other aircraft, propeller aircraft will be divided into zones according to the predominant source of vibration, and separate default test spectra will be proposed for each zone. The default test spectrum consists of four narrow band random vibration spikes superimposed on a low level broad band random vibration background. Flight data from the C-130 and the P-3 aircraft were used to derive the test requirements for the default spectrum.

Summary of the Discussion from the Floor

1. Many comments or questions concerned the test requirements for simulating the cargo transportation vibration environment.

   (a). It might be difficult to reproduce the multiple frequency break points in the tactical vehicle test schedules.

   (b). Stating the frequencies to multiple decimal places might lead to difficulties in satisfying test requirements because some digital vibration test control equipment might round off the frequencies to the nearest integer value.

   (c). Why not envelope the spectra?

   To answer these questions, several members of the panel pointed out their experience with digital vibration test control equipment. It is capable of reproducing a spectrum with multiple freqency break points; in addition, some test control equipment provides the frequency values in multiple decimal places instead of integers. The panel also stressed the fact that the test spectra shown in MIL-STD-810D are "default" values, to be used only where field data are not available. Users are encouraged to use field data to set laboratory test requirements.

2. Another question about transportation concerned the meaning of transportation vibration measurements, and how data from the test courses relate to the real-world transportation environment. The answer to this question was the test schedules derived from measurements made on test courses represent foreign theater transportation scenarios, exclusive of common carrier transportation.

3. It is not realistic to assume that transportation inputs to different points on large packages will be the same. What effect will the size of a package have on test requirements for simulating the transportation vibration environment? The answer to this question and comment was that the test requirements should be tailored to properly reflect service conditions.

4. Questions were raised about the possible overconservatism of the minimum integrity test, and what would be the impact of not running this test. The concern was the Minimum Intergrity Test conditions might be more severe than the field environment. The answer to this question was the test tailoring process in this version of the standard requires a rational environmental engineering plan to be developed early in the system's development program, and the need for various environmental tests should be determined then.

5. Another issue was the justification for using acceleration or exaggeration factors in developing test requirements. Further, specific factors should be defined. The justification for applying exaggeration factors is that one never knows if the worst case has been measured therefore, these exaggeration factors are factors of conservatism which are applied to cover this situation. There was no answer to the second part of this comment.

6. A question of whether we were going too far in requiring random vibration for simulating many of the vibration environments was raised. A specific example was the simulation of the vibration environment for equipment for propeller driven aircraft, which is a complex periodic motion. The justification for using random vibration is that the propeller aircraft test requirements were developed from C-130 and P-3 aircraft vibration data which contain a low level broad band random background with superimposed narrow band periodic "spikes" that are not necessarily at discrete frequencies. However, it is also possible to tailor the laboratory vibration test to include discrete sinusoids instead of the narrow band random vibration if warranted.

7. Several comments concerned parts of the standard that were not clear. These included:

   (a). The nature of the vibration spikes in the default test spectrum for equipment installed on helicopters. Answer: The spikes are intended to represent discrete frequencies.

(b). The definition of damage in paragraph I - 3.2.2.4(c) might conflict with the criteria for damage stated in an equipment development specification.

(c). The various test schedule curves should be linked to the appropriate references contained at the end of the vibration test method (Method 514.3). Answer: This change will be made in the final document.

(d). The standard does not state whether shipboard equipment shall be exposed to both the random vibration and the sinusoidal vibration tests. Answer: Both tests will be required.

(e). The flow chart in Appendix 1 is too complex to be understood by some acquisition personnel. The intent of this standard is to ensure that only qualified personnel use it to set test requirements.

PYROTECHNIC SHOCK AND SHOCK TESTING AND ANALYSIS

PYROTECHNIC SHOCK TEST AND TEST SIMULATION

M. E. Hughes
Martin Marietta Corporation
Orlando Aerospace
Orlando, Florida

Mechanical shock was measured at 18 locations during 5 ground tests of flight vehicle structures. The shock was generated by a linear shaped charge (LSC) cutting 0.063-in. aluminum skin to separate a reentry vehicle from a booster. Of the 5 tests, 4 used 10 grains/ft and 1 used 12.5 grains/ft. A maximum shock response spectra of 32,000 g was measured 5 in. from the LSC cutting plane. The data were statistically treated to define the source environment and distance attenuation. A pyro shock simulation fixture was developed for equipment testing.

INTRODUCTION

A major problem with the use of pyrotechnics is the prediction of shock to equipment.

There is no reliable analytical method available to predict shock transmissions in a complex structure. Therefore, most shock predictions are based on scaling of available data. At the start of design a literature search was performed to gather the most applicable data. Ref. [1] was found to be the most comprehensive source of shock information. However, sufficient data of similar ordnance charge and configuration size was not found. A ground test program was therefore developed. There were two types of tests performed:

1. Development tests to prove the functional capability of the separation system design and to collect shock data for equipment requirements.

2. Verification tests to prove the capability of the final design and to verify that the flight equipment would function properly after exposure to the shock environment.

The data collected during the development test were statistically treated to define the source environment and distance attenuation used to predict equipment requirements.

A shock simulation fixture was developed for equipment testing during the design phase and for qualification testing after design.

TEST DESCRIPTION

The test configurations were flight vehicle structures (a heatshield wrapped aluminum skin, fully equipped reentry vehicle (RV), and an empty motor section - see Fig. 1). The configuration for the development tests and verification tests was similar; however, there were three differences which affect the shock response characteristics: 1) missile section splice joints, 2) equipment mass loading, and 3) LSC and installation.

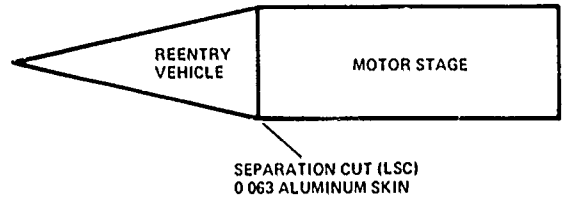

Fig. 1 - Test Configuration

The configuration was hung by four nylon straps with the missile centerline parallel to the ground. An axial load was applied to the motor section to represent drag and provide motor separation after the ordnance cuts. Bolted and bonded aluminum mounting blocks were used for all accelerometers except at two locations where equipment prevented bolting and only bonding was used.

Fig. 2 shows the typical accelerometer mounting. The heatshield shown is rubber

modified silica phenolic. Results of previous tests have shown the presence of this material to have a negligible effect on the accelerometer response.

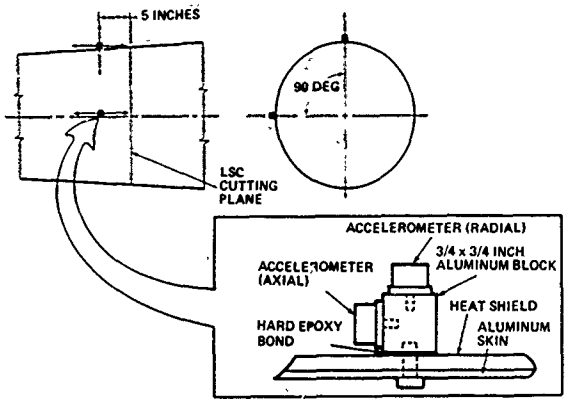

Fig. 2 - Typical Accelerometer Mounting

The data acquisition system was Endevco 2225 and 2225-M5 accelerometers, Endevco 2735 charge amplifiers, Honeywell 5620 wide band FM tape recorders, and a Spectral Dynamics 321 shock spectrum analyzer.

SOURCE SHOCK

The shock environment was generated by LSC cutting 0.063-in. aluminum skin to separate the RV from the booster. The source level was measured by 4 accelerometers per test located in pairs (radial and axial) 90 degrees apart on the RV circumference, 5 in. from the cutting plane (Fig. 2).

Recognizing that pyro shock data varies widely and requires statistical treatment, a test program was instituted to acquire the maximum possible experimental data base (using a single skin thickness) and processed with the same data acquisition system.

The results of these test are presented in Table 1 as the commonly used shock spectra peak g. The frequencies at which the peaks occurred varied from test to test and a plateau criteria (discussed later) was used that minimizes the peak and frequency dependence. The three development tests were identical and were all successful. However, a new ordnance vendor was obtained before the verification tests. Test 4 used the same size charge (10 grains/ft) as the development test, but failed to produce full skin penetration and separation. A new installation procedure and tolerance control and an increase from 10 grains/ft to 12.5 grains/ft for increased reliability was incorporated before test 5.

There is no significant or consistent difference between the axial and radial measurements of Table 1 as seen by comparing the test to test variations and averages for the development test. However, the data from test 4 and 5 require explanation.

Test 4 failed to produce full skin penetration or separations, but the ordnance went high order as expected. On this test note that both radial measurements were significantly higher than the axial measurements. In test 5, where both full skin penetration and separation occurred, both axial measurements were higher than the radial measurements. This difference suggests the possibility that when predominantly higher radial measurements occur, the ordnance is producing a near marginal cut.

A comparison of tests 4 and 5, which used charge sizes 25 percent different and produced the same average shock levels, suggests that the charge size had a second order effect on the shock levels.

TABLE 1

Source Shock Data
Skin Thickness = 0.063 in. Aluminum
$C/C_c = 0.025$

Shock Spectra Peak g

ORIENTATION \ TEST NO.		DEVELOPMENT TEST NO. 1	NO. 2	NO. 3	N	AVG	1σ	VERIFICATION TEST NO. 4	NO. 5
AXIAL	0 deg	7,800	11,000	11,000	3	9,933	1,847	23,000	27,000
RADIAL	0 deg	19,000	11,000	14,000	3	14,660	4,040	30,000	23,000
AXIAL	90 deg	21,000	12,000	13,000	3	15,330	4,932	17,000	32,000
RADIAL	90 deg	21,000	10,000	12,000	3	14,330	5,000	30,000	17,500
TEST AVG		17,200	11,000	12,500		13,556	4,170	25,000	24,875
1σ		6,340	816	1,290				6,271	6,142
OVERALL					12	13,556	4,381	N = 8 AVG = 24,940 1σ = 5,747	
TOTAL N = 20 AVG = 18,000 1σ = 7,681									

A comparison of the average values of the tests show that the verification tests are approximately 11,000 g higher than the development tests. This difference is attributed to the change in ordnance vendors. The previously mentioned configuration changes of mass distribution and splice joint occur more than 40 in. away from the source measurement and should have a small effect. Test 4 used the same installation and charge size as the development test. For the same charge size each vendor has a different design and fabrication procedure which affects the cutting plasma jet that produces the shock environment.

The local structural resonances of the unique structure being tested have a strong influence on the frequency and peak values of the shock spectrum. Therefore, a plateau concept was established to reduce this effect for comparisons of various locations and other configurations.

The plateau value was determined by judgment, i.e., fairing a curve between 2 kHz and 10 kHz at a constant g level, which represents an average of the peaks and valleys of the shock spectrum. This valve provides a more realistic comparison of energy induced into the structure than a comparison of peaks. Table 2 presents the test data as shock spectra plateau values. The test shock spectra are presented in Fig. 3 with the peak and plateau statistical data overlayed.

TABLE 2

Source Shock Data
Skin Thickness = 0.063 in. Aluminum
$C/C_c = 0.025$

Shock Spectra Plateau g

ORIENTATION \ TEST NO.		DEVELOPMENT TEST						VERIFICATION TEST	
		NO. 1	NO. 2	NO. 3	N	AVG	1σ	NO. 4	NO. 5
AXIAL	0 deg	4,000	9,000	9,000	3	7,330	2,886	14,000	21,000
RADIAL	0 deg	15,000	9,000	10,000	3	11,330	3,214	25,000	18,000
AXIAL	90 deg	16,000	3,500	9,000	3	9,500	6,264	13,000	20,000
RADIAL	90 deg	15,000	8,000	9,000	3	10,660	3,786	24,000	14,000
TEST AVG		12,500	7,375	9,250		9,708	4,037	19,000	18,250
1σ		5,686	2,625	500				6,377	3,095
OVERALL					12	9,708	3,954	N = 8 AVG = 18,625 1σ = 4,660	
TOTAL N = 20 AVG = 13,300 1σ = 5,940									

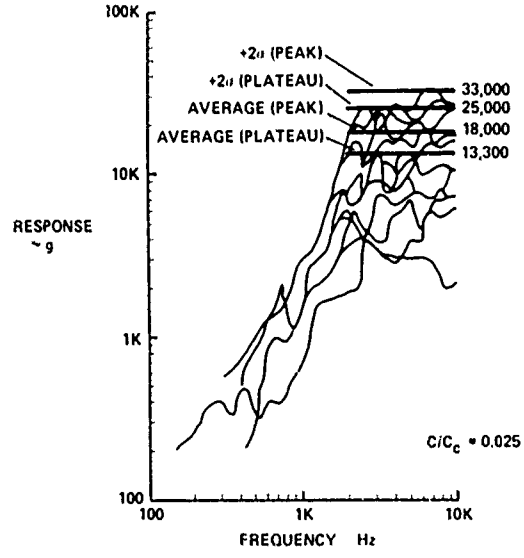

Fig. 3 - Source Shock Spectra Development and Verification Test

The data presented in Fig. 3 show a quantative comparison of the shock variation and criteria. As an example, the average plateau value +3σ variations = 31,000 g. The average peak value +2σ = 33,000 g. The values are approximately the same and in either case represent less than 3 percent probability of exceedence.

The results of these tests were correlated with 4 other full-scale shock tests. All configurations compared has diameters from 18 to 50 in. and lengths from 100 to 300 in. Three of these tests were in-house tests from other missile configurations which cut a 0.09, 0.10 and 0.135-in. aluminum skin. The fourth test was a Spartan test which cut a 0.17-in. aluminum skin (Ref. [1]).

The data for the 0.135-in. skin were corrected to reflect the same source location as the other test. The 0.135-in. skin test referenced a bulkhead location that is not on the primary skin shock path. Data were found on 3 tests that had the same source location as the other test and a measurement on a bulkhead similar to the 0.135-in. skin test. The average of

the ratio of g (source)/g (bulkhead) was 1.8, which was used to correct the data.

The g levels for correlation were directly related to the skin thickness by assuming that near optimum charge weights were used - therefore having a small effect. The assumption of correlation between skin thickness and shock is questionable to many; however, the results shown in Fig. 4 appear to support correlation.

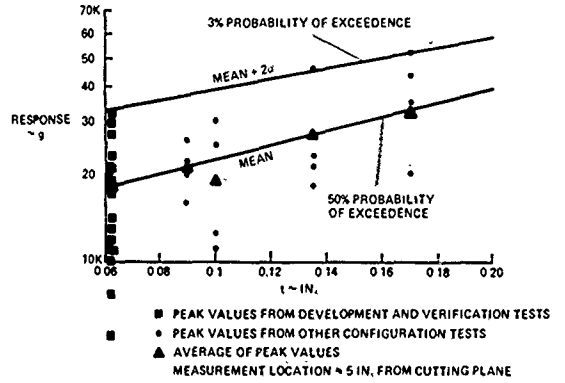

Fig. 4 - Expected Source Shock Spectra Peaks versus Skin Thickness

DISTANCE ATTENUATION

The distance attenuation was determined by measurements at 18 locations along the RV body. The distance attenuation measured reflects the uniqueness of the configuration (mass loading and stiffness characteristics).

A statistical evaluation of the development tests data was performed and Fig. 5 shows the results as a 3σ curve along the body.

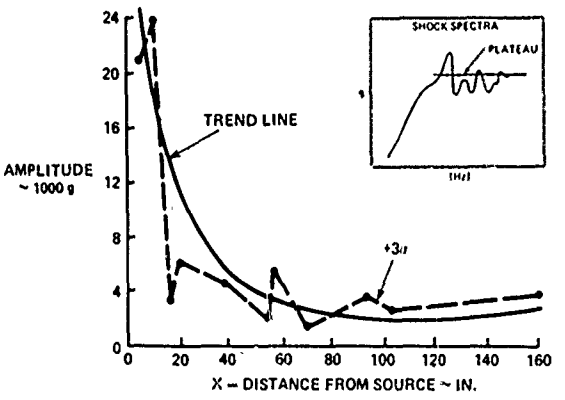

Fig. 5 - Development Test (Plateau "g" versus Distance)

The discontinuities in the curve are attributed to local effects of mass loading and stiffness changes.

A trend line was established by curve fitting the test data, and then the line was used for data correlation studies. An empirical expression was developed to represent the trend line which simplified the correlation process. The expression used for the trend line is:

$$g_x = g_o e^{-[0.0135(x-5) + 1.3 \sin(\pi(x/L)]}$$

where

x = > 5 and x = < 160
x = distance from cutting plane
g_o = source "g" level
L = 160 in. (RV length)
g_x = g level at x distance from cutting plane

The trend line is presented in Fig. 5 for comparison with test data. The low points of the test data reflect accelerometer locations near high local mass locations, and the higher levels reflect skin measurements.

Fig. 6 presents data from verification tests and the trend line for comparison. It is evident the verification test had more attenuation at the forward end of the body than did the development test.

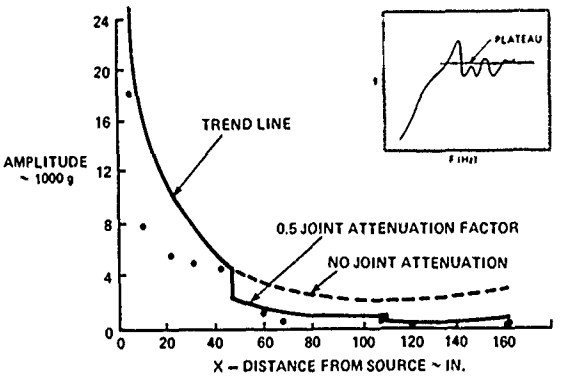

Fig. 6 - Verification Test (Plateau "g" versus Distance)

Fig. 7 presents a comparison of the splices used in the tests. The shear splice was used in development tests (attenuation factor = 0), and the internal "V" band (attenuation factor = 0.5 for matched angle splices) was used in the verification tests. By applying the 0.5 joint attenuation factor (Ref. [1] for matched angle splices) at the splice locations, 47 in. and 110 in. from the source shock, the attenuation prediction agrees with the tests.

The data presented herein are a departure from the normal use of distance attenuation which is only used with time history data. However, a need for a shock spectra correlation

existed. Therefore, the plateau criteria was used, and a trend line was established for the shock spectra (more usable) rather than the time history g levels.

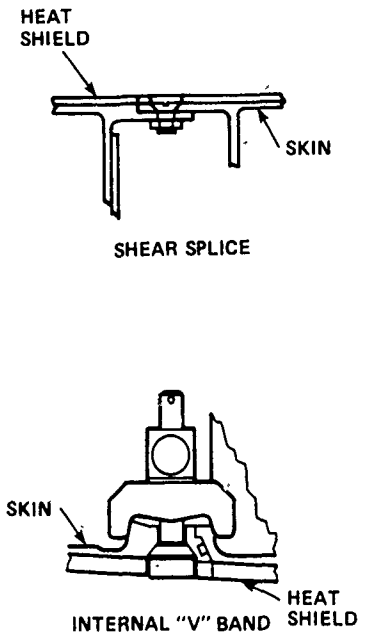

Fig. 7 - Missile Section Splice Joints

PYROTECHNIC SHOCK SIMULATION

Several methods of shock simulation are presently being used: 1) a shaker induced transient, 2) 1/2 sine pulse shock machine, 3) ordnance test, and 4) various impact fixtures. The limitations of some of these methods are as follows:

1 The shaker is limited to lower amplitudes of approximately 500 g

2 The 1/2 sine pulse produces a shock spectra with 6 db/octave roll off on the low frequency end which overtests equipment in the lower frequency bands

3 Ordnance test is expensive and less repeatable.

The simulation fixture presented here is in the fourth category. The general criteria established was that the equipment must remain stationary and the fixture must induce a complex transient to the equipment that will yield a shock spectrum similar to the pyrotechnic shock. The guidelines used that established the fixture configuration are as follows:

1 The anvil mass must be large relative to the equipment to be tested. This reduces the influence of the equipment feedback on the shock spectra.

2 The impact mass must be small relative to the anvil to allow a high intensity and low impulse similar to the pyrotechnic shock.

3 The anvil must have a large number of modes below 10,000 Hz to minimize the number of large amplitude narrow band resonances.

4 The shock spectra must be repeatable.

5 The design range of shock spectra plateau is from 3000 g to 25,000 g.

6 The maximum expected equipment weight is 30 pounds.

A circular steel plate was selected as the anvil because of its many radial and circumferencial modes below 10,000 Hz. The combination of these modes and the capability to vary the strike location was felt to provide the most versatility to obtain the required shock spectra. A Bungee cord is used to accelerate the impact mass to the velocity required to meet the shock spectra amplitude. The mass is a solid steel cylinder 4 in. in diameter and approximately 10 in. long.

Fig. 8 shows a sketch of the fixture, and Fig. 9 shows a photograph of the installation.

The aluminum blocks and rubber pads shown in Figs. 8 and 9 are used to support the 3-in. plate. The location and number of blocks and pads (usually 3 or 4), along with the impact location, can be varied to tailor the shock spectrum.

The higher shock spectra are usually produced by impacting the plate near the edge with the test item located near the edge across the plate approximately 180 degrees away.

Figs. 10 and 11 present 2 typical shock spectra within the range of amplitude capability. Once the desired spectrum is obtained the repeatability is typically within 1 db. A comparison of Fig. 11 (simulation spectrum) with Fig. 3 (typical pyrotechnic shock spectra) shows the similarity of the simulation. This fixture has been used for several years to test equipment and isolation systems, and it has been found to be versatile in tailoring spectra, inexpensive to use, and repeatable.

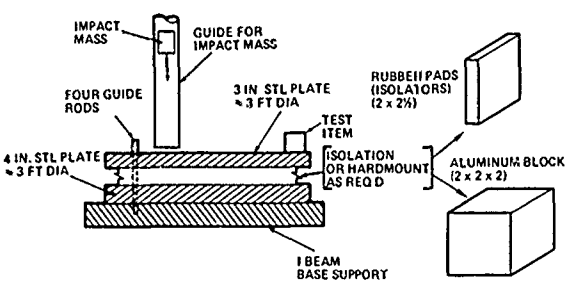

Fig. 8 - Shock Simulation Fixture

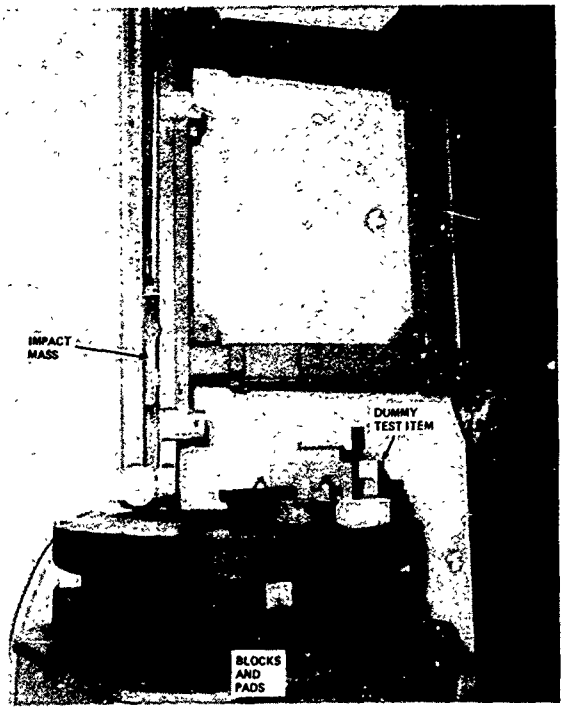

Fig. 9 - Block and Pad Installation

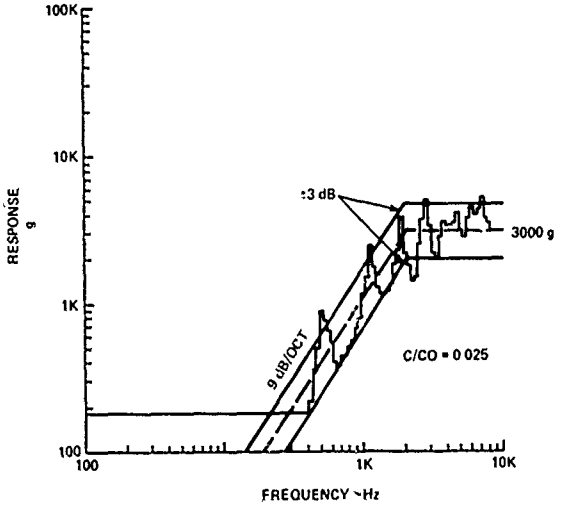

Fig. 10 - Shock Spectra - Shock Simulation Fixture

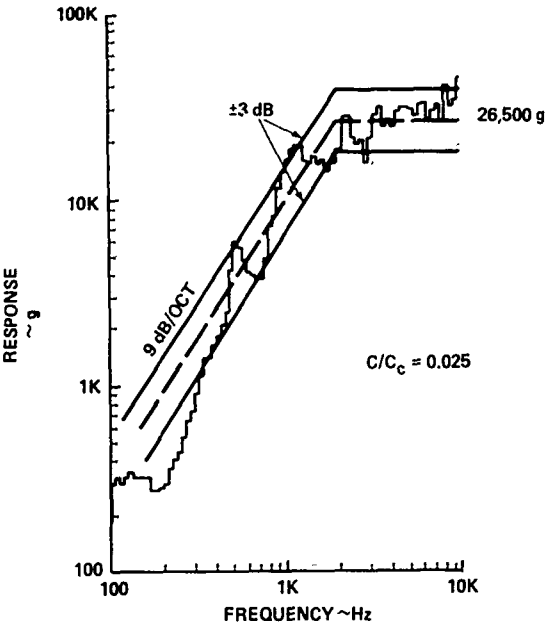

Fig. 11 - Shock Spectra - Shock Simulation Fixture

CONCLUSIONS

1. Multiple measurements and a statistical treatment are required to define source shock level
2. For near optimum charge size, the size has a secondary effect, and source shock levels can be directly correlated to skin thickness
3. Shock levels vary with vendor design for the same charge size
4. Splice attenuation factors agree with Ref. [1].

REF. [1] "Aerospace Systems Pyrotechnic Shock Data" MCR-69-611, prepared by Martin Marietta Denver Division for NASA, Goodard Space Flight Center.

STRAIN HISTORIES ASSOCIATED WITH STAGE SEPARATION SYSTEMS USING LINEAR SHAPED CHARGE

D. R. Powers
McDonnell Douglas Astronautics Company
Huntington Beach, California

A series of design optimization tests were performed on subscale and full-scale vehicle interstage separation systems. Aluminum sheathed, 30 grains/foot, linear shaped charge (ALSC), was used to cut 1-1/2 by 3 foot panels and 8-foot-diameter 6-foot-high cylindrical sections. Acceleration and strain histories and shock response spectra are presented from representative firings. Recorders were run in both the direct and FM modes giving frequency responses of 600 kHz and 80 kHz respectively. Shock response spectra amplitudes exceeding 200,000 g plotted to 100 kHz and strain histories exceeding 80,000 μin./in. at rates greater than 3,000 in./in./sec are shown.

INTRODUCTION

Vehicle stage separation is normally accomplished by an ordnance-activated device. The most severe shocks are produced by devices that sev . the skin holding the stages together. Shock response spectra values exceeding 100,000 g have been reported near separation planes that are cut with linear shaped charge or mild detonating fuze [1]. Volumes of data obtained from accelerometers (acceleration histories and shock response spectra) are available to the analyst for prediction purposes [2]. However, very little data exist on the strain that produces these accelerations.

A series of design optimization tests were recently conducted in which strain measurements were obtained near high-energy separation joints. On one of the subscale tests, data from accelerometers were obtained. The acceleration data are presented not because they are new, but because the response data are plotted to 100 kHz. Past experimenters have usually stopped their analysis at 10 or 20 kHz.

This paper relays to the technical community characteristic strain histories that are associated with skin-cutting separation systems and delineates the instrumentation used to accurately record these high-frequency transients.

TEST SPECIMEN DESCRIPTIONS

Tests were performed on subscale and full-scale specimens. Subscale specimens measured approximately 1-1/2 by 3 feet with the charge cutting the long direction. A typical joint configuration is shown in Figure 1. The charge was aluminum sheathed, RDX, 30 grains/foot, linear shaped charge, and the material severed was 7075-T7351 aluminum, 0.140 inch thick.

Full-scale tests were performed on cylindrical sections measuring approximately 8 feet in diameter and 6 feet high. The joint configuration, material, and charge size was the same as was used for the subscale specimens.

FLAT PANEL TEST WITH ACCELEROMETERS

This test was performed to obtain acceleration histories and shock response spectra data. Nine Endevco Model 2225M5A accelerometers were mounted as shown in Figure 1 on a 1-1/2 by 3 foot panel. All of the accelerometers were mounted perpendicular to the panel except the one at location 9 which was mounted on a 1-inch block perpendicular to the separation plane. Installation of the accelerometers was in accordance with a procedure previously described in Ref. [3].

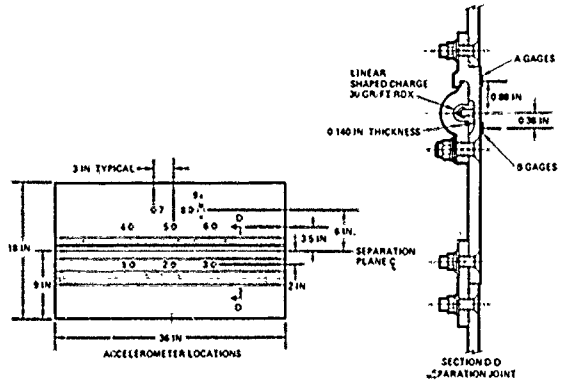

Figure 1. Typical LSC Separation System

A Honeywell 101 recorder run at 120 inches/second double extended (432-kHz carrier) was used to give a frequency response of 80 kHz. Unholtz Dickie Model D11 charge amplifiers with the filters removed were used for signal conditioning. Acceleration histories were obtained with a Nicolet Model 660A spectrum analyzer. The tape recorder was played into a Nicolet with a 1,000 word memory at a digitizing rate of 256,000 samples/second giving a time increment of

4 milliseconds. Note that for an 80-kHz signal, this rate gives only 3.2 samples/cycle and consequently true peak amplitudes would be sightly higher than those displayed.

Shock response spectra were generated with an MB982 Shock Spectrum Analyzer with a quality factor (Q) of 10. These data are presented in Figures 2 through 5. The signature from accelerometer 4 exhibited a DC shift and is not presented. Note that while spectra are plotted to 100 kHz, data above 80 kHz are attenuated by tape recorder rolloff.

FLAT AND CURVED PANEL TESTS WITH STRAIN GAGES

Subscale tests were performed to determine exact gage positions for maximum strains, to select the best cement for adequate gage bonding, and to check out signal conditioning and recording equipment. Rather extensive studies were performed on explosive nuts and bolts [4], but little information on strain rates near skin-cutting separation systems was available for guidance. For a first try, a Honeywell 101 recorder was set to record in the direct mode medium band and was run at 120 inches/second giving a frequency response between 300 Hz and 600 kHz. Since the frequency response of the available DC ampifiers was only 100 kHz, no amplifiers were used and the gage outputs were played directly into the recorder. The tape recorder input/output voltages were set to optimize the dynamic range for the low-strain gage outputs.

Panels measuring 6 by 12 inches were used to check adhesive, gage mounting techniques, and the optimum position for the gages. The results of these tests showed that Measurement Group Model No. CEA-13-125VW-350 gages bonded with AE10 and cured at room temperature gave the best results.

Gages were positioned 0.88 inch above and 0.28 inch below the separation plane centerline. These positions, as shown in Figure 1, corresponded to points of maximum stress concentrations. After separation, the material above the separation plane was bent outward approximately 30 degrees at the gage locations labeled A. The material below the separation plane fractured at the gage locations labeled B.

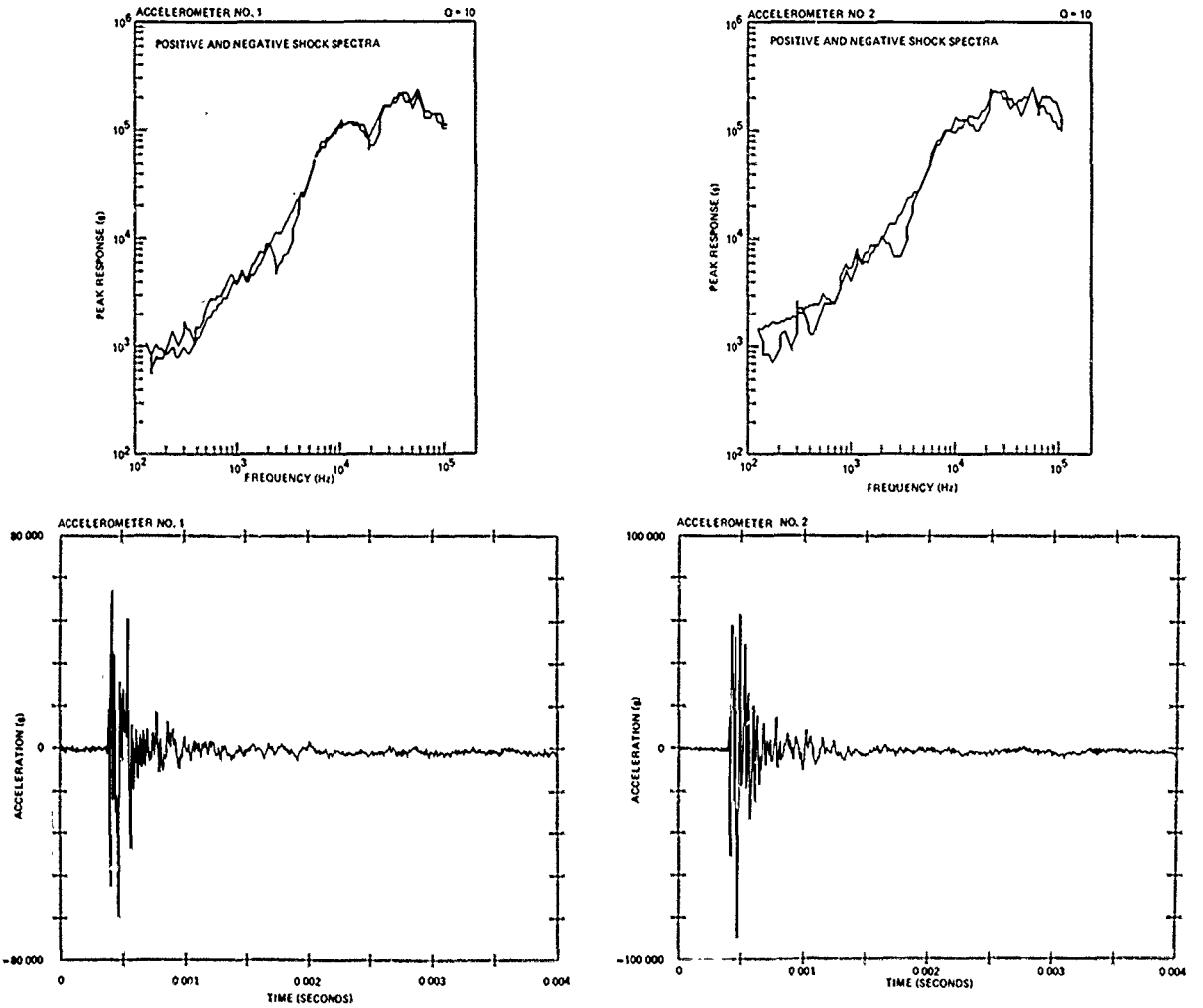

Figure 2. Spectra and Acceleration Histories 1-1/2 x 3 Foot Panel

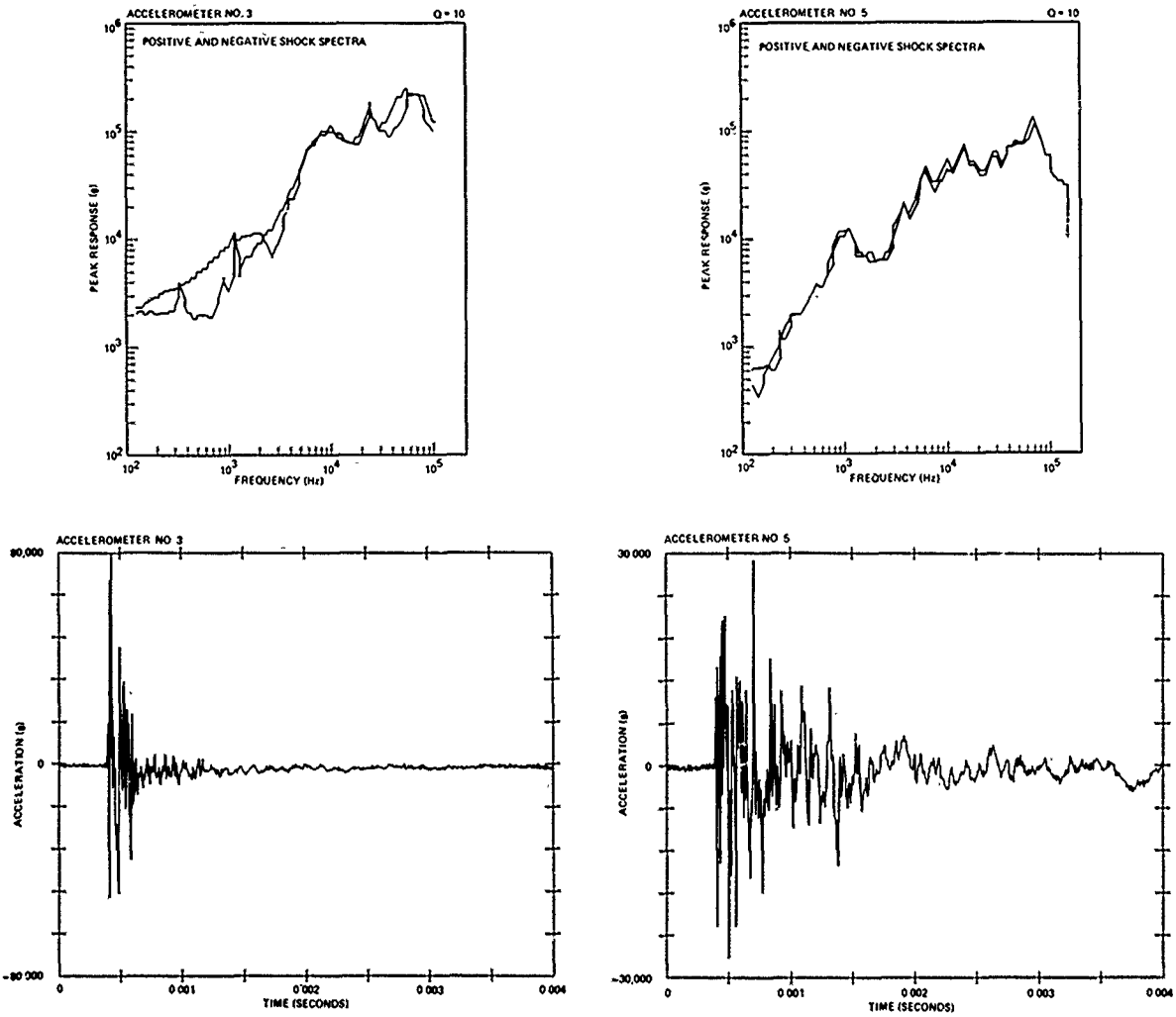

Figure 3. Spectra and Acceleration Histories 1-1/2 x 3 Foot Panel

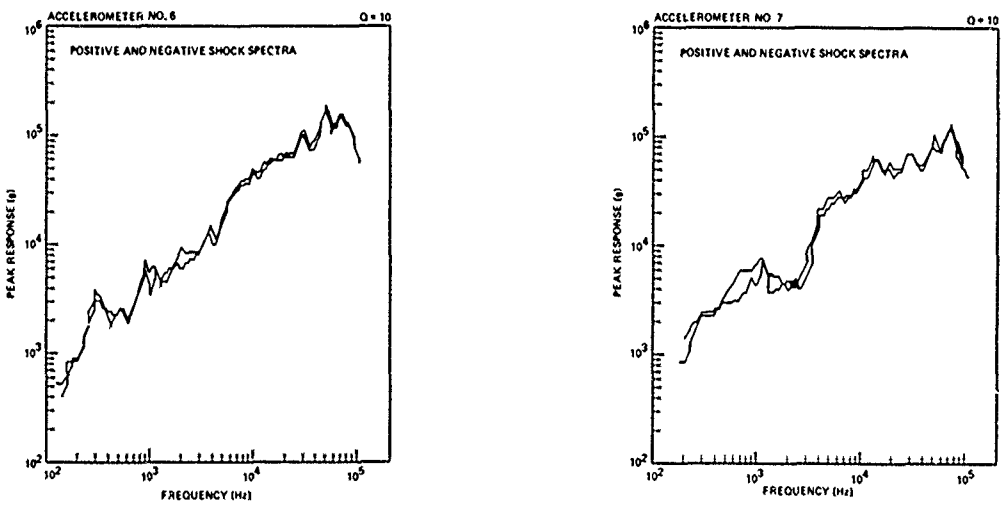

Figure 4. Spectra and Acceleration Histories 1-1/2 x 3 Foot Panel

The author also mounted an accelerometer on one of these small panel tests to examine spectra above 80 kHz. An Endevco Model 2225M5 with a published mounted resonance frequency of 80 kHz and an acceleration limit of 100,000 g was used. Rasanen [3] has reported that this frequency could be as low as 34 kHz, depending upon the mounting technique used.

The acceleration history and shock response spectra plots generated from the output of this accelerometer are presented in Figure 6. While the recorder has a frequency reponse of 600 kHz, the data above 100 kHz are attenuated because of charge amplifier rolloff.

Curved panels measuring 1-1/2 by 3 feet with a radius of 4 feet were gaged at positions as described above and in Figure 1. The Honeywell 101 recorder, configured with direct and FM cards, was run at 120 inches/second giving the direct cards a frequency response of 300 Hz to 600 kHz and the FM cards a frequency response of DC to 80 kHz. This was done to determine if the FM 80 kHz response was adequate to accurately record the strain histories. Figure 7 shows the outputs from the same strain gage, one recorded direct and the other FM. As can be seen, the outputs were the same except in the range of constant strain where the direct mode shows rolloff.

By using the recorder in the FM mode, data reduction was simplified. Since FM responds down to DC, tape recorder playback speed could be reduced without sacrificing the low end of the spectrum. With FM it was not necessary to use a memoscope or high-

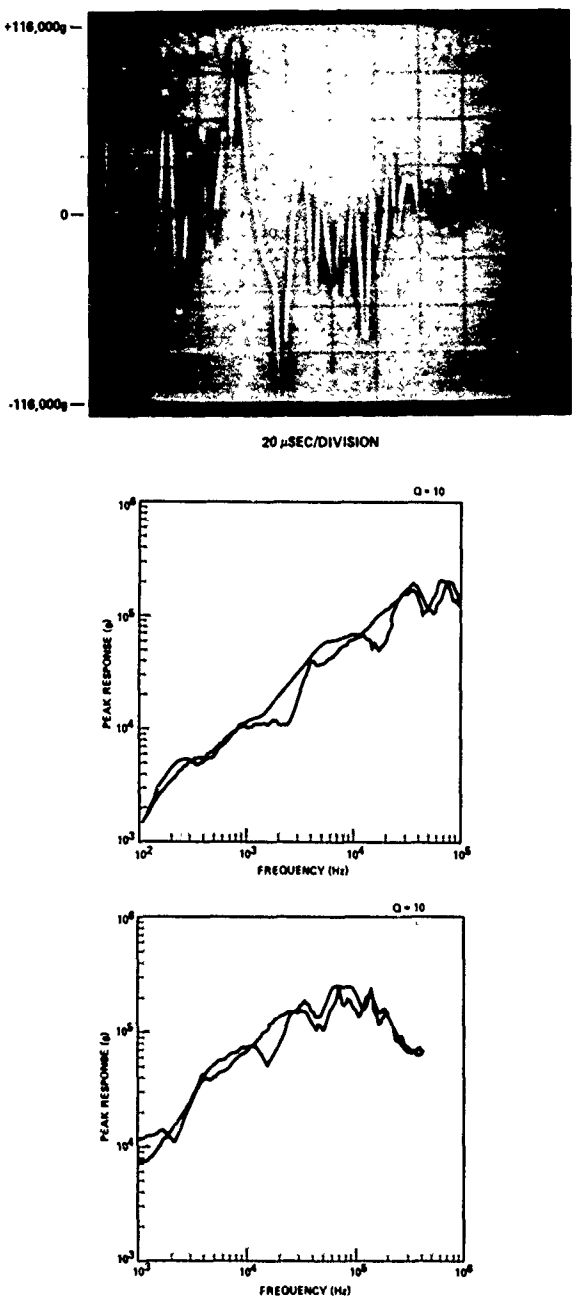

Figure 6. Spectra and Acceleration History 6 x 12 Inch Plate

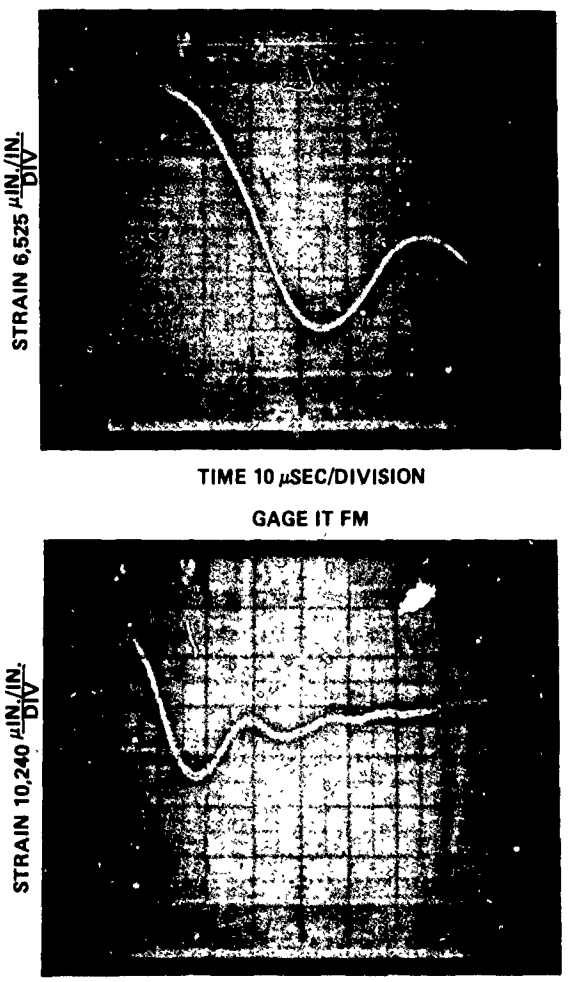

Figure 7. Strain History Comparisons Between FM and Direct Recording

speed transient capture device to retain the signature. Playback speed could be adjusted to be within the frequency response of a conventional oscillograph. This made it possible to look at several gage outputs and to determine accurate timing between the outputs with the aid of breakwire.

A total of eight strain gages were placed on 8-foot-diameter sections at the longitudinal positions shown in Figure 1. They were placed circumferentially around the section in pairs and labeled 1 through 4. The gages above and below the separation plane were designated A and B respectively.

Two full-scale firings were performed. The sections were identical except for minor differences in the joint configurations.

Data from both tests were recorded on a Honeywell 101 recorder operated at 120 inches/second double extended (432 kHz carrier) giving a frequency response of 80 kHz.

Data were played back at 1.87 inches/second (speed reduction of 64/1) and viewed on an oscillograph. The data were then played back at the same rate and captured in a Zonic DMS Data Memory System. With the 64/1 speed reduction the Zonic had an effective digitizing rate of 12.8 samples/microsecond.

The strain histories are presented in Figures 8 through 11. Circumspection must be used when interpreting these plots. The plots for the gages above the separation plane (those labeled 1A-4A) are correct. They all show an extremely high rise time (3000 in./in./sec), reach a maximum strain, drop to a value of approximately 60% the initial peak, and then oscillate about this mean value until the gage wire breaks or the gage becomes unbonded (seen on oscillographs with greater record lengths).

These gages were mounted on a surface that was permanently deformed. The joint was bent outward from the charge at about 30 degrees from its unstressed condition. When the charge cut through the skin, the material was pushed outward from internal joint pressure, reached yield and then sprung back and oscillated about the deformed position.

The plots for the gages located below the separation plane (those labeled 1B-4B) are correct only for the period showing the initial rise and peak. These gages were located on a section that fractured and flew away from the joint. The gage outputs for gages 1B, 2B, and 4B for the first full-scale firing (Figure 9) show the strain dropping to zero after the initial peak is reached. The reason for this is that the gages become unbonded and are flying through the air in this time period. The output from gage 3B is clipped past 100 microseconds. The outputs from gages 1B, 2B, and 3B from the second full-scale firing (Figure 11) show the strain increasing sharply after the initial peak is reached. This occurred because the strain gage wires were broken putting 14 volts DC into the recorder causing it to go into complete saturation. Gage 4B became unbonded before gage wire fracture and its output dropped to zero.

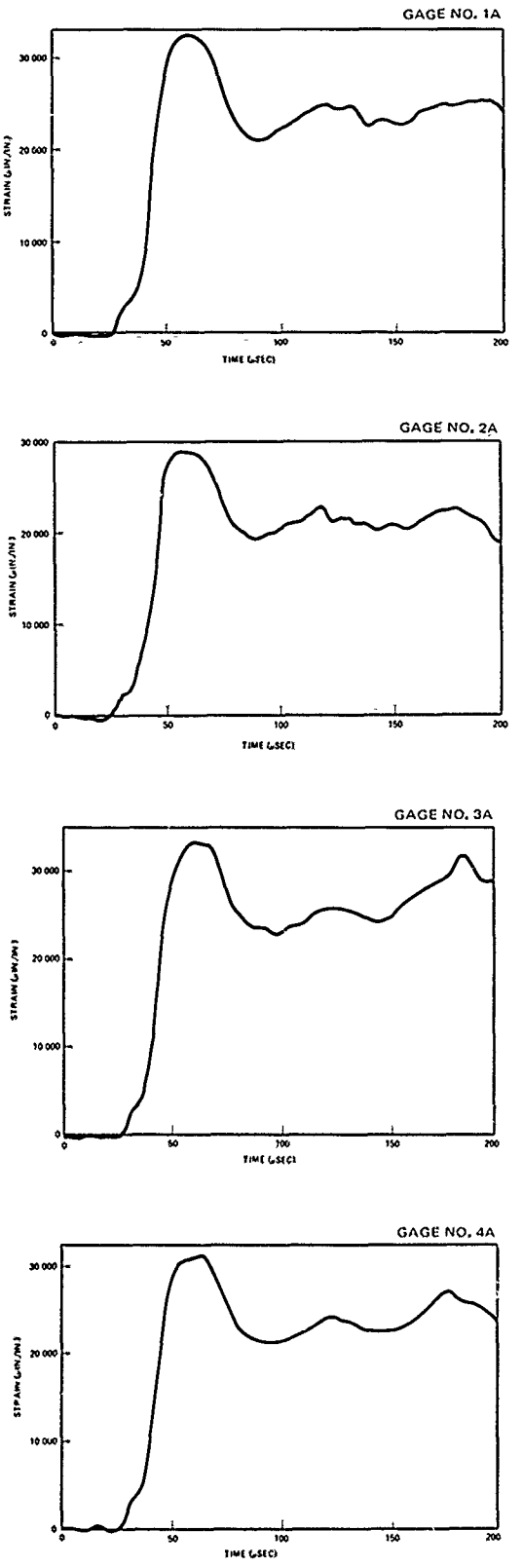

Figure 8. Upper Strain Gages First Full-Scale Separation

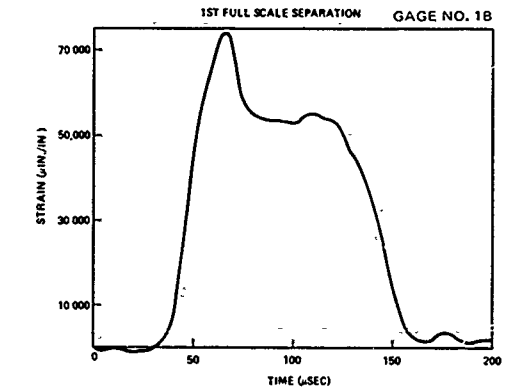

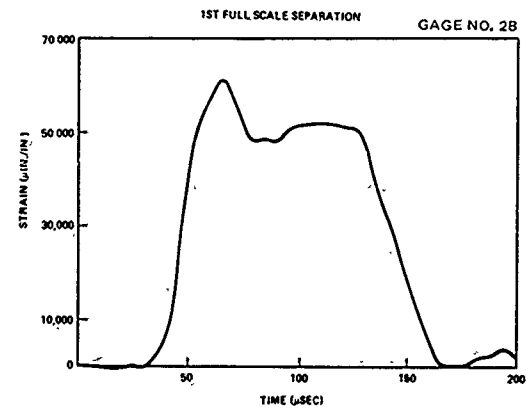

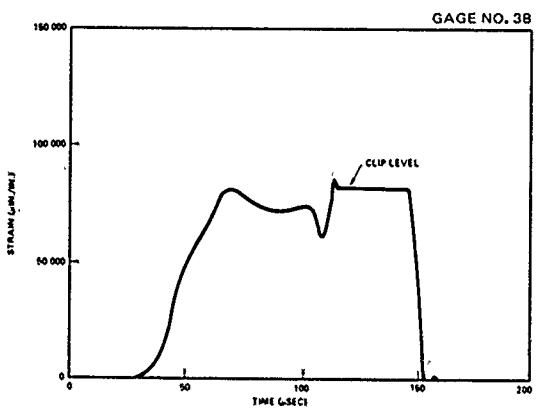

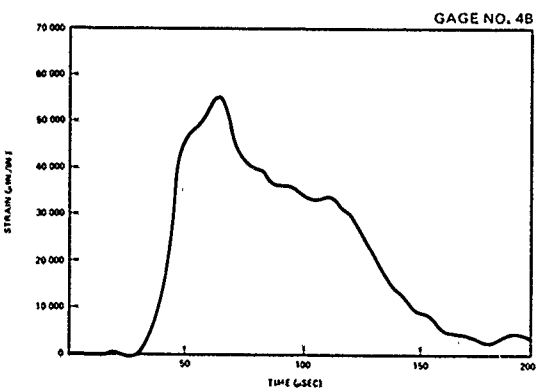

Figure 9. Lower Strain Gages First Full-Scale Separation

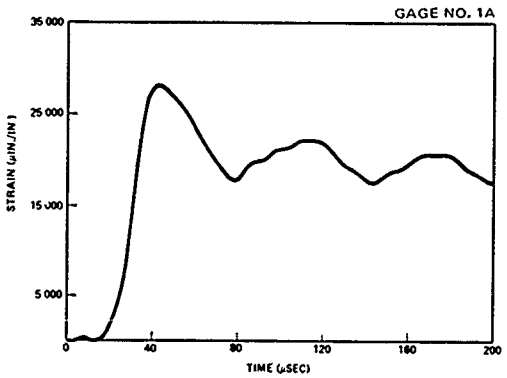

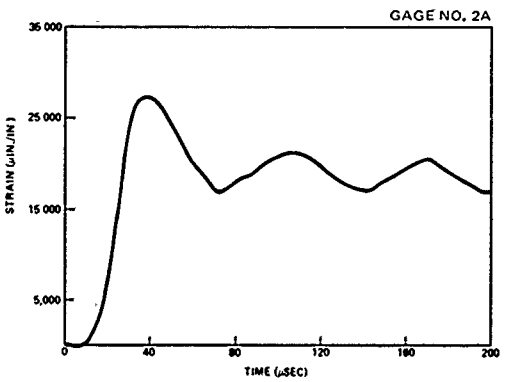

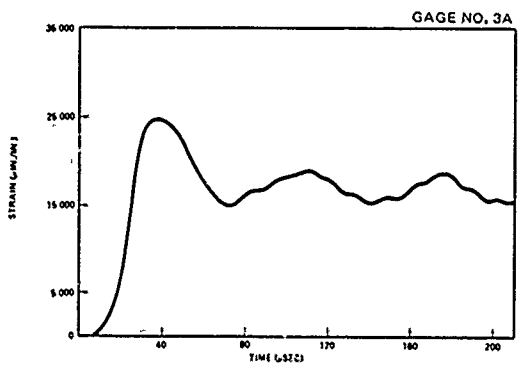

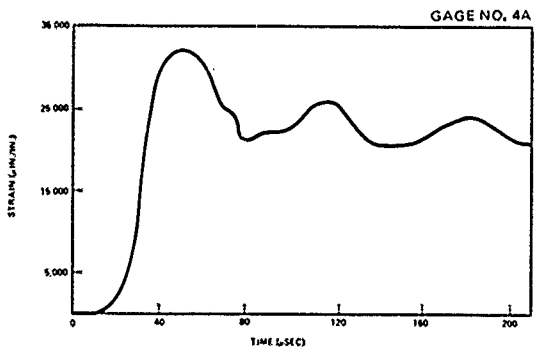

Figure 10. Upper Strain Gages Second Full-Scale Separation

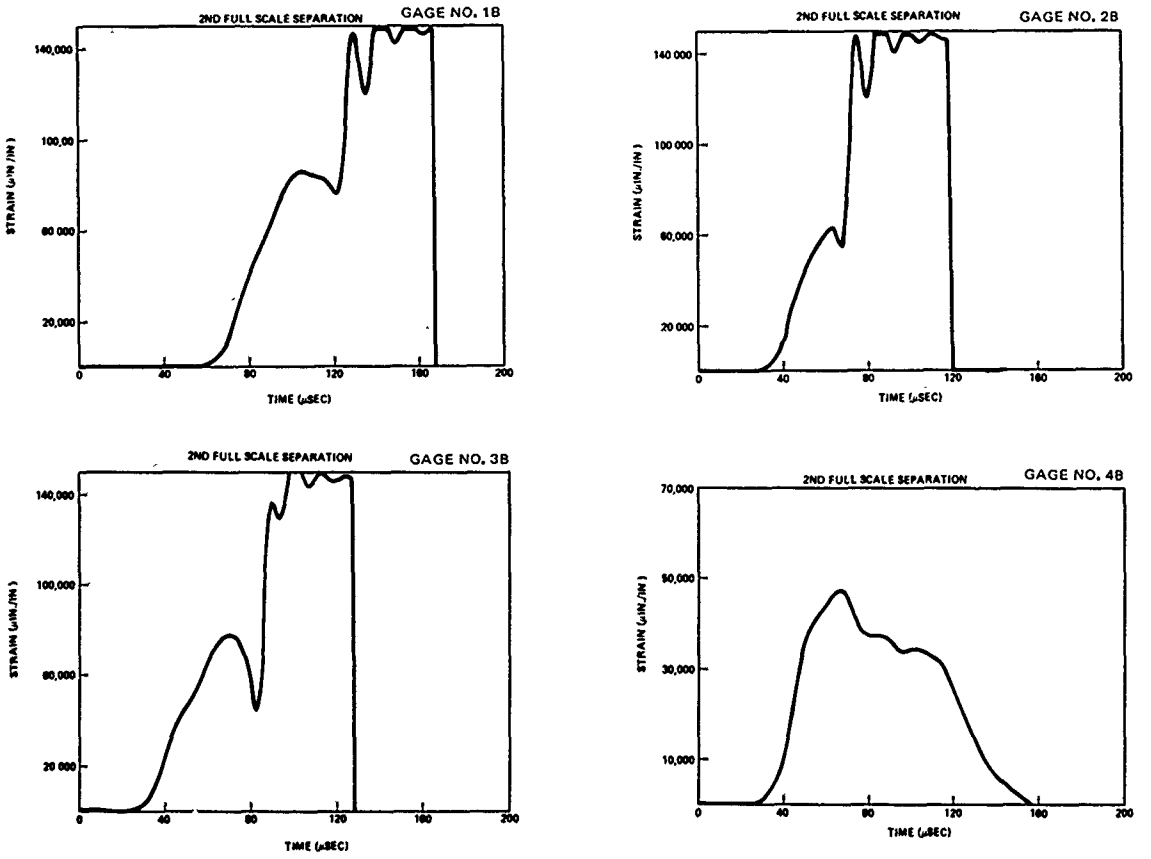

Figure 11. Lower Strain Gages Second Full-Scale Separation

CONCLUSIONS AND RECOMMENDATIONS

It can be concluded from the results of this test series that meaningful strain gage data can be obtained at locations very close to high-energy separation joints. While some of the gages may fly off or fracture within 60 microseconds after detonation, the peak strains are reached within 25 microseconds and can be accurately recorded.

Signal conditioning and data acquisition systems should have a flat frequency response to 80 kHz to ensure that the high-frequency peak strains are accurately recorded.

It is beneficial to use a breakwire to identify a zero time base and to use as a trigger during data reduction. If an 80-kHz oscillator is used rather than a DC offset, it can be used as an exact check on tape recorder/oscillograph playback speed. The oscillator/breakwire is very helpful in locating the data on an oscillograph. Even with a 64/1 speed reduction in recorder playback speed, an oscillograph must be run at 120 inches/second to get adequate resolution for an 80 kHz signal (10 cycles/inch).

Extensive care must be exercised in both the positioning and bonding of the strain gages. The manufacturer's recommendation for surface preparation, curing time, and temperature must be followed. Gage leads must be positioned to minimize blast effects.

REFERENCES

1. D. R. Powers, "Simulation of Pyrotechnic Shock in a Test Laboratory," 22nd Annual Technical Meeting Institute of Environmental Sciences, pp 5-9, 1976

2. R. J. Kacena, III, et al., "Aerospace Systems Pyrotechnic Shock Data (Ground Test and Flight)," Martin Marietta Corporation, Denver, Colorado, 7 March 1970. Distributed by National Technical Information Service, U.S. Dept. of Commerce, Springfield, VA.

3. D. R. Powers, "Development of a Pyrotechnic Shock Test Facility," Shock and Vibration Bulletin 44, Part 3, pp 73-82, August 1974.

4. V. H. Neubert and R. P. Parker, "Timewise Output of Pyrotechnic Bolts," Shock and Vibration Bulletin 44, Part 3, pp 101-110, August 1974.

SHOCK SPECTRAL ANALYSIS BY PERSONAL COMPUTER, USING THE IFT ALGORITHM

Charles T. Morrow
Consultant
Encinitas, California

In THE ENVIRONMENTAL SPECIFICATION AS A TECHNICAL MANAGEMENT TOOL, the author has recommended that the undamped residual shock spectrum (as opposed to damped or undamped maximax) be the primary mode of spectral analysis for shock. The only specific objection raised thus far to conforming to this in environmental specifications is that no instrument is yet commercially available to perform the spectral computations. Conversely, no instrument manufacturer would be sure enough of a market to develop such an instrument before the undamped residual is recognized by specifications. Partly as a step to resolve this, the author reports his progress in the development of a program for personal computers, based on an algorithm that is comparable in practice to the FFT in computation time but much less demanding of computer memory. The current program is designed for 301 logarithmically spaced frequencies and deals with phase as well as magnitude in plottable form.

INTRODUCTION

In 1962, O'Hara[1] showed that the undamped residual shock spectrum was simply related to the Fourier transform and proposed a method for shock response computation that could also be made to yield a spectrum. At the 52nd Shock and Vibration Symposium, Morrow[2] reported an extension to permit computation of responses and residual spectra on the HP-97 or HP-67 card-programmable calculator, and labelled the algorithm the Indirect Fourier Transform (IFT) because, from O'Hara's relationship, the Fourier transform, if desired, could be computed indirectly. That paper was not prepared, however, until after Morrow had explored the potential of the algorithm for a personal computer and carried out a demonstration on a Radio Shack TRS-80 Model 1 computer with 16 kilobytes of random access memory, at the 51st Shock and Vibration Symposium, in San Diego in 1980.

At the time of the demonstration, three programs on tape had been developed, all for data inputs from the keyboard, which are simplest for exploratory work and will retain utility even after program development is more complete. Two of the programs permitted spectral computation for shock data with variable and constant time increments, respectively, without requiring memory for data storage. The third, using a hybrid time increment approach with any integral number of constant time increments between data inputs, and storing the data, demonstrated the feasibility of computation and plotting of the response of an arbitrary mechanical system to shock, so as to explore in advance any benefits from design changes. It contained subroutines only for absolute acceleration and relative displacement of a damped simple mechanical resonator but had a framework that would support extension to multiple-degree-of-freedom systems.

Since the demonstration, the computer has been expanded to have 48 kilobytes of RAM and the capability to support development of programs on floppy disk. Most of the work has been completed to combine the three programs, improve the computer-user interaction, and include machine language processing of the spectral matrix. The last improvement is capable of speeding up a typical data input processing from about 20 seconds to about 1 second.

The arguments in favor of the undamped residual spectrum[3] are briefly that (1) because of its simple relationship to the Fourier transform it is a more fundamental shock description than a maximax, (2) being less dominated by the peak magnitude of the excitation, it is more indicative of what will be multiplied up by multiple-degree-of-freedom systems and (3) for the same reason, it has less tendency to obscure spectral holes or nulls and is therefore a better description for both customer and contractor. The customer should not by his choice of spectrum inadvertently permit a test shock with a residual hole or null. For example, a square wave has a series of nulls indicating no response persisting after the excitation comes to an end unless damping is high. At such a frequency only a brittle part will be likely to fail. Again, at high frequencies a maximax spectrum can not fall below the peak magnitude of the excitation even if there is no shock energy. Finally, the customer should be permitted to know from reduced data whether the actual shock simulated in test had a hole such that a deviation in response to a test failure might be justifiable instead of a redesign.

Eventually more response subroutines will be added and a provision will be made for inputs from an analog to digital converter. In the meantime, the present paper will serve to report the strategy for implementation of the spectral computation by computer and the special considerations that arise from this capability.

FUNDAMENTAL THEORY

The fundamental theory of the IFT algorithm was reported in the previous paper[2], which also compared the IFT with the FFT in computation speed. Only a brief summary of the theory is necessary here.

The central idea underlying the algorithm has been that an excitation approximated by a series of straight lines is equivalent to a summation of a sequence of RAMP's, or perhaps RAMP's and STEP's, determined by the successive acceleration-time data points. Therefore the response of any linear mechanical system to the shock can be computed if its responses to a unit-slope RAMP and a unit STEP are known. For the computation of the undamped residual shock spectrum, the system selected is an undamped simple mechanical resonator, and no actual evaluation of response is carried out. It is necessary only to evaluate the cosine and sine coefficients in the expression for the residual responses.

Let the acceleration for the time t_{k-1} be a_{k-1} and that for time t_k be a_k, producing a RAMP input. The slope of the

SHOCK SPECTRAL ANALYSIS BY PERSONAL COMPUTER, USING THE IFT ALGORITHM

Charles T. Morrow
Consultant
Encinitas, California

In THE ENVIRONMENTAL SPECIFICATION AS A TECHNICAL MANAGEMENT TOOL, the author has recommended that the undamped residual shock spectrum (as opposed to damped or undamped maximax) be the primary mode of spectral analysis for shock. The only specific objection raised thus far to conforming to this in environmental specifications is that no instrument is yet commercially available to perform the spectral computations. Conversely, no instrument manufacturer would be sure enough of a market to develop such an instrument before the undamped residual is recognized by specifications. Partly as a step to resolve this, the author reports his progress in the development of a program for personal computers, based on an algorithm that is comparable in practice to the FFT in computation time but much less demanding of computer memory. The current program is designed for 301 logarithmically spaced frequencies and deals with phase as well as magnitude in plottable form.

INTRODUCTION

In 1962, O'Hara[1] showed that the undamped residual shock spectrum was simply related to the Fourier transform and proposed a method for shock response computation that could also be made to yield a spectrum. At the 52nd Shock and Vibration Symposium, Morrow[2] reported an extension to permit computation of responses and residual spectra on the HP-97 or HP-67 card-programmable calculator, and labelled the algorithm the Indirect Fourier Transform (IFT) because, from O'Hara's relationship, the Fourier transform, if desired, could be computed indirectly. That paper was not prepared, however, until after Morrow had explored the potential of the algorithm for a personal computer and carried out a demonstration on a Radio Shack TRS-80 Model 1 computer with 16 kilobytes of random access memory, at the 51st Shock and Vibration Symposium, in San Diego in 1980.

At the time of the demonstration, three programs on tape had been developed, all for data inputs from the keyboard, which are simplest for exploratory work and will retain utility even after program development is more complete. Two of the programs permitted spectral computation for shock data with variable and constant time increments, respectively, without requiring memory for data storage. The third, using a hybrid time increment approach with any integral number of constant time increments between data inputs, and storing the data, demonstrated the feasibility of computation and plotting of the response of an arbitrary mechanical system to shock, so as to explore in advance any benefits from design changes. It contained subroutines only for absolute acceleration and relative displacement of a damped simple mechanical resonator but had a framework that would support extension to multiple-degree-of-freedom systems.

Since the demonstration, the computer has been expanded to have 48 kilobytes of RAM and the capability to support development of programs on floppy disk. Most of the work has been completed to combine the three programs, improve the computer-user interaction, and include machine language processing of the spectral matrix. The last improvement is capable of speeding up a typical data input processing from about 20 seconds to about 1 second.

The arguments in favor of the undamped residual spectrum[3] are briefly that (1) because of its simple relationship to the Fourier transform it is a more fundamental shock description than a maximax, (2) being less dominated by the peak magnitude of the excitation, it is more indicative of what will be multiplied up by multiple-degree-of-freedom systems and (3) for the same reason, it has less tendency to obscure spectral holes or nulls and is therefore a better description for both customer and contractor. The customer should not by his choice of spectrum inadvertently permit a test shock with a residual hole or null. For example, a square wave has a series of nulls indicating no response persisting after the excitation comes to an end unless damping is high. At such a frequency only a brittle part will be likely to fail. Again, at high frequencies a maximax spectrum can not fall below the peak magnitude of the excitation even if there is no shock energy. Finally, the customer should be permitted to know from reduced data whether the actual shock simulated in test had a hole such that a deviation in response to a test failure might be justifiable instead of a redesign.

Eventually more response subroutines will be added and a provision will be made for inputs from an analog to digital converter. In the meantime, the present paper will serve to report the strategy for implementation of the spectral computation by computer and the special considerations that arise from this capability.

FUNDAMENTAL THEORY

The fundamental theory of the IFT algorithm was reported in the previous paper[2], which also compared the IFT with the FFT in computation speed. Only a brief summary of the theory is necessary here.

The central idea underlying the algorithm has been that an excitation approximated by a series of straight lines is equivalent to a summation of a sequence of RAMP's, or perhaps RAMP's and STEP's, determined by the successive acceleration-time data points. Therefore the response of any linear mechanical system to the shock can be computed if its responses to a unit-slope RAMP and a unit STEP are known. For the computation of the undamped residual shock spectrum, the system selected is an undamped simple mechanical resonator, and no actual evaluation of response is carried out. It is necessary only to evaluate the cosine and sine coefficients in the expression for the residual responses.

Let the acceleration for the time t_{k-1} be a_{k-1} and that for time t_k be a_k, producing a RAMP input. The slope of the

straight line between the two points is

$$S_k = (a_k - a_{k-1})/(t_k - t_{k-1}). \quad (1)$$

The change from the previous slope is

$$\Delta S_k = S_k - S_{k-1}. \quad (2)$$

The incremental instantaneous response to the RAMP is

$$\Delta a(t \geq t_{k-1}) = \Delta S_k [t - t_{k-1}) - (1/2\pi f_i)\sin 2\pi f_i (t - t_{k-1})]. \quad (3)$$

This would hold indefinitely if there were no further data inputs. It must be added to all previous incremental responses to obtain the total instantaneous response for $t \geq t_{k-1}$.

Now let a discontinuity Δa_k in acceleration occur at time t_k, producing a STEP input. The incremental instantaneous response to the STEP is

$$\Delta a(t \geq t_k) = \Delta a_k [1 - \cos 2\pi f_i (t - t_k)]. \quad (4)$$

It is a convenience to have the computer set the excitation slope arbitrarily to zero after a STEP input. If this is not actually true of the shock excitation, the next RAMP will correct it. However, it simplifies the data inputs when there is a terminal STEP and provides a way of setting the slope to zero after a terminal RAMP without advancing the time beyond the end of the shock. The incremental instantaneous response to the STEP with slope nullification is

$$\Delta a(t \geq t_k) = \Delta a_k [1 - \cos 2\pi f_i (t - t_k)] - S_{k-1} [t - t_k - (1/2\pi f_i)\sin 2\pi f_i (t - t_k)]. \quad (5)$$

This persists indefinitely in the absence of further data inputs. Like Equation (3), it must be added to all previous incremental responses to obtain the total instantaneous response. An equation sufficiently general to represent any such sum is given by

$$a(t \geq t_k) = B_k + C_k t + D_{ik} \cos 2\pi f_i t + E_{ik} \sin 2\pi f_i t. \quad (6)$$

where B_k, C_k, D_{ik}, and E_{ik} are constants to be evaluated for each time interval.

Accordingly, equations (3), (5) and (6) are the foundation for the IFT algorithm applied to computation of undamped residual spectra. Since no actual computation of instantaneous response of the undamped simple mechanical resonator concurrently with the spectral computation is contemplated, only the cosine and sine coefficients in Equation (6) (for the i'th frequency and k'th time instant) need be updated after a data input. It would be nice if this could be limited to adding the cosine and sine factors from Equation (3) or (5). However, closer inspection shows that the cosines and sines in the latter equations are functions of $t - t_k$ or $t - t_{k-1}$, whereas those of Equation (6) are functions of t. Therefore, before any such addition, there must be a time shift according to the trigonometric identities

$$\cos(\theta \pm \phi) = \cos\theta \cos\phi \mp \sin\theta \sin\phi \text{ and} \quad (7)$$

$$\sin(\theta \pm \theta) = \sin\theta \cos\phi \pm \cos\theta \sin\phi. \quad (8)$$

In Method 1, which is useful for variable time increments and simple pulses, these equations are applied to Equation (3) or (5) to yield functions of t. This is slow because new trigonometric functions must be computed for each data input. However, after the last data input, for $k = n$, the coefficients D_{in} and E_{in} directly describe the residual undamped response, complete with phase information, as if this response were extended back to the origin and examined for $t = 0$.

For constant time increments, this same method could be speeded up by computing and storing the trigonometric functions for the time increment before the data inputs and obtaining all other trigonometric functions by recursion, using Equations (7) and (8). However, each shift would require that these equations also be applied a second time, using the results of the first operation.

Therefore, in Method 2, with trigonometric functions corresponding to the constant time increment computed and stored in the first and second columns of the matrix in advance, the multiply-add-on operations of these equations are applied once for each shift, to ratchet along Equation (3) with trigonometric functions of $t - t_k$ or $t - t_{k-1}$. Each computation is similar to the multiply-add-on operation of the FFT, but there is no constraint on the number of frequencies in the spectrum or on their numerical relationships. For correct spectral phase after completion of data inputs, new trigonometric functions corresponding to the entire duration must be computed and Equations (7) and (8) applied a final time for a reverse shift to restore functions of t.

For Method 2, with constant time increments, if the instantaneous response of a system is to be computed, it can be done most simply immediately after a shift. For computing response to simple shock wave shapes that can be defined by a few data inputs, a hybrid method has been devised that permits any integral number of constant time increments between data inputs. This permits a corresponding number of shifts and response computations between the stored data inputs. For computation of shock responses of an arbitrary system by Method 2, the data must likewise be stored as input from the keyboard. However, no response computations are necessary for the evaluation of undamped residual shock spectra.

For the spectral computation from hybrid data inputs, there is a choice of procedure. If there are only a few constant time incrments between data inputs, it is quickest for the computer to update the coefficients by successive shifts as in response computation. For a larger number, it is quicker for the computer to evaluate new trigonometric functions corresponding to the total time interval and perform one shift.

SPECTRAL COMPUTATIONS AND PLOTS

Method 1 variable-time-increment data are not stored because there is no convenient way of using the data for subsequent response computations.

For all spectral computations, 301 frequencies, logarithmically spaced from 2 to 2000 Hz, are used. This amounts to an availability of 101 spectral points per decade or 30 per octave. The frequencies are not stored in memory but computed as required by successive multiplications of an initial value by a constant factor.

The spectral computations utilize a 301 by 5 matrix, chosen over other options because it lends itself to use of machine language subroutines with a minimum of hunting for

variables. Except in Method 1, the first and second columns hold the cosines and sines, respectively, of $2\pi f_i$ times a constant time increment—for Method 1,there is no advantage to storing sines and cosines. The third and fourth columns hold the coefficients D_{ik} and E_{ik}. The remaining column is reserved for Apparent Starting Time, to be computed after the data inputs are complete.

Computations after each data input begin at 2 Hz and proceed through all frequencies one by one to 2000 Hz. In Method 2, each shift requires four multiplications and two summations for each frequency. A STEP input without slope adjustment would require also an addition, but it is the multiplications that take the time. A RAMP input requires instead a multiplication and addition, increasing the computation time about 25 percent—a RAMP term is established first for 2 Hz and for each successive frequency this term is multiplied by a constant factor. A STEP input with slope nullification needs about the same computation time as the RAMP.

Figure 1 shows the undamped residual spectrum, computed by Method 1 for the range from 2 to 2000 Hz, for a terminal peak sawtooth of 100 g and 10 milliseconds. To comply with the display limitations of the video monitor, this contains points only for every third frequency, or 10 points per octave. However, any of the three decades can be examined by itself at the full resolution of 30 points per octave. For example, Figure 2 shows the second decade of the same spectrum, for 20 to 200 Hz, at this resolution. This frequency scale change capability is especially helpful when spectra are more irregular.

The Fourier transform is a powerful theoretical tool and a powerful computational device, but do we really want to see it plotted? Figure 3 is a magnitude plot for the terminal-peak sawtooth, from 2 to 2000 Hz. It provides good visibility at low frequencies where the spectrum is predictable from the area under the shock excitation curve, but not at high frequencies where more of interest may be happening. If the vertical scale were expanded for the high frequencies, the 6 db-per-octave slope inherent in a comparison of Fourier transform to undamped residual would still confuse the interpretation of the curve. The units that are most useful to the shock and vibration engineer are displacement (at low frequencies) and acceleration. The Fourier transform has the dimensions of a velocity, which is neither here nor there. Accordingly, although the program can provide the Fourier transforms in either a curve or a number table, it is doubtful that the plotting capability will often be used.

Figure 4 shows the undamped residual spectrum, for 2 to 2000 Hz, for a square wave of 100 g and 10 milliseconds, which with sufficient precision and resolution would exhibit a null at every 100 Hz. Figure 5, for 20 to 200 Hz, shows the first null more vividly. If one watches the third decade, from 200 to 2000 Hz, being plotted in the same way, the second null is quite clear, and it is discernable in Figure 6, but the remainder of the curve looks like a random function. Fortunately, the square wave appears to be coming into disuse as a standard pulse shape for shock testing. As implemented in practice with a drop tower, it is unlikely to duplicate the high frequency portion of the spectrum shown here, but there is no reason to expect practical deviations from the standard acceleration-time curve to result in significantly better properties. In any event, the "ideal" square wave is unlikely to produce failures at null frequencies except in parts that are extremely brittle.

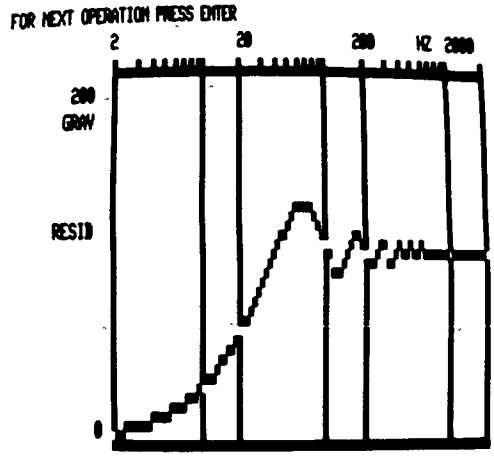

Fig. 1 — Three-decade undamped residual for 100-g 10-millisecond sawtooth

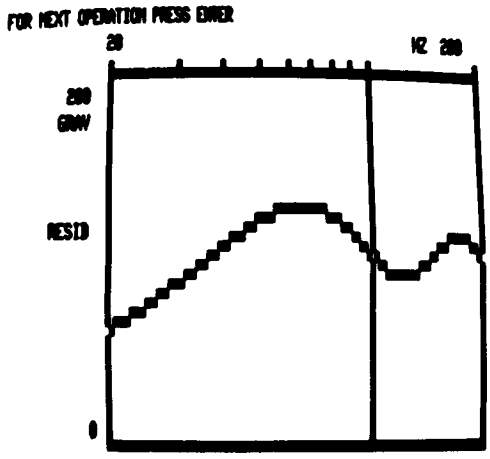

Fig. 2 — Sawtooth undamped residual for second decade of frequencies

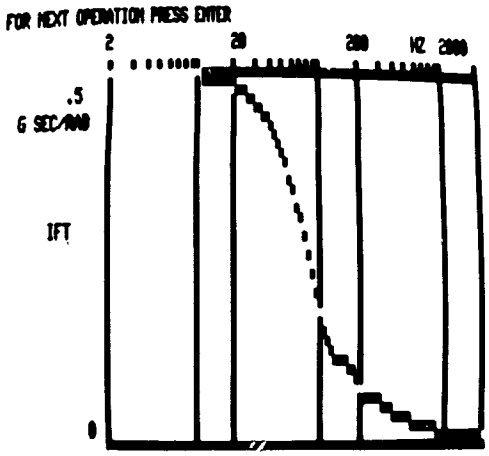

Fig. 3 — Three-decade sawtooth fourier transform

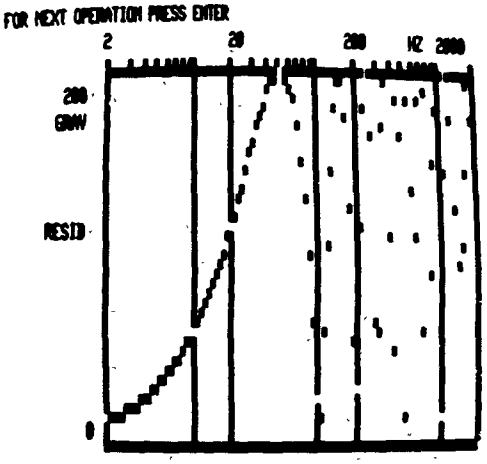

Fig. 4 — Three-decade undamped residual for 100-g 10-millisecond square wave

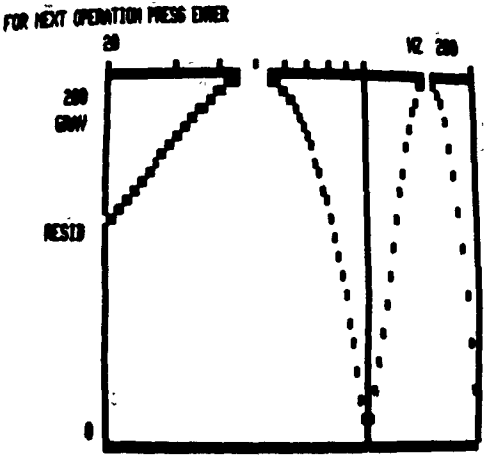

Fig. 5 — Square-wave undamped residual for second decade of frequencies

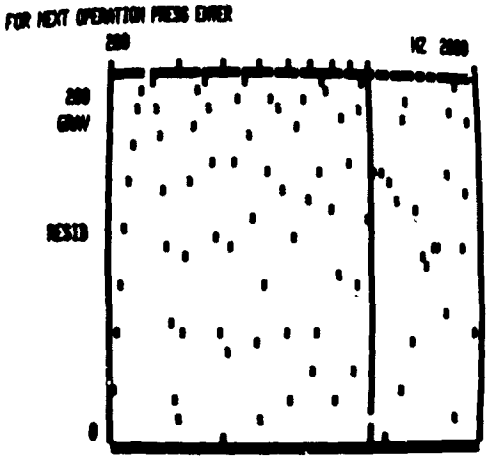

Fig. 6 — Square-wave undamped residual for third decade of frequencies

PHASE AND APPARENT STARTING TIME (AST)

One fundamental property of the Fourier transform is that if both magnitude and phase are known as functions of frequency, the original time-domain function can be reconstructed by an inverse transformation. The shock spectrum has been criticized because as usually defined it does not include phase information and does not permit a reconstruction. Therefore, whether residual, initial or maximax, it does not uniquely describe a shock excitation. However, the undamped residual shock spectrum as defined by the operations reported here inherently contains phase information that, in conjunction with one acceleration value, does permit uniquely describing a shock excitation.

From the previous paper[2], the cosine transform at the frequency f is given by

$$F_c(f) = E_n/2\pi f, \tag{9}$$

where n indicates the subscript k for the last data input, for the end of the shcok. The sine tranform is given by

$$F_s = D_n/2\pi f. \tag{10}$$

Inspection shows that the undamped residual is not simply the derivative of the Fourier transform because of a difference in sign in one equation. Nevertheless, the undamped residual does have a phase angle that is uniquely related to that of the Fourier transform. For any non-zero frequency, the Fourier transform is uniquely determined if the undamped residual is known.

For either spectrum, the phase itself, though of fundamental importance, is difficult to work with directly and almost impossible to plot in a useful way because it can change so rapidly with frequency. However, the derivative of the residual phase angle in radians with respect to angular frequency in radians per second turns out to be a well behaved function with a physical meaning. It has the dimensions of time and it describes the Apparent Starting Time of the residual transients, based on their properties after the shock is over.

Computation is more devious, however, than computing angles and dividing each angle increment by a frequency increment, because the angles and even the differences in angle may be many times 2π radians, especially for long durations and toward the highest frequencies. Computation starts with the lowest pair of frequencies to minimize the initial angle change and proceeds in order upward through the higher pairs of adjacent frequencies. The multiply-add-on operations of Equations (7) and (8) are applied to the contents of columns 3 and 4 of the matrix for successive adjacent frequency pairs. The coefficients D_k and D_{k-1} are taken to be proportional respectively to $\cos\theta$ and $\cos\phi$. The coefficients E_k and E_{k-1} are taken to be proportional respectively to $\sin\theta$ and $\sin\phi$. The antitangent of the ratio of the results yields the angular difference, which is then divided by the angular frequency difference. If, as the frequency increases, the angular difference approaches π, a switch is made to predicting the next value of AST or, in equivalent manner, predicting the next angle of the undamped residual. A correction, obtained by applying Equations (7) and (8) to the discrepancy between predicted and actual values, is added. Finally, if an angular difference or a correction close to $-\pi$ appears when the AST is close to half the shock duration, it is assumed that the two frequencies are straddling a null, and the computer adds a phase reversal correction of π

radians. By this procedure, most shock excitations up to 1 second in duration can be made to yield AST curves to 1000 Hz without wild points. Computation and storage in the final column of the matrix is done concurrently with plotting a 2 to 2000 Hz curve to relieve the user of the boredom of an inactive video screen. After this, the values are readily available for any frequency range plot or for a numbers printout.

Figure 7 is a 2 to 2000 Hz plot of the AST for the 100-g 10-millisecond terminal-peak sawtooth. At low frequencies it is opposite the center of the area of the pulse—roughly two thirds of the duration. At high frequencies, where everything that happens in response results from the final discontinuity, it equals the shock duration. In between, as the frequency increases, the AST approaches the duration, overshoots, and wavers back and forth before it settles down.

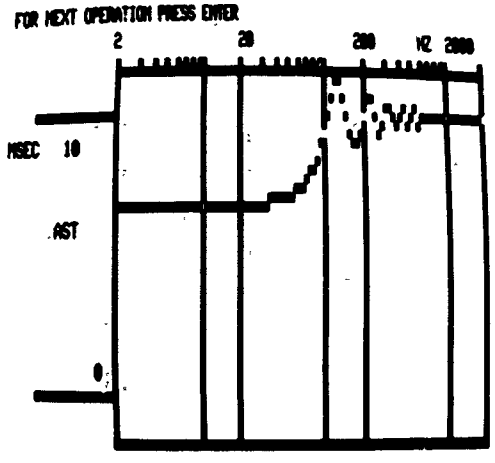

Fig. 7 — Three-decade AST for 10-millisecond sawtooth

Figure 8 is a 2 to 2000 Hz plot of the AST for the 100-g 10 millisecond square wave—a uniform straight line at half the duration. It should not be presumed that any part of the response is actually starting at this time—the AST a weighted value to which in this case the initial and terminal acceleration discontinuities contribute equally regardless of frequency.

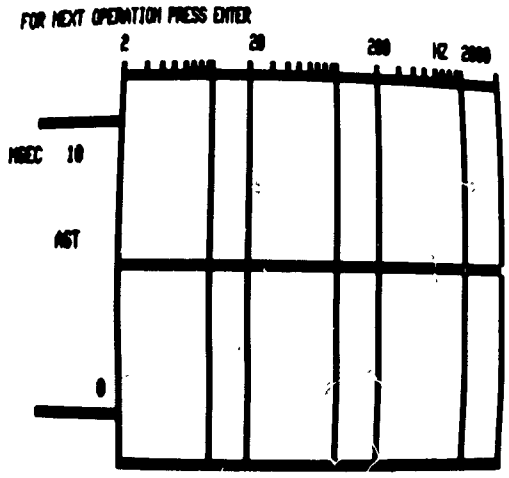

Fig. 8 — Three-decade AST for 10-millisecond square wave

As can be seen, the AST is well behaved and readily plottable—sometimes more so than the corresponding magnitude spectrum. Experiments on the computer indicate that it remains finite even for shocks that have no definite ending. An upper limit on AST can be used in a specification to ensure a degree of simultaneity of shock responses in test. The engineer who wishes to experiment with "reconstruction" of a time history from a prescribed spectrum will find the AST more convenient to work w...l than the phase function directly. Integration to obtain angle is simple, except that one value of phase angle must be supplied to determine the integration constant.

NUMBER TABLES

Once the AST has been computed and stored in the memory matrix, the computer can print, either on the video screen or on paper, a number table with all representations of the undamped residual and the Fourier transform. Figure 9 shows the beginning of a 2 to 2000 Hz video number display for the 100-g 10-millisecond sawtooth, at 10 frequencies per octave. Alternatively, the computer can print a table for any of the three decades, or for the entire range, at the full resolution of 30 frequencies per octave.

IFT AND UNDAMPED RESIDUAL

I	F(I) HZ	IFT MAG	RAD	COS	SIN		RESID MAG	DEG	MSEC
0	1.995	0.500	6.28	0.498	-0.042		6.3	95.	
3	2.138	0.500	6.19	0.498	-0.045		6.7	95.	6.64
6	2.291	0.500	6.19	0.497	-0.048		7.2	95.	6.66
9	2.455	0.500	6.18	0.497	-0.051		7.7	96.	6.66
12	2.630	0.500	6.17	0.497	-0.055		8.3	96.	6.65
15	2.818	0.500	6.17	0.496	-0.059		8.8	97.	6.67
18	3.020	0.499	6.16	0.496	-0.063		9.5	97.	6.67
21	3.236	0.499	6.15	0.495	-0.067		10.2	98.	6.66
24	3.467	0.499	6.14	0.494	-0.072		10.9	98.	6.67
27	3.715	0.499	6.13	0.493	-0.077		11.7	99.	6.67
30	3.981	0.499	6.12	0.492	-0.083		12.5	100.	6.67

TO CONTINUE HIT ENTER, ELSE EXIT (/)? _

Fig. 9 — First frame of number table for every third frequency

CONCLUSION

The IFT algorithm as developed in the previous[2] and present papers is based on geometry, which makes understanding easier and provides an intuitive idea of the quality of the approximation achieved by the data inputs. The RAMP input, which provides to the computer both realistic data points and realistic slopes between them, may be a unique feature. It requires only a 25 percent increase in computation time over that of a STEP without slope adjustment. The excitation curve could, of course, be approximated by a series of such steps, essentially in ascending and descending staircases, for a slight increase in speed per data input. However, the roughness in the approximation would result in some deterioration in accuracy of high-frequency spectra so that a larger number of data points would be desirable. One can imagine a higher order of approximation using data points in triplets to make the derivative of the slope usually more realistic, but this would probably require more computation time per data input than it would be worth. For spectral algorithms that originate more purely in analysis,

a geometric reinterpretation might provide some useful insight into high-frequency accuracy.

To avoid aliasing error, if in the future provision is made for obtaining RAMP data inputs from a digital-analog converter for IFT spectral analysis, then, as in the case of the FFT and all other spectral algorithms, it will be necessary to install a low-pass filter before the converter to eliminate frequencies above the highest of interest and to use time increments no larger than half the period corresponding to the cutoff frequency. For most excitations, this will eliminate one potentially large source of error. With data inputs from the keyboard, on the other hand, the user will intuitively pick his points so that he tends to perform the equivalent of such a filtering as may be necessary. However, as in the case of other algorithms, the mere avoidance of aliasing is not sufficient to ensure accuracy at the highest frequency. The two data points per period that would be marginally adequate according to a purely aliasing criterion could occur at a maximum and a minimum, or at zeros for that frequency component. It is desirable that the analog to digital converter provide at least 8 data points per period at 2000 Hz in order to describe all shock excitation wave shapes adequately. However, this need not result in an overwhelming burden in data quantity. For example, for a shock 10 milliseconds in duration, this criterion would prescribe only 160 data points. For longer durations, compromises may be possible because of a decreased probability of energy as high as 2000 Hz. The same high-frequency criteria will apply also to response computation.

If the data inputs for the sawtooth and square wave spectra illustrated in this paper had utilized a hybrid time increment rather than a variable time increment, a variation of the response computation routine would permit displaying the excitation wave shape from the stored data, so as to verify that the data were entered correctly, however, computation of instantaneous response by the IFT algorithm on a personal computer is another story, to be introduced in the next paper. That will not end the story, however, as there is no limit to the number of dynamical configurations potentially of interest to the shock and vibration engineer.

In contrast, the potential ramifications of spectral computation by personal computer are finite, so that in principle the IFT algorithm in this application can be perfected so that little further change is beneficial. For the immediate future, detail improvement will continue. In the meantime, the present paper has shown that the algorithm is a practical way of obtaining the undamped residual with phase information included. If the author's motivation were immediate financial gain, he would take care to couple in a response subroutine and a max value subroutine so as to make computation of maximax spectra also possible. However, for the foreseeable future, he will develop the spectral algorithm as he would like to see it used—for the computation of the undamped residual only. The algorithm makes possible a more refined definition of the undamped residual shock spectrum than has been available previously.

REFERENCES

1. G. J. O'Hara, "A Numerical Procedure for Shock and Fourier Analysis", NRL Report 5772, June 5, 1962.

2. C. T. Morrow, "Indirect Fourier Transform and Shock Response", SHOCK AND VIBRATION BULLETIN 52, Part 4, 37-45, The Shock and Vibration Information Center, 1982.

3. C. T. Morrow, THE ENVIRONMENTAL SPECIFICATION AS A TECHNICAL MANAGEMENT TOOL, 59-62, The Shock and Vibration Information Center, November, 1981.

AN EXPLOSIVE DRIVEN SHOCK TUBE FOR VERIFYING SURVIVAL OF RADIOISOTOPE HEAT SOURCES DURING SPACE SHUTTLE LAUNCH ACCIDENT

F. H. Mathews
Sandia National Laboratories
Albuquerque, New Mexico

Decay of radioactive isotopes provides a heat source for flights into deep space. Environmental concerns dictate that these heaters retain and immobilize their toxic contents in the event of a space shuttle detonation on the launch pad. This paper describes the planning, conduct, and analysis of experiments which employed explosive driven shock tubes to simulate such a blast. Trials were conducted using a 102 mm diameter tube filled with air with an attached expendable driver section containing explosive. Analysis indicated dimensionless parameters which allowed scaling of pressure and impulse data to design of a larger shock tube, although this was complicated by distortion due to the greater relative roughness of the large tube. Scaled results were used to design a 0.3 m diameter by 18 m tube driven by 74 kg of Composition C-4 plastic explosive to produce the 14 MPa (2000 psi) static overpressure and 37 kPa·s (5.4 psi·s) impulse for the heat source survivability tests. Experimental measurements included shock arrival time, pressure, and flash radiographs of the heat source capsule. Analysis of blast wave motion in the shock tube provided a convenient description of peak pressures to which measurements could be compared. Results describing shock tube impulse and pressure performance from 13 tests are included. Two radioisotope heater capsules were recovered after testing. Although their metallic shells were deformed, detailed examination indicated that they were not ruptured, thus verifying that the design met its objective in this challenging environment.

INTRODUCTION

The Galileo Spacecraft will carry numerous radioisotope-powered heaters [1] attached so that critical mechanical joints can be warmed to assure easy movement. Because of environmental concerns, the toxic-radioactive contents must be retained, and therefore immobilized, within a protective capsule in the unlikely event of a launch accident. Analysis indicates the worst case accident is equivalent to the blast wave occurring 30 meters from the surface after detonation of a 7000 metric ton sphere of conventional explosive [2].

This paper is concerned with the experimental survival verification program* which used an explosive driven shock tube to generate the blast environment.

Specifications involved recovering the 9 mm diameter by 14 mm long radioisotope source after subjecting it to a blast wave of 14 MPa (2000 psi) static overpressure of sufficient duration to produce a 37 kPa·s (5.4 psi·s) static impulse. We elected to extend our experience with various explosive driven

*Sandia National Laboratories was contracted by Los Alamos National Laboratory, the power supply developer, to conduct this testing program.

shock tubes [3] which are employed at much lower blast pressures to achieve these conditions. For these devices, static impulse can be increased by lengthening the shock tube. Thus, a desired peak static overpressure-impulse combination could be produced simply by finding an appropriate explosive quantity and tube length.

A warning of difficulty was suggested in Reference 4 where the flow limitations associated with boundary layer growth in relatively long, thin tubes is discussed. Energy transport down the tube is restricted producing limit conditions where large increases in explosive weight result in little pressure increase. Since an appropriate analysis was not available, trials employing a 102 mm shock tube were conducted to obtain performance data useful for sizing of larger hardware necessary for testing at specified blast levels.

DIMENSIONAL ANALYSIS

Methods of dimensional analysis from Reference 4 were used considering parameters listed in Table 1. The explosive energy density, Item 9, is the product of the explosive weight (W) and its specific energy of detonation (E) divided by the tube's area (A). This formulation allows rough comparison of results obtained using composition C-4 explosive, specific energy of 1400 kcal/g, with different types of explosive.

Because static impulse and static pressure are linked by an auxiliary equation, i.e., the time integral of pressure, these parameters may be considered separately. Two dimensionless equations were formed as indicated below:

$$\frac{P_s}{P_0} = f\left(\gamma, \frac{x}{d}, \frac{\varepsilon}{d}, \frac{P_0 x A}{WE}\right) \qquad (1)$$

$$\frac{I_s C_0 A}{WE} = G\left(\gamma, \frac{x}{d}, \frac{\varepsilon}{d}, \frac{P_0 x A}{WE}\right) \qquad (2)$$

Note that use of the same gas and explosive in geometrically similar tubes produces replica scaling. However, readily available steel tubing included a drawn steel tube of 102 mm bore which was relatively smoother than the rolled and welded 300 mm bore tube used in full-scale tests. This distortion proved important in subsequent use of model data.

MODEL SHOCK TUBE

A sketch of the 102 mm bore shock tube is given in Figure 1. Drawn 12 mm wall tubing was arranged with a sequence of pressure gages spaced at approximately 0.6 m intervals along a 2.4 m instrumented section. A non-instrumented tube was placed between the explosive and the instrumented section to allow testing with longer tubes. When using this latter configuration, stress waves originating

TABLE 1
Parameters for Dimensional Analysis

Variable	Symbol	Dimensions[1]
1. Static Overpressure	P_s	F/L^2
2. Static Impulse	I_s	FT/L^2
3. Ratio of Specific Heats	γ	No Units
4. Tube Position	x	L
5. Tube Diameter	d	L
6. Surface Roughness	ε	L
7. Initial Pressure	P_0	F/L^2
8. Sound Velocity	C_0	L/T
9. Explosive Energy Density	$\frac{WE}{A}$	$\frac{F}{L}$

(1) F = Force L = Length T = Time

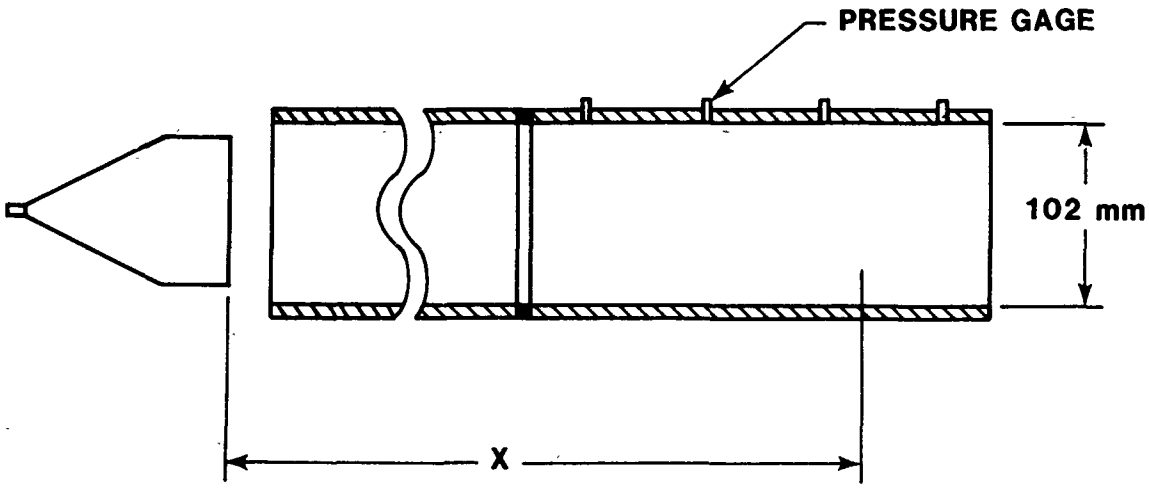

Fig. 1 - Small-Scale Shock Tube

from impact between tubes caused acceleration-induced pressure gage excitation on several experiments. A plywood gasket placed between tubes provided cushioning, thus alleviating this problem.

Several explosive configurations evolved during the model study. A conical arrangement, initiated at its apex, with no surrounding confinement as shown in Figure 2, was used during early low-pressure tests. As explosive weights increased, this evolved into an unconfined cone-cylinder arrangement with a maximum diameter of 97 mm. The explosive output face was placed 13 mm from the tube breech when unconfined assemblies were fired. Refer to Tables 2 and 3 for a summary of setup conditions.

During experiments with very long shock tubes and large explosive weights, the explosive energy losses to the sides of unconfined assemblies were unacceptably large. Accordingly, three different confined explosive assemblies depicted in Figure 2 were used in Tests 9 through 11. Refer to Table 2 for specifics. The setup for Shot 9 involved a cone-cylinder 97 mm in diameter placed inside a 13 mm wall by 102 mm bore steel tube with open back. The steel tube was completely filled for Shot 10, and a 13 mm steel back plate was added for Shot 11. This torturous development resulted from concern that metal fragments from the confinement would be ingested into tube flow and become a potential threat to downstream instrumentation; however, fragment ingestion was not observed during model tests.

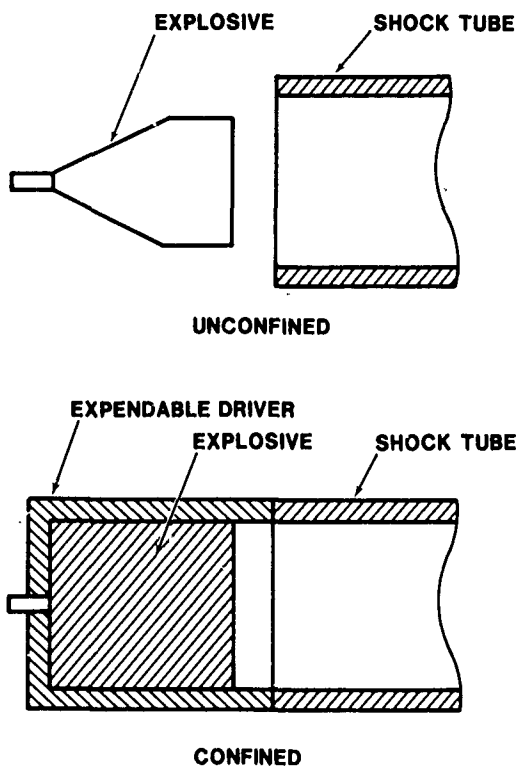

Fig. 2 - Typical Explosive Driver Sections

PRESSURE MEASUREMENTS

Kulite HKM-375 pressure transducers rated at 2000 psi which employ a diaphragm-mounted semiconductor sensor

TABLE 2
Test Summary for 102 mm Diameter Model Tube

Test	Explosive				Tube Geometry			
	Type	Mass g	Space mm	Diameter mm	Length(1) m	Gage Location m First	Gage Location m Final	Gage Number
1	Cone(2)	23	12.7	38	3.37	0.88	3.35	6
2	Cone(2)	23	12.7	38	3.37	0.88	3.35	5
3	Cone(2)	45	12.7	47	3.37	0.88	3.35	5
4	Cone(2)	68	12.7	54	3.37	0.88	3.35	5
5	Cone(2)	108	12.7	64	3.37	1.49	3.35	5
6	Cone(2)	283	12.7	86	3.37	1.49	3.35	5
7	Cone(2)	410	12.7	97	3.22	0.88	3.21	6
8	Cone-Cylinder(2)	760	12.7	97	4.40	1.97	4.31	6
9	Cone-Cylinder(3)	1137	--	97	7.16	4.63	6.95	6
10	Cylinder(3)	1964	--	102	7.16	4.63	5.85	3
11	Cylinder(4)	2620	--	102	7.16	4.63	6.95	5

(1) Measured from explosive output face
(2) No confinement
(3) Confined sides, open back
(4) Confined sides and back

TABLE 3
Test Summary for 300 mm Diameter Full-Scale Tube

Test	Explosive			Tube Geometry			
	Type(1)	Mass Kg	Diameter mm	Length m	Gage Location m First	Gage Location m Final	Gage Number
14	Cylinder	73.5	305	18.0	11.1	17.3	6
15	Cylinder	73.5	305	18.3	13.9	17.5	4
16	Cylinder	73.5	305	18.3	--	--	0

(1) Confined sides and back on all tests

were used in the first six experiments. Thermally-induced shifts frequently occurred even when grease covered the diaphragm. This problem prevented accurate integration to obtain static impulse. Inertially-induced overshoot due to grease and side wall motion further obscured pressure records, making interpretation for peak pressure uncertain. Fortunately, time of shock wave arrival based upon pressure signals allowed accurate timing of shock wave position from which calculations of shock pressure were possible.

Kulite HKS-375 pressure gages rated at 10,000 psi and equipped with standard ablative thermal protection, proved more satisfactory. Use of these gages in all subsequent tests provided acceptable pressure readings for impulse determination as well as time of arrival data. During these experiments, pressure gages suffered approximately 5% attrition per measurement due to a variety of damage mechanisms.

DATA ANALYSIS

The instrumented tube section served two immediate purposes. First, to allow shot-to-shot comparison of peak static overpressures, and second, to define the static impulse. Our objective was to apply dimensional analysis and obtain an estimate of the shock tube configuration required to meet test specifications. The analysis described here served these purposes. The data applying to Shot 9 will be reviewed in detail since this experiment gave a good data return and is representative of the analysis necessary for a high pressure experiment.

A pressure gage record of representative but better than average quality is shown in Figure 3. The maximum indicated pressure, 1820 psia, is substantially larger than a value of 1660 psia derived from shock wave speed. It is clear that mechanical resonance associated with motion of the tube responding as an elastic member is also occurring. This high gage pressure apparently results from overshoot caused by acceleration-induced gage output. A faired peak pressure reading can be obtained by drawing a mean line through the resonance to obtain a corrected peak pressure value of 1700 psi as indicated in Figure 3.

A more satisfactory peak pressure value can be derived by measuring the shock wave velocity and using Rankin-Hugoniot relationships for a normal shock wave in air to derive expected

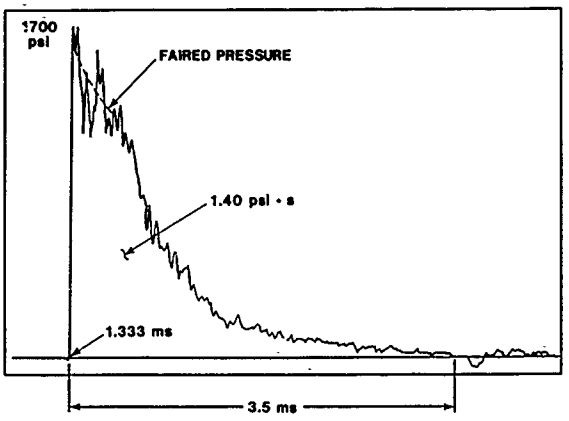

Fig. 3 - Record of Static Overpressure 6.45 m From Explosive on Test 9

pressures. Since timing errors of a few microseconds are important, we elected to use least squares methods and fit a quadratic curve to the position versus time of arrival data. Then, a continuous velocity equation was obtained by differentiation. Comparison of the time of arrival functio: and data is given in Figure 4. A summary of experimental data is given in Table 4.

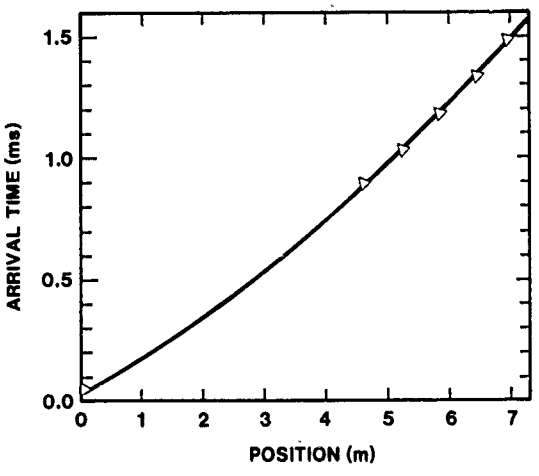

Fig. 4 - Quadratic Curve Fit to Time of Shock Wave Arrival for Test 9

Application of the normal shock relationships with a specific heat ratio of 1.25 which accounted for dissociation of air produced the velocity-pressure function shown in Figure 5. Both the measured peak and faired peak pressure values are included for comparison. The peak pressure versus position curve derived from time of arrival over the instrumented tube length was taken as the most accurate indication of peak static overpressure.

TABLE 4
Data Summary From Test 9

Data from 102 mm Shock Tube
TEST #9 1137 g C-4 3/22/82

Setup Parameters
Confinement-Steel
Bore = 102 mm
Wall = 12.7 mm
WHE = 1137 g
Gas Gamma = 1.25
Initial Pressure (kPa) = 575 kPa
Sound Velocity (m/s) = 338 m/s
Test Temperature (deg K) = 301 K

Constants for Quadratic X versus T Fit
A1 = .02425 ms
A2 = .14007 ms/m
A3 = .009847 ms/m^2

Data Summary

Gage ID	Position m	Time ms	Pmax MPa	Pfaired MPa	Impulse kPa·s
BREAKOUT	0.000	.024	0.00	0.00	0.0
P2D90	4.628	.886	16.07	15.34	9.4
P4D90	5.237	1.029	14.48	14.13	8.6
P7D90	5.847	1.177	14.07	13.45	9.9
P11D90	6.455	1.333	13.38	11.72	9.7
P21D90	6.953	1.477	12.55	11.03	11.0
P23D0	6.953	1.477	12.48	10.69	12.1

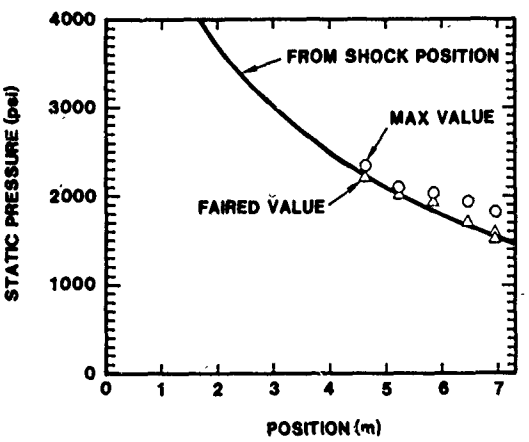

Fig. 5 - Comparison of Measured and Desired Peak Overpressures for Test 9

Impulse data was obtained by integration of the pressure records until the static pressure crossed the ambient pressure line. In cases where this zero crossing appeared delayed or did not occur due to zero shift, integration was terminated based on zero pressure crossings of adjacent pressure gages. The resultant impulse versus position data for Test 9 is given in Figure 6. Impulse data was so badly scattered by problems of zero shift during Shots 1 through 6 that impulses derived from this data were meaningless. However, by changing to gages with ablative coated diaphragms on Test 7, the data scatter was acceptable with results comparable to Figure 6 on all subsequent firings.

EXPERIMENTAL RESULTS

Nondimensional results are plotted in Figures 7 through 9 where the

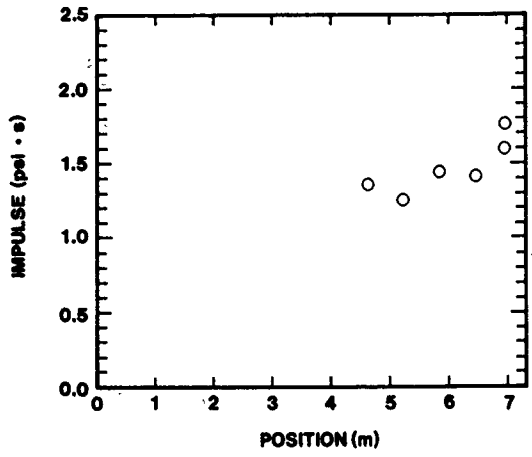

Fig. 6 - Impulse Data for Test 9

nondimensional parameters are defined as given below:

$\frac{P_s}{P_0}$ Nondimensional Pressure

$\frac{P_0 x A}{WE}$ Nondimensional Distance

$\frac{I_s C_0 A}{WE}$ Nondimensional Impulse

with the individual variables defined in Table 1.

Nondimensional Pressure versus Distance data based upon the time of arrival curve is shown for Tests 1 through 7 in Figure 7. Coefficients for this quadratic function are listed in Table 4. This group of experiments are directly comparable since only a single tube length was used; thus, no functional distortions existed either in the length parameter, L/D, or the surface roughness parameter, ε/D. The only distortion over this range involved the geometric distortion of the explosive assembly at the largest explosive weights. This distortion

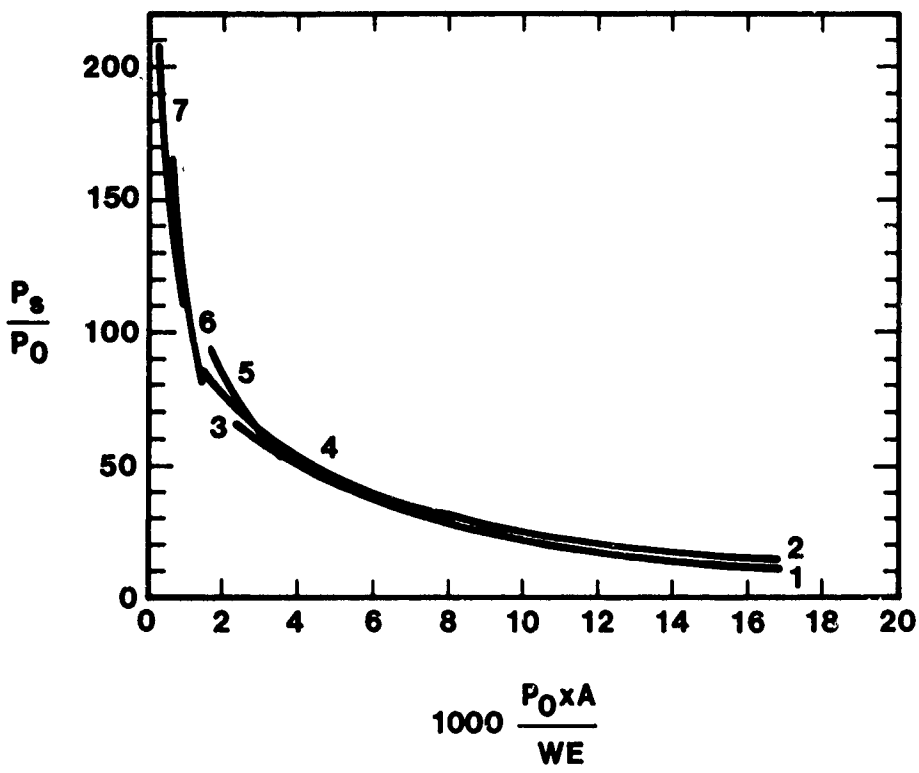

Fig. 7 - Nondimensional Pressure Versus Distance From Time of Arrival Curves for Seven Tests

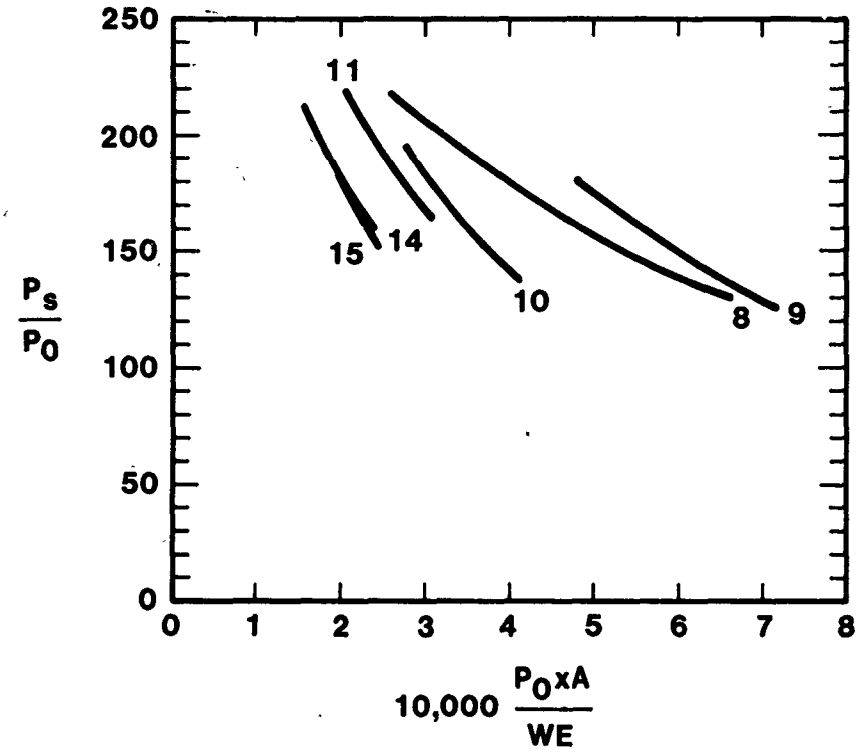

Fig. 8 - Nondimensional Pressure Versus Distance From Time of Arrival Curves for Tests 8 Through 15

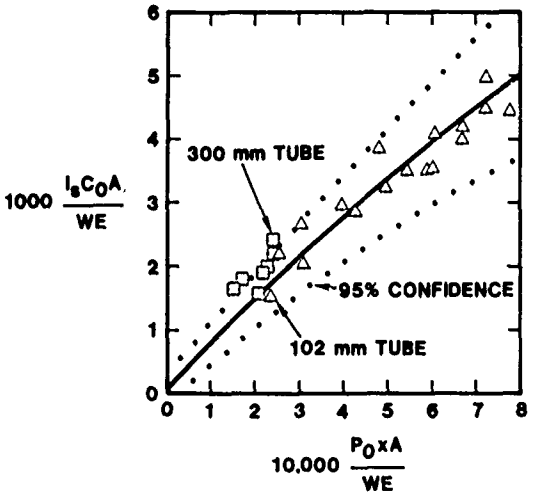

Fig. 9 - Nondimensional Impulse Versus Distance Data with Curve Fit to Triangular Points

allowed a relatively larger portion of the explosive energy to escape laterally on the higher pressure trials and is believed to explain why Test 7 is to the left of Test 6. Overall repeatability is indicated by a comparison of Tests 1 and 2 and is valid, at least at relatively low pressures. It is concluded that Figure 7 establishes a nondimensional calibration curve of pressure versus explosive weight for a relatively smooth shock tube with a maximum L/D of 33. Since a single curve can be drawn through this data, the edge loss distortion is evidently not important.

Similar curves are given in Figure 8 for Shots 9 through 11 as summarized in Table 2. Curves 14 and 15 are from a larger tube for conditions summarized in Table 3. Curve 8 involves a somewhat lengthened tube with the largest unconfined charge fired. Curve 9 involves an even longer tube with a confined explosive charge. The relative positions of these curves demonstrate the importance of confinement. Curves 9, 10, and 11 all involve the longest tube with an overall L/D ratio of 70 where both confinement and charge weight are increasing with test number.

Rather than the expected upward relative positioning of these curves, they are shifted primarily to the left indicating that additional explosive and confinement had a diminishing influence upon peak pressure. Apparently, boundary layer growth (Reference 4) in these relatively long tubes is restricting the down tube energy transport required to sustain extremely intense shock waves. It was concluded that a nondimensional pressure of 163 (2000 psi) could be generated at a nondimensional distance of .00031 in a smooth tube at a L/D position of 66, corresponding to the lower right edge of Curve 11. Nondimensional impulse versus distance data is plotted for Tests 7 through 15 in Figure 9. Data associated with the full-scale tube are represented by square symbols and will be discussed later. A least squares quadratic fit to small tube data is also shown together with 95% confidence intervals. This equation is:

$$\frac{I_s C_0 A}{WE} = .0000842 + 7.1712 \frac{P_0 x A}{WE} - 1253 \left(\frac{P_0 x A}{WE}\right)^2 , \quad (3)$$

$$\frac{P_0 x A}{WE} < .002 .$$

The impulse curve, unlike the pressure results, is not strongly affected by roughness or by length to diameter considerations, at least within indicated data scatter. Evidently, boundary layer growth allows sufficient energy flow to sustain pressures at lower levels after shock wave passage so that the lack of high pressure is compensated by longer pressure durations resulting in less sensitivity to tube length and friction than was the case for pressure. This is a useful finding of our model experiments.

PROTOTYPE SHOCK TUBE DESIGN

Two thick-walled steel pipes were readily available for full-size Radioisotope Heater Experiments. Using the dimensional analysis, the largest tube of 550 mm inside diameter was estimated to produce desired test conditions requiring a 155 kg composition C-4 explosive with a confined driver. The prospect of meeting other test requirements such as cost, post-test recovery of heat sources, and recovery of x-ray information in the presence of this explosive firing did not appear promising.

An intermediate-size pipe 18 m long of 300 mm bore and 28 mm wall was also available. Results from Test 11, when extrapolated to this configuration, indicated that a confined explosive charge of 59 Kg would produce a peak pressure of 14 MPa (2000 psi) and an impulse of 32 kPa s (4.7 psi s) at its muzzle. However, this tube was relatively much rougher than the model tube, suggesting that more frictional resistance could be expected. Since cost and time limited our calibration effort, we elected to adjust the explosive upward to 74.5 kg during the only calibration trial to allow some compensation for an expected pressure shortfall. Note that explosive requirements have been reduced by one half using the intermediate diameter pipe. The expected performance values were:

$$\frac{P_0 x A}{WE} = 0.000257$$

$$\frac{I_s C_0 A}{WE} = 0.0020$$

$$\frac{P_s}{P_0} \leq 180$$

Hence,

$$I_s \cong 36 \pm 7 \text{ kPa·s (5.2 psi·s)}$$

$$P_0 \leq 15.4 \text{ MP (2220 psi)}$$

CALIBRATION EXPERIMENT

With this background, a trial involving 73.5 kg of C-4 explosive was conducted representing nearly the maximum explosive possible. The test produced adequate conditions at the 17.7 m muzzle station to allow testing of Radioactive Heat Sources.

The prototype shock tube was constructed from three sections of schedule 120, 300 mm bore welded steel pipe. Under dynamic conditions, pipe sections were marginal at the breech where internal static overpressures near 35 MPa (5000 psi) could produce yielding. A 305 mm diameter by 610 mm long C-4 explosive charge contained in a 25 mm thick steel tube, closed at one end by a 25 mm steel plate and open toward the shock tube, comprised the expendable explosive driver. Plywood discs placed between flanged joints served to interrupt the path of stress waves traveling along the tube walls. A thick layer of moistened and tamped earth covered 10 m of tube providing additional stress attenuation.

Pressure instrumentation was mounted in the wall of the 8 m muzzle section.

INSTRUMENTATION

Six Kulite type HKS-375 10,000 psi pressure gages employing ablative thermal protection and mounted in phenolic inserts were spaced at 1.2 m intervals along the tube muzzle. Data is summarized in Table 5, and a pressure time record obtained at 16 m is given in Figure 10.

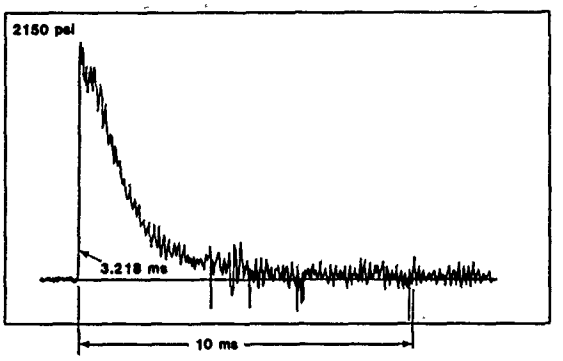

Fig. 10 - Record of Static Overpressure 16.3 m From Explosive on Test 15

Impulse associated with the measured static overpressure was obtained by integration. Obvious data deficiencies such as dropouts were replaced with faired lines as indicated. Based upon the scatter observed during model tests, error bars of about 3 KPA·s should apply.

Pressure gage time of arrival data was fit to a quadratic function using least squares techniques to produce the coefficients given in Table 6. The derived maximum nondimensional static overpressure versus position curve is shown in Figure 8 and labeled Test 14. This curve represents the best description of the tube peak presure performance. Measured peak faired pressure values are in reasonable agreement for the four of six gages which survived to generate usable pressure results.

In order to investigate target response without damaging a very expensive heater assembly during this calibration, a dummy of aluminum was constructed to mock the heater pellet and its surrounding carbon jacket. This unit was included so that, as it exited the shock tube, x-ray images could be obtained on film placed in protective cassettes near the muzzle. Only a rough estimate of expected velocity was available.

Target recovery was attempted by placing a berm of sawdust and fine soil in an enclosure built from massive concrete blocks 2 m from the tube muzzle. We estimated that the aluminum would penetrate 1 m into the catcher from a velocity of 300 m/s.

The pressure results indicated that useful test levels were obtained since a pressure of 14 MPa occurred at a station 16.8 m from the explosive output face where a static impulse of 38 $\pm$ 4 kPa·s was produced. The shock tube remained intact without evidence of plastic deformation except at the interface between the explosive driver and tube breech. At this location, steel was torn and burned from the tube edge and entered with the explosion gas flow. Evidence of fragment impact corresponded to one damaged pressure gage, and a few steel fragments were recovered in the catcher. An x-ray image of the dummy heat source was obtained from a film cassette which had been blown 100 m from its initial position. This image corresponded to the extraordinary target velocity of 1500 m/s. This lead to a more detailed study of target loading and motion in the blast flow with the tentative conclusion that most of the target acceleration occurs during the dense explosion product gas flow which generates stagnation pressures nearing 350 MPa (50,000 psi). The dummy heat source was successfully recovered. Substantial damage to the catcher occurred involving venting and movement of its concrete sides.

HEAT SOURCE TESTS

Two firings of the prototype shock tube were conducted to test heat sources. The first, Test 15, involved a single radioisotope heater assembly filled with inert fuel simulants and placed on an aluminum mounting plate at the 17.8 m station where results from Test 14 indicated that static overpressure would be 10% below desired values, while the impulse should be somewhat higher than desired. This compromise in test conditions allowed use of the tube without the expense of modifications. The expendable driver section was lengthened 200 mm to reposition its output face 305 mm from the tube muzzle to reduce fragment ingestion.

The heat source was thus subjected to a static overpressure of 13 MPa (1850 psi) and a static impulse of 38 kPa·s (5.6 psi·s). The nondimensional

TABLE 5
Data Summary From Test 15

Data from 300 mm Shock Tube
TEST #15 73.5 kg C-4 5/13/82

Setup Parameters
Confinement-Steel
Bore = 300 mm
Wall = 25.4 mm
WHE = 73.5 g
Gas Gamma = 1.25
Initial Pressure (kPa) = 84.8 kPa
Sound Velocity (m/s) = 341 m/s
Test Temperature (deg K) = 306 K

Constants for Quadratic X versus T Fit
A1 = .08103 ms
A2 = .14241 ms/m
A3 = .003053 ms/m^2

Data Summary

Gage ID	Position m	Time ms	Pmax MPa	Pfaired MPa	Impulse kPa·s
BREAKOUT	0.000	.081	0.00	0.00	0.0
P45	13.879	2.647	0.00	0.00	0.0
P49	15.104	2.928	14.00	13.65	28.3
P53	16.323	3.218	14.76	14.07	35.2
P57	17.525	3.516	14.89	13.58	39.3

TABLE 6
Coefficients for Quadratic Position Time Data

$T = A1 + A2 * X + A3 * X^2$; T(ms),X(m)

Test	A1 (ms)	A2 (ms/m)	A3 (ms/m^2)
1	.00685	.2780	.09617
2	.00435	.3108	.07473
3	.00732	.3029	.04293
4	.01238	.2792	.03183
5	.01086	.2359	.02808
6	.01179	.1619	.02788
7	.02275	.1860	.01757
8	.01550	.1715	.01207
9	.02425	.1401	.00984
10	.02400	.1353	.00927
11	.02971	.1460	.00702
14	.10340	.1487	.00305
15	.08103	.1424	.00305

static overpressure position data for this experiment is plotted in Figure 8, while nondimensional impulse data is indicated by squares in Figure 9. Shock tube performance was essentially identical to the calibration test verifying good shot-to-shot repeatability. An x-ray image of the Heat Source Capsule was obtained as shown in Figure 11, indicating that the capsule remained intact. Capsule position is consistent with a blast-induced velocity of approximately 1300 m/s. The capsule was not found after an extensive search of the catcher material. Since the catcher was disrupted by the blast and because some sawdust was blown away, we suspected that the heat source was carried out of the catcher with this debris.

A repeat test was conducted for the purpose of recovering capsule assemblies for detailed laboratory examination. Three heat source assemblies were all mounted on a single plate. The catcher was strengthened and moved to a position 3 m from the tube. As an economy measure, no instrumentation was included since repeatablility had already been demonstrated.

Two of the three capsules were recovered and found to be flattened on one side. Because the x-ray from the previous test had shown no deformation after the blast encounter, this damage is thought to result from impact into the dirt and sawdust-filled catcher. Even with this deformation, laboratory examination showed that the capsule wall was not breached and it retained the simulated radioactive contents. Thus, even in this extreme "worst case" blast environment, the capsule design objectives were realized.

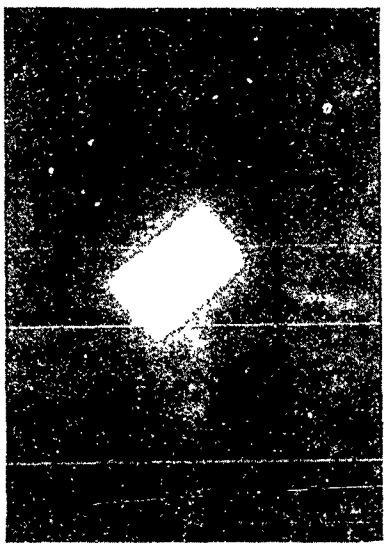

Fig. 11 - X-Ray Image of Capsule in Flight Just Before Entering Catcher

ACKNOWLEDGEMENTS

The assistance of Tom Witherspoon, Richard Bohannon, and Duane Smith, all of Sandia National Laboratories, is gratefully acknowledged. We worked with Stanley Bronisz and C. Melvin Seabourn of Los Alamos National Laboratory.

REFERENCES

1. R. E. Tate, "The Light Weight Radioisotope Heater Unit (LWRHU): A Technical Description of the Reference Design," Los Alamos National Laboratory, LA-9078-MS, US-33a, Jan. 1982

2. W. B. Leisher, "Shock Tube Explosive Charge Geometries, Performance and Scaling," Sandia National Laboratories; Proceedings of the Third Conference on the Military Application of Blast Simulators, 1972

3. Dept. of the Army Technical Manual, TM 5-1300; Dept. of the Navy Publication, NAVFAC P-397; Dept. of the Air Force Manual, AFM 88-22, "Structures to Resist the Effects of Accidental Explosions"

4. A. G. Gaydon, D.Sc., F.R.S., University of London and I. R. Hurle, Ph.D. (Cantab.), Cornell Aeronautical Laboratory, Inc., Cornell Univ., "The Shock Tube in High-Temperature Chemical Physics," Reinhold Publishing Corp., New York, 1963

5. Wilfred E. Baker, Peter S. Westine, Southwest Research Institute; Frnklin T. Dodge, Univ. of Tennessee, "Similarity Methods in Engineering Dynamics," Hayden Book co., Inc., Rochelle Park, New Jersey

DISCUSSION

Voice: You went through a great deal of trouble to get these high pressures in the air. Did you consider using water as a medium, thereby reducing the amount of explosive necessary and so forth? If it were just a pressure pulse you wanted, you would get that. This is just an idea.

Mr. Mathews: The problem became one of trying to represent the gas flow field in the vicinity of the test article. The introduction of a non-realistic medium would have complicated things beyond the realm of environmental verification, so those methods were not considered.

CALCULATION OF THE SHOCK WAVE FROM A PENTOLITE TAPERED CHARGE

James T. Gordon and David K. Davison
Physics International Company
San Leandro, California 94577

Results are presented from two-dimensional computations simulating the shock wave produced by the underwater detonation of a small-scale, 2.66 pound Pentolite tapered charge. These calculations were performed using the nonlinear explicit finite-difference computer code PISCES 2D ELK. The numerical model employed represented the Pentolite high explosive by a finely zoned Eulerian mesh and used the JWL (Jones-Wilkens-Lee) equation of state. The water region surrounding the tapered charge was modeled by a Lagrangian grid and used a single-phase equation of state developed by Walker and Sternberg. This water model gives pressure as a function of density and internal energy on the Hugoniot, and for adiabatic release off the Hugoniot for initial shock pressures up to 250 kbar. The coupled Euler-Lagrange technique is quite beneficial from a computational standpoint since the calculation tends to run more smoothly when the explosive grid remains fixed in space thus eliminating mesh distortion difficulties. The two-dimensional finite-difference calculation was run to 1200 μs after detonation of the high explosive. Results presented include pressure contours, mesh plots, and pressure time histories. The growth of the gas bubble produced by the detonation products is shown in mesh plots at various times during the calculation. Pressure contour plots show the planarity of the shock wave produced by the tapered charge. A comparison of computed pressure histories with digitized experimental records shows excellent agreement.

INTRODUCTION

Tapered charges are explosives designed to generate long duration shock waves. The pressure field produced by a tapered charge is directional with the maximum duration times being obtained along the longitudinal axis of the charge. The duration of the shock wave is long compared to the duration produced by an equivalent amount of explosive in spherical or constant radius cylindrical form. Tapered charges have been built in sizes ranging from a few ounces to over 15,000 pounds. Their purpose is to provide a pressure pulse which will simulate nuclear shock wave loading on scaled models. The 2.66 pound Pentolite tapered charges are used to provide shock wave loading on small scale three inch diameter models. These models were evaluated at the Explosion Test Pond Facility at Carderock in the Nuclear Damage Rule Development Program instigated by the David W. Taylor Naval Ship Research and Development Center (Reference 1).

This paper documents numerical studies conducted using the nonlinear explicit finite-difference computer code PISCES 2D ELK to simulate and predict the shock wave produced by the underwater detonation of a small-scale 2.66 pound Pentolite tapered charge. The goal of this numerical simulation was to demonstrate the applicability of the explicit finite-difference technique in predicting the shock loadings produced by tapered charges. Although the greatest amount of experimental data is available for HBX-1 tapered charges, a Pentolite charge was selected for analysis because the equation of state is better known for Pentolite than for HBX-1. Also, the parameters required to apply the existing method for predicting tapered charge shockwaves are unknown for Pentolite.

TAPERED CHARGE DESCRIPTION

A tapered charge consists of a series of truncated cones or cylinders arranged on a common axis. The charge is detonated at one end and the detonation wave propagates down the length of the charge at a fixed velocity (the detonation velocity) as depicted in Figure 1. The 2.66 pound Pentolite tapered charge simulated in these calculations is shown in Figure 2. The 18.3 inch long charge has a diameter which tapers from 0.5 inches at the nose to 1.5 inches at the end of the first tapered section. The charge then tapers to a diameter of 1.93 inch at its other end. Figure 3 shows a

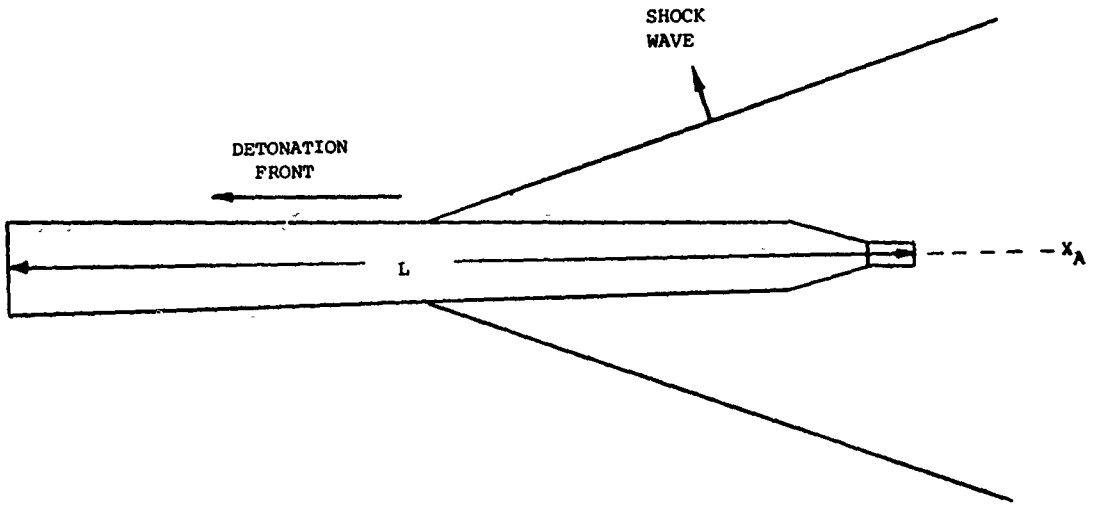

Figure 1 - Detonation of Tapered Charge

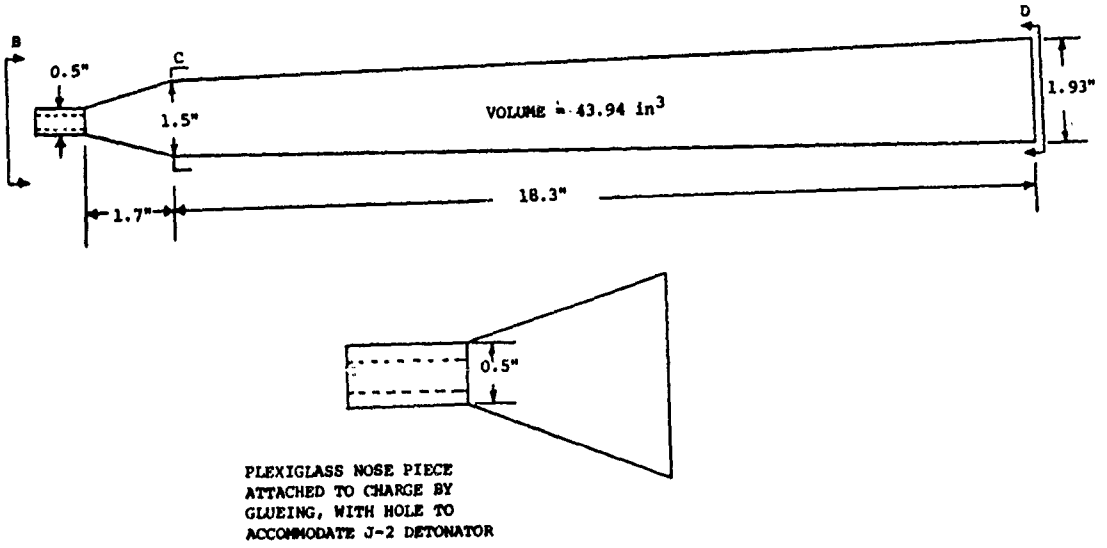

Figure 2 - 2.66 Pound Tapered Charge Design for Use on Small Scale Models

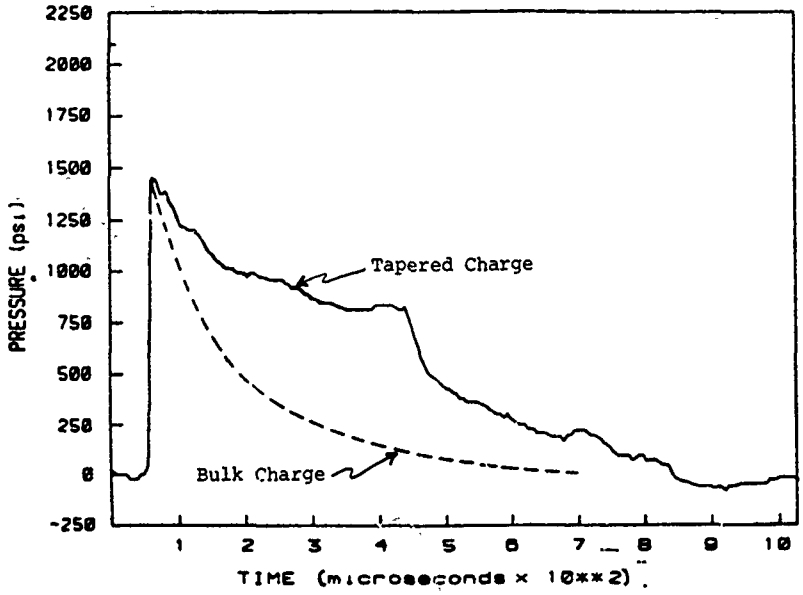

Figure 3 - Pressure-Time History Comparison Between a Tapered Charge and a Bulk Charge

a pressure history obtained from a 2.66 pound Pentolite tapered charge at a 70 inch standoff. Also shown in this figure is a comparison with the pressure history predicted using a bulk charge of equivalent weight to generate the same peak pressure. The advantage of a tapered charge is evident when simulating long duration shock wave loading.

PROBLEM SIMULATION

The numerical simulation of the underwater detonation of a Pentolite tapered charge has been performed using the nonlinear explicit finite difference code PISCES 2D ELK. These two-dimensional calculations have applied a coupled Euler-Lagrange technique in which separate Eulerian and Lagrangian finite-difference grids are allowed to interact. This method allows a cost effective zoning scheme to be employed with the appropriate zoning to resolve the shock applied in each grid. In these numerical simulations, the Pentolite high explosive was modeled with a finely zoned Eulerian mesh (grid fixed in space). The fine zoning is necessary to resolve the initial shock wave. The water region surrounding the tapered charge was modeled by a Lagrangian grid (constant mass zones). The Lagrangian grid must maintain a sufficiently fine zoning to resolve the shock in the water but is inherently less expensive than the Eulerian computational scheme. This coupled Euler-Lagrange technique is quite beneficial from a computational standpoint. When the explosive grid remains fixed in space, the calculation tends to run more smoothly and mesh distortion difficulties are eliminated.

The Pentolite tapered charge in these calculations is about 50 cm long and 5 cm in diameter. Figure 4 is a diagram of the tapered charge and the experimental pressure gage stations. The objective of the PISCES 2D ELK calculation was to compare the pressures computed at certain close-in locations to those obtained in the experiments. Figures 5 and 6 show the initial configurations of the Lagrangian water mesh and the Eulerian mesh containing the Pentolite high explosive, respectively. A nominal initial zone size of 2 cm was selected for the water mesh in the gage region and a nominal size of 1 cm was chosen for the explosive mesh. The calculation was performed in axial symmetry. In Figures 5 and 6, the axis of symmetry is the bottom edge of the mesh. In Figure 5 the boundary of the Euler mesh containing the explosive is shown for reference. The outline of the tapered charge is seen centered in the Euler mesh. In Figure 6, the boundary of the Lagrangian water mesh is shown for reference. The third row of the Euler mesh coincides with the edge of the long tapered section of the charge. The back of the charge coincides with column number 75 as indicated in Figure 6. The Lagrangian water mesh consists of 1830 zones (31 x 62 grid points). The Eulerian high explosive mesh contains 3510 zones (40 x 91 grid points).

The edges of the Lagrangian water mesh were modeled as non-reflecting boundaries using the transmitting boundary option in the PISCES 2D ELK computer code (References 2 and 3). The transmitting boundary option is discussed in Reference 2. It is fundamentally a stress boundary condition which damps longitudinal and shear waves.

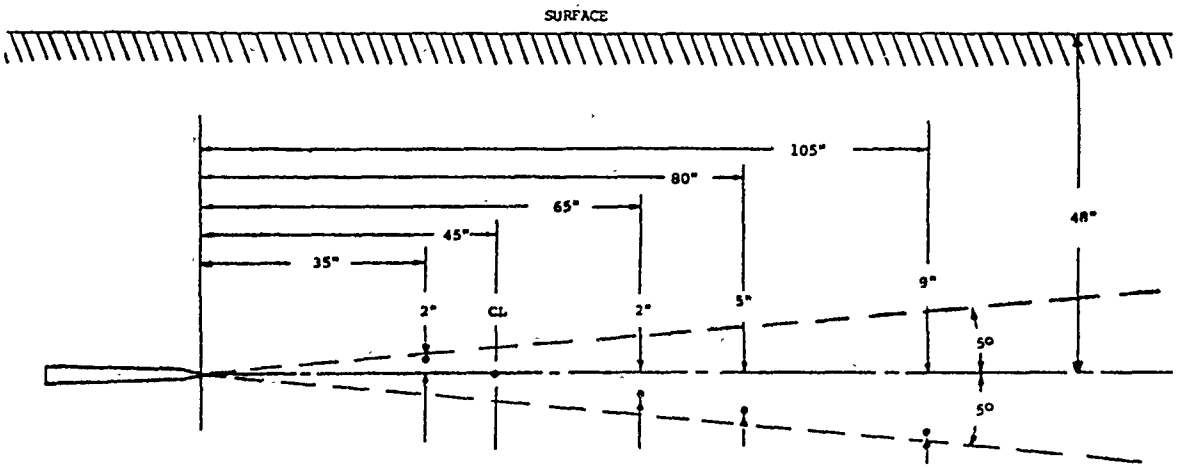

Figure 4 - Test Arrangement to Determine Free Field Pressure Measurements

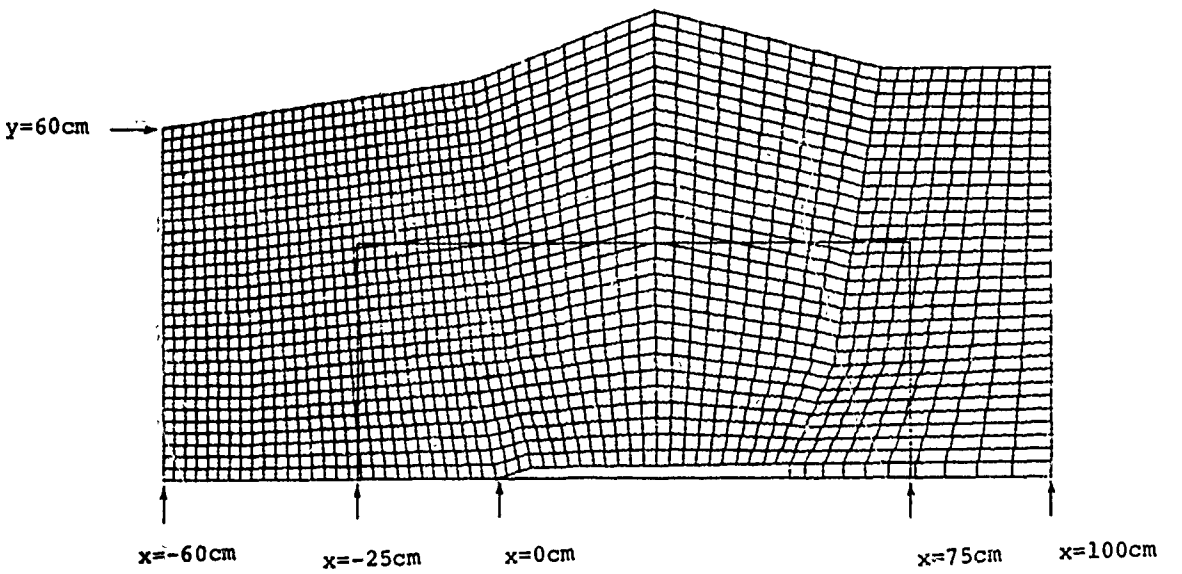

Figure 5. Initial configuration for the Lagrange water mesh. The axis of symmetry is the bottom edge of the mesh. The boundary of the Euler mesh containing the explosive is included for reference. The outline of the tapered charge is seen centered in the Euler mesh.

The explosive behavior of the Pentolite was modeled by the JWL (Jones-Wilkens-Lee) equation of state. The equation of state for Pentolite is well represented by the JWL model. This model describes the adiabatic expansion of the explosion products for many explosives and is widely accepted. Table 1 presents a summary of the JWL parameters for Pentolite used in these calculations. These values and a complete description of the JWL model are given in Reference 4.

The water equation of state selected is that of Walker and Sternberg (Reference 5). This model gives pressure as a function of density and internal energy on the Hugoniot, and for adiabatic release off the Hugoniot for initial shock pressures up to 250 kbar. Table 2 summarizes this water equation of state in computer code units. Figure 7 shows the comparison of isentropes for this equation of state (EOS) with those obtained from Butkovich (Reference 6). The Walker-Sternberg EOS does not attempt to model the production of steam below the saturation line, so the two models disagree below

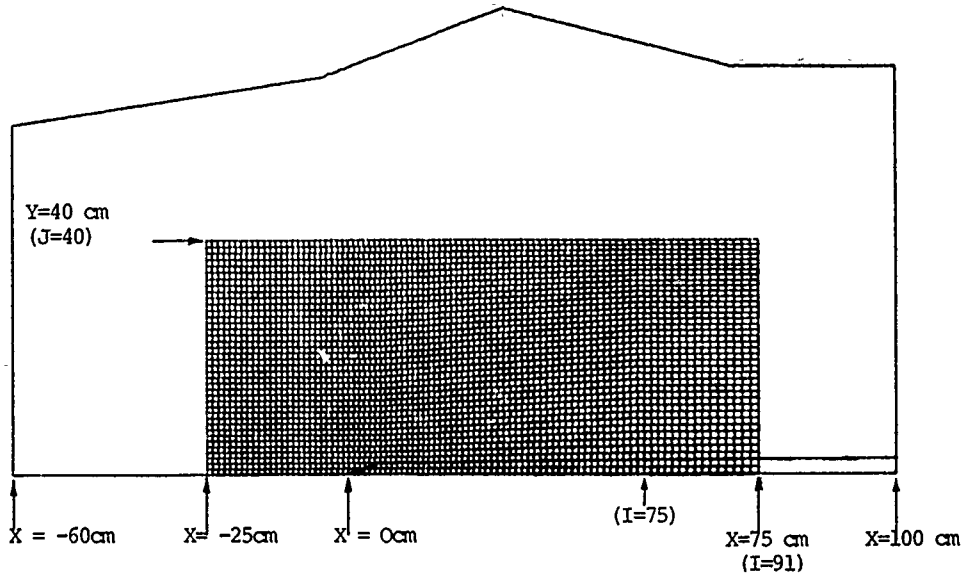

Figure 6. Euler mesh containing the explosive. The boundary of the Lagrange water mesh is included for reference. The third row of the Euler mesh coincides with the edge of the long tapered section of the charge, and the back of the charge coincides with column number 75.

TABLE 1.

JWL EOS Parameters for Pentolite
50/50 Composition: 50/40 TNT/PETN

A = 5.4094 Mbar	E_o = 0.081 Mbar-cm^3/cm^3
B = 0.093726 Mbar	ρ_o = 1.68 gm/cm^3
R_1 = 4.5	D = 0.753 cm/μsec (Detonation velocity)
R_2 = 1.1	P_{cj} = 255.0 kbar (C-J Pressure)
ω = 0.35	γ_{cj} = 2.78 (Energy released per unit HE mass)

that point. Above the saturation line, however, the two models agree well. Walker and Sternberg examined the contribution of steam-generated pressure within the bubble for Pentolite explosions detonated in water (Reference 5). They concluded that steam, even if generated, would not significantly raise the pressure within the bubble.

The importance of steam production was considered in previous studies of explosion bubble pulsation caused by the deep underwater detonation of a tapered charge (Reference 7). The question of steam generation was investigated by a series of cylindrically symmetric one-dimensional calculations. The results of these calculations showed that a cylindrical envelope surrounding the charge with an approximate thickness of 6 cm could possibly generate steam when the pressure within that region of shocked water falls below the corresponding pressure on the saturation curve. This corresponds to a pressure of about 10 bars, or about one-third of the hydrostatic pressure at a depth of 305 m. Thus, it was concluded that steam production could contribute (if it forms at all) only to the late-time pressure within the bubble, i.e., near the time when the bubble reaches its maximum radius. Hence, it will not contribute significantly to the initial bubble growth. The peak bubble radius occurs at times much greater than the times of interest in the current small-scale Pentolite calculations. Thus, neglecting steam production is a conservative assumption.

Table 2. Summary of water EOS model of Walker and Sternberg

$$p\ (\text{mbar}) = f_1\,\rho + f_2\,\rho^3 + f_3\,\rho^5 + f_4\,\rho^7$$

ρ = current density (g/cm^3); $\rho_o = 0.9982$ g/cm^3

$0 < E < 0.006$

$$f_1 = 0.005722427 - 1.240522\,E + 50.42535\,E^2 - 1.400579 \times 10^3 E^3 + 4.137950 \times 10^6 E^4 - 2.726437 \times 10^8 E^5 - 1.295684 \times 10^{11} E^6 + 1.437988 \times 10^{13} E^7$$

$0.006 < E < 0.017$ ($E' = E - 0.006$)

$$f_1 = 0.001015091 - 0.3270122\,E' + 6.734616\,E'^2 + 1.552785 \times 10^4 E'^3 - 2.926440 \times 10^6 E'^4 + 2.139341 \times 10^8 E'^5 - 5.61538 \times 10^9 E'^6$$

$0.017 < E$ ($E'' = E - 0.017$)

$$f_1 = 5.607572 \times 10^{-4} + 0.1122840\,E'' + 5.27579\,E''^2 + 82.21745\,E''^3 - 147.1514\,E''^4 - 4.044093 \times 10^3 E''^5 - 3.130131 \times 10^4 E''^6$$

$0 < E < 0.0032$

$$f_2 = -0.02748180 + 1.691130\,E + 17.12981\,E^2 + 1.483364 \times 10^4 E^3 - 1.549072 \times 10^7 E^4 + 3.415591 \times 10^9 E^5 - 2.357818 \times 10^{11} E^6$$

$0.0032 < E < 0.0245$ ($E' = E - 0.0032$)

$$f_2 = -0.02215430 + 1.510990\,E' - 10.56299E'^2 - 5.411856 \times 10^3 E'^3 + 6.176871 \times 10^5 E'^4 - 1.810118 \times 10^7 E'^5 - 6.205700 \times 10^8 E'^6 + 4.406075 \times 10^{10} E'^7 - 6.587460 \times 10^{11} E'^8$$

$0.0245 < E$ ($E'' = E - 0.0245$)

$$f_2 = 0.002499950 + 0.9374720\,E'' - 4.624610\,E''^2 - 44.52203\,E''^3 + 375.1364\,E''^4$$

$$f_3 = 0.0268 - 0.4148\,E$$

$$f_4 = -0.005 + 0.0741\,E$$

E = internal energy in mbar-cm^3/g

DESCRIPTION OF CALCULATION

The calculation was completed in four stages, to 1200 μs after detonation of the high explosive:

1. Time 0-150 μs. Initial grids are shown in Figures 5 and 6. The Euler mesh was rezoned at 100 μs; alternate rows and columns were removed, as were the outer 15 rows.
2. Time 150-600 μs. The Lagrange mesh was expanded along the axis of symmetry and radially as shown in Figures 8-10. The Lagrange water mesh was also rezoned in the vicinity of the tapered charge and along the axis of symmetry.
3. Time 600-1037 μs. The calculation was restarted at 600 μs and terminated unexpectedly early, at time 1037 μs, due to zone tangling in the Lagrange

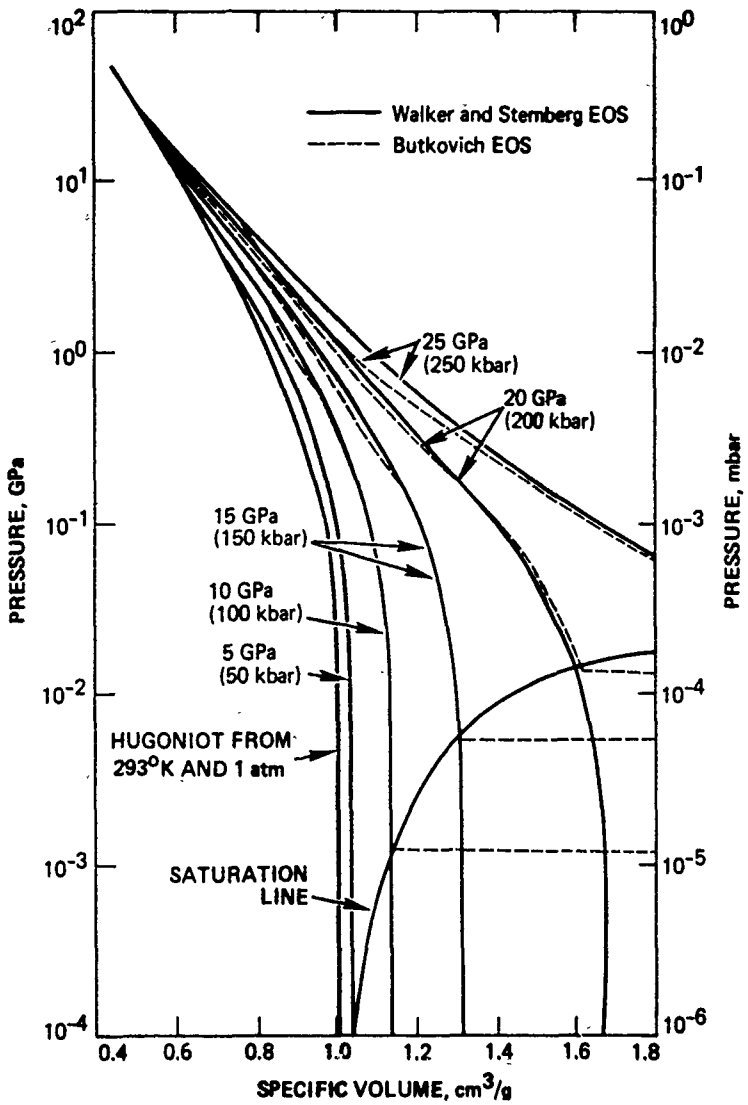

Figure 7. Water isentropes calculated using the Walker and Sternberg EOS model compared with those calculated by Butkovich.

mesh near coordinate X = 0 cm.

4. Time 1037-1186 μs. The troublesome part of the mesh was rezoned, and the calculation restarted and run to completion.

Figure 8 shows the Lagrange water mesh at 300 μs after detonation. Additional zones have been added to both ends of the initial grid shown in Figure 5. Figure 9 shows the Lagrange water mesh at 600 μs for an initial calculation (without expanding the mesh in the radial direction). Figure 9 also shows the Euler mesh containing the explosive gages. The Euler mesh was rezoned at 100 μs by removing alternate rows and columns. In addition, the outer fifteen rows of the Euler mesh were eliminated. Examination of the pressure histories and contours for this initial calculation showed formation of a rarefaction wave at the upper boundary of the water grid. This reflected wave was formed by the interaction of the shock front with the boundary. The transmitting boundary condition which was applied at the upper boundary of the Lagrange mesh did not achieve complete shock transmission. This result occurred because the non-reflecting boundary option used in PISCES 2D ELK will achieve complete shock transmission only for normal incidence shock waves. A proper treatment of oblique shocks can be accomplished but requires a more complicated boundary logic. The simplest solution to eliminate this problem was to extend the mesh in the radial direction. Figure 10 shows the expanded Lagrange mesh for elimination of boundary effects. The boundary was extended sufficiently far from the charge to ensure that reflected waves (generated by

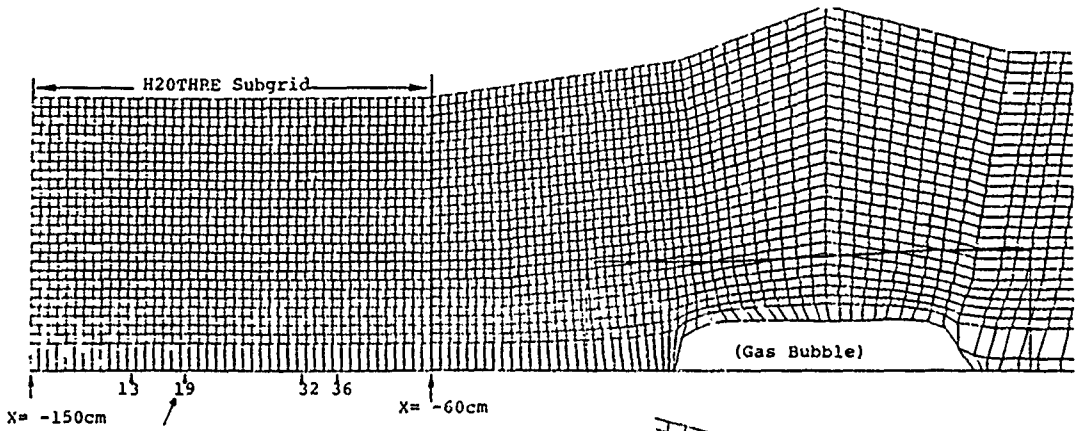

Column Indices
Corresponding to
Gage Station Locations

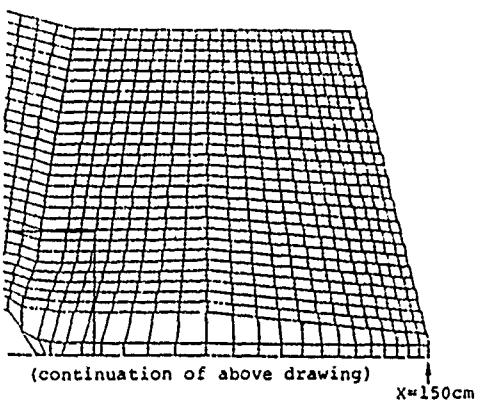

Figure 8. Lagrange water meshes at time 300 us. Additional zones have been added to both ends of the initial mesh (Figure 5.). The Lagrange mesh rezone was performed at 5ime 150 us.

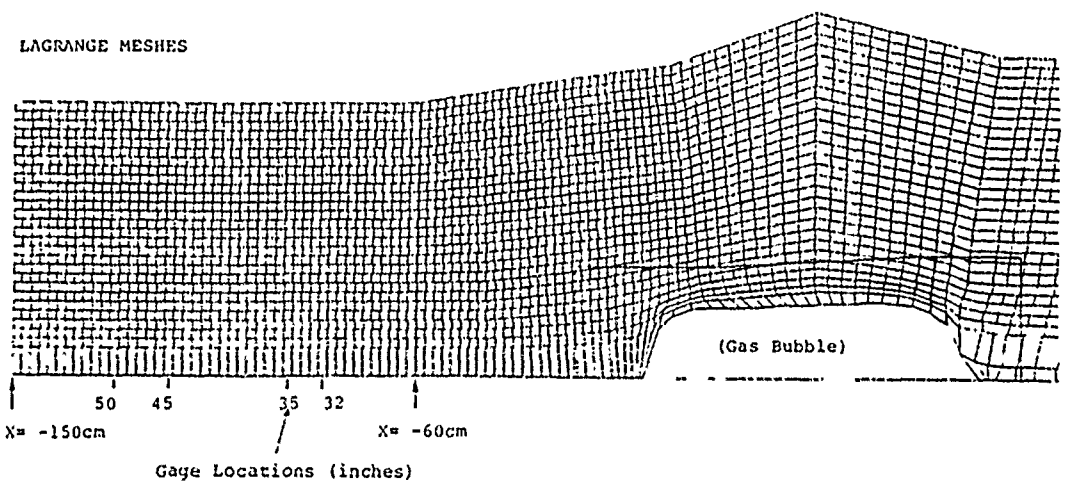

Figure 9. Left end of Lagrange water meshes at time 600 us and rezoned Eulermesh. The outline of the Euler mesh is shown in the upper diagram.

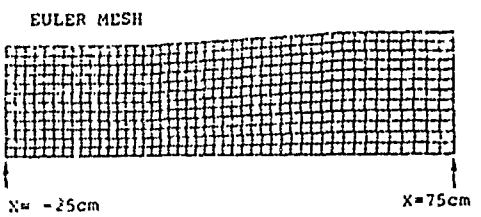

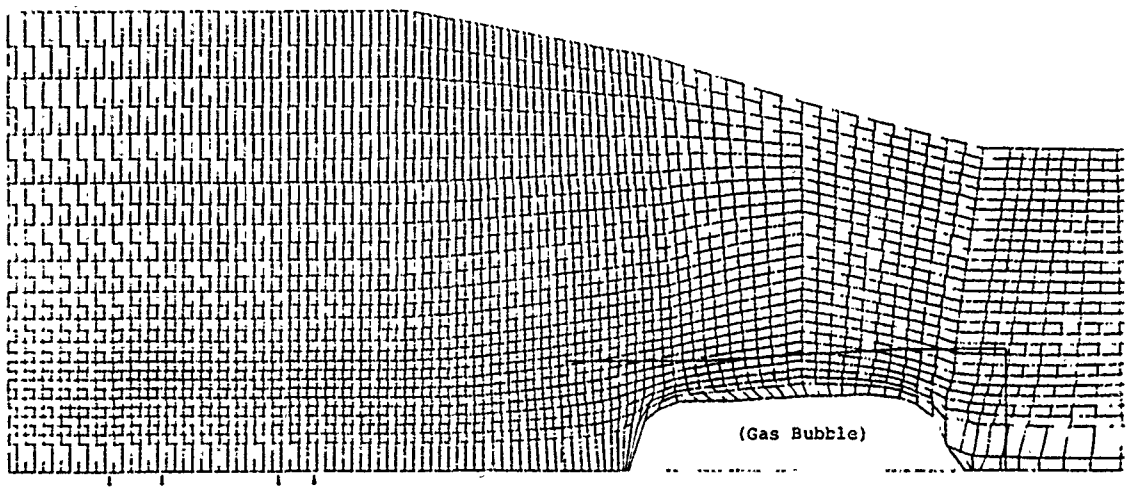

Figure 10. Expanded Lagrange mesh for elimination of boundary effect. The radius of the left end of the mesh was increased from 60 cm to 100 cm. This is a plot of the mesh at time 600 μs, and it can be compared with Figure 9. The gage locations are indicated.

incomplete shock transmission) would not arrive at the gage stations during times of interest. With this modification of the grid, the calculation was restarted and run until zone tangling unexpectedly occurred in the Lagrange water mesh at 1037 μs. The mesh was rezoned and the calculation was restarted and run to completion.

Figures 11 and 12 show the calculated pressure histories for gage stations at 32, 35, 45, and 50 inches standoff from the tapered charge. In these figures, plots of P and P + Q versus time are shown, where P = pressure and Q = artificial viscosity. The theoretical duration of the pressure plateau, 340 μs, is shown on these plots. This time is defined to be the longest shock wave duration possible with a given charge. It is a function of the charge length, the detonation velocity, and the shock propagation speed in the water near the charge. It is obtained along the extended charge axis on the initiation side of the detonation. A good approximation of this theoretical value is given by charge length divided by the speed of sound in water (Reference 1).

Figure 13 shows pressure contours in the vicinity of the gage stations at times 750 μs and 900 μs. Note the planarity of the pressure wave near the axis of the charge. Figure 14 shows pressure contours near the gage stations at time 1050 μs. Note that the boundary has induced a compressive shock front for the final zoning (expanded in the radial direction and along the charge axis). If the initial zoning had been used for the entire calculation, a rarefaction wave would have been produced by the oblique shock reflection and would have affected the gage station pressures during the times of interest.

COMPARISON WITH EXPERIMENT

Two of the experimental pressure traces in Reference 1 were digitized and transformed for direct comparison with the calculated pressure histories. Figure 15 shows a comparison of experimental and calculated pressures at 32 and 35 inch standoffs. The agreement at 32 inches standoff is excellent, and at 35 inches, very good. The peak pressures are quite close to the experimental values. Figure 16 shows a comparison of calculated peak pressures with experimental peak values from Reference 1 in the standoff interval from 30 to 55 inches. The agreement is seen to be very good. The computed curves tend to lie above the experimental data. Thus, estimates of pressure loading effects based on computed values will tend to be conservative.

The rise time of the calculated pressure peak is about 100 μs. The observed rise time was between 12 and 15 μs. There are several reasons which could account for this discrepancy. First, in the calculation, the steepness of the shock is controlled in part by the artificial viscosity coefficient and the size of the mesh zones. A rise time of 100 μs is consistent with the viscosity values and zone sizes used in this calculation. Secondly, the tapered charge was modeled with a pointed nose as seen in Figure 5. This was done primarily to minimize computational costs by avoiding the use of additional zones within the high explosive region. However, the steepness of the shock front is determined largely by the blunt nose of the charge design. A sharp nose charge would have a much longer rise time than a blunt nosed charge of the same design.

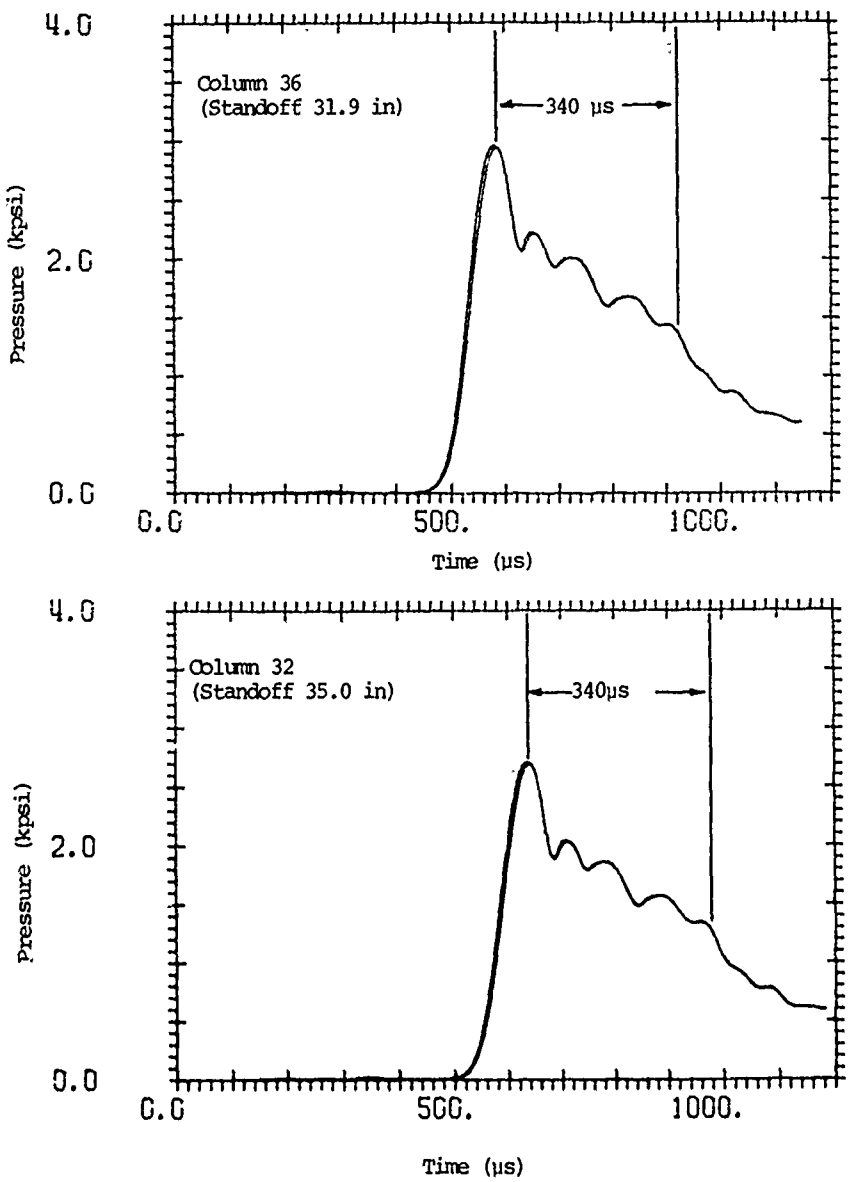

Figure 11. Pressures at standoffs 32 and 35 inches. (Both P and P+Q are plotted. The theoretical plateau duration is marked.)

There are three criteria for evaluating the adequacy of the computational model: the peak pressure, the pressure plateau duration, and the plateau pressure. Comparison of computational and experimental results shows that the first two aspects of the pressure traces are adequately modeled by the present technique. Since the pressure traces for the Pentolite tapered charge do not have a persistent, flat plateau at the close-in standoff distances investigated here, it is difficult to draw conclusions about the third aspect. Estimates were made of the pressure immediately prior to the exponential fall-off which occurs approximately 340 µs after the peak. Figure 17 compares the values derived from the calculation with those taken from the short standoff traces in Reference 1. The experimental scatter is large. Consequently, the adequacy of the derived plateau pressure cannot be fully confirmed. Future calculations on HBX-1 tapered charges should resolve this question since these charges produce well-defined pressure plateaus. A fourth possible evaluation criterion is pressure impulse. Since the shock rise time was considerably larger than the measured value, a good comparison at early times was precluded. For times after the peak pressure is attained, the comparison should be good since the pressure histories compare quite favorably. Future work

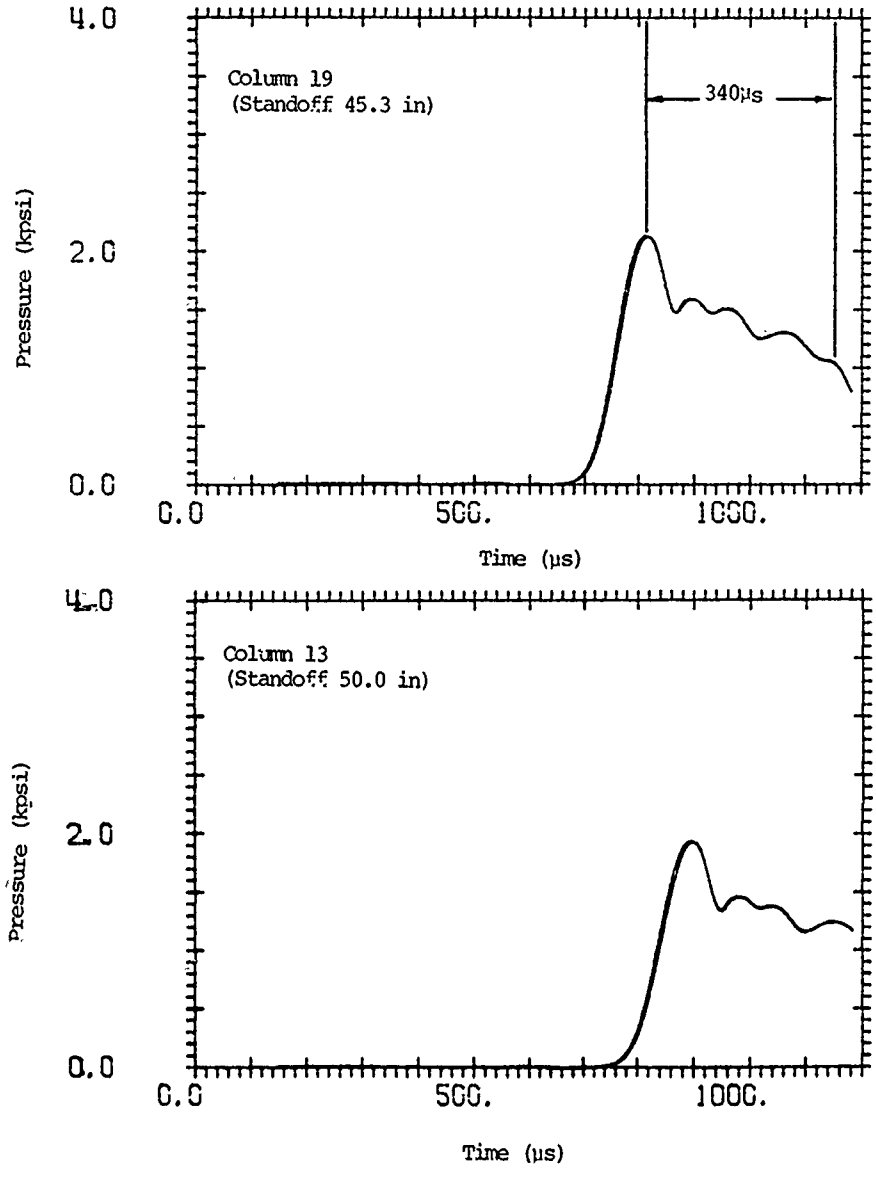

Figure 12. Pressures at standoffs 45 and 50 inches. Both P and P+Q are plotted, as in Figure 15. The theoretical plateau duration is marked on the 45 inch standoff wave.

will focus on improving the calculated shock rise time with more detailed modeling of the blunt nose of the tapered charge.

CONCLUSION

Results from two-dimensional computations simulating the shock wave produced by the underwater detonation of a Pentolite tapered charge have been presented. Comparison of these results with experimental data has demonstrated the capability of the coupled Euler-Lagrange finite-difference calculational technique to predict pressure loadings produced by tapered charges. The calculation was performed in axial symmetry. The numerical model represented the Pentolite high explosive by a finely zoned Eulerian mesh and used the JWL (Jones-Wilkens-Lee) equation of state. The water region surrounding the tapered charge was modeled by a Lagrangian grid and used a single-phase equation of state developed by Walker and Sternberg. A comparison of computed pressure histories with digitized experimental records showed excellent agreement. Three criteria were used for evaluating the adequacy of the computational model: the peak pressure, the pressure plateau duration, and the plateau pressure. Comparison of computational and experimental results showed that the first two aspects of the pressure traces were adequately modeled by the present technique. The pressure traces for the Pentolite charge

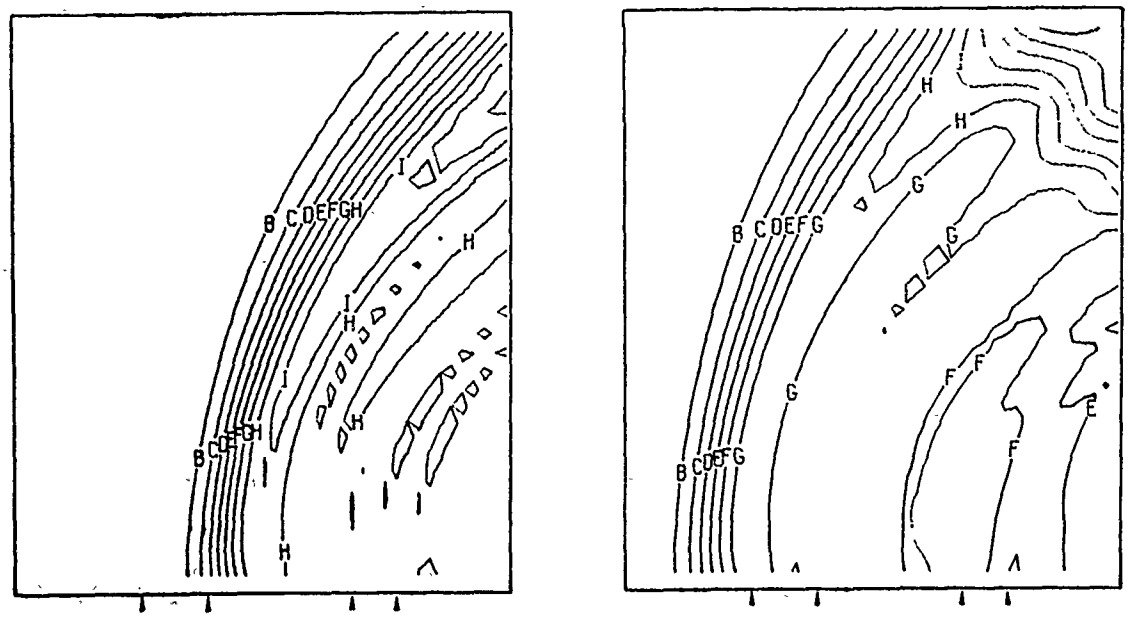

a. 750 μs

b. 900 μs

Figure 13. Pressure contours near the gages at times 750 μs and 900 μs. Contour increment is 20 bars (280 psi); contour B is 20 bars. The gage stations are marked.

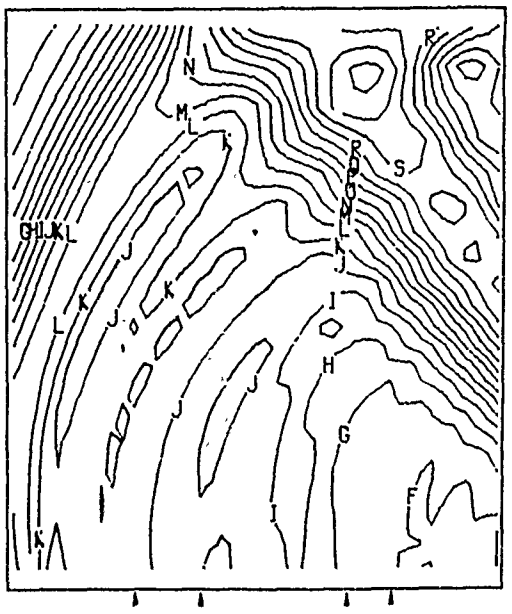

Figure 14. Pressure contours near the gages at times 1050 μs. Contour increment is 10 bars (140 psi); contour B is 10 bars. The gage stations are marked. Note that the boundary induces a compressive shock front for this zoning; for the initial zoning the shock is a rarefaction wave.

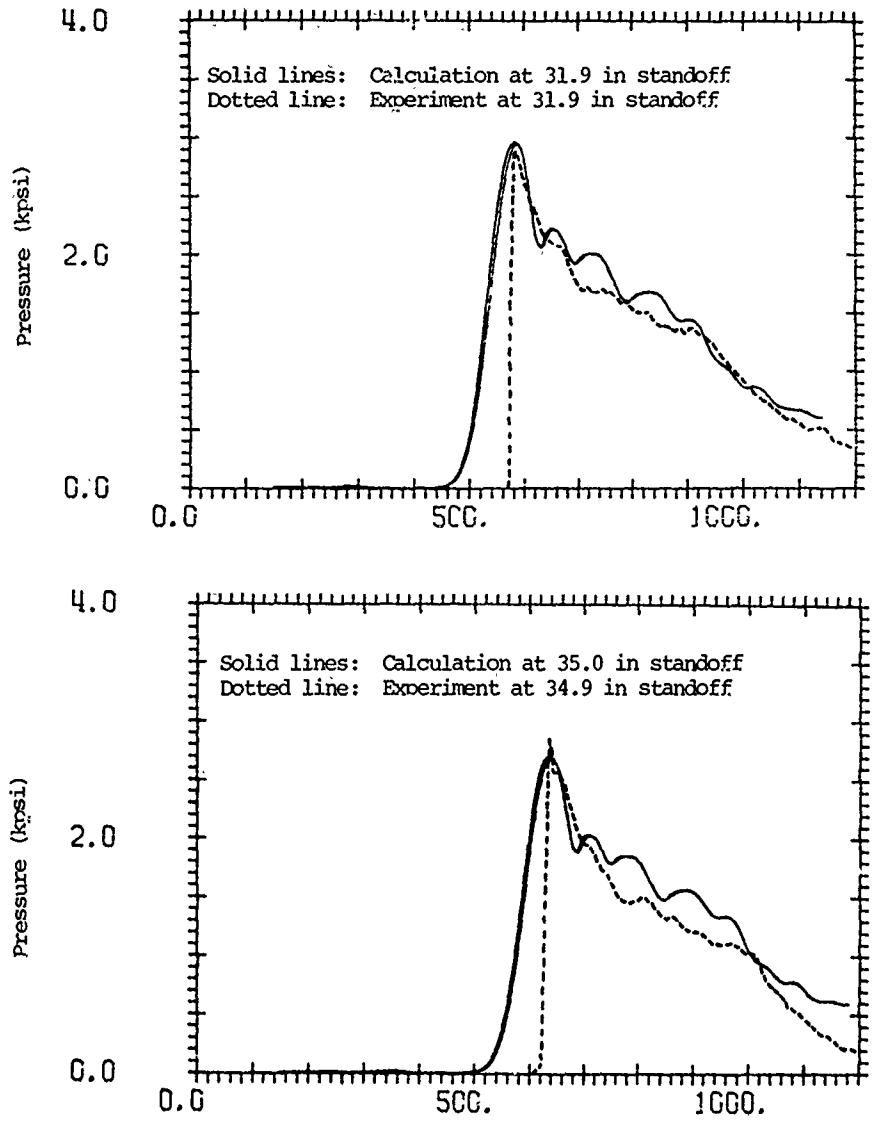

Figure 15. Comparison of calculated and experimental pressure traces at 32 and 35 in standoff.

did not have a flat plateau and the experimental scatter was large. Consequently, it was not possible to fully confirm the adequacy of the derived plateau pressure.

ACKNOWLEDGEMENT

This work was sponsored by the Defense Nuclear Agency under RDT&E RMSS Code B3440-82466 Y99QAX D 00018 H2590D. The contract technical manager was Commander Thomas J. Deevy, Shock Physics Directorate, SPSS.

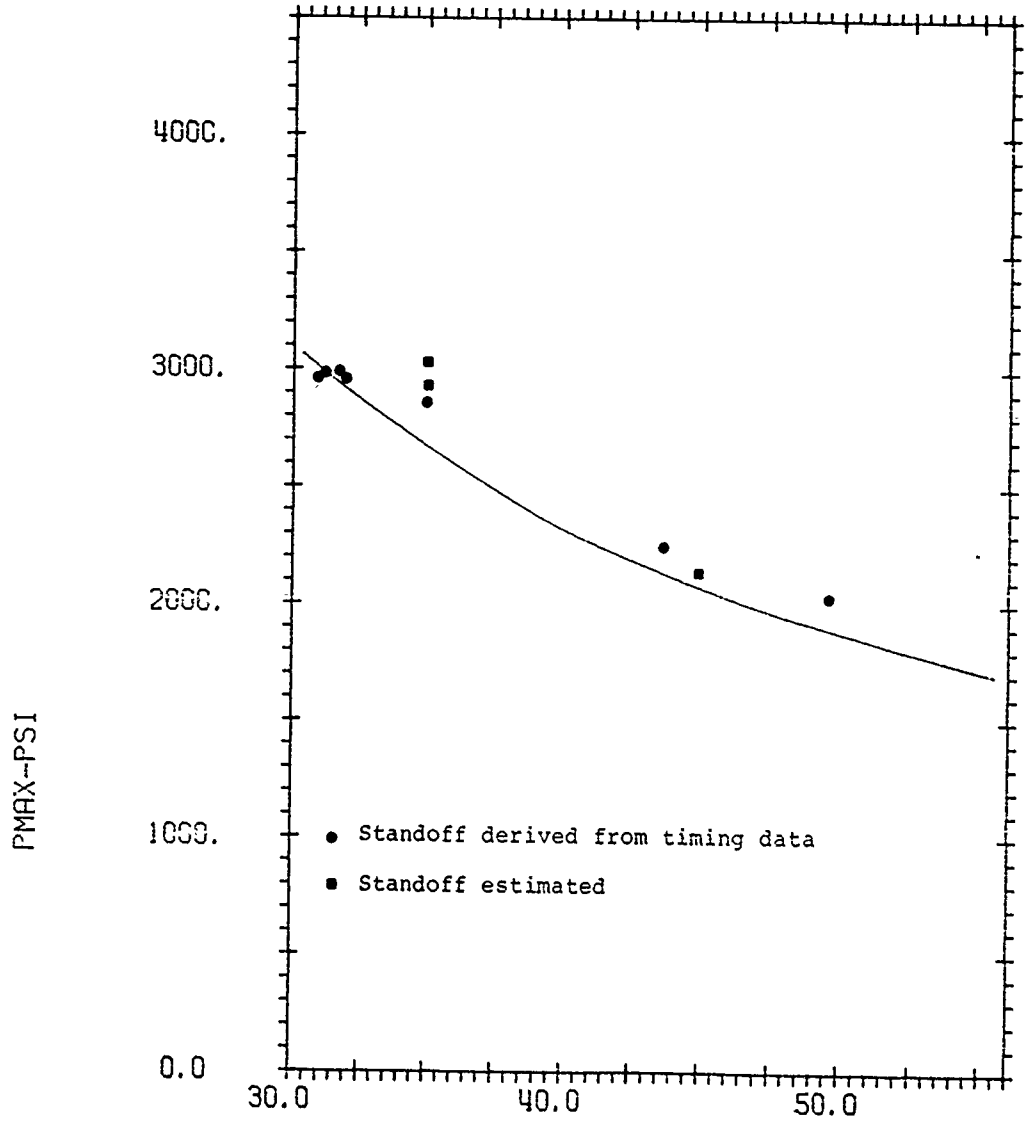

Figure 16. Comparison of calculated peak pressures (solid line) and experimental values.

REFERENCES

1. W. R. Conley, W. T. Bersson and D. A. Koch, Evaluation of a 2.66 Pound Tapered Charge Used to Simulate Nuclear Shock Wave Loading," David W. Taylor Naval Ship Research and Development Center Report, June 1980.

2. M. Trigg, S. Hancock, P. Kavaler and H. Hancock, "PISCES 2D ELK User's Manual," Physics International Company, San Leandro, California 94577, April 1981

3. S. L. Hancock, "Finite Difference Equations for PISCES 2D ELK, A Coupled Euler Lagrange Continuum Mechanics Computer Program," Technical Memo TCAM 76-2, Physics International Company, San Leandro, California 94577, April 1976.

4. B. M. Dobratz, "LLNL Explosives Handbook - Properties of Chemical Explosives and Explosive Simulants," UCRL-52997, Lawrence Livermore National Laboratory, Livermore, California, March 1981.

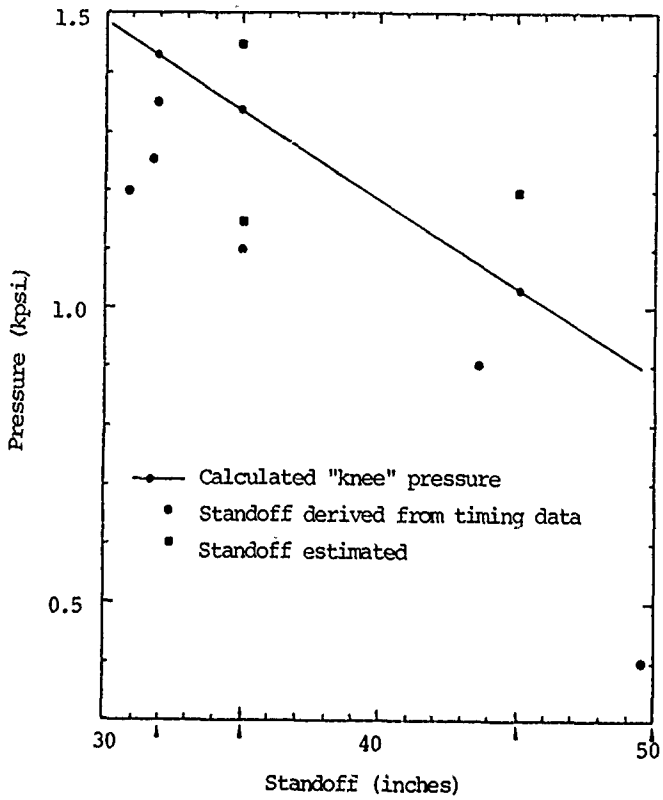

Figure 17. Comparison of calculated and experimental "knee" pressures. "Knee" pressure is the pressure just before the exponential pressure dropoff, approximately 340 μs after peak pressure.

5. W. A. Walker and H. M. Sternberg, "The Chapman-Jouget Isentrope and the Underwater Shockwave Performance of Pentolite," Fourth Symposium on Detonation, Department of the Navy, Office of Naval Research, 1965.

6. T. R. Butkovich, "The Influence of Water in Rocks on Underground Nuclear Explosions Effects," UCRL-72558, Lawrence Radiation Laboratory, June 1970.

7. J. M. Thomsen and S. F. Ruhl, "Mitigation of Explosion Bubble Pulsation Caused by the Deep Underwater Detonation of a Tapered Charge," DNA 5531 Final Report for Contract No. DNA 001-80-C0125, Prepared for Defense Nuclear Agency by Physics International Company, San Leandro, California, 31 October 1980.

DISCUSSION

Mr. Walter (Sandia National Laboratories): Were your predictions of the pressure time profiles static pressures or stagnation pressures? When you showed the discrepancies in your rise time, what instrumentation techniques did you use to measure the experimental data that you presented?

Mr. Gordon: Let me answer the experimental question first. I really don't know the details of that because the measurements were made by UERD. Those were static pressures that were measured under water.

EFFECT OF MEASUREMENT SYSTEM PHASE RESPONSE ON SHOCK SPECTRUM COMPUTATION

Patrick L. Walter
Sandia National Laboratories
Albuquerque, New Mexico

A shock spectrum is the envelope of peak responses of an infinite number of single-degree-of-freedom linear oscillators to an input transient. The shock spectrum provides a technique to assess the results of different shock stimuli by comparing the similarities in peak responses they elicit from the assemblage of oscillators. The principal application of the shock spectrum in aerospace technology is to permit component shock test specifications to be generated independent of specific time histories. Computation of a shock spectrum first depends on a successful measurement of the transient acceleration-time history a component experiences in application. Acceleration mesurement systems can all be described as low-pass filters; i.e., systems which pass frequencies from at or near 0 Hz to some upper frequency limit. This upper frequency limit, typically characterized by 3 dB attenuation, is due to constraints in the bandwidth of the analog signal conditioning amplifiers, filtering due to distributed cable capacitance, anti-aliasing filters designed into digital systems, or analog filters associated with FM demodulators. All transient acceleration data pass through some combination of these filters. This article specifically investigates the effect of nonlinear phase response in systems measuring transient signals. The results of phase modification of input signals to measurement systems are illustrated. Distorted waveforms, erroneous signal amplitudes, and different pulse durations are shown to occur. The important role of measurement system phase response in shock spectrum computation is demonstrated and system design guidelines are provided to assure the generation of valid component shock test specifications.

INTRODUCTION

One of the standard methods for characterizing mechanical shock is by means of the shock spectrum. The principal application of the shock spectrum in aerospace technology is to permit component shock test specifications to be generated, independent of specific time histories. Inattention to the dynamics of the instrumentation system used to measure mechanical shock can result in distorted test data. Erroneous component test specifications will originate from shock spectra calculations based on these distorted data.

A shock spectrum is the envelope of peak responses of an infinite number of single-degree-of-freedom linear oscillators to an input transient at their foundation. The shock spectrum can be specified for a variety of input-response relationships. For each particular input-response relationship, there are at least nine different ways of specifying shock spectra; the major divisions are primary (during pulse application), residual (after the pulse), and maximax (all time), with subdivisions of positive, negative, and maximum. The shock spectrum provides a technique to assess the results of different shock stimuli by comparing the similarities in peak responses they elicit from the assemblage of oscillators. In this article, the oscillators are treated as undamped.

The shock spectrum concept originated at the Department of Aeronautics, California Institute of Technology. First reported in 1933[1], a theory was presented which provided a method of evaluating the action of random impulses on vibrating systems.

Computation of a shock spectrum first depends on a successful measurement of the transient acceleration-time history which a component experiences in application. As a minimum, an acceleration measurement system is comprised of an accelerometer, signal conditioning amplifier, and FM tape recorder. If data are required in digital form, the FM tape recorder is replaced by an anti-aliasing filter, analog to digital converter, and a digital tape machine or a computer. If the system cannot be continuously connected by cables, it may contain an intermediate radio frequency link for space transmission.

These measurement systems can all be described as low-pass filters; i.e., systems which pass frequencies from at or near 0 Hz to a specified upper frequency limit. This upper frequency limit, typically characterized by 3 dB attenuation, is due to constraints in the bandwidth of the analog signal conditioning amplifiers, filtering due to distributed cable capacitance, anti-aliasing filters designed into digital systems, or analog filters associated with FM demodulators. All transient acceleration data pass through some combination of these filters.

The frequency response function of any linear measurement system* can be represented as:

$$H(j\omega) = A(\omega)e^{-j\phi(\omega)} \qquad (1)$$

where $A(\omega)$ describes the system amplitude response and $\phi(\omega)$ its phase response with frequency (ω). If $A(\omega)$ is not a constant, the amplitude of the spectral content of a transient acceleration signal recorded by the system will be modified causing signal distortion with resultant error in the computed shock spectrum. Figure 1a illustrates a transient acceleration signal and Figure 1b its spectral content. In this example, a filter with constant amplitude response to 300 Hz will not introduce distortion due to signal attenuation; however, the influence of filter phase response is not so apparent.

Figure 2 presents the amplitude-frequency and phase-frequency responses of two typical filters. The six-pole Chebyshev is the best approximation

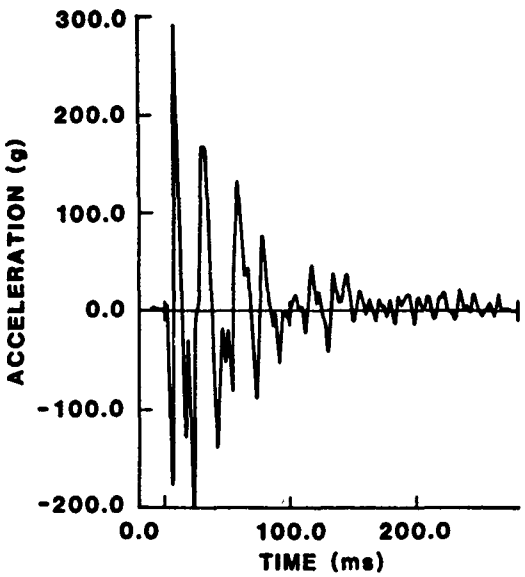

Fig. 1a: Acceleration Time Record

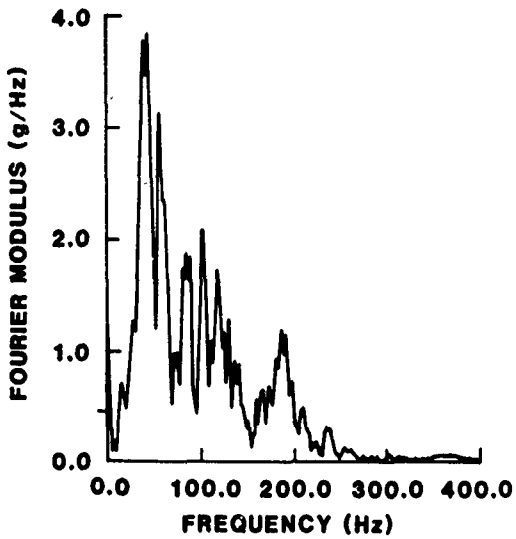

Fig. 1b: Magnitude of Fourier Transform of Acceleration-Time Record

Fig. 1: Acceleration Measurand Which Might Be a Stimulus to a Measurement System

to an ideal "boxcar" filter in the amplitude domain (see Figure 2a), but its phase response is more nonlinear than that of the six-pole Bessel as shown in Figure 2b.

The remaining portion of this article investigates the effect of nonlinear phase response in systems which measure transient signals and the influence of this response on computed shock spectra. The general problem of acquiring valid structural dynamics measurements has been described elsewhere.[3]

*Reference 2 discusses the problem of nonlinear measurement systems.

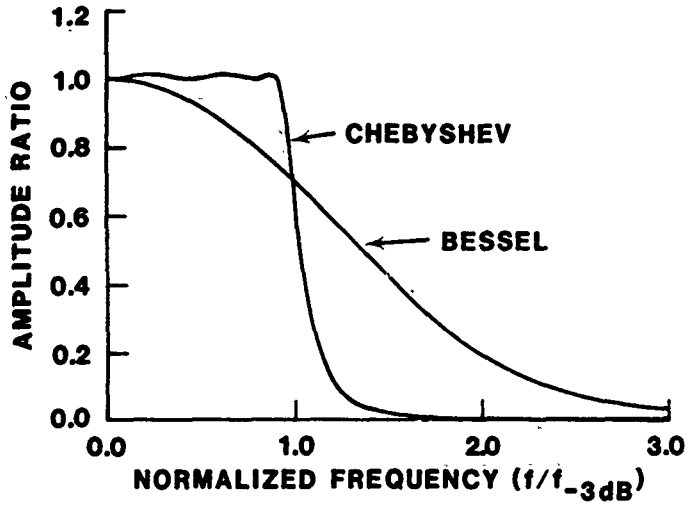

Fig. 2a: Amplitude Frequency Response

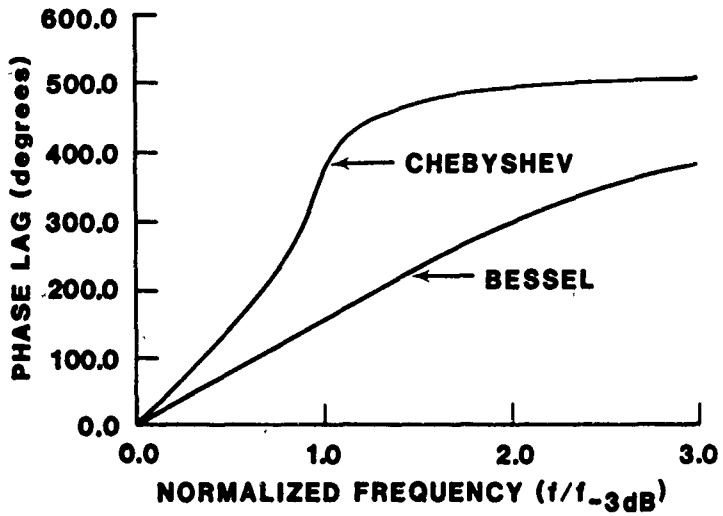

Fig. 2b: Phase Frequency Response

Fig. 2: Amplitude Frequency and Phase Frequency Plots For 6-Pole Chebyshev and Bessel Filters

Nonlinear Phase Effects on Signals

The effects of nonlinear phase response on the input signals to measurement systems are qualitatively depicted in Figures 3 and 4. Figure 3a illustrates a pulse train with a period of one second. Over any period, the time function f(t) can be represented as:

$$f(t) = 1, \quad .3 \leq t \leq .7 \qquad (2)$$

$$f(t) = 0 \text{ elsewhere in } 0 \leq t \leq 1.$$

The Fourier series representation of this periodic function is:

$$f(t) = 0.4 + (2/\pi)A \qquad (3)$$

$$A = \sum_{n=1}^{\infty} [(-1)^n/n]\sin(0.4\pi n)\cos(2\pi nt+\phi_n)$$

where ϕ_n is initially equated to zero. This function will be aproximated by summing its first 25 harmonics. This

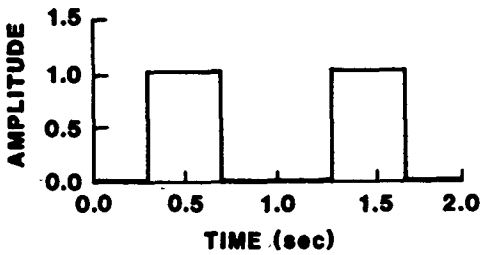

Fig. 3a: Periodic Time Function

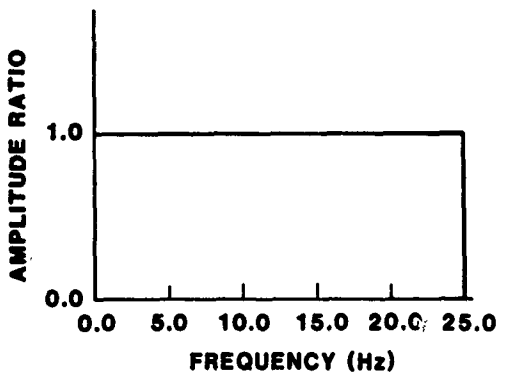

Fig. 3b: Amplitude Frequency Response

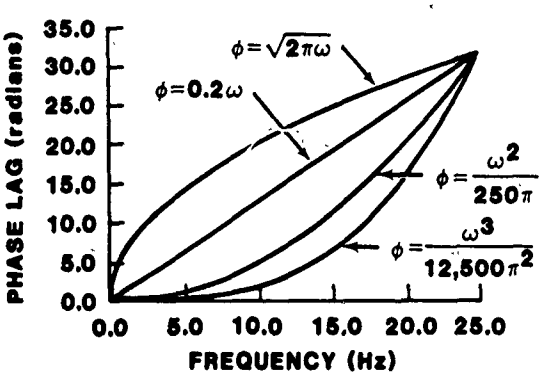

Fig. 3c: Phase Frequency Responses

Fig. 3: Periodic Time Function And Idealized Filter Response Plots

is equivalent to passing the function through the ideal "boxcar" filter described in Figure 3b with no accompanying phase shift. The resultant filtered signal can then have the various linear and nonlinear phase responses of Figure 3c associated with it. These are respectively:

$$\phi_n = \sqrt{2\pi\omega_n}, \qquad (4.1)$$

$$\phi_n = .2\omega_n, \qquad (4.2)$$

$$\phi_n = \omega_n^2/(250\pi), \text{ and} \qquad (4.3)$$

$$\phi_n = \omega_n^3/(12{,}500\pi^2) \qquad (4.4)$$

where $\omega_n = 2\pi n$. These phase responses are normalized to produce a phase shift of 10π radians at 25 Hz, the highest harmonic in the filtered signal.

Figure 4a shows the result over one period of the time function when it is passed through the filter in Figure 3b. The ripple on top of the pulse is due to truncation of the higher frequencies and is called Gibbs phenomenon.[4]

Figure 4b shows the effect of shifting the phase of the signal in Figure 4a in the linear fashion described by Eq. (4.2) and illustrated in Figure 3c. As predicted by theory[5], only a constant time delay occurs and signal distortion is avoided.

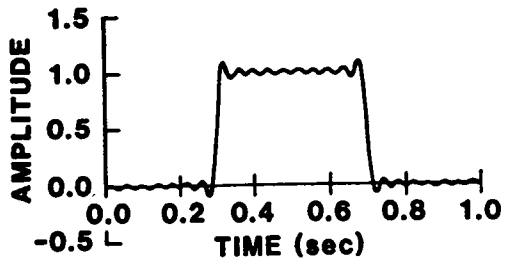

Fig. 4a: Amplitude Distortion Only

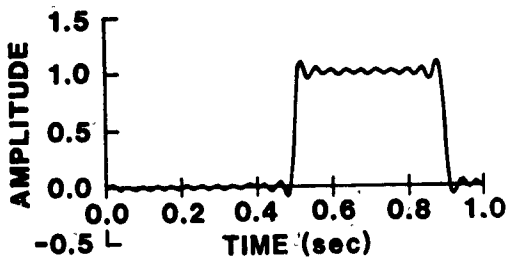

Fig. 4b: Linear Phase Shift

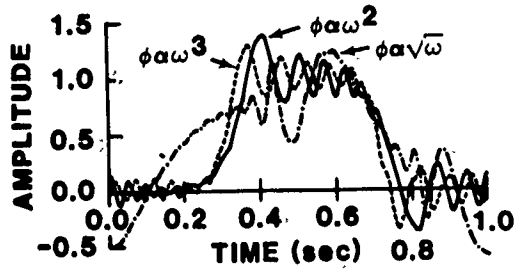

Fig. 4c: Nonlinear Phase Shifts

Fig. 4: One Cycle Of Periodic Time Function Passed Through Idealized Filter Of Figure 3

Figure 4c superposes results of shifting the phase of the signal in Figure 4a in a nonlinear fashion according to Eqs. (4.1), (4.3), and (4.4) also illustrated in Figure 3c. (In Figure 4c α denotes proportional.) The distorted waveforms, erroneous signal amplitudes, and modified pulse durations are solely attributable to the various nonlinear filter phase responses.

Application to Shock Spectra

In practice, an infinite variety of acceleration transients exist in nature and can be input to measurement systems. Each measurement system will add varying amounts of linear or nonlinear phase shift to the spectral content of these input transients.

The initial and terminal peak sawtooth pulses of Figure 5 will be used to illustrate the influence of measurement system phase response on shock spectrum computation. The terminal peak sawtooth pulse is widely used in component shock testing due to unique properties of its shock spectrum.[6]

Figure 6a plots the magnitudes of the Fourier transform of both the initial and terminal peak sawtooth pulses. Note that these magnitudes are identical! Figure 6b and 6c show the pulse phase relations, however, to be quite different. Both pulses then contain identical frequency content but differ in its time of occurrence. An initial peak sawtooth can be turned into a terminal peak sawtooth by modifying its phase relationship and vice-versa.

Figure 7 shows that the maximax undamped acceleration shock spectra of these two pulses are grossly different. Since both pulses contain identical frequency content, dissimilarities are due solely to the difference in phase relations. While measurement systems are often designed only around amplitude response considerations, this example demonstrates the important role of measurement system phase response in subsequent shock spectrum computations. Nonlinear phase response can result in severe distortion of recorded acceleration transients and the resultant computed shock spectra.

Measurement System Design Guidelines

The majority of the phase shift associated with the systems being considered is introduced by analog

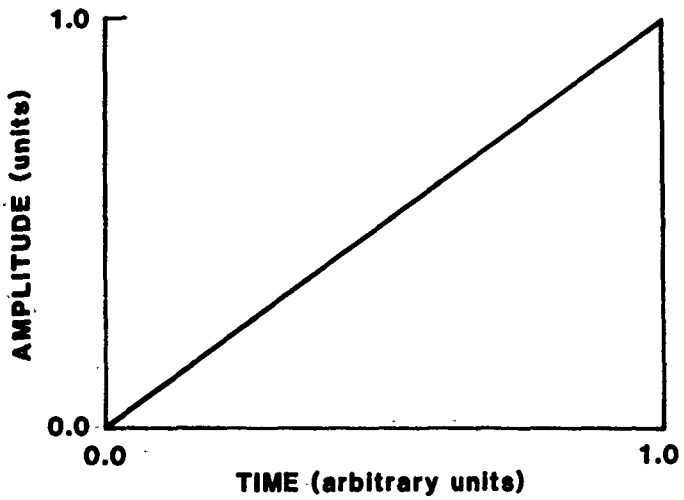

Fig. 5a: Terminal Peak Sawtooth Pulse

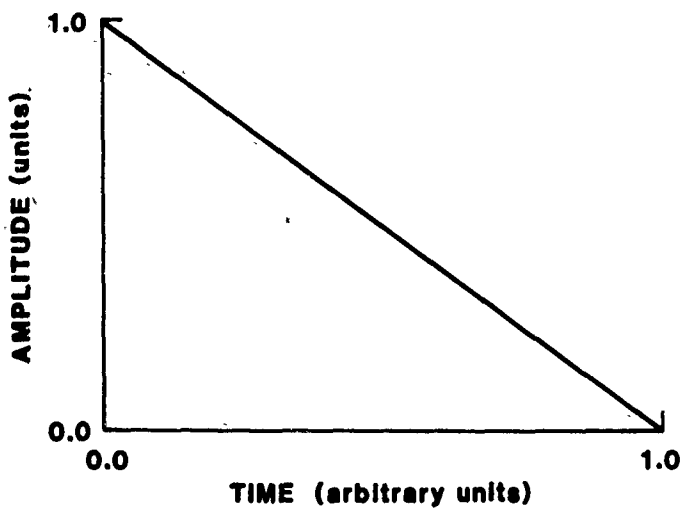

Fig. 5b: Initial Peak Sawtooth Pulse

Fig. 5: Sawtooth Pulses

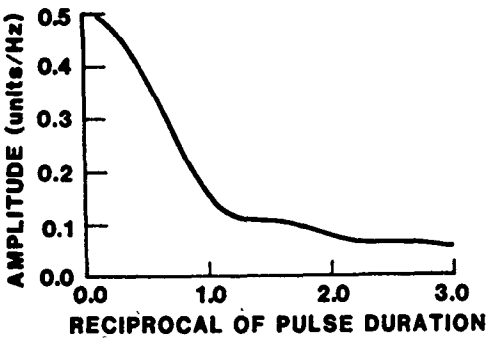

Fig. 6a: Magnitude of Fourier Transform of Both Terminal and Initial Peak Sawtooth Pulses

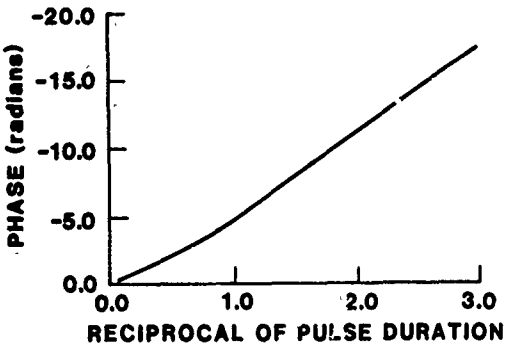

Fig. 6b: Phase of Fourier Transform of Terminal Peak Sawtooth Pulse

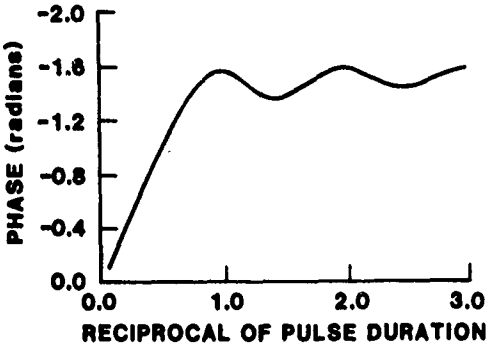

Fig. 6c: Phase of Fourier Transform of Initial Peak Sawtooth Pulse

Fig. 6: Fourier Spectra of Sawtooth Pulses of Figure 5

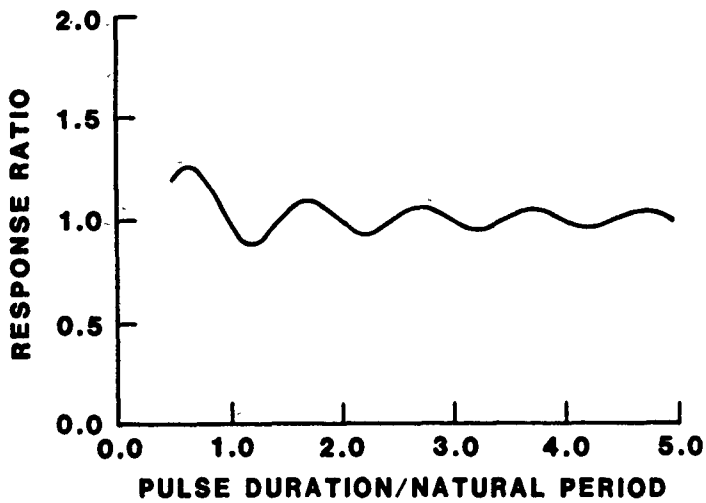

Fig. 7a: Shock Spectrum of Terminal Peak Sawtooth Pulse

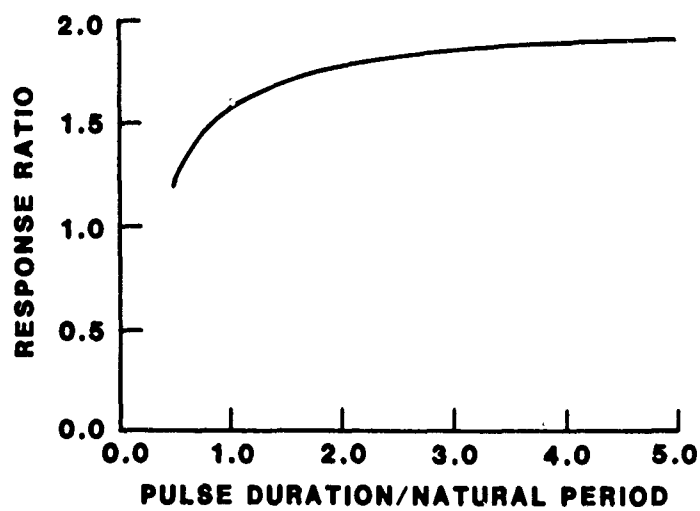

Fig. 7b: Shock Spectrum of Initial Peak Sawtooth Pulse

Fig. 7: Maximax Undamped Acceleration Shock Spectra of Terminal and Initial Peak Sawtooth Pulses

	Filter Type		
	Butterworth	Bessel	0.1 dB Chebyshev
2 poles	.573	.399	.522*
4 poles	.575*	.399	.489*
6 poles	.541*	.392	.418*
8 poles	.506*	.389	.372*

*upper limit due to phase nonlinearity

filters. Since the introduction of the modular transistorized operational amplifier operational amplifier in the 1950's, active filters have become almost universally applied in structural measurements. As noted earlier, these filters are used to preclude aliasing in digital systems and as part of FM signal demodulation.

Modern filter theory involves the approximation of the filter specifications by a frequency response function and the design of a network which realizes this frequency response function. The rate of attenuation of a filter is specified in decibels/octave. Each filter pole provides 6 dB/octave ultimate attenuation. The more common filters in current use are the Butterworth, Bessel, and Chebyshev.

Frequently, filters are selected solely due to their amplitude response characteristics with phase considerations ignored. The above table, based on calculations made by the author, provides improved selection guidelines for the three previously described filter types with two, four, six, and eight poles of attenuation. Numeric values presented are the ratio of the upper frequency limit at which the filter should be used to that of its -3 dB frequency. This upper frequency limit is based on the lesser of the two values at which the filter deviates either five percent from a flat amplitude response or five degrees from phase linearity based on its initial phase slope. These criteria should assure waveform reproduction without distortion, since they provide a reasonable approximation to an ideal low-pass filter.

An example will show how to use this table. A six-pole Butterworth and a six-pole 0.1 dB Chebyshev filter with a 1,000 Hz -3 dB frequency would be limited in application to 541 and 418 Hz respectively because of phase nonlinearities. A six-pole Bessel would become limited at 392 Hz due to its deviation from a flat amplitude response.

Conclusion

Measurement system design is frequently based upon amplitude response considerations with phase response ignored. In structural testing, nonlinear phase response in measurement systems results in distorted transient data being recorded for analysis with resultant error in the computed shock spectra. Design guidelines are provided in this work to preclude these errors from occurring.

References

1. M. Biot, "Theory of Elastic Systems Vibrating Under Transient Impulse with an Application to Earthquake-Proof Buildings," Proceedings National Academy of Sciences, 19, pp. 262-268, 1933

2. P. K. Stein, "Measurement on and with Non-linear Systems: Problems and Approaches," International Measurement Confederation, IMEKO IX, Berlin, West Germany, May 1982

3. P. L. Walter, H. D. Nelson, "Limitations and Corrections in Measuring Structural Dynamics," Experimental Mechanics, 19(9), pp. 309-316, Sept. 1979

4. P. M. Chirlian, Signals, Systems, and the Computer, Intext Educational Publishers, NY, Ch. 2, pp. 47-50, 1973

5. C. M. Harris, C. E. Crede, Shock and Vibration Handbook, McGraw Hill Book Co., NY, Ch. 12, pp. 12-15, 1976

6. R. Lowe, R. D. Cavanaugh, "Correlation of Shock Spectra and Pulse Shape with Shock Environment," Environmental Engineering, pp. 24-29, Feb. 1959

Voice: The noise distortion is very wide, and you really can't do anything else but use phase distorting antiabasing filters.

Mr. Walter: I have done a little work in that area, and one of the fellows that works for me is spending a great deal of time on that right now. Essentially, can you work the process backwards? Can you take an instrumentation system that induces distortion, and then can you back that distortion out of the signal? The answer is "Yes, that is possible." If you take a signal, feed it to an instrumentation system, there is an analytical expression that relates to that. That is just convolution, so the inverse process is deconvolution. That is exactly true, and I have some articles I can refer you to that give the detailed procedures for that. Basically, you have to watch for an instability problem. You must be sensitive to that problem, because if you think of a filter as something that attenuates at high frequencies, then to correct that you must put in gain at high frequencies. So you are correcting for the phase, but you're also inducing gain. So if you have high frequency noise in your signal, and you start putting in the inverse function to a filter, and then putting in horrendous gains to boost up this filter roll-off, you can get into instability problems. That can be handled, but that is beyond the time I have to properly respond to that question.

EFFICIENT ALGORITHMS FOR CALCULATING SHOCK SPECTRA ON GENERAL PURPOSE COMPUTERS

Frank W. Cox
Computer Sciences Corporation
Houston, Texas

We note that standard shock spectral analysis is merely a problem in the time domain; thus, transform methods such as the FFT are both slow and superfluous on general purpose hardware. We write the solution to the differential equation in ways that are formally exact. What has been neglected in traditional computation is that recursive algorithms can be devised that circumvent numerous evaluations of transcendental functions. Further, shock spectra often exhibit minor oscillations other than the obvious peaks expected at resonant frequencies. We show that these secondary oscillations are theoretically legitimate.

INTRODUCTION AND SUMMARY

In shock spectral analysis, structural response to impulsive excitation is modeled by an ensemble of damped linear oscillators, each with a different natural frequency. The maximum acceleration response observed for each oscillator during the combined impulse and residual time intervals is plotted versus the corresponding oscillator natural frequency, providing a spectral distribution of response and a standardized measure of potential structural damage. The governing equation for each oscillator is a linear 2nd order differential equation with constant coefficients. At some installations, these equations have been solved by use of the Fast Fourier Transform (FFT). However, the concept of shock spectra is fundamentally a problem in the time domain, frequency being a parameter of interest but not the basic independent variable in the governing equations. Transform methods such as the FFT are both slow and superfluous unless special purpose hardware is employed.

Another disadvantage of the FFT in this problem is the need for zero fill time, that is, a substantial number of zero values must be appended to the excitation profile beyond the impulse time range to avoid possible distortion induced by the inherently periodic nature of the Fourier transform. Direct methods provide improvements in speed, accuracy, and range of applicability.

The solution to the differential equation can be written in ways that are formally exact. What has been neglected in traditional computation is that recursive algorithms can be devised which circumvent the need to evaluate transcendental functions at all the numerous sample points throughout the impulse time range. A short special calculation in the residual time range saves additional time.

Shock spectra often exhibit minor oscillations other than the obvious peaks expected at resonant frequencies contained in the input excitation. We show that these secondary oscillations are not numerical instabilities but are, in fact, theoretically legitimate. We also present a compact numerical scheme based on the Euler-Maclaurin sum formula.

In closing, we show practical graphical examples and short FORTRAN routines for use on general purpose computers.

MATHEMATICAL DESCRIPTION - A DIRECT METHOD

Referring to Fig. 1, the differential equation for the mass displacement x(t) is:

$$M\ddot{x}(t) + D[\dot{x}(t) - \dot{s}(t)] + \frac{1}{K}[x(t) - s(t)] = 0 \quad (1)$$

The function s(t) is the wall displacement:

$$\ddot{s}(t) = a(t) \text{ the given excitation} \quad (2)$$

$$\dot{s}(t) = \dot{s}(0) + \int_0^t a(\tau)d\tau$$

The initial conditions for Eq. (1) are:

$$x(0) = 0 \qquad s(0) = 0$$

$$\dot{x}(0) = 0 \qquad \dot{s}(0) = 0 \quad (3)$$

To avoid the quadrature in Eq. (2), make the following substitution changing the dependent variable.

Let

$$y = x - s \quad (4)$$

$$\ddot{y} = \ddot{x} - \ddot{s}$$

and

$$\ddot{x} = \ddot{y} + \ddot{s}$$

Substituting the definitions of Eq. (4) into Eq. (1), we obtain

$$M\ddot{y} + D\dot{y} + \frac{1}{K}y = -M\ddot{s}(t) \quad (5)$$

with the initial conditions

$$y(0) = 0$$

$$\dot{y}(0) = 0 \quad (6)$$

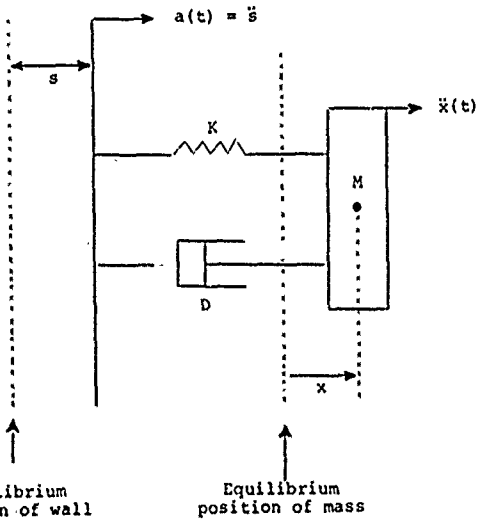

a(t) = Excitation Acceleration
D = Damping
K = Compliance
M = Mass
s = Displacement of Wall
x = Displacement of Mass

Fig. 1 - Individual linear oscillator responding to excitation

This strategy enables us to deal directly with the input excitation a(t) and eliminates the need to be concerned with values of s, ṡ, x, or ẋ. The desired output is the oscillator response acceleration ẍ(t), which can be recovered by noting from Eqs. (4) and (5) that

$$M\ddot{x} = -D\dot{y} - \frac{1}{K}y \quad (7)$$

Thus, we solve Eq. (5) for y(t) and ẏ(t) and compute ẍ(t) from Eq. (7).

The ultimate goal is to determine both the maximum positive and the maximum negative values attained by the response acceleration, ẍ(t). These global extrema will occur either during the impulse time range while the excitation is in effect or possibly during the residual time range, which is limited to one cycle beyond the excitation cut-off.

Make the definitions

$$\omega = \frac{1}{2M}\left|D^2 - \frac{4M}{K}\right|^{\frac{1}{2}} \quad (8)$$

and

$$\alpha = \frac{D}{2M}$$

The complementary solution to Eq. (5) is:

$$y_c(t) = e^{-\alpha t}\left(C_1 \sin \omega t + C_2 \cos \omega t\right) \quad (9)$$

where C_1 and C_2 are arbitrary constants.

The fundamental inputs are D, K, M, s̈(t), y(0), and ẏ(0). However, the damping, D, and compliance, K, are not input directly. Instead, they are computed from special input parameters, namely the response frequency f_R and the damping "quality factor" Q.

Quality of damping, Q, is defined as:

$$Q = \frac{D \text{ critical}}{2D} \quad (10)$$

where

$$D \text{ critical} = 2\sqrt{\frac{M}{K}} \quad (11)$$

Thus, Q and ω are implied by D and K and vice versa.

That is,

$$(Q,\omega) \leftrightarrow (D,K) \quad (12)$$

In a typical case, we are given:

$$M = 1$$
$$y(0) = \dot{y}(0) = 0 \quad (13)$$
$$\ddot{s}(t) = a(t) \quad \text{(discrete points)}$$

We are also given the value Q and a range of values for response frequency f_R. Then, for each f_R, we have:

$$\omega = 2\pi f_R \qquad K = \frac{4 - \frac{1}{Q^2}}{4\omega^2} \tag{14}$$

and

$$D = \frac{1}{Q}\sqrt{\frac{1}{K}}$$

This parameterization is desirable since, in the study of shock spectra, the damping quality and a prescribed range of natural response frequencies are convenient basic inputs.

The particular solution to the non-homogeneous equation depends on how we choose to represent the excitation function, a(t). In practical applications, the excitation is defined by a table of discrete sample points, equally spaced in time. Overall trends are usually highly oscillatory, and individual points appear to vary erratically. (Only in theoretical checkout runs is the excitation given by an analytical expression.) When the input excitation points are closely spaced, corresponding to a satisfactory sample rate, it is both convenient and effective to assume linear variation between sample ordinates. This facilitates the determination of the necessary particular solution that must be added to the complementary solution. The linear approximations must be changed from point to point; however, this turns out to be convenient, and an efficient recursion algorithm is available for evaluating the solution at all points in the impulse time range. A short special calculation is made to determine possible extrema of the acceleration response in the residual time range.

We write both the excitation function and the response solution specifically for the discrete jth time subinterval used in the recursion relation. That is, consider the equally spaced points,

$$t_j = jh \tag{15}$$

where $j = 0,1,\ldots N$; the value, Nh, being the impulse time range.

The input excitation acceleration a(t) is defined by the values $a_0, a_1, \ldots a_N$ with the assumption that a_{N+1} and subsequent values are zero (although a "zero fill" array is not needed in this approach).

The basic equation for the jth time step is:

$$\ddot{y} + D\dot{y} + \frac{1}{K}y = -\left(1-\frac{t-jh}{h}\right)a_j - \left(\frac{t-jh}{h}\right)a_{j+1} \tag{16}$$

The general solution in the interval $jh \le t \le (j+1)h$ is:

$$y(t) = \underbrace{A_j + B_j(t-jh)}_{\text{(particular)}} + \underbrace{e^{-\alpha(t-jh)}\left[C_j\cos\omega(t-jh) + D_j\sin\omega(t-jh)\right]}_{\text{(complementary)}} \tag{17}$$

and

$$\dot{y}(t) = B_j + e^{-\alpha(t-jh)}\left[\left(\omega D_j - \alpha C_j\right)\cos\omega(t-jh) + \left(-\omega C_j - \alpha D_j\right)\sin\omega(t-jh)\right] \tag{18}$$

The arbitrary constants are subscripted since they must be changed for each jth subinterval corresponding to a changing linear approximation to the excitation $\ddot{s}(t) = a(t)$.

At each jth step of the recursive algorithm,

$$B_j = \frac{(a_j - a_{j+1})K}{h}$$

$$A_j = \left(-a_j - DB_j\right)K \tag{19}$$

$$C_j = y_j - A_j$$

$$D_j = \frac{\dot{y}_j - B_j + \alpha C_j}{\omega} \tag{20}$$

The solution at the next time t_{j+1} is:

$$y\left(t_j+h\right) = A_j + B_j h + e^{-\alpha h}\left(C_j\cos\omega h + D_j\sin\omega h\right) \tag{21}$$

and

$$\dot{y}\left(t_j+h\right) = B_j + e^{-\alpha h}\left[\left(\omega D_j - \alpha C_j\right)\cos\omega h + \left(-\omega C_j - \alpha D_j\right)\sin\omega h\right] \tag{22}$$

The oscillator acceleration response at $t = t_j + h$ is:

$$\ddot{x}\left(t_j+h\right) = -D\,\dot{y}\left(t_j+h\right) - \frac{1}{K}y\left(t_j+h\right) \tag{23}$$

The formal procedure used is equivalent to imagining that the functions y, $\dot{y}$, and $\ddot{s}$ emanate continually from a moving origin and thus the exponential and trigonometric functions need not be evaluated for all values of t in the impulse range but only for t = 0 and t = h. The values $e^{-\alpha h}$, sin ωh, and cos ωh can be

evaluated once, stored, and used repeatedly without recomputation.

Another notation can be useful for viewing the process in condensed form. The governing differential equation is:

$$Ly = \ddot{y} + D\dot{y} + \frac{1}{K}y = -\ddot{s}(t) \tag{24}$$

The general solution is:

$$\begin{bmatrix} y \\ \dot{y} \end{bmatrix} = e^{-\alpha t}\begin{pmatrix} \sin \omega t & \cos \omega t \\ \omega \cos \omega t - \alpha \sin \omega t & -\omega \sin \omega t - \alpha \cos \omega t \end{pmatrix}\begin{bmatrix} C_1 \\ C_2 \end{bmatrix} + \begin{bmatrix} p(t) \\ \dot{p}(t) \end{bmatrix} \tag{25}$$

or

$$\bar{y}(t) = Q(t)\,\bar{c} + \bar{p}(t)$$

with (26)

$$\bar{p}(t) = \begin{bmatrix} A + Bt \\ B \end{bmatrix}$$

where $\bar{p}$ is the particular solution (and its derivative) to the equation

$$L\,p(t) = -\ddot{s}(t) \tag{27}$$

in the time subinterval $jh \leq t \leq jh + h$ over which the excitation $s(t)$ is considered linear. At time zero,

$$\bar{C}_o = Q_o^{-1}\left(\bar{y}_o - \bar{p}_o\right) \tag{28}$$

Then at $t = h$,

$$\bar{y}(h) = Q(h)\bar{C}_o + \bar{p}(h) \tag{29}$$

And, in general,

$$\bar{y}(t+h) = Q(t+h)Q^{-1}(t)\ [\bar{y}(t) - \bar{p}(t)] + \bar{p}(t+h) \tag{30}$$

We must show that the matrix product, $Q(t+h)Q^{-1}(t)$, is independent of time.

Write $Q(t)$ as

$$Q(t) = e^{-\alpha t}\,M(t) \tag{31}$$

where

$$M(t) = \begin{pmatrix} \sin\omega t & \cos\omega t \\ \omega\cos\omega t - \alpha\sin\omega t & -\omega\sin\omega t - \alpha\cos\omega t \end{pmatrix} \tag{32}$$

then

$$[Q(t+h)]\,Q^{-1}(t) = \left[e^{-\alpha t}e^{-\alpha h}\,M(t+h)\right]\ e^{\alpha t}\,M^{-1}(t) = e^{-\alpha h}\,M(t+h)M^{-1}(t) \tag{33}$$

and the time-dependent exponential is already removed.

The trigonometric matrix $M(t)$ has some convenient properties because special combinations of its time-dependent elements yield constants. Let M, Eq. (32), be abbreviated as:

$$M(t) = \begin{pmatrix} S & C \\ U & V \end{pmatrix} \tag{34}$$

Since $(\sin^2 + \cos^2 = 1)$, we have the special relations

$$\begin{aligned} S^2 + C^2 &= 1 \\ U^2 + V^2 &= \omega^2 + \alpha^2 \\ SU + CV &= -\alpha \\ \det(M) &= SV - UC = -\omega \end{aligned} \tag{35}$$

Further,

$$M^{-1}(t) = \frac{1}{-\omega}\begin{pmatrix} V & -C \\ -U & S \end{pmatrix} \tag{36}$$

Now we must study the matrix $M(t+h)$ in Eq. (33).

$$M(t+h) = \begin{pmatrix} \sin(\omega t+\omega h) & \cos(\omega t+\omega h) \\ \omega\cos(\omega t+\omega h) - \alpha\sin(\omega t+\omega h) & -\omega\sin(\omega t+\omega h) - \alpha\cos(\omega t+\omega h) \end{pmatrix} \tag{37}$$

The expressions in Eq. (37) must be expanded further, making use of the trigonometric identities for sine and cosine of a binomial. After some factoring and rearrangement, we can write

$$M(t+h) = \cos\omega h\begin{pmatrix} S & C \\ U & V \end{pmatrix} + \sin\omega h\begin{pmatrix} C & -S \\ V & -U \end{pmatrix} \tag{38}$$

A few more manipulations can show that the matrix product, $Q(t+h)Q^{-1}(t)$, is a function of h, α, and ω, but not of time t.

The possibility exists that the global extrema of the response acceleration $\ddot{x}(t)$ may occur during the residual time range. It is not necessary to interrogate all points in the residual time interval as must be done when exercising the recursive algorithm throughout the impulse range. Since the acceleration response is

$$\ddot{x}(t) = -D\dot{y} - \frac{1}{K}y \tag{39}$$

its derivative is

$$\dddot{x}(t) = -D\ddot{y} - \frac{1}{K}\dot{y} \tag{40}$$

After the excitation $\ddot{s}(t)$ drops to zero, we can find constants A and δ such that

$$\ddot{x}(t) = A\, e^{-\alpha t} \sin(\omega t+\delta) = 0 \tag{41}$$

or merely

$$\sin(\omega t+\delta) = 0 \tag{42}$$

where the value of t is greater than the excitation cut-off time. It is required that the quantity $\omega t + \delta$ be an integral multiple of π. We are concerned only with the first two values of t beyond excitation cut-off for which Eq. (42) will hold.

The multiple of π, which must be equated to the argument $\omega t + \delta$, will be 0, 1, or 2. We determine which multiple to use depending on whether the translation term δ is positive or negative. Specifically, we compute two values of time t_1 and t_2 according to the following rules:

$$\text{If } \delta < 0$$
$$\omega t_1 + \delta = 0 \tag{43}$$

$$\text{If } \delta \geq 0$$
$$\omega t_1 + \delta = \pi \tag{44}$$

In either case,

$$\omega t_2 + \delta = \omega t_1 + \delta + \pi \tag{45}$$

By substituting the values t_1 and t_2 into a special form of Eq. (39), we examine the possibility of global extrema in the residual time range. (Sometimes even these two calculations can be avoided.)

To determine the response acceleration needed in the residual time range and the phase angle δ prominent in Eqs. (41) through (45), consider the following.

When t = Nh, the impulsive vibration ceases and the excitation $\ddot{s}(t)$ drops abruptly to zero.

$$\text{Let } \hat{t} = t - Nh \quad \text{where } t \geq Nh \tag{46}$$

The entire problem of response may be viewed anew at this point since the governing differential equation becomes homogeneous for all $t \geq Nh$. Vibrations are no longer forced, and simple damped oscillations will ensue.

$$y(\hat{t}) = e^{-\alpha\hat{t}}\left(C_1 \sin \omega\hat{t} + C_2 \cos \omega\hat{t}\right) \tag{47}$$

and

$$\dot{y}(\hat{t}) = e^{-\alpha\hat{t}}\left[\left(-\omega C_2-\alpha C_1\right) \sin \omega\hat{t} + \left(\omega C_1 - \alpha C_2\right) \cos \omega\hat{t}\right] \tag{48}$$

or renaming constants,

$$\dot{y}(\hat{t}) = e^{-\alpha\hat{t}}\left(A_1 \sin \omega\hat{t} + A_2 \cos \omega\hat{t}\right) \tag{49}$$

where

$$A_1 = -\omega C_2 - \alpha C_1 \tag{50}$$
$$A_2 = \omega C_1 - \alpha C_2$$

and

$$C_2 = y_N \tag{51}$$
$$C_1 = \left(\dot{y}_N + \alpha C_2\right)/\omega$$

for all $t > Nh$ ($\hat{t} > 0$).

Then,

$$\ddot{x}(\hat{t}) = -e^{-\alpha\hat{t}}\left[\left(DA_1 + \frac{C_1}{K}\right) \sin \omega\hat{t} + \left(DA_2 + \frac{C_2}{K}\right) \cos \omega\hat{t}\right] \tag{52}$$

By standard procedures, we can find the functions $\dddot{y}$, $\dddot{x}$, and the angle δ. This phase angle δ determines the values t_1 and t_2 in Eqs. (43) through (45).

In some instances, it is not even necessary to evaluate $\ddot{x}(t)$ at the two candidate points t_1 and t_2. Eq. (52) reveals that $\ddot{x}(t)$ in the residual time range is bounded from above by the quantity,

$$\hat{A} = \left[\left(DA_1 + \frac{C_1}{K}\right)^2 + \left(DA_2 + \frac{C_2}{K}\right)^2\right]^{1/2} \tag{53}$$

Therefore, if the positive and negative extrema already encountered in the impulse time range are both greater in absolute value than the bound $\hat{A}$, those extrema are global and there is no need to examine the residual time range.

In some applications, modern investigators focus on the residual time range with no damping. The assumption, D = 0, presents no

difficulty in the above calculations and, in fact, shortens the algorithm.

ALTERNATE QUADRATURE METHODS

A general technique for solving linear differential equations is the Lagrange Variation of Parameters or "reduction to quadrature." The core of the method is as follows:

Suppose $$Ly = \ddot{y} + p\dot{y} + qy = R \tag{54}$$

and suppose we know functions $y_1(t)$ and $y_2(t)$, both of which satisfy the homogeneous form of Eq. (54).

Functions A(t) and B(t) can be found, in principle, such that the general solution to Eq. (54) is:

$$y(t) = c_1y_1(t) + c_2y_2(t) + A(t)y_1(t) + B(t)y_2(t) \tag{55}$$

It turns out that

$$A = -\int \frac{\dot{y}_2 R}{W}\,dt \text{ and } B = \int \frac{y_1 R}{W}\,dt \tag{56}$$

where W(t) is the Wronskian $y_1\dot{y}_2 - \dot{y}_1y_2$.

In our shock spectral problem, Eq. (55) becomes

$$y(t) = \frac{e^{-\alpha t}\sin \omega t}{\omega}\int_o^t e^{\alpha s}\cos(\omega s)R(s)ds - \frac{e^{-\alpha t}\cos \omega t}{\omega}\int_o^t e^{\alpha s}\sin(\omega s)R(s)ds \tag{57}$$

We now devise an algorithm wherein the negative exponential outside the integral and the positive exponential inside the integral are merged into a recursion relation that will require no exponentiation at all except for the quantity $e^{-\alpha h}$ where h is the step size. We also avoid excessive computation of the trigonometric functions.

We will find the general form to be

$$y_{i+1} = f_1(y_i, \dot{y}_i, R_i, R_{i+1}, \alpha, \omega, h)$$

and

$$\dot{y}_{i+1} = f_2(y_i, \dot{y}_i, y_{i+1}, R_i, R_{i+1}, \alpha, \omega, h) \tag{58}$$

where neither of the functions f_1 nor f_2 contain t explicitly. To begin, we return to Eq. (57) and substitute t = t + h, also separating each integral into two terms. We can write

$$\omega\, e^{\alpha t}e^{\alpha h}\, y(t+h) = \sin(\omega t+\omega h)\left\{\int_o^t e^{\alpha s}\cos(\omega s)\,R(s)ds + \int_t^{t+h} e^{\alpha s}\cos(\omega s)\,R(s)ds\right\} - \cos(\omega t+\omega h)\left\{\ldots \text{ etc.}\right\} \tag{59}$$

The above must be expanded and regrouped to eliminate explicit appearance of transcendental functions in the symbol t. The basic strategic tools are:

a. Use the trapezoidal rule for the integrals from t to t + h.
b. Leave the integrals from o to t intact because they help constitute the definition of y(t).
c. Be prepared to recognize the derivative $\dot{y}(t)$, also in terms of integrals from o to t.
d. Make use of familiar trigonometric identities.

A convenient form of the final result is

$$y(t+h) = \frac{e^{-\alpha h}}{\omega}\left[y(t)\,(\alpha \sin \omega h + \omega \cos \omega h) + \sin \omega h\left(\dot{y}(t) + \tfrac{h}{2}R(t)\right)\right] \tag{60}$$

and

$$\dot{y}(t+h) = e^{-\alpha h}\left[y(t)\,(\alpha \cos \omega h - \omega \sin \omega h) + \cos \omega h\left(\dot{y}(t) + \tfrac{h}{2}R(t)\right)\right] - \alpha y(t+h) + \tfrac{h}{2}R(t+h) \tag{61}$$

If the above strategy is exercised using the mid-point rule for quadrature, we can derive an alternate algorithm,

$$y(t+h) = \frac{e^{-\alpha h}}{\omega}[y(t)(\alpha \sin \omega h + \omega \cos \omega h) + \dot{y}(t) \sin \omega h] + \rho_1[R(t) + R(t+h)] \tag{62}$$

and

$$\dot{y}(t+h) = e^{-\alpha h}[y(t)(\alpha \cos \omega h - \omega \sin \omega h) + \dot{y}(t) \cos \omega h] - \alpha\, y(t+h) + \rho_2[R(t) + R(t+h)] \tag{63}$$

where

$$\rho_1 = \frac{h}{2\omega}\, e^{-\alpha\frac{h}{2}}\left[\sin(\omega h)\cos(\omega\tfrac{h}{2}) - \cos(\omega h)\sin(\omega\tfrac{h}{2})\right] \tag{64}$$

and

$$\rho_2 = \frac{h}{2}\, e^{-\alpha\frac{h}{2}}\left[\sin(\omega h)\sin(\omega\tfrac{h}{2}) + \cos(\omega h)\cos(\omega\tfrac{h}{2})\right] \tag{65}$$

Note that the recursion relations using the two different quadrature methods result in expressions of the

same form. Therefore, an average of the two formulae will again yield expressions of the same form with alterations involving only the constants ρ_1 and ρ_2 and the terms in R(t) and R(t+h). A weighted average of one third of the trapezoidal formula plus two thirds of the mid-point formula is recommended since it simulates quadrature by Simpson's rule.

A NUMERICAL METHOD EMPLOYING THE EULER-MACLAURIN SUM FORMULA

Consider the time points $t_n = nh$ and the function Y(t), which may be a vector. One convenient truncated form of the Euler-Maclaurin sum formula states that

$$Y_{n+1} = Y_n + \frac{h}{2}\left(\dot{Y}_{n+1} + \dot{Y}_n\right) - \frac{h^2}{12}\left(\ddot{Y}_{n+1} - \ddot{Y}_n\right) + Oh^5 \quad (66)$$

This relation constitutes a 4th order method for solving a system of ordinary differential equations (ODE's)

$$\dot{Y} = F(t,Y) \quad (67)$$

with prescribed initial conditions. Specifically, consider

$$\dot{Y} = AY + f \quad (68)$$

where $\dot{A} = 0$.

Then, $$\ddot{Y} = A^2Y + Af + \dot{f} \quad (69)$$

We can solve for Y_{n+1} in terms of Y_n, A, f_n, f_{n+1}, $\dot{f}_n$, and $\dot{f}_{n+1}$, the latter quantities being known at each step.

The basic shock spectral problem is

$$\ddot{y} + p\dot{y} + qy = R(t) = -\ddot{s}(t) \quad (70)$$

Eq. (70) is equivalent to

$$\frac{d}{dt}\begin{bmatrix} y \\ \dot{y} \end{bmatrix} = \begin{bmatrix} 0 & 1 \\ -q & -p \end{bmatrix}\begin{bmatrix} y \\ \dot{y} \end{bmatrix} + \begin{bmatrix} 0 \\ R(t) \end{bmatrix} \quad (71)$$

which is in the form $\dot{Y} = AY + f$. Here,

$$Y = \begin{bmatrix} y \\ \dot{y} \end{bmatrix}, \quad f = \begin{bmatrix} 0 \\ R(t) \end{bmatrix} \quad (72)$$

and

$$A = \begin{bmatrix} 0 & 1 \\ -q & -p \end{bmatrix} \quad (73)$$

To isolate the unknown Y_{n+1}, we perform manipulations that lead to the following relation,

$$\left(I - \frac{h}{2}A + \frac{h^2}{12}A^2\right)Y_{n+1} - \left(I + \frac{h}{2}A + \frac{h^2}{12}A^2\right)Y_n + \begin{Bmatrix} \frac{-h^2}{12}\left(R_{n+1} - R_n\right) \\ \frac{h}{2}\left(R_n + R_{n+1}\right) - \frac{h^2}{12}\left[\dot{R}_{n+1} - \dot{R}_n - p\left(R_{n+1} - R_n\right)\right] \end{Bmatrix} \quad (74)$$

where I is the 2 by 2 identity matrix.

Fortunately, the only appearance of derivatives in Eq. (74) occurs in the form of a difference of end-point values. The function R(t) is defined as linear in the closed interval $t_n \leq t \leq t_n + h$. The derivative $\dot{R}(t)$ is, therefore, constant, but only in the open interval $t_n < t < t_n + h$. Nevertheless, we are tempted to suggest that

$$\dot{R}_{n+1} - \dot{R}_n \cong 0 \quad (75)$$

for each individual interval used in the recursive procedure defined by Eq. (74). This is a natural consequence of connecting the sampled excitation points with straight lines - an artifice deemed acceptable in the previously discussed methods.

Eq. (74) may be written simply as

$$MY_{n+1} = NY_n + r_n \quad (76)$$

or

$$Y_{n+1} = M^{-1}\left(NY_n + r_n\right) \quad (77)$$

where, for example,

$$M = I - \frac{h}{2}A + \frac{h^2}{12}A^2 = \begin{pmatrix} 1 - \frac{h^2}{12}q & -\frac{h}{2}\left(1+\frac{h}{6}p\right) \\ \frac{h}{2}q\left(1+\frac{h}{6}p\right) & 1 + \frac{h}{2}p + \frac{h^2}{12}\left(-q+p^2\right) \end{pmatrix} \quad (78)$$

Since the matrices M and N are merely of dimension 2 by 2, some preliminary algebra can be done by hand to render Eq. (77) of the form

$$Y_{n+1} = G\left(h, p, q, Y_n, R_n, R_{n+1}\right) \quad (79)$$

where G represents a short algorithm.

COMPARISON WITH FOURIER TRANSFORM METHOD

In classical shock spectral analysis, the direct analytical method is preferable to the FFT method for reasons of speed, accuracy, and range of applicability. However, when the

input parameters are in ranges such that the FFT method is valid, the two methods should give comparable results. Experience has shown the FFT to be valid when

$$f_R t_Z > Q \tag{80}$$

where

f_R = response frequency

t_Z = zero fill time

Q = damping quality factor

In this discussion, the zero fill time is always

$$t_Z \cong 32768h - T \tag{81}$$

where

h = 1/(sample rate)
T = impulse width

At this point, see Figs. 2 and 3.

Since the Fourier transform method is equivalent to assuming that the input excitation is periodic (which, in general, it is not), in principle, the zero fill time should be as great as possible. However, computer storage limitations have imposed the constraint of Eq. (81).

The "validity" criterion of Eq. (80) is also called the "distortion" criterion for the FFT since it defines a critical response frequency,

$$\hat{f}_R = \frac{Q}{t_Z} \tag{82}$$

For values of f_R below the critical value, distortion is expected to appear in shock spectra computed by the FFT.

Consider the problem:

$$\ddot{s}(t) = 25 \sin [2\pi(300)t] \text{ G units/sec}^2$$
Q = 10 (dimensionless)
Sample rate = 5000 points/sec
h = 1/5000 sec
T impulse = 1 sec (83)
$t_Z = 32768h - T \cong 5.6$ sec
$\hat{f}_R = \frac{Q}{t_Z} = \frac{10}{5.6} < 2$ hz

f_R = 10, ... 1000 hz

Logarithmic frequency spacing with six subdivisions per octave

Since all response frequencies are greater than the critical value $\hat{f}_R$, both the transform and the direct methods produce highly similar shock spectra (Figs. 4 and 5).

The UNIVAC system routine, SUPTF, was used to time both runs. Timings on the UNIVAC 1108 were:

FFT Method: 154 SUP SECS
DIRECT Method: 20 SUP SECS
Improvement Ratio: $\cong$ 7.7

Now consider:

$$a(t) = \ddot{s}(t) = \sin[2\pi(2)t] \text{ G units/sec}^2$$
Q = 10 (dimensionless)
Sample rate = 10,000 points/sec
h = .0001 sec
T impulse = 1 sec
$t_Z = 32768h - T \cong 2.3$ sec (84)
$\hat{f}_R = \frac{Q}{t_Z} = \frac{10}{2.3} \cong 4.3$ hz
f_R = 1, ... 4 hz with Δf_R = .1 hz

In this case, distortion should be expected in the FFT method throughout most of the response frequency range (Figs. 6 and 7). The difficulties observed are intrinsic to the FFT method, which, in this example, does not have enough zero fill to simulate the fact that the simple excitation wave is truncated for all time after t = 1.

Computer Run Times for Case in Eq. (84)

FFT Method: 210.3 SUP SECS
DIRECT Method: 31.6 SUP SECS
Improvement ratio $\cong$ 6.7

EXAMPLE OF NON-MONOTONIC VARIATION

Consider the following test case, which uses a single-frequency sinusoidal excitation sampled at a rate of 8192 points/second:

T(impulse) = 1 sec
$\ddot{s} = \sin(100\pi t)$ G units, $0 \leq t \leq 1$
$\ddot{s} = 0$ G units, $t > 1$
Q = 50 (dimensionless)
f_R = (0,100) hz

Fig. 8 is the resulting shock spectrum. The sharp peak is expected. Although not obvious in this broadly scaled graph, some secondary oscillations are present at low frequencies. A resolution blowup of Fig. 8 is shown in Fig. 9, in which the non-monotonic behavior becomes predictable. Peaks and troughs occur alternately at $f_R = n - 1/2$ and $f_R = n$, where n is any integer between 1 and approximately 20. Neither noise nor instabilities occur in the algorithm,

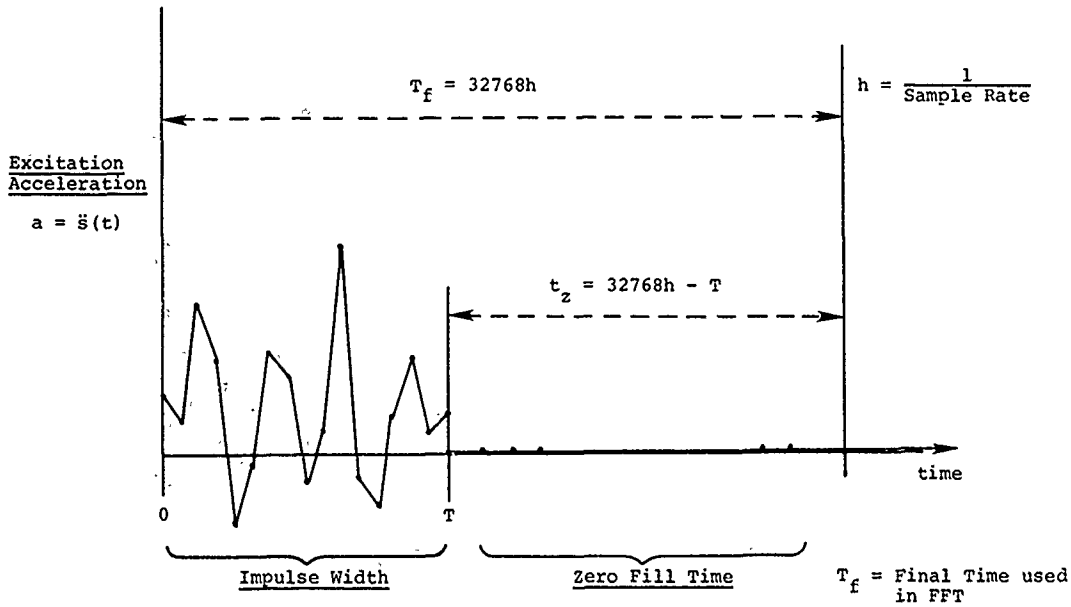

Fig. 2 - Time segmentation in FFT

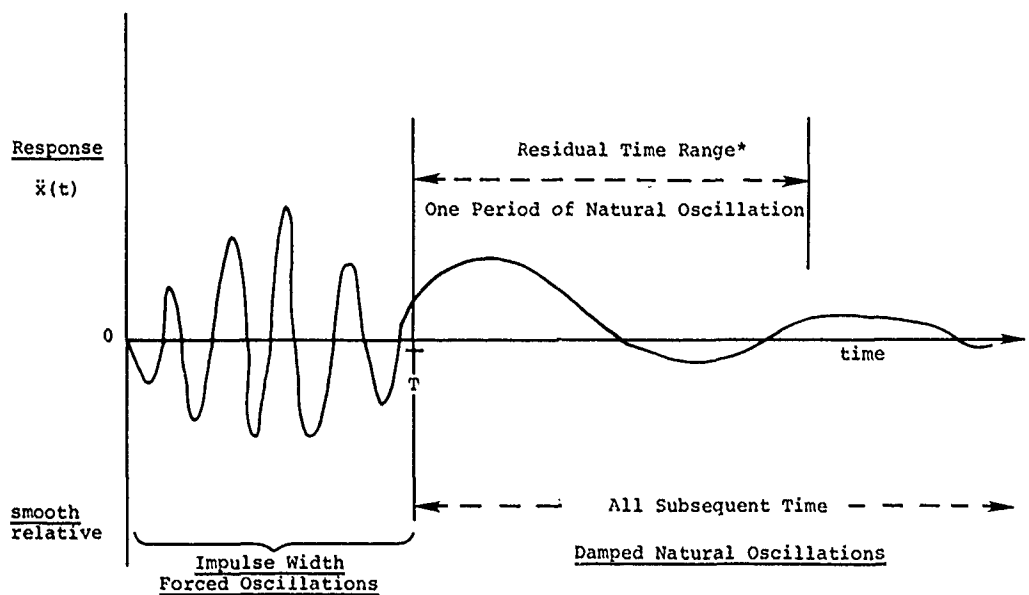

*Note: "Residual Time Range" Not Equal to "Zero Fill Time".
(There is no zero fill the direct method.)

Fig. 3 - Example response acceleration (any method)

Using FFT

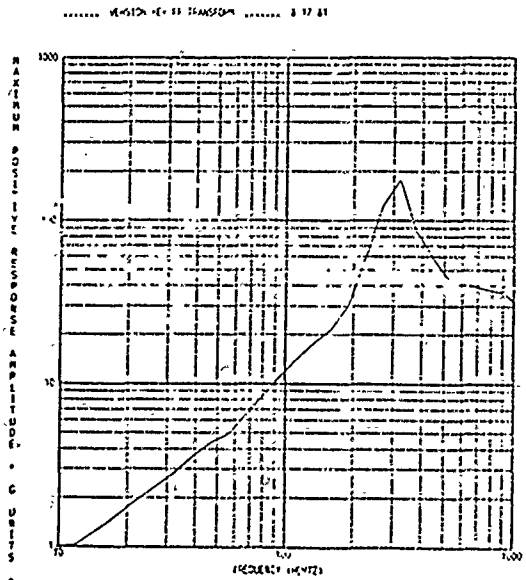

Fig. 4 - Shock spectrum - maximum positive response case of Eq. (83), using FFT

Using FFT

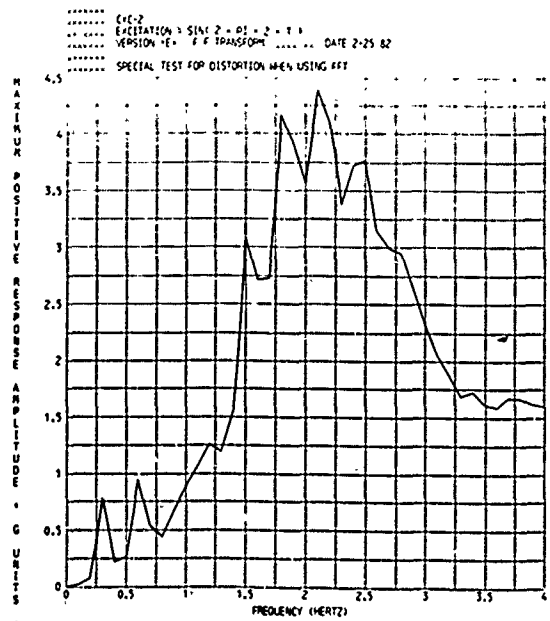

Fig. 6 - Shock spectrum - maximum positive response case of Eq. (84), using FFT

Direct Method

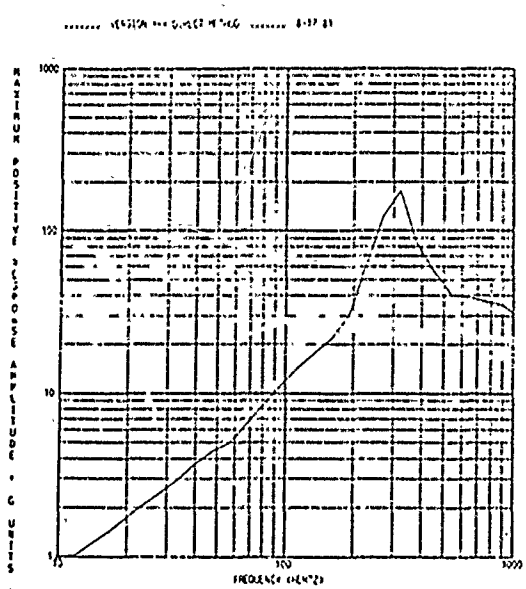

Fig. 5 - Shock spectrum - maximum positive response case of Eq. (83), using direct method

Direct Method

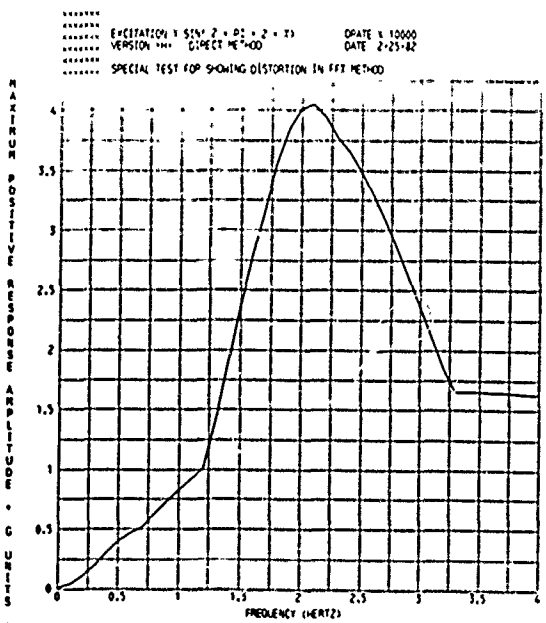

Fig. 7 - Shock spectrum - maximum positive response case of Eq. (84), using direct method

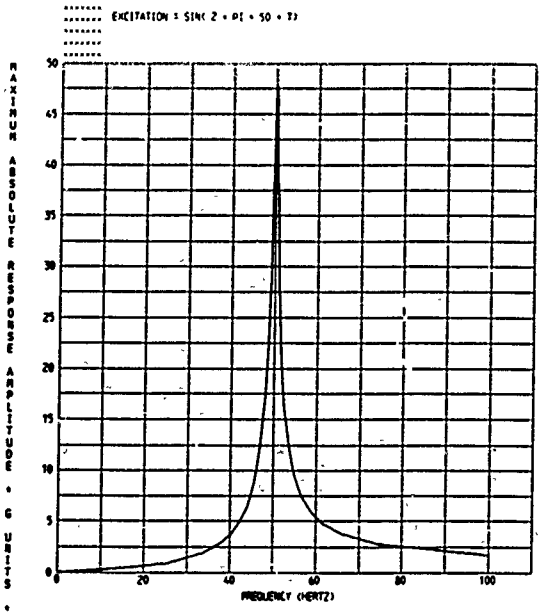

Fig. 8 - Example shock spectrum, maximum absolute response

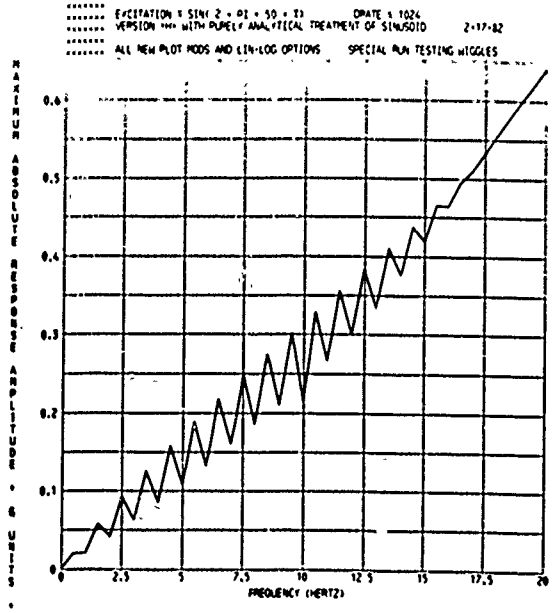

Fig. 9 - Finer resolution blowup of fig. 8

and we will show that the secondary oscillations are mathematically legitimate.

EXPLANATION OF NON-MONOTONIC VARIATION

Suppose a linear oscillator with variable natural frequency is subjected to a purely sinusoidal excitation with a single driving frequency, as was the case above. Suppose further that the natural response frequency f_R is allowed to vary from $f_R = 0$ up to a value near the excitation frequency f_E where, upon coinciding, the value $f_R = f_E$ may be called the resonant frequency. One might suspect that the maximum response acceleration would increase monotonically as f_R varies from zero up to f_E where the resonant peak occurs. Certainly, this is the overall trend. However, this smooth variation is not realized when the graph is examined with greater resolution. At the time of excitation cut-off, the values of response at the end of the impulse time range become the initial values in a new homogeneous (unforced) problem in the residual time range. These critical values of response at the junction of the two time ranges turn out to be multiplicative in a factor that is non-monotonic in the response frequency f_R. Thus, the resulting shock spectrum can exhibit minor oscillations in its ascent toward the resonant peak.

In this case of sinusoidal excitation, the problem can be solved analytically. The differential equation becomes

$$\ddot{y} + D\dot{y} + \frac{1}{K}y = -\sin(\beta t) \qquad (85)$$

Proceeding in traditional fashion, the solution is of the form:

$$\begin{aligned} y(t) &= e^{-\alpha t}(C_1 \sin \omega t + C_2 \cos \omega t) + a \sin \beta t + b \cos \beta t \\ \dot{y}(t) &= e^{-\alpha t}(B_1 \sin \omega t + B_2 \cos \omega t) + a\beta \cos \beta t - b\beta \sin \beta t \end{aligned} \qquad (86)$$

Recall that the damping-compliance pair, D and K, is implied by the quality-frequency pair, Q and ω, and vice versa. The conventional parameterization takes Q and ω to be fundamental. Thus, we prefer to write the final solutions exclusively in terms of Q, ω, and β, or alternately, in terms of Q, f_R, and f_E, since $\omega = 2\pi f_R$ and $\beta = 2\pi f_E$.

The usual assumption of $Q \geq 10$ gives

$$\frac{1}{K} \cong \omega^2 \qquad D \cong \frac{\omega}{Q} \qquad (87)$$

The frequency values we first consider are in the ranges

$$f_R \lesssim 5$$

$$f_E \cong 50 \quad ; \quad \text{any integer near 50} \tag{88}$$

Therefore, it is safe to write $\omega^2 << \beta^2$.

This assumption will subsequently be relaxed, but temporarily, we are seeking simple coefficients.

The solution functions $y(t)$ and $\dot{y}(t)$ in Eq. (86) become

$$y(t) = e^{\frac{-\omega t}{2Q}}\left(\frac{1}{\omega\beta}\sin\omega t - \frac{\omega}{Q\beta^3}\cos\omega t\right) + \frac{1}{\beta^2}\sin\beta t + \frac{\omega}{Q\beta^3}\cos\beta t$$

$$\dot{y}(t) = \frac{1}{\beta}e^{\frac{-\omega t}{2Q}}\left(\frac{1}{2Q}\sin\omega t - \cos\omega t\right) + \frac{1}{\beta}\left(-\frac{\omega}{Q\beta}\sin\beta t + \cos\beta t\right) \tag{89}$$

Our goal is to evaluate the response acceleration $\ddot{x}(t)$ and its derivative $\dddot{x}(t)$ at the end of the impulse time range. These critical values become the initial conditions for a related but new problem in the residual time range in which the vibrations are naturally decaying with no forcing excitation. Let the impulse width equal 1 second. We substitute $t = 1$ into Eq. (89) and note that

$$\sin\beta = \sin 2\pi f_E = 0$$

and

$$\cos\beta = \cos 2\pi f_E = 1 \tag{90}$$

since the driving frequency f_E is an integer.

We will temporarily consider the response frequency, f_R, taking on the values

$$f_R = 0, \tfrac{1}{2}, 1, 1\tfrac{1}{2}, \ldots 4\tfrac{1}{2}, 5$$

Therefore, $\sin\omega = \sin 2\pi f_R = 0$ (91)

However, $\cos\omega = \cos 2\pi f_R = \pm 1$ (92)

with the sign depending on whether f_R is an integer or a multiple of one-half.

Substituting $t = 1$ into Eq. (89), we have for $y(1)$

$$y(1) = \frac{\omega}{Q\beta^3}\left(1 - e^{\frac{-\omega}{2Q}}\cos\omega\right) \tag{93}$$

or

$$y(1) = \frac{\omega}{Q\beta^3}\left(1 \pm e^{\frac{-\pi f_R}{Q}}\right) \tag{94}$$

where the (+) is associated with $f_R = n + 1/2$, and the (-) with $f_R = n$ (any integer). The quantity in parentheses in Eq. (94) is called $\eta = (f_R, Q)$

$$\eta = \eta(f_R, Q) = 1 \pm e^{\frac{-\pi f_R}{Q}} \tag{95}$$

and we have

$$y(1) = \frac{\omega}{Q\beta^3}\eta \tag{96}$$

Returning to Eq. (89), we have

$$\dot{y}(1) = \frac{1}{\beta}\left(1 - e^{\frac{-\omega}{2Q}}\cos\omega\right) \tag{97}$$

or

$$\dot{y}(1) = \frac{1}{\beta}\eta$$

The familiar relation

$$\ddot{x} = -D\dot{y} - \frac{1}{K}y \tag{98}$$

is now

$$\ddot{x} \cong -\omega\left(\frac{1}{Q}\dot{y} + \omega y\right) \tag{99}$$

Therefore,

$$\ddot{x}(1) \cong -\frac{\omega\eta}{Q\beta}\left(1 + \frac{\omega^2}{\beta^2}\right) \tag{100}$$

or if $\omega^2 << \beta^2$,

$$\ddot{x}(1) \cong -\frac{\omega}{Q\beta}\eta \tag{101}$$

Further manipulations can yield $\dddot{x}(1)$, which as expected, is also multiplicative in the factor η. See Table 1 for a summary of the critical response values and Table 2 for a brief tabulation of the function $\eta = \hat{\eta}(f_R, Q)$.

The solution to a linear homogeneous 2nd order differential equation is exponentially damped sinusoidal in time but linear in the initial values of the solution and its derivative. As the response acceleration $\ddot{x}(t)$ varies through the residual time range $t > T$ impulse, all its values, including the extrema, are multiplicative in the factor $\eta(f_R, Q)$, which is oscillatory in the response frequency f_R. Thus, the secondary peaks in the shock spectra of Fig. 9 are explained.

The condition $\omega^2 << \beta^2$ can be relaxed; it was introduced merely to simplify coefficients in Eq. (89). Even if the natural frequency and excitation driving frequency are not widely separated in magnitude, the critical values of response will still be multiplicative in the parameter

$\eta(f_R,Q)$. Of course, when f_R takes on large values, the multiplier, η, oscillates tightly about unity, and its effect on a shock spectral graph becomes negligible.

In Table 3, we summarize the critical response values for the more general case where ω may be either smaller or larger than β but not equal. The natural frequency f_R may now be considered to vary continuously; however, in this analysis, the excitation frequency remains an integer so that Eq. (90) can hold. The magnitudes of the critical response values oscillate between relative extrema as the natural frequency f_R varies through alternate multiples of unity or one-half.

See Fig. 10 for qualitative sketches of typical situations. Also, see the tabulation in Table 4 for a quantitative corroboration of what we suspect when $\omega^2 << \beta^2$. The case is specifically

$$\begin{aligned} &a(t) = \ddot{s}(t) = \sin [2\pi(50)t] \text{ G units} \\ &Q = 50 \text{ (dimensionless)} \\ &T \text{ impulse} = 1 \text{ sec} \\ &f_E = 50 \text{ hz} \end{aligned} \qquad (102)$$

$$f_R \leq 10 \text{ hz}$$

When f_R is a multiple of one-half, the critical multiplier η is at a peak and both global extrema of $\ddot{x}(t)$ are in the residual time range. When f_R is an integer, the critical multiplier, η, is at a trough and thus lacks the augmentive "strength" to produce residual extrema greater than those already encountered in the impulse time range.

TABLE 1
Approximate Critical Response Values[a]

$y(1) = \frac{\omega}{Q\beta^3}\ \eta$	T impulse = 1
$\dot{y}(1) = \frac{1}{\beta}\ \eta$	$\eta = 1 - e^{\frac{-\pi f_R}{Q}} \cos 2\pi f_R$
$\ddot{x}(1) = -\frac{\omega}{Q\beta}\ \eta$	$\omega = 2\pi f_R$
$\dddot{x}(1) = -\frac{\omega^2}{\beta}\ \eta$	$\beta = 2\pi f_E$
[a]Here, $\omega^2 << \beta^2$	

TABLE 2
Critical Multiplier, η, as Function of f_R and Q

Q	f_R	f_R/Q	η
50	0.5	.01	1.969
50	1.0	.02	.061
50	1.5	.03	1.910
50	2.0	.04	.118
--			
50	4.5	.09	1.754
50	5.0	.10	.270
--			
50	60.5	1.21	1.022
50	61.0	1.22	.978
--			
10	0.5	.05	1.855
10	1.0	.10	.270
10	1.5	.15	1.624
10	2.0	.20	.467
--			
10	4.5	.45	1.243
10	5.0	.50	.792
--			
10	20.5	2.05	1.002
10	21.0	2.10	.999

TABLE 3
More General Expressions for Critical Response Values

$y(1) = \frac{\omega\beta\eta}{Q(\omega^2 - \beta^2)^2}$	T impulse = 1
$\dot{y}(1) = \frac{-\beta\eta}{\omega^2 - \beta^2}$	$\eta = 1 - e^{\frac{-\pi f_R}{Q}} \cos 2\pi f_R$
$\ddot{x}(1) = \frac{-\omega\beta^3\eta}{Q(\omega^2 - \beta^2)^2}$	$\omega = 2\pi f_R$
$\dddot{x}(1) = \frac{\omega^2\beta\eta}{\omega^2 - \beta^2}$	$\beta = 2\pi f_E$
	f_R = any value other than f_E
	f_E = any integer
	$\frac{1}{Q^2} << 1$

FINAL EXAMPLE AND COMPARATIVE SPEED OF METHODS

It has been demonstrated that the direct analytical method is considerably faster than the transform method using the FFT. Improvement factors of 4 to 10 are common, with 6 or 7 being typical as shown. In fact, our principle purpose is to discourage the use of transform methods for calculating shock spectra on general purpose computers (although not necessarily on array processors). A preferred choice from the alternate methods offered in this paper is not obvious since the relative speeds are not widely disparate. We will quote approximate relative run times for four methods described in the previous sections. The values are based on UNIVAC 1108 experience but can also be estimated by counting the number of multiplications in the inner loop of each routine. The methods are:

ANALYT-DIRECT - Direct analytical solution

VARPAR-TRAP - Quadrature (Trapezoidal)

VARPAR-SIMP - Quadrature (Simpson)

EULMAC-4TH - Euler-Maclaurin 4th order

The approximate relative run times are:

Method	Approximate Relative Run Time
ANALYT-DIRECT	1.0
VARPAR-TRAP	.7
VARPAR-SIMP	1.0
EULMAC-4TH	1.3

User facilities vary more greatly than the above timing ratios. However, the author prefers the basic direct method, ANALYT, because it involves only one assumption, namely, that the sample rate is great enough to permit the polygonal representation of the excitation function. The other methods make even further demands on smallness of time step to justify the classical numerical techniques. (Of course, no method can accurately examine the acceleration response peaks if the time step is too large.)

The following is a convenient case for timing and checkout. The input excitation is the sum of four sine waves, each with unit amplitude having driving frequencies of 10, 20, 30, and 40 hz. The wave truncates to zero for all t > 1. The complete description of input is:

$$a(t) = \ddot{s}(t) = \sum_{k=1}^{4} \sin [2\pi(10k)t]$$

G units
T(impulse) = 1 sec
Δt = 1/8192 sec
Q = 50 (dimensionless) (103)
f_R = (0,50) with Δf_R = .5 hz

This case has also been published by Rockwell International. Note the graphs in Figs. 11 and 12. The resolution in the Rockwell graph does not expose the secondary oscillations at low frequencies since this effect was not pertinent to the overall purpose of their investigation. We emphasize the 2nd order effect for theoretical completeness.

The reader may also note Tables 5 and 6, which offer some comparisons of methods and sample rates.

TABLE 4
Behavior of Low Frequency Response due to Higher Frequency Excitation

f_R	t_{min}	$\ddot{x}_{min}$	t_{max}	$\ddot{x}_{max}$
.5	1.49	-.019	2.49	.018
1.5	1.16	-.056	1.50	.055

9.5	1.03	-.301	1.08	.292

1.0	.74	-.020	.25	.0202
2.0	.36	-.040	.11	.041

10.0	.07	-.209	.02	.215

a(t) = sin[2π(50)t] G units
T impulse = 1 sec
Q = 10 (dimensionless)
f_E = 50 hz

$f_R < f_E$

Noting Minor Oscillations

f_R	$\ddot{x}_{max}$	
0.5	.018	
1.0	.020	
1.5	.055	
2.0	.041	non-monotonic

9.5	.292	
10.0	.215	non-monotonic

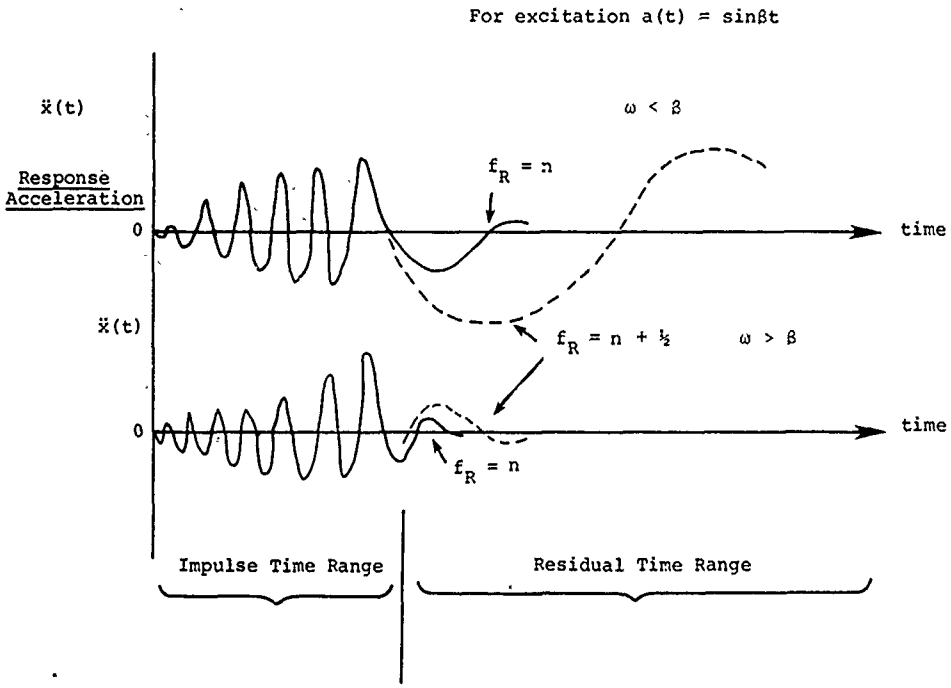

Fig. 10 - Qualitative parametrics of response acceleration caused by sinusoidal excitation

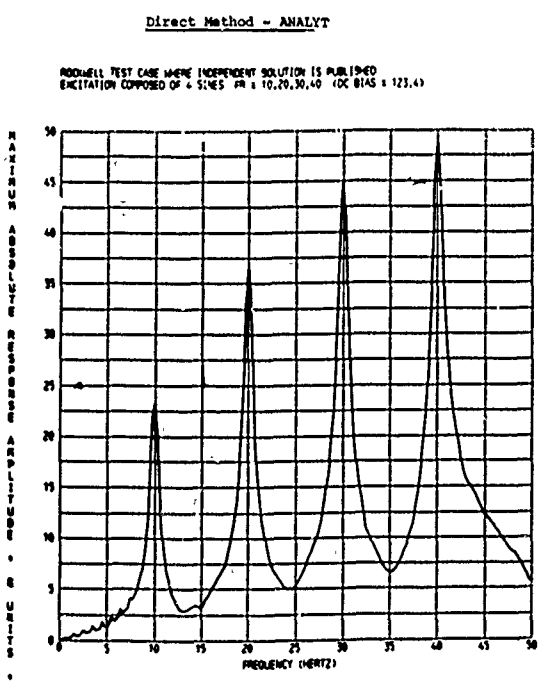

Fig. 11 - Shock spectrum for a composite sinusoidal excitation, maximum absolute response

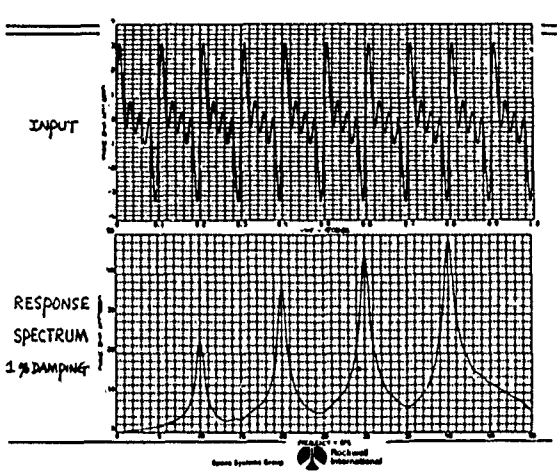

Fig. 12 - Shock spectrum method verification (Courtesy Rockwell International)

TABLE 5
Maximum Absolute Acceleration Response
(G Units) Case of Eq. (103), Sample Rate = 8192/sec

f_R (hz)	ANALYT	SIMPSON	TPAPZ	EULMAC
1.0	.21254	.21271	.21271	.21272
1.5	.59498	.59537	.59538	.59542
2.0	.42213	.42217	.42217	.42218
2.5	.98646	.98670	.98670	.98685

19.5	25.237	25.237	25.237	25.238
20.0	36.506	36.506	36.506	36.509

29.5	32.977	32.976	32.978	32.978
30.0	44.790	44.789	44.791	44.792

39.5	36.671	36.671	36.673	36.672
40.0	48.710	48.710	48.713	48.713

50.0	5.6670	5.6670	5.6671	5.6670

TABLE 6
Noting Different Sample Rates -
Case of Eq. (103)

Response Frequency Sample Rate Method f_R	Maximum Absolute Acceleration Response			
	8192 ANALYT Response	1024 ANALYT Response	8192 SIMPSON Response	1024 SIMPSON Response
1	.21254	.21238	.21217	.21240
2	.42213	.42152	.42217	.42152
20	36.506	36.477	36.506	36.447
30	44.790	44.541	44.791	44.540
40	48.710	48.407	48.713	48.406
50	5.667	5.641	5.667	5.641

FORTRAN LISTINGS

In closing, we present FORTRAN routines for two of the principle algorithms developed in this paper. Note that the routines accept the damping coefficient and the compliance as inputs. These can be computed in a calling routine from the damping "quality," Q, and the response frequency, f_R. The values of Q and f_R can be as numerous and arbitrary as desired.

For a copy of the complete paper, contact Frank Cox, Computer Sciences Corporation, 1300 Bay Area Blvd., Houston, TX. 77058.

```
FD7-A04606*TPF$(G).ANALYT(1S)
      1            SUBROUTINE ANALYT(NFIN,W,D,CONK,R,H,BIG,SMALL,ABMAX)
      2      C.....    BASIC DIRECT METHOD
      3      C... INPUT :  NFIN = NO. OF PTS. IN IMPULSE TIME RANGE
      4      C... INPUT :  W = 2*PI*RESPONSE FREQUENCY
      5      C... INPUT :  D = DAMPING COEFFICIENT  (NOT DAMPING 'QUALITY' Q)
      6      C... INPUT :  CONK = COMPLIANCE  (RECIPROCAL OF SPRING 'STIFFNESS')
      7      C... INPUT :  R(I) = EXCITATION ACCELERATION
      8      C... INPUT :  H = TIME STEP
      9      C... OUTPUT :  BIG = MAX ACC RESPONSE
     10      C... OUTPUT :  SMALL = MIN ACC RESPONSE
     11      C... OUTPUT :  ABMAX = MAX ABSOLUTE RESPONSE
     12            DIMENSION R(1)
     13            DATA PI /3.14159265 /
     14            BIG = -100000.
     15            SMALL = 100000.
     16            REPK = 1./CONK
     17            REPW = 1./W
     18            D2 = D/2.
     19            Y1 = 0.
     20            Y2 = 0.
     21            WH = W*H
     22            E = EXP(-D2*H)
     23            S = E*SIN(WH)
     24            C = E*COS(WH)
     25            U =  W*C - D2*S
     26            V = -W*S - D2*C
     27            CONKH = CONK/H
     28            RTO = -R(1)
     29      C.....  AS OF 12-31-82 THIS IS FASTEST VERSION OF ANALYT
     30            DO 10  I = 2,NFIN
     31            R1 = -R(I)
     32            A = CONKH*(R1 - RTO)
     33            B = CONK*(RTO - D*A)
     34            C2 = Y1 - B
     35            C1 = (D2*C2 + Y2 - A)*REPK
     36            Y1 = S*C1 + C*C2 + A*H + B
     37            Y2 = U*C1 + V*C2 + A
     38            RTO = R1
     39            DDX = -D*Y2 - Y1*REPK
     40            IF(DDX .GT. BIG) BIG = DDX
     41            IF(DDX .LT. SMALL) SMALL = DDX
     42       0010 CONTINUE
     43            C1 = (D2*Y1 + Y2)/W
     44            C2 = Y1
     45            A1 = -W*C2 - D2*C1
     46            A2 =  W*C1 - D2*C2
     47            ENUF = SQRT((D*A1 +REPK*C1)**2 + (D*A2 +REPK*C2)**2)
     48            IF(BIG .GT. ENUF .AND. ABS(SMALL) .GT. ENUF) GO TO 50
     49            B1 = -W*A2 - D2*A1
     50            B2 =  W*A1 - D2*A2
     51            P1 = D*B1 + A1*REPK
     52            P2 = D*B2 + A2*REPK
     53            P = ATAN2(P2,P1)
     54            IF(P .LT. 0.) WT = ABS(P)
     55            IF(P .GE. 0.) WT = PI - P
     56            DO 20  J = 1,2
     57            S = SIN(WT)
     58            C = COS(WT)
     59            U =  W*C - D2*S
     60            V = -W*S - D2*C
     61            E = EXP(-D2*WT/W)
     62            Y1 = E*(S*C1 + C*C2)
     63            Y2 = E*(U*C1 + V*C2)
     64            DDX = -D*Y2 - Y1*REPK
     65            IF(DDX .GT. BIG) BIG = DDX
     66            IF(DDX .LT. SMALL) SMALL = DDX
     67            WT = WT + PI
     68       0020 CONTINUE
     69       0050 ABMAX = AMAX1(BIG,-SMALL)
     70            RETURN
     71            END
```

```
FD7-AC46C6*TPF$(C),SIMPSON-QUAD(16)
      1            SUBROUTINE VARPAR(NFIN,W,D,CONK,R,H,H2,H3,H6,BIG,SMALL,ABMAX)
      2      C...                                  QUADRATURE WITH SIMPSON RULE
      3      C... INPUT :  NFIN = NO. PTS. IN IMPULSE TIME RANGE
      4      C... INPUT :  W = 2*PI*RESPONSE FREQUENCY
      5      C... INPUT :  D = DAMPING COEFFICIENT  (NOT DAMPING QUALITY 'Q')
      6      C... INPUT :  CONK = COMPLIANCE  (RECIPROCAL OF SPRING 'STIFFNESS')
      7      C... INPUT :  R(I) = EXCITATION ACCELERATION
      8      C... INPUT :  H = TIME STEP,   H2=H/2   H3=H/3   H6=H/6
      9      C... OUTPUT :   BIG = MAX ACC RESPONSE
     10      C... OUTPUT :  SMALL = MIN ACC RESPONSE
     11      C... OUTPUT :  ABMAX = MAX ABSOLUTE RESPONSE
     12            DIMENSION R(1)
     13            DATA PI  /3.14159265
     14            BIG = -1C0C0.
     15            SMALL = 1C000.
     16            REPK = 1./CONK
     17            A = D/2.
     18            ERT = EXP(-A*H2)
     19            E = ERT * ERT
     20            HE = H3 * ERT
     21            EW = E/W
     22            WH = W*H
     23            WH2 = WH/2.
     24            S = SIN(WH)
     25            C = COS(WH)
     26            S2 = SIN(WH2)
     27            C2 = COS(WH2)
     28            P1 = HE*(S*C2 - C*S2)/W
     29            P2 = HE*(S*S2 + C*C2)
     30            EWB1 = EW*(A*S + W*C)
     31            EB2 = E*(A*C - W*S)
     32            EWS = EW*S
     33            EC = E*C
     34            HS = H6*EWS
     35            HC = H6*EC
     36            Y = C.
     37            DY = 0.
     38            RO = -R(1)
     39            DO 10  I = 2,NFIN
     40            R1 = -R(I)
     41            RR = RO + R1
     42            EB2Y = EB2*Y
     43            Y = EWB1*Y + EWS*DY + P1*RR + HS*RO
     44            DY = -A*Y + EB2Y + EC*DY + P2*RR + HC*RO + H6*R1
     45            RO = R1
     46            DDX = -D*DY - Y*REPK
     47            IF(DDX .GT. BIG) BIG = DDX
     48            IF(DDX .LT. SMALL) SMALL = DDX
     49       0010 CONTINUE
     50            C1 = (A*Y + DY)/W
     51            C2 = Y
     52            A1 = -W*C2 - A*C1
     53            A2 =  W*C1 - A*C2
     54            ENUF = SQRT((2*A1 +REPK*C1)**2 + (D*A2 +REPK*C2)**2)
     55            IF(BIG .GT. ENUF .AND. ABS(SMALL) .GT. ENUF) GO TO 50
     56            B1 = -W*A2 - A*A1
     57            B2 =  W*A1 - A*A2
     58            P1 = D*B1 + A1*REPK
     59            P2 = D*B2 + A2*REPK
     60            P = ATAN2(P2,P1)
     61            IF(P .LT. 0.) WT = ABS(P)
     62            IF(P .GE. 0.) WT = PI - P
     63            DO 40  J = 1,2
     64            S = SIN(WT)
     65            C = COS(WT)
     66            U =  W*C - A*S
     67            V = -W*S - A*C
     68            E = EXP(-A*WT/W)
     69             Y = E*(S*C1 + C*C2)
     70            DY = E*(U*C1   V*C2)
     71            DDX = -D*DY - Y*REPK
     72            IF(DDX .GT. BIG) BIG = DDX
     73            IF(DDX .LT. SMALL) SMALL = DDX
     74            WT = WT + PI
     75       0040 CONTINUE
     76       0050 ABMAX = AMAX1(BIG,-SMALL)
     77            RETURN
     78            END
```

DISCUSSION

Voice: Is it basically computing the convolution through the FFT procedure?

Mr. Cox: That is correct. I should have shown what we did with the FFT. When I worked down there, which was for quite a long time, people would look at the differential equation. They would use the Fast Fourier transform, and then they also had to do the inverse transform. The way that procedure works is to simply do the FFT with the input excitation acceleration. We also write a transfer function that involves the LaPlace transform, and that is something you can do by hand. Then you multiply the inverse Fourier transform, done by the FFT, by this transfer function, using a slightly different code, and you get the X double dot that you want. But it means using the FFT twice, and if you use the FFT, you need some zero fill time. So you find yourself performing the transform even on zero fill points. It is necessry to do that, and it take more time than you would suspect. The FFT is certainly faster than discrete Fourier transform in any other way. But for this particular simple problem, the direct method in the time domain is much faster.

Voice: If you have a hardware processer, or an array processer, for the FFT, wouldn't that be faster? Or would it be better to still do it in the time domain with some sort of a convolution?

Mr. Cox: I am not really sure of that. I make it a point to say that at the end of my paper, and I even showed the Fortran routines. I believe that these algorithms are essentially as fast as possible for general purpose computers, but not necessarily for array processors. However, I am not positive of that. If a person had an array processor, they might be able to output that FFT so fast that it might be competitive. However, the direct solution is just a very short algorithm. The loop usually only involves 10 or 12 lines of Fortran code with no transcendental functions, just multiplications and additions.

EVALUATION AND CONTROL OF CONSERVATISM IN DROP TABLE SHOCK TESTS*

Thomas J. Baca
Sandia National Laboratories
Albuquerque, New Mexico 87185

Absolute acceleration shock spectra are the most common means of characterizing mechanical shock. These shock spectra are of limited use in making a quantitative evaluation of the conservatism contained in a laboratory shock test. This paper presents a technique for evaluating and controlling the conservatism in drop table shock tests. Alternative characterizations of shock transients are introduced which compensate for the limitations of absolute acceleration shock spectra in representing shock environments. A method of analyzing both field and laboratory shock environments is developed which can be used for any type of shock characterization to account for the variability in the description of the environments. An index of conservatism (IOC) is defined which quantifies conservatism between the field and laboratory shock environments. The IOC can be calculated for any response characteristic of interest. This measure of conservatism possesses the attribute of incorporating information on the uncertainty in either of the shock environments. Control of the level of conservatism in a shock test in terms of a given response characterization is shown to be possible through the derivation of test modification factors associated with desired IOC values. These shock data analysis procedures are demonstrated using field and drop table shock data measured on a simple cantilever beam structure. Curves are generated showing the factor by which the amplitude of the drop table input pulse must be modified to produce the required index of conservatism.

INTRODUCTION

Mechanical shock testing of aerospace structures and their components has traditionally been the means by which such hardware is qualified for use in an operational shock environment. Drop table shock tests are the most common type of shock testing technique. (The basic elements of a drop table shock machine are shown in Figure 1.) The objective of this paper is to consider the evaluation and control of conservatism in drop table shock tests. Alternate characterizations of shock environments will first be considered in order to provide a more sound basis for comparing field and laboratory environments. These alternate means of describing the shock environment are necessary to supplement the informational limitations of shock spectra which are presently used as the basis for the specification of drop table shock tests. A statistical analysis of each response characteristic allows consideration of the uncertainty in the description of any shock environment. It then becomes possible to determine an index of conservatism (IOC) which incorporates this knowledge of the uncertainty in the shock characterization. Once the degree of conservatism associated with enveloping absolute acceleration shock

*This work was supported by the United States Department of Energy.

spectra (which is the current means of specifying drop table shock tests) has been determined, a test modification factor can be found which indicates how the drop table test input must be modified to produce a desired index of conservatism.

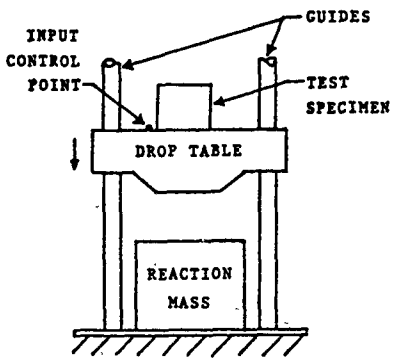

Figure 1 Drop Table Shock Machine.

CURRENT PROCEDURES

In order to appreciate the usefulness of the results of this paper more fully it is necessary to be aware of the procedures currently employed in the specification, execution, and interpretation of drop table shock tests. Figure 2 summarizes the major steps in the process of qualification shock testing. Acceleration data recorded in the field shock environment are analyzed in terms of absolute acceleration shock spectra (SAA) using standard methods [1,2]. [The SAA spectrum is a plot of the maximum value of the absolute acceleration response of a single degree of freedom (SDOF) system versus the natural frequency of the SDOF system.] The field shock environment is defined by the envelope of all the shock spectra collected for the particular shock event of interest. Specification of an appropriate drop table shock input involves the selection of a simple haversine pulse shape (defined by its amplitude A_H and duration T_H) whose SAA spectrum will exceed the SAA envelope of the field data. The drop table shock test is then performed by creating an acceleration pulse at the input control point having the amplitude and duration called out in the test specification. Analysis of test data once again involves the calculation of SAA spectra. Interpreting the results of the test requires both an evaluation of test conservatism and an assessment of whether or not the test specimen survived the shock test. A shock test is considered to be conservative if its SAA spectrum exceeds the SAA spectrum envelope of the field data. While determining whether the test item is operable after the test may be straightforward, the implications of the functional outcome of the test may be less clear. The lack of a quantitative procedure for comparing

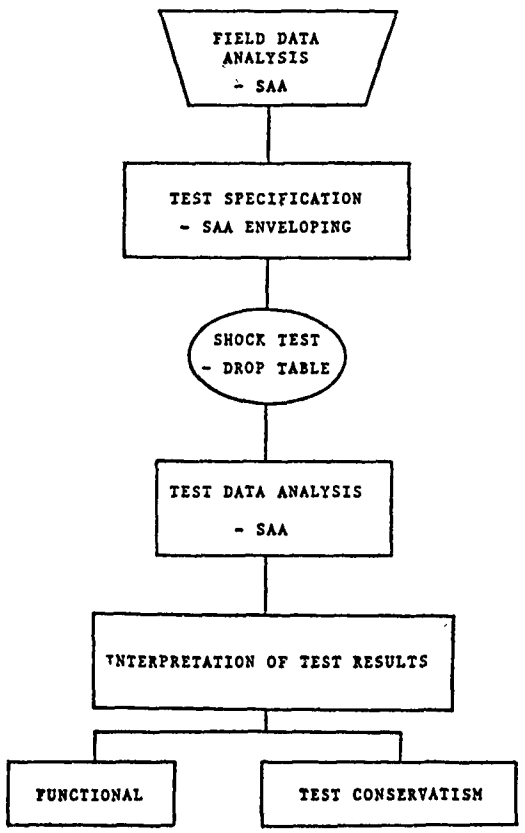

Figure 2 Schematic Diagram Summarizing the Current Process of Qualification Shock Testing.

the field and test shock environments makes it difficult to say at what point a drop table test would be considered to be overconservative. Thus, it is difficult to judge whether it is necessary to totally redesign a test specimen which has failed in a drop table test solely on the basis of shock spectrum enveloping.

This dilemma can be illustrated by considering the SAA spectra in Figure 3. A theoretical test spectrum is shown which envelops the field spectrum. Both the actual and the theoretical test spectra deviate from the field spectrum by different amounts at different frequencies. While the current method of shock spectrum enveloping would judge the actual test to be conservative, it would give no guidance as to the degree of conservatism. The amount of enveloping between the actual test spectrum and the field spectrum can be seen to vary greatly as a function of frequency.

The significance of actual shock spectrum values depends on the extent to which the structure being tested behaves like a brittle SDOF system. Since brittle structures fail if their ultimate load resisting capacity is exceeded, the analysis of loads on

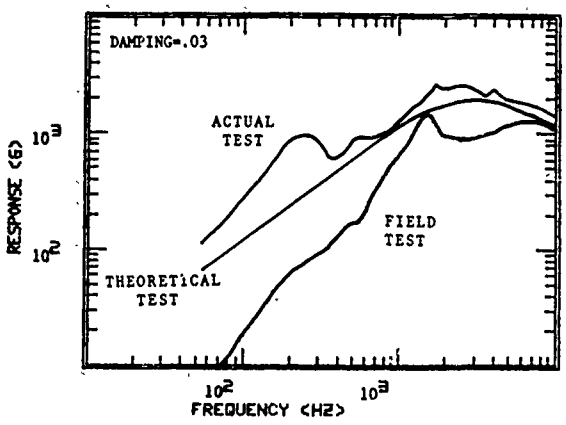

Figure 3 Comparison of Actual Test, Theoretical Test, and Field SAA Spectra.

this type of structure is not concerned with the number or magnitude of other acceleration peaks in the shock time history. Few real structures, however, are realistically modelled by the brittle SDOF system. For structures that do not behave as brittle SDOF oscillators, the calculation of SAA spectra is only useful as a qualitative description of the frequency content and overall magnitude of a shock transient.

One final indication of the limitations of SAA spectra in characterizing shock environments is revealed in the study of the two time histories which produced the "field" and "test" shock spectra in Figure 3. The "test" shock in Figure 4 has a peak acceleration over twice that of the "field" shock in Figure 5. The drop table test input exhibits the desired initial pulse shape but it has secondary peaks which exceed the primary peak in the field shock test. (This behavior also demonstrates the difficulty that exists in producing high level, short duration classical pulse shapes using actual test fixtures and drop table machines.)

Given these limitations, the general justifications behind the use of the drop table shock test are:

1) It is the only practical way to produce high level (e.g., greater than ~500g) shock inputs.

2) Drop table test machines are relatively common in most production facilities.

3) The initial pulse shapes are relatively easy to control.

4) Experience shows that components qualified to drop table shock test specifications derived through shock spectrum envelopes will be able to survive in the operational shock environment.

The striking disparity between Figures 4 and 5, however, supports the contention that components tested according to current shock test specification procedures are being qualified to a shock environment which bears little resemblance to the actual shock environment.

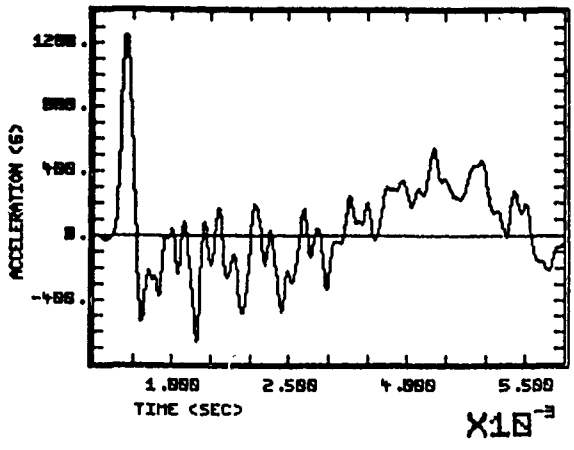

Figure 4 Actual Drop Table Shock Test Input.

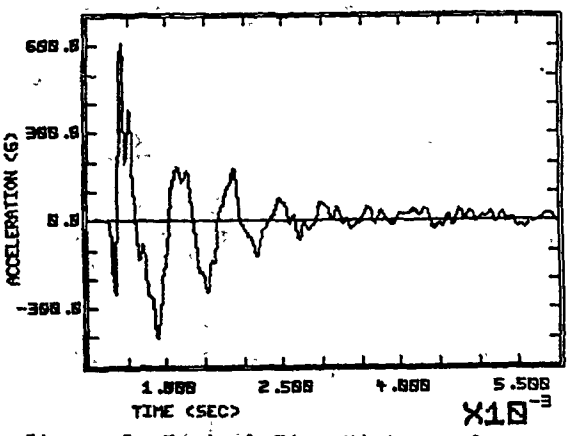

Figure 5 Typical Time History of Pendulum Impulse Test Input.

Recent efforts to quantify the conservatism between test and field environments fall short of being able to provide the capability necessary for achieving this goal. Paez's method [3] does not allow consideration of the simple pulse shapes associated with drop table inputs since his approach to the problem assumes that both the field and test inputs are represented by stationary Gaussian time histories modulated by deterministic intensity functions. Another effort to characterize shock test conservatism is that of Hart, Hasselman, and Jones [4]. This method decomposes shocks into a deterministic and random component, but does not account for the variation between field and test shocks from the same shock source. Both of these methods characterize shocks in terms of their shock spectra so they are subject to restrictions regarding the applicability of SAA spectrum to real structures.

ALTERNATE SHOCK CHARACTERIZATIONS

An improved characterization of both the field and drop table test shock environments must be implemented before any progress can be made in comparing these two shock environments in a meaningful way. Three promising alternative characterizations have been introduced recently [5]. These descriptive quantities include the ranked peaks (PKA) in the acceleration time history and the root mean square (RMS) acceleration as a function of time (TRMS) or of frequency (FRMS). In contrast to the SAA spectrum which characterizes a shock in terms of its "effects" on a collection of SDOF oscillators, these alternative types of data analysis provide insight into the distinguishing features of the shock transient itself.

Peak acceleration values in a shock time history are defined to be the maximum absolute values attained by the time history between changes in sign of the response. This definition of peaks is distinct from the purely mathematical definition of maxima and minima which locates points of zero slope in the acceleration time history. A ranking of all of the peak values from highest to lowest provides the engineer responsible for analyzing the data with a much more complete description of the shock input time history. For example, information on the magnitude of subsequent peaks is particularly important when it is necessary to evaluate the significance of secondary peaks in test inputs (e.g., Figure 4) which should ideally have only one peak, namely that of the classical haversine pulse.

The time domain RMS acceleration (TRMS) provides a way of quantifying average acceleration levels as a function of time during the shock event. The TRMS values versus time are given by the following equation:

$$\mathrm{TRMS}(\tau) = \left(\frac{1}{\tau}\int_0^{\tau} \ddot{x}^2(t)\,dt\right)^{\frac{1}{2}} \quad , \; 0<\tau<TD \qquad (1)$$

Calculation of this integral from the beginning to the end of the shock provides a useful means of comparing the change in the average magnitude of two different shock pulses as a function of time. It should be noted that the use of RMS acceleration as a measure of shock intensity for structures has been advocated by researchers in the field of earthquake engineering [6,7].

The calculation of RMS acceleration as a function of frequency is an important step in the characterization of a shock time history because it provides a means of revealing the frequency content of the transient. Such frequency domain information can replace the indirect view of the frequency content in the acceleration signal that has been given in the past by the SAA shock spectrum. By applying Parseval's theorem [8] and a symmetry argument, the RMS acceleration as a function of frequency is given by:

$$\mathrm{FRMS}(F) = \left(\frac{2}{TD}\int_0^{F} |\ddot{X}(f)|^2\,df\right)^{\frac{1}{2}} \qquad (2)$$

where F is the frequency up to which the RMS is calculated and $\ddot{X}(f)$ is the Fourier transform of $\ddot{x}(t)$. Equation 2 gives the RMS contribution of all frequencies below F for the transient time history having a duration of length TD. The duration of both time histories must be the same for this comparison to be meaningful.

Selection of one or more response characterizations will be governed by the engineer's knowledge of the dominant failure mode of the test item. Table 1 summarizes the structural characteristics that are normally of greatest interest during the selection of an appropriate response characteristic.

Table 1 Summary of Appropriate Response Characteristics for Different Types of Structures.

RESPONSE CHARACTERISTIC	TYPE OF STRUCTURE
SAA	Brittle SDOF Structure
PK1	Brittle Structure
TRMS (OVERALL)	Structure Sensitive to Repeated Load Reversals
FRMS	Structure Sensitive to Repeated Load Reversals in a Particular Frequency Range

The SAA spectrum is of interest when the structure being tested is brittle and behaves as an SDOF system. Few structures can be adequately modelled in this fashion, so the maximum peak value (PK1) becomes the most meaningful response characteristic for brittle structures.

The overall TRMS acceleration (TRMS-OVERALL) is a significant indicator of the average shock intensity for structures which are susceptible to degradation as the result of an accumulation of damage due to stress reversals. Ranked peak values (PKA) provide more detailed information on the number of peaks which exceed a critical acceleration level in cases that require a more detailed assessment of successive peak acceleration levels.

Frequency domain RMS acceleration (FRMS) information is most useful if the test structure is known to have a limited tolerance to certain frequency ranges. This type of sensitivity might occur in an electronic component which has miniature internal parts (e.g., printed circuit boards or integrated circuit chips) that fail when exposed to high frequency excitations.

INDEX OF CONSERVATISM

The need to quantify the degree of conservatism between the shock test environment and the field shock environment has led to the development of an index of conservatism (IOC) [5]. First, a response characteristic C (e.g., SAA, PKA, TRMS, or FRMS) is chosen as the most appropriate descriptor of the shock environment. A random variable representing the margin of conservatism M is then defined as the difference between random variables C_T and C_F which represent the corresponding response characteristics in the test and field shock environments, respectively:

$$M = C_T - C_F \tag{3}$$

A shock test is said to be conservative if M is greater than zero. The variability in M is introduced into the analysis by dealing with the mean $\overline{M}$ and standard deviation σ_M of the margin of conservatism. The index of conservatism is defined as the ratio of these two quantities:

$$IOC = \frac{\overline{M}}{\sigma_M} \tag{4}$$

If C_T and C_F are independent, the IOC can be expressed directly in terms of the means ($\overline{C}_T$ and $\overline{C}_F$) and standard deviations (σ_T and σ_F) of the test and field response characteristics:

$$IOC = \frac{\overline{C}_T - \overline{C}_F}{\sqrt{\sigma_T^2 + \sigma_F^2}} \tag{5}$$

Figures 6 and 7 help to express the variables in equation 5 graphically. These figures show that the IOC is a measure of both the difference between the average levels of the test and field environments and of the dispersion of these response characteristics about their mean values as expressed by the standard deviations.

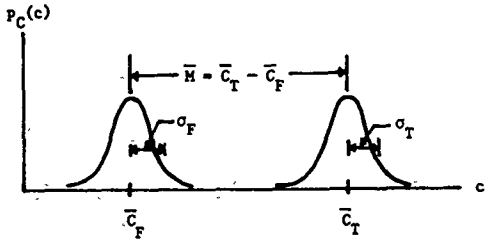

Figure 6 Probability Density Functions of Field and Laboratory Test Shock Environments.

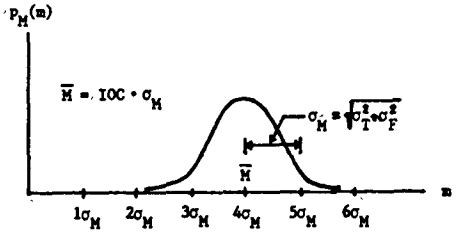

Figure 7 Probability Density Function of the Margin of Conservatism for IOC = 4.

Formulation of an index of conservatism was motivated by a practical approach to reliability assessment in structures [9,10] which was developed to assess structural reliability in terms of the first and second moments of available data on load and resistance. This approach is practically oriented because it does not depend on the selection of probability density functions in the process of calculating reliabilities. In the context of quantifying drop table shock test conservatism, the IOC can be interpreted as a measure of test reliability (i.e., the probability that a conservative test was conducted).

One other advantage of the IOC stems from the fact that it is dimensionless. This attribute allows the evaluation of shock test conservatism in terms of any appropriate response characteristic.

TEST MODIFICATION FACTOR

It is now assumed that IOC values associated with a drop table test specified by the current procedure of enveloping SAA spectra have been determined for the response characteristic of interest. The derivation of a test modification factor is necessary if there is a desire to obtain a shock test which has a predetermined index of conservatism.

The desired drop table pulse shape is a haversine having amplitude A_H and duration T_H. Assuming that the test environment response characteristic C_T varies linearly with A_H, the modification of A_H is the most direct means of controlling the mean value of the shock test response characteristic $\bar{C}_T$. Let the subscript I refer to the desired IOC level which is to relate the test and field data. The test modification factor W_I is defined as the factor by which $A_{H,IOC}$ must be multiplied to obtain $A_{H,I}$ or simply:

$$W_I = \frac{A_{H,I}}{A_{H,IOC}} \qquad (6)$$

As a result of the linearity assumption, the following relationship can be written:

$$W_I = \frac{A_{H,I}}{A_{H,IOC}} = \frac{\bar{C}_{T,I}}{\bar{C}_{T,IOC}} \qquad (7)$$

Introducing $\bar{C}_F$ into the right side of Equation 7 gives

$$W_I = \frac{\bar{C}_{T,I} \,/\, \bar{C}_F}{\bar{C}_{T,IOC} \,/\, \bar{C}_F} \qquad (8)$$

By defining R_{IOC} as the ratio between $\bar{C}_T$ and $\bar{C}_F$ for the completed drop table test (i.e., $R_{IOC} = \bar{C}_{T,IOC}/\bar{C}_F$) and defining R_I as the ratio between the mean test and field response characteristics (i.e., $R_I = \bar{C}_{T,I}/\bar{C}_F$) for the desired IOC level, the final form of the test modification factor is

$$W_I = \frac{R_I}{R_{IOC}} \qquad (9)$$

Now let k_T and k_F be the coefficients of variation ($k_T = \sigma_T/\bar{C}_T$, $k_F = \sigma_F/\bar{C}_F$) for the test and field shock environments, respectively. Assuming that $\bar{C}_F$ and σ_F are known and that k_T remains constant in spite of changes in $\bar{C}_T$, it has been shown [5] that the value of the ratio R_I for a particular IOC value I can be obtained by utilizing the following equation:

$$R = \begin{cases} \dfrac{1 + \sqrt{B}}{1 - \sqrt{Q_T^2}} & , \text{if } Q_T^2 < 1 \\ \dfrac{1 - \sqrt{B}}{1 - \sqrt{Q_T^2}} & , \text{if } Q_F^2 < 1 \end{cases} \qquad (10)$$

where $B = Q_T^2 + Q_F^2 - Q_T^2 Q_F^2$, $Q_T = IOC \cdot k_T$,

and $Q_F = IOC \cdot k_F$

After W_I is found by taking the ratio of R_I and R_{IOC} according to Equation 9, the new drop table test specification level $A_{H,I}$ is determined by multiplying the original test specification level $A_{H,IOC}$ by the test modification factor W_I.

ANALYSIS OF SHOCK DATA

The methodology for analyzing shock test conservatism introduced in the preceding discussion was applied to a collection of shock records collected from "field" and drop table test environments. Acceleration measurements were made on the fixed and free ends of a 5 x 1 x 1/4 inch aluminum cantilever beam which was mounted in a relatively massive box-like fixture. The "field" environment was generated by having a pendulum hammer impact the base of the fixture while it was suspended by support cables. This pendulum impulse shock was chosen as a representative "field" shock environment because it exhibits many of the same characteristics (e.g., high acceleration and high frequency content) as shock inputs generated in aerospace vehicles by pyrotechnic events. The ensemble of "field" data consisted of measurements made during twenty-two pendulum tests. An example of the shock transient at the base of the cantilever beam is shown in Figure 5. A drop table shock test specification consisting of a 1300 g x 0.33 ms haversine pulse was then derived using the current procedure of enveloping shock spectra. Data were analyzed from twenty-three drop table tests. A typical drop table shock input is shown in Figure 4.

Figures 8-15 compare mean and mean plus three standard deviation plots for SAA, FRMS, PKA, and TRMS response characteristics at the fixed (Figures 8-11) and free (Figures 12-15) ends of the cantilever beam. The plots substantiate the expectation that a shock test which is conservative in terms of SAA will also be conservative in terms of the newly introduced shock characterizations.

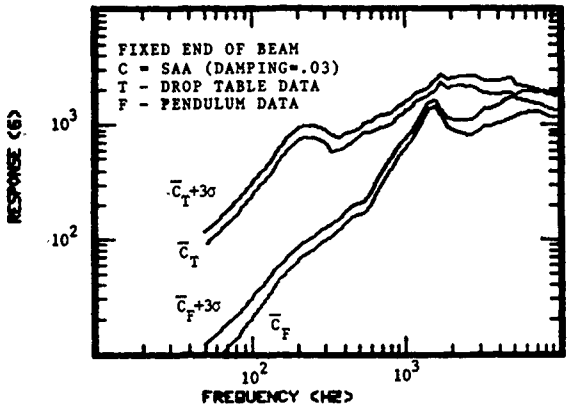

Figure 8 Comparison of SAA Mean and Mean Plus Three Standard Deviation Plots for Drop Table and Field Test Data at Fixed End of Beam.

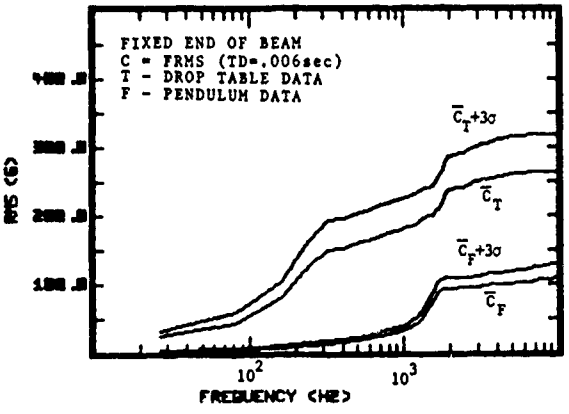

Figure 9 Comparison of FRMS Mean and Mean Plus Three Standard Deviation Plots for Drop Table and Field Test Data at Fixed End of Beam.

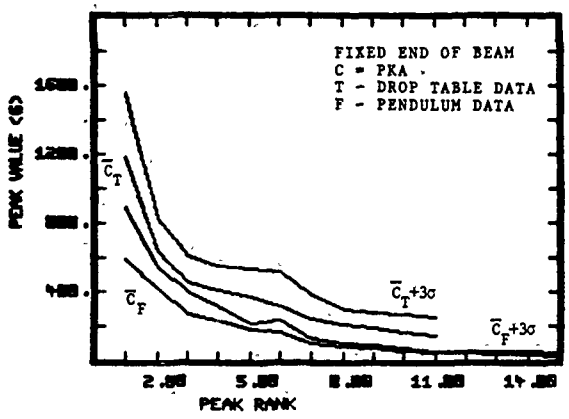

Figure 10 Comparison of PKA Mean and Mean Plus Three Standard Deviation Plots for Drop Table and Field Test Data at Fixed End of Beam.

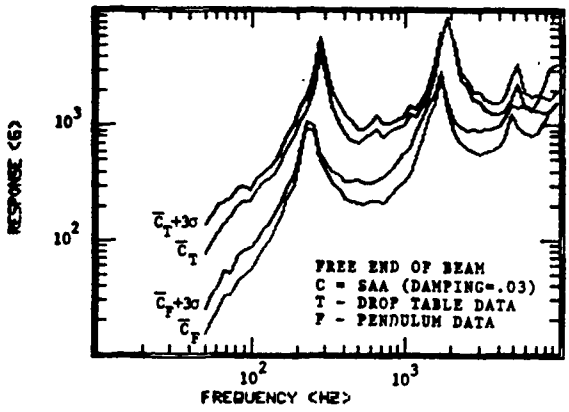

Figure 12 Comparison of SAA Mean and Mean Plus Three Standard Deviation Plots for Drop Table and Field Test Data at Free End of Beam.

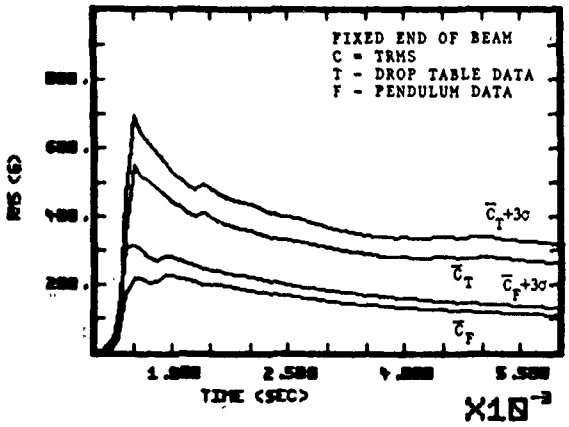

Figure 11 Comparison of TRMS Mean and Mean Plus Three Standard Deviation Plots for Drop Table and Field Test Data at Fixed End of Beam.

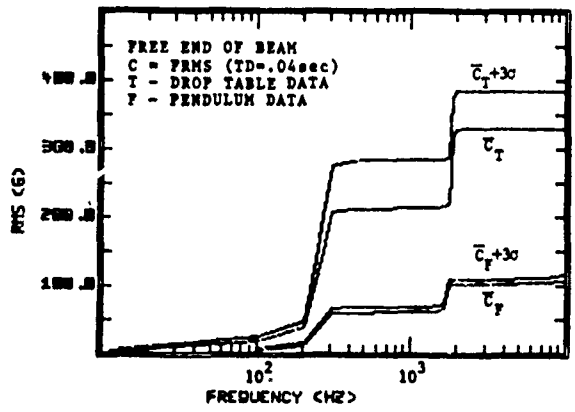

Figure 13 Comparison of FRMS Mean and Mean Plus Three Standard Deviation Plots for Drop Table and Field Test Data at Free End of Beam.

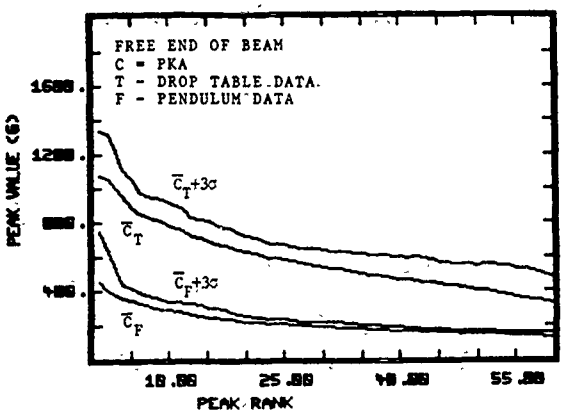

Figure 14 Comparison of PKA Mean and Mean Plus Three Standard Deviation Plots for Drop Table and Field Test Data at Free End of Beam.

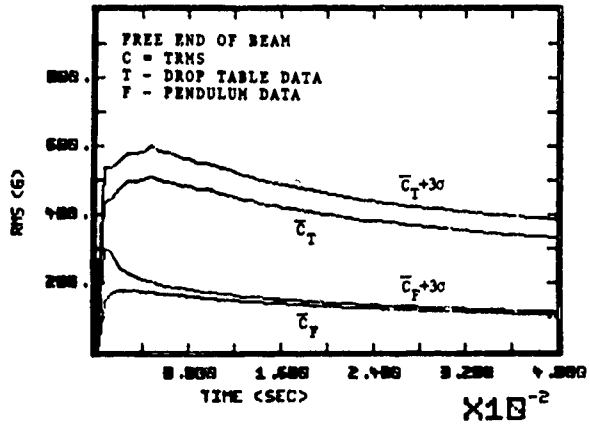

Figure 15 Comparison of TRMS Mean and Mean Plus Three Standard Deviation Plots for Drop Table and Field Test Data at Free End of Beam.

Consideration of these plots greatly improves the engineer's understanding of the two shock environments. The very use of the statistical moments in representing the response characteristics is important in that it underlines the variability in these quantities which is so often ignored when enveloping of SAA spectra is employed as a means of summarizing available shock data. Plotting FRMS (Figures 9 and 13) is quite helpful in showing which frequencies contribute most to the shock time histories. Unlike SAA plots, the FRMS plots give quantitative information on the relative importance of the predominant frequencies at the free and fixed ends of the beam in each shock environment. Consideration of the ranked peaks (PKA in Figures 10 and 14) provides a complete picture of the peak acceleration levels reached in each shock environment. It is interesting to note that the PKA plot at the base of the beam (Figure 10) reveals that not only the initial peak in the drop table test, but subsequent peaks as well, exceeded those of the field environment. The graphs of TRMS versus time in Figures 11 and 15 emphasize the sharper rise in the average acceleration level that was experienced during the drop table test series than in the pendulum tests.

Plots of IOC corresponding to the response characterizations in Figures 8-15 are shown in Figures 16-23. These plots are the culmination of the effort to demonstrate the quantitative evaluation of the conservatism in drop table shock tests. It is of interest to note that the SAA plots of IOC (Figures 16 and 20) are much more erratic than those of the other response characterizations (FRMS, PKA, and TRMS). This type of behavior would tend to encourage the use of those alternate characterizations in the calculation of test modification factors so that one test modification factor would apply over a greater range of the variable for which the response characterization is evaluated (i.e., frequency, peak rank, or time). It should be pointed out that the reason the IOC values for SAA and PKA are generally less than those of FRMS and TRMS is that the coefficients of variation k_T and k_F for SAA and PKA response characteristics are higher (ranging between 0.10 and 0.20) than those of the RMS quantities (which are between 0.05 and 0.05 and .10). The coefficient of variation of the RMS characterizations is reduced as a result of the averaging process that is involved in the calculation of these quantities.

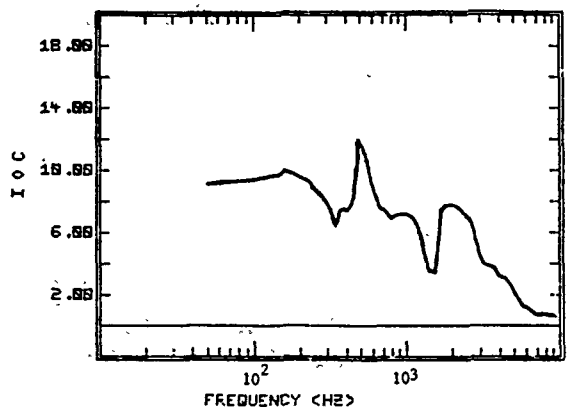

Figure 16 IOC Plot for SAA (Damping=.03) at Fixed End of Beam.

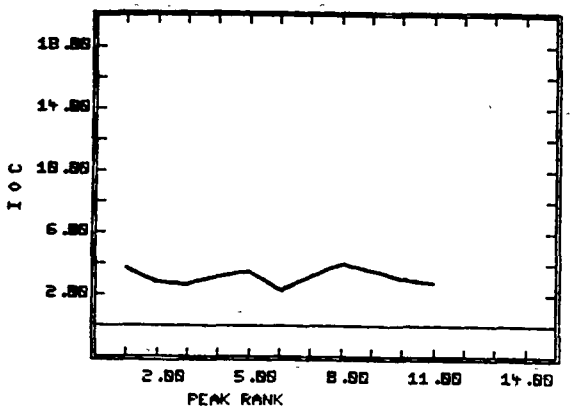

Figure 18 IOC Plot for PKA at Fixed End of Beam.

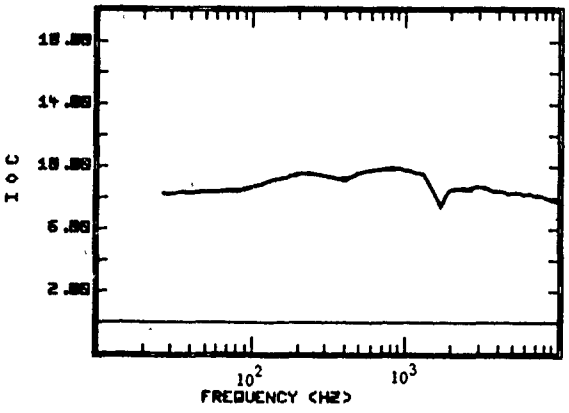

Figure 17 IOC Plot for FRMS (TD = .006 sec) at Fixed End of Beam.

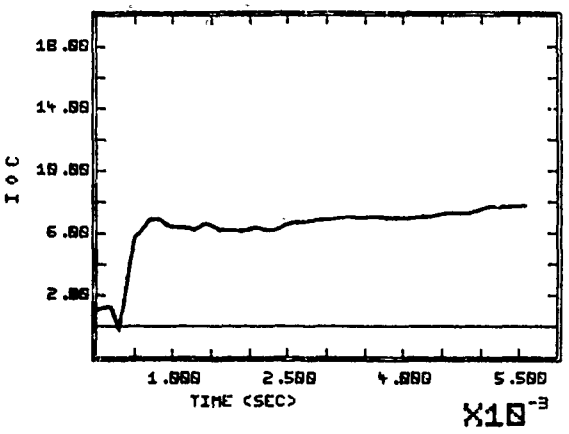

Figure 19 IOC Plot for TRMS at Fixed End of Beam.

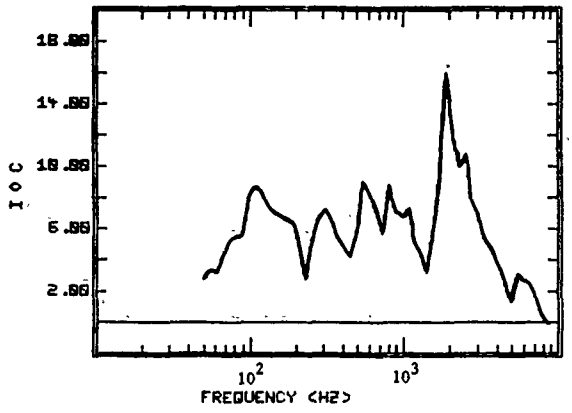

Figure 20 IOC Plot for SAA (Damping=.03) at Free End of Beam.

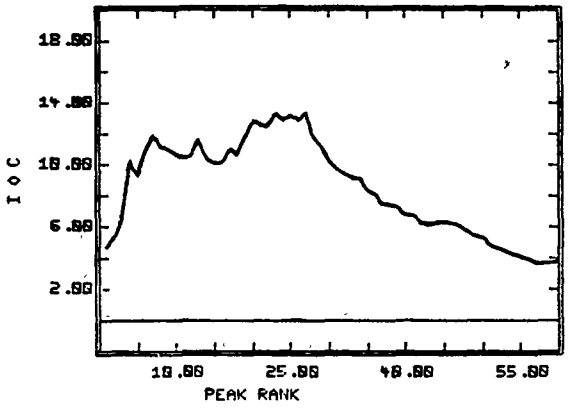

Figure 22 IOC Plot for PKA at Free End of Beam.

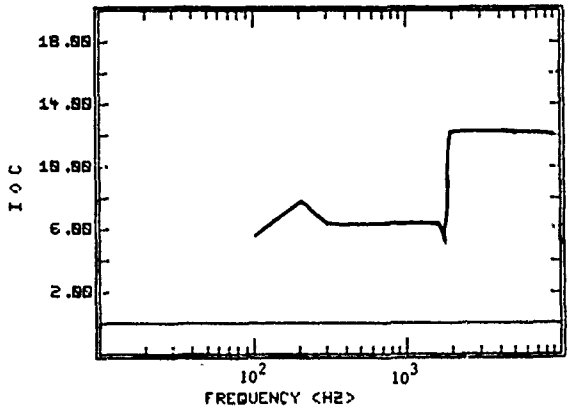

Figure 21 IOC Plot for FRMS (TD=.04 sec) at Free End of Beam.

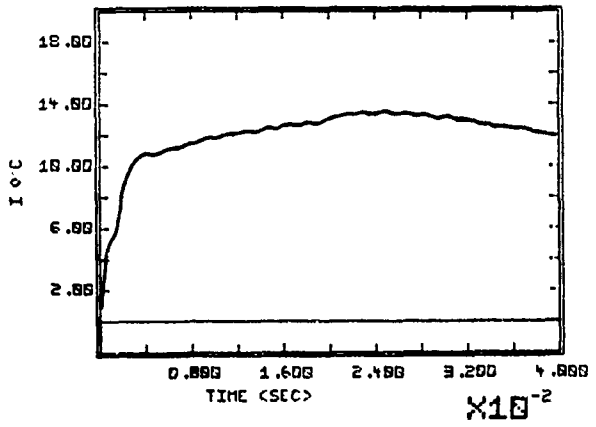

Figure 23 IOC Plot for TRMS at Free End of Beam.

In order to demonstrate the calculation of the test modification factor W_I, Figures 24 and 25 were constructed to show W_I as a function of the desired index of conservatism I for the fixed and free ends of the cantilever beam, respectively. Four specific response characteristics were analyzed in these plots. Values of W_I for SAA and FRMS were averaged in the frequency range between 1000 Hz and 2000 Hz since there appears to be significant frequency content in this range (see Figures 9 and 13) at both locations on the cantilever beam. The test modification factors for the highest peak acceleration PK1 and for the overall RMS acceleration were also studied since they represent response characteristics of particular interest.

The implication of Figures 24 and 25 is that regardless of the type of response characterization, the current method of drop table shock test specification does produce a conservative test. The significance of particular IOC and corresponding W_I values may be interpreted in two ways. First, calculation of IOC values for the drop table shock test specifications of existing aerospace components will serve to calibrate the degree of conservatism that is currently being built into shock resistant structures in terms of IOC values. This type of analysis would establish a baseline from which the conservatism (i.e., the IOC level) of future drop table shock tests would be specified. Second, statistical analyses

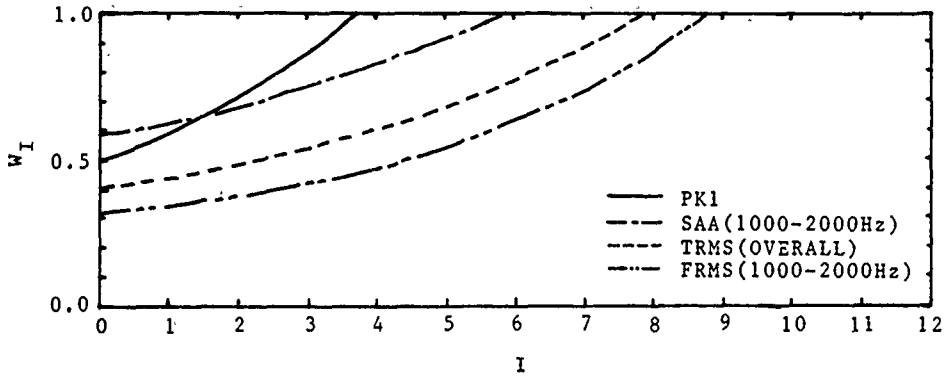

Figure 24 Test Modification Factor W_I versus Index of Conservatism I Plot for Fixed End of Beam.

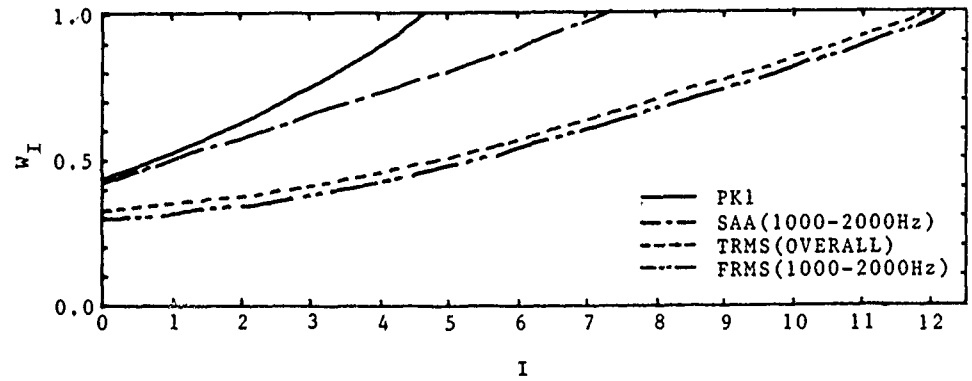

Figure 25 Test Modification Factor W_I versus Index of Conservatism I Plot for Free End of Beam.

of response characteristics such as PKI and overall RMS have been shown to substantiate the assumption that these quantities are normally distributed [5]. Such an assumption would then lead to the conclusion, for example, that a 99.9 percent probability test conservatism would be obtained if an IOC of three is chosen. Values of IOC equal to zero, one, and two correspond to test reliability levels of 50, 84.1 and 97.9 percent, respectively. Thus, if an IOC level of three can be interpreted as a sufficient requirement for shock test conservatism, the amplitude of the drop table test specification could be reduced between 38 to 87 percent, depending on the response characteristic that is chosen as being most important for the particular test item. A lower IOC requirement might be chosen if it is known, for example, that some level of conservatism already existed in the field data. This might be the case if the field data were generated during some type of subsystem ground tests.

CONCLUSIONS

A technique for quantifying the conservatism in drop table tests specified by the enveloping of absolute acceleration shock spectra has been presented. The index of conservatism can be calculated for the standard shock spectrum representation of the field and test shock environments as well as for alternative characterizations such as ranked peak accelerations and time or frequency domain RMS acceleration. Use of these alternative response characterizations gives the engineer greater insight into both the test and field shock environments. The fact that knowledge regarding the uncertainty in the characterization of the shock environment is incorporated into the analysis of test conservatism represents a considerable improvement over the use of simple enveloping techniques. The development of a test modification factor provides a new means of controlling the degree of shock test conservatism in drop table shock testing. Test modification factors as low as 30 percent were found to be possible depending on the response characterization and degree of conservatism (i.e., IOC value) used in the calculation procedure.

The use of these test modification factors will provide a means of assuring greater uniformity in the degree of conservatism required in qualification shock tests performed on drop table shock machines. The ability to select an appropriate response characteristic and a desired level of test conservatism greatly enhances the engineer's potential for conducting and interpreting the results of drop table shock tests.

REFERENCES

1. Kelly, R. D., and G. Richman, Principles and Techniques of Shock Data Analysis, The Shock and Vibration Information Center, USDOD, SVM-5, 1969.

2. Rubin, S., "Concepts in Shock Data Analysis," Shock and Vibration Handbook, Second Edition, Harris, C. M., and C. E. Crede, eds., New York: McGraw-Hill, 1976, pp. 23-1,30.

3. Paez, T. L., "Conservatism in Shock Analysis and Testing," Shock and Vibration Bulletin, Vol. 50, Part 4, September 1980, pp. 117-135.

4. Hart, G. C., T. K. Hasselman, and W. N. Jones, "Estimation of Ship Shock Parameters for Consistent Design and Test Specifications," Shock and Vibration Bulletin, Vol. 46, Part 2, August 1976, pp. 155-167.

5. Baca, T. J., "Characterization of Conservatism in Mechanical Shock Testing of Structures," Ph.D. Dissertation, Department of Civil Engineering, Stanford University, September 1982.

6. Housner, G. W. and P. C. Jennings, "Generation of Artificial Earthquakes," Journal of the Engineering Mechanics Division, ASCE, Vol. 90, No. EM1, Proc. Paper 3806, February 1964, pp. 113-150.

7. McCann, M. W., Jr., and H. C. Shah, "RMS Acceleration for Seismic Risk Analysis: An Overview," Proceedings of the 2nd U. S. Conference on Earthquake Engineering, EERI, Stanford, CA, August 1979, pp. 883-897.

8. Bracewell, R. N., The Fourier Transform and Its Applications, 2nd ed., New York: McGraw-Hill, 1978.

9. Ang, A. H.-S., and C. A. Cornell, "Reliability Bases of Structural Safety and Design," Journal of the Structural Division, ASCE, Vol. 100, No. ST9, Proc. Paper 10777, September 1974, pp. 1755-1769.

10. Hasofer, A. M., and N. C. Lind, "Exact and Invariant Second-Moment Code Format," Journal of the Engineering Mechanics Division, ASCE, Vol. 100, No. EM1, Proc. Paper 10376, February 1974, pp. 111-121.

DISCUSSION

Voice: You test by making two different drop tests, one to simulate the low frequency domain, and one to simulate the high frequency part of the shock spectra.

Mr. Baca: That is the kind of flexibility, I think, that we would like to investigate further. But I like to think I have some way of doing that in a quantitative sense so that I could see the effects of both the low frequency and the high frequency, to make a more meaningful evaluation of the test.

ICE IMPACT TESTING OF SPACE SHUTTLE THERMAL PROTECTION SYSTEM MATERIALS

By

Paul H. DeWolfe
Rockwell International
Downey, California

An ice impact test program is currently in progress to evaluate the damage resistance of the various Space Shuttle thermal protection system materials when subjected to impact by ice projectiles shed from the external tank during ascent. This program required the development of a test method before material evaluation could begin. The development of the test method, as well as progress in material tesing during 1982, are the subject of this paper. Descriptions of the impact, including ice source, velocity, incidence angle, and location are included. Five significant conclusions have been drawn to date and are reported. The direction taken for future testing is also described.

INTRODUCTION

The possibility of ice impact damage to the Space Shuttle orbiter's thermal protection system (TPS) was discovered when it was determined that ambient humidity at the launch sites could condense and form ice on the external tank (ET) between fueling and lift-off. It was predicted that this ice could break loose from the ET during ascent and impact critical portions of the orbiter lower surface TPS. Initial analytical work had predicted the magnitude and geometry of the worst case impact. Further analysis, though limited by a lack of rigorous methods, indicated that there was a potential for ice impact damage serious enough to be considered a threat to vehicle safety (i.e., loss of vehicle during entry). To minimize this threat, constraints were initiated on acceptable weather conditions and hold times for the launch and countdown sequences to minimize ice formation. During the first four orbiter missions, ice damage was observed during the post-flight TPS inspection.

Early in 1982, a test program to evaluate the ice impact threat was developed as a part of the on-going independent research and development program at Rockwell's Space Transportation and Systems Group (ST&SG). There were three goals of the test program: to develop a reliable method of testing within given impact parameters, to evaluate the impact durability of baseline and second generation TPS materials, and to devise methods of improving the impact durability of TPS materials and validate by testing. This program was run under contract with the Southwest Research Institute of San Antonio, Texas, which provided the test facilities and aided in developing the test program.

BACKGROUND

The space transportation system (Fig. 1) consists of four major components: the orbiter, the ET, and two solid rocket boosters (SRB's). In order to more clearly understand the ice impact problem, descriptions of the ice source, the impact parameters (mass, velocity, and incidence angle), and the impact locations are needed.

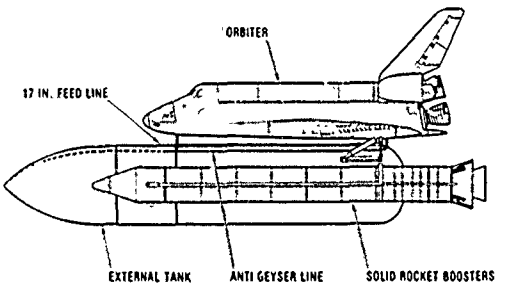

Fig. 1-The space transportation system

As stated previously, the ice source is the ET. The ET is actually two tanks in tandem: a liquid oxygen (LO_2) tank and a liquid hydrogen (LH_2) tank. The smaller LO_2 tank is mounted forward into the ogive (nose) portion of the ET. A 17-inch feedline and a separate antigeyser line run aft along the outside of the tank to the aft end of the ET, where they run up into the aft fuselage of the orbiter. The ET ogive, the 17-inch feedline, the antigeyser line, and the line support bracketry, are all considered sources of ice projectiles.

The orbiter TPS consists of several insulating materials with high temperature performance capabilities (Fig. 2). The majority of the insulation consists of 6 by 6 in. ceramic tiles. Lower temperature regions have flexible blanket insulation and the highest temperature regions of the vehicle, the wing leading edges and the nosecap, are reinforced carbon-carbon (RCC) hot structure. A detailed description of each of these classes of material follows.

Four types of ceramic tile are used on the orbiter. They can be generally described as a low density, fiber-reinforced

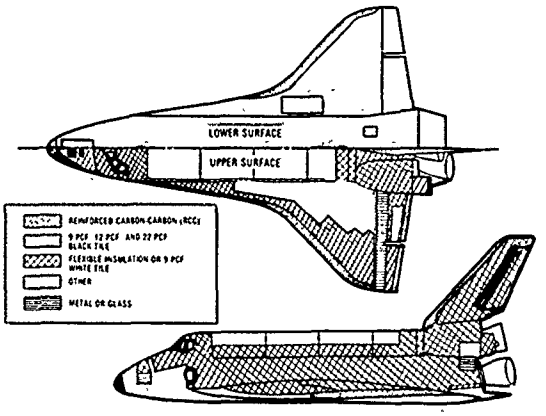

Fig. 2-Thermal protection system; Orbiters 103 and 104, Discovery and Atlantis

ceramic matrix. The most widely used of these materials is a 9 pcf high purity silica tile, which is coated with one of two glass coatings. For regions where the maximum temperature does not exceed 1,200°F the coating is a white borosilicate glass of a nominal 8 to 10 mils thickness. In higher temperature regions, up to 2,300°F and including the entire lower surface of the vehicle, a high emissivity black glass coating called reaction cured glass (RCG) is used, which is nominally 15 mils thick. The third type of tile is a 22 pcf high purity silica tile coated with the high emissivity black glass coating. This denser material has increased strength, and is used in areas where the thermal or mechanical loading exceeds the capabilities of the 9 pcf material. The fourth tile material is a 12 pcf composite ceramic consisting of silica and alumina-boria-silica fibers in a semiordered matrix. This tile is also coated with the high emissivity black coating and is used as a lighter weight replacement for the 22 pcf material on orbiters Discovery and Atlantis. Installation details are shown in Fig. 3.

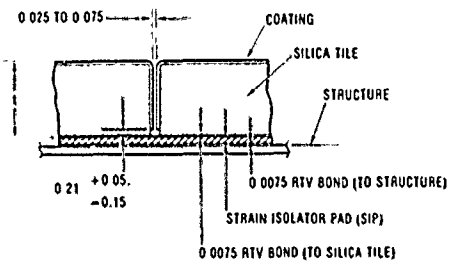

Fig. 3-Typical tile joint baseline

A quilted blanket insulation material known as flexible insulation (FI), is being developed as a replacement for tile materials in regions where the maximum temperature does not exceed 1,500°F. The inner layer of the quilted FI is fiberglass and the outer layer is a quartz cloth. These fabrics are used as covers for a low density ceramic batt material, and the whole package is stitched together with quartz thread. Installation details are shown in Fig. 4.

RCC is a composite pyrolyzed carbon matrix coated with silicon carbide to retard oxidation. This material is used

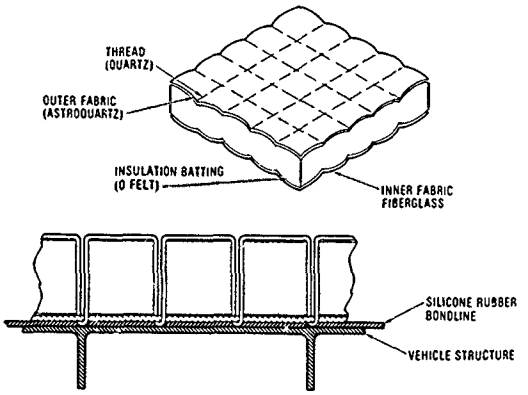

Fig. 4-Flexible insulation construction

to form the nosecap and wing leading edge of the orbiter where temperatures are in excess of 2,300°F. The leading edge panels and nosecap attach indirectly to the aluminum primary structure of the orbiter through an intricate system of insulated connections. An improved carbon-carbon composite is currently being developed as a replacement for RCC. Called advanced carbon-carbon (ACC), it has improved material properties and service life at high temperatures in comparison to RCC.

Because all of these materials are subject to possible ice impact on ascent, each must be evaluated for impact durability.

In evaluating the threat to the TPS materials from ice impact, it is necessary to understand the magnitude and physical characteristics of the worst case impact. A study by Rockwell's Aero Sciences Department resulted in a prediction of the parameters for the worst case impact. This definition was accomplished by a study of the drag, gravitational, and pressure forces acting on the ice particles after separation from the ET. The velocity of the ice particle was calculated by setting these forces into equilibrium and solving for the particle acceleration. From the particle acceleration, the velocity at impact is easily obtained. The angle of incidence was calculated by plotting the motion of particles that break loose from several locations on the ET and determining the maximum angle at which a particle impacts the vehicle. This study indicated that the maximum relative projectile velocity at impact was 500 feet per second, the maximum incidence angle was 12 degrees, and the maximum dimensions of the projectile would be 3.0 in. by 1.5 in. by 0.5 in. The evaluation of the ice impact threat to the orbiter TPS is based on these parameters.

The regions of the vehicle that have experienced impact damage, or which can be expected to sustain damage based on the first two flights of Columbia, are illustrated in Fig. 5. Not all of this damage is ice damage. The lower surfaces of the fuselage and body flap have sustained the most damage during the first five Shuttle missions. Minor damage has been sustained by the fuselage sidewalls, the lower wing surfaces, and the forward fuselage upper surface. The forward surfaces of the orbital maneuvering system (OMS) pods have also sustained impact damage during Flights 1 through 5. All

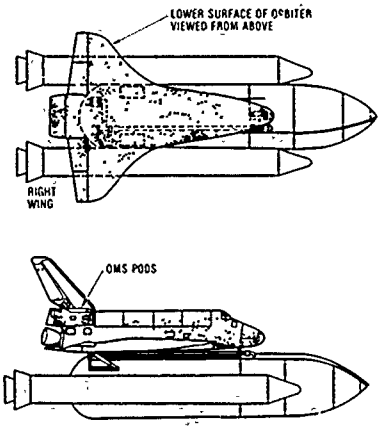

Fig. 5-Locations of impacts from all sources; missions 1 and 2

of the TPS materials described previously are used in one or more of these regions, and must therefore be tested for impact durability.

TEST METHOD DEVELOPMENT

The planning of a test program to evaluate the ice impact threat first required the development of a test method. After consultation with the test conductor, Southwest Research Institute, it was agreed to use a modified version of a method used in many lightweight projectile tests. The basic method involves the use of a compressed gas gun (Fig. 6) to fire projectiles at targets. The projectile is usually mounted in a sabot, a device that adapts the projectile to the barrel of the gun and prevents projectile damage during firing. The sabot is mechanically stripped from the projectile after the assembly has left the gun barrel, and the projectile travels on to the target alone. The sabot also acts to seal in the expanding gas in the gun, increasing the velocity capabilities of the gun. Because the ice projectile diameter requirements closely matched the maximum gun bore diameter available, the sabot had to be eliminated. This resulted in two compromises to the method's efficiency. First, the projectile does not seal the barrel as well as a sabot, allowing the expanding gas to leak out ahead of the projectile. This limits the velocity capability of the gun, but not to an extent that it inhibits the ice impact tests. The second problem that arises from the elimination of the sabot is that the projectile is not shielded during the rapid acceleration along the barrel during firing. This occasionally results in the breakup of the projectile before it reaches the target, the end result being a test of questionable quality.

The projectile is made from a solution of water and orange vegetable dye. Initial tests were run using projectiles made of water only, but it was decided to add the dye to improve visibility of the projectile in the high-speed films. The projectile is slowly frozen in a mold at temperatures between 20°F and 30°F. This slow freezing process is used to minimize thermal stress cracking and eliminate trapped air bubbles.

The projectile is approximately 3.5 inches long and 0.88 inch in diameter and weighs 31 grams. A cylindrical shape was chosen to represent the rectangular block of the predicted projectile shape because the cylinder was more easily adapted to ballistic testing. The predicted mass of the projectile was duplicated and the maximum length-to-width ratio of 6 was not exceeded. It was recognized that a cylinder of ice would not breakup on impact as easily as a rectangular block of similar mass. This meant that the cylinder should cause greater damage to the target than the rectangular block, resulting in a conservative (low) estimate of damage resistance. The conservative nature of the test method was taken into account when the test results were evaluated.

The projectile is weighed and then breech-loaded into the gun. The breech is cooled with liquid nitrogen to approximately 0°F to prevent melting or cracking of the ice projectile. Two 36-gauge copper wires, spaced 6 inches apart, are rigged across the muzzle of the gun and connected to an electronic timer. As the projectile breaks these wires, it starts and stops the electronic timer. Given the spacing of the wires and the time to travel that distance, the projectile exit velocity can be calculated. The target (Fig. 7) is mounted to an aluminum plate that can be adjusted to the proper angle of incidence, and is located approximately 30 inches from the muzzle of the gun.

Continuous photo recording of the test was done using a Hycam II 16mm high-speed camera operating at a film speed of 4,000 frames per second and a shutter speed of 1/10,000 second to reduce image smear. In addition, still photographs of the target are taken before and after a test run.

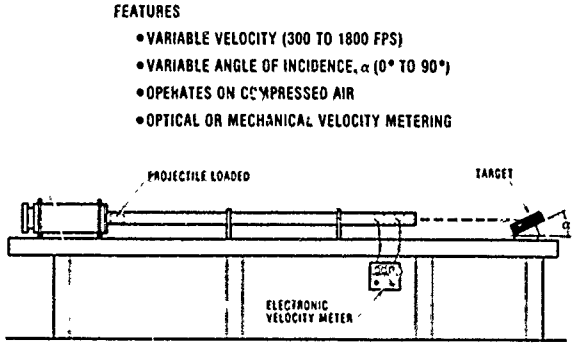

Fig. 6-Low velocity air gun; Southwest Research Institute

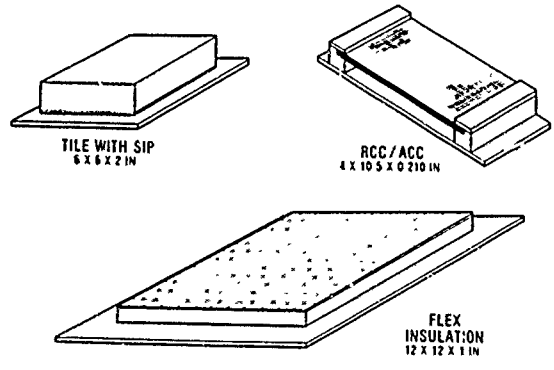

Fig. 7-Test articles

TEST PLAN EVOLUTION

The expanded test plan for this program evolved from a one phase comparative durability test to a multiphase program of material development and testings. As each phase of testing concludes, new avenues of investigation are revealed. As necessary, the master test plan is revised to incorporate these new investigations. At this writing, the program now consists of four series of tests.

Series 1 testing was conducted in April, 1982, with target materials including RCC, 9 and 22 pcf silica tiles, and 8 and 12 pcf composite tiles. Three goals were set for this test series: validation of the test method, evaluation of the durability of the tiles and RCC at the predicted worst case impact, and an estimate of the impact threshold of RCC damage.

Series 2 testing was conducted in late May, 1982. The targets for this test series were FI blankets with two different thicknesses of outer fabric. The goals of this series of tests were to develop qualitative knowledge about the impact durability of FI, and to make a qualitative comparison of this durability with the materials tested during Series 1.

Series 3 testing, conducted during August and September, 1982, is by far the most extensive phase of the test program to date. This test series can be further broken down into five subsets of tests, each with a different goal. The first subset of tests was intended to test 9 pcf tiles of a thickness comparable to the FI blankets previously tested, so as to develop a direct durability comparison. The second subset of tests was designed to evaluate several methods of enhancing the durability of the 9 pcf and 12 pcf tiles. These enhancement methods included thicker glass coatings, densifying the outer layers of the tile material under the coating, and combinations of the two methods. The third subset of tests involved the evaluation of advanced composite tiles developed by the NASA Ames Research Center and 12 pcf composite tiles with fiber reinforced coatings developed by the Lockheed Missiles and Space Company. The fourth subset of tests was designed to evaluate the extent of damage the ice projectile causes in acreage TPS. (As used in this paper, acreage denotes more than a single tile in a contiguous grouping or array.) To this end, arrays of 9 pcf silica tiles and arrays of FI blankets were tested to observe the extent of damage to these arrays when subjected to several levels of impact energy. And, finally, the fifth subset of tests was a preliminary evaluation of the durability of ACC. The immediate goal of this subset (ACC) was to develop an estimate of the minimum thickness of ACC required to withstand the predicted worst case ice impact. The long term goal of this subset was to provide preliminary information for the Series 4 testing, and to provide data for correlation with previous RCC impact tests.

Series 4 testing, to be conducted in early 1983, is planned to be an in-depth evaluation of ACC. ACC is currently under development by the Vought Corporation as a replacement for the RCC currently used on the orbiter. Preliminary studies indicate ACC will have improved mechanical properties and longer life at higher temperatures than RCC. The goal of the Series 4 testing will be to obtain an accurate prediction of the impact durability of ACC. Target panels will be inspected before and after testing using ultrasonic methods to reveal subsurface damage extent.

TEST RESULTS

The results of the three completed test series can best be characterized by the type of material tested. Tiles, blankets, and carbon-carbon panels each have unique failure modes. Differences in material properties may vary the extent of damage, but the basic character of the damage is unchanged.

Silica and Composite Tile

The pure and composite silica tiles are gouged by the projectile (Fig. 8) along the direction of travel. The length, width, and depth of the gouge are dependent on the tile material properties, coating thickness, and the magnitude of the impact. In general, the composite tile materials are more damage resistant than the pure silica tiles. This is thought to be the result of two material characteristics of the composite tile. First, it is known that the fiber-to-fiber bond between silica and the alumina-boria-silica fibers in the composite tile is far stronger than the fiber-to-fiber bond between silica fibers in the pure silica tile. The result of this greater bond strength is a greater capacity to withstand strain, or strain energy, before damage occurs. The second inherent strength of the composite tile material is a residual compressive stress in the coating. This residual stress is the result of different coefficients of thermal expansion of the coating material and tile material. As the coated tile cools at the completion of the coating firing process, a residual stress in the coating results. As stated previously, the residual coating stress for the composite tile is compressive. This compressive stress increases the amount of induced tensile strain the material can withstand, and thus also improves damage propagation resistance. The pure silica tile has a tensile residual stress in the coating, which acts to reduce the ability to withstand tensile strain and the ability to resist damage propagation.

It was also noted that increased damage resistance was directly related to increased material density. For maximum incidence angle, all tiles, except the 9 pcf pure silica tiles, deflect the ice projectile away from the impacting surface, reducing the possibility of downstream damage. In the testing of single 9 pcf tiles, the projectile passed through the downstream side of the tile, implying damage to adjacent

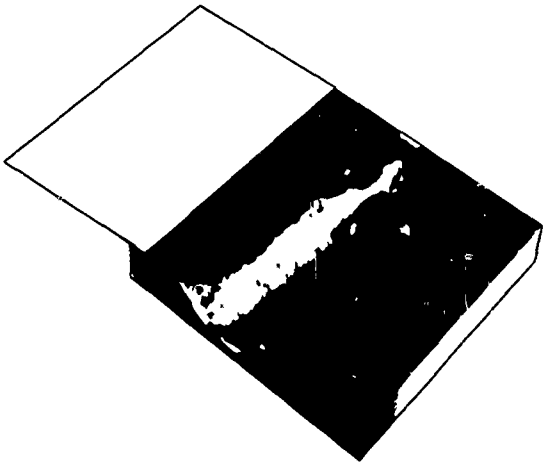

Fig. 8-Typical tile damage for 9 pcf pure silica tile

tiles. The test of 9 pcf 4-tile arrays confirmed this implication. The arrays tested in this program were constructed of tiles 4 inches thick, roughly the maximum thickness at any point on the orbiter lower surface. This allowed the projectile to expend all of its energy in tile damage and gave a truer measure of the destructive capability of the projectile.

Flexible Insulation Blankets

The FI blankets tested were also damaged by gouging (Fig. 9). These test blankets tended to show no improvement over the 9 pcf tile in impact resistance. Two types of outer fabric, a light gauge and a heavy gauge, were tested to compare their respective impact durabilities. While the heavy gauge fabric was more impact durable than the light gauge, it had the effect of deflecting more of the projectile into the insulation batt. This resulted in more extensive damage to the batt than observed on the light gauge blankets. Overall, heavy gauge fabric blankets have no better impact durability than the light gauge specimens.

RCC and ACC Panels

The RCC and ACC specimens tested were 4 by 10 inches of varying thickness and clamped in a fixture along two 4-inch sides (Fig. 7). The test panel dimensions were calculated such that the panel would react as a plate, and not as a beam, when impacted, and maximum use could be made of a limited source of test material. Plate behavior was desired because the RCC components of the TPS are plate (or shell) structures. The failure shown in Fig. 10 confirms that plate behavior was achieved.

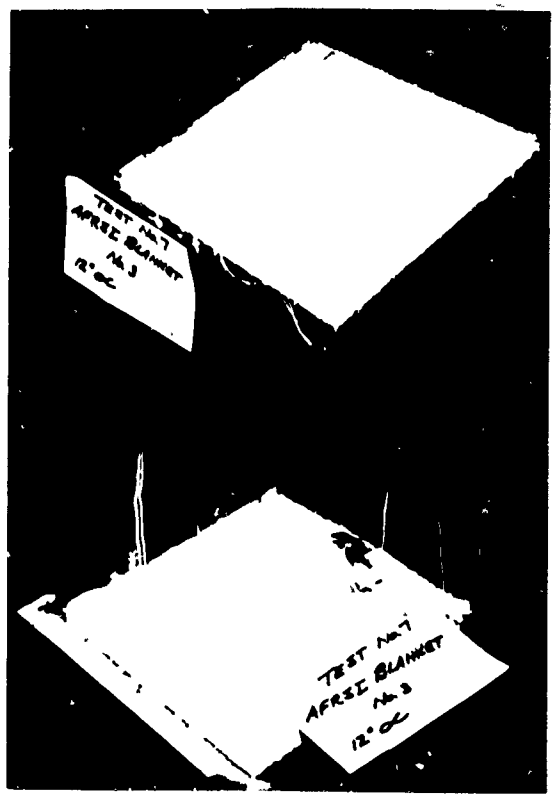

Fig. 9-FI specimen before (top) and after impact (typical)

The type of damage incurred by the RCC and ACC panels varied with the thickness of the panels. Thin panels of these materials, 66 to 88 mils thick, failed in a combination of penetration and spalling. Moderate thickness panels, 105 mils thick, failed in bending with lateral cracking the only visible evidence of failure. Heavy gauge panels, 175 to 210 mils thick, were undamaged by the predicted worst case impact. The thickest panel did not fail until the impact energy was increased to 10 times the predicted worst case impact. At this energy level, the failure mode was perforation caused by massive far side spalling (Fig. 10). (It should be noted that the minimum thickness of RCC currently used on the Shuttle is 210 mils.) These test results tend to confirm that the orbiter RCC panels should not experience damage from ice impact.

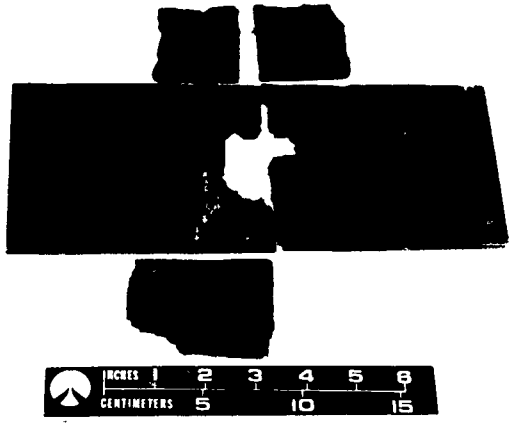

Fig. 10-RCC panel damage impact energy; 10 times predicted worst case

It should also be stated that the RCC panel tests were limited to visual inspection, and that the presence of internal damage occurring before visible external damage would not have been detected. The four ACC panel tests already conducted and the further 23 tests scheduled for early 1983 include requirements for ultrasonic inspection to reveal any interior failure that occurs prior to, or simultaneously with, visible exterior damage.

CONCLUSIONS

Five significant conclusions have come from the testing completed to date. First, the test method developed is a valid representation of actual flight conditions. This has been confirmed by comparisons of test tiles with flight damaged tiles. Second, by comparing damaged test tiles with tiles damaged during actual flight, it has been concluded that the ice impact problem is not a threat to vehicle safety. This conclusion is based on the similarity of worst case damage incurred in testing with actual flight damage, and the fact that the vehicle has returned safely after each of four missions. Third, the RCC components of the TPS are not damaged by the predicted worst case damage. This has led to the development of a concept known as the ice breakup threshold. If the target material is strong enough, it will shatter the ice projectile and remain undamaged. One part of the Series 3 testing was aimed at hardening the fragile tile materials so that they might approach this ice breakup threshold. The results of this

part of the Series 3 testing led to the fourth conclusion that several methods of durability enhancement for tiles are available, but none totally eliminate impact damage. And fifth, the flexible insulation blankets, originally thought to be more durable than the 9 pcf silica tile, actually are not any more durable.

An overview of the ice impact test program reveals four benefits that are directly a result of the test program.

1. A better understanding of the ice impact problem has been developed through the program.

2. The development of a working test method has permitted the evaluation of proposed solutions to the ice impact threat.

3. The result of the early phases of testing have generated additional potential solutions to be evaluated.

4. The development of a test method has added another tool for use in future TPS material development programs.

DISCUSSION

Mr. Walter (Sandia National Laboratories): During your presentation you talked about simulating the L to D ratios of the projectiles, but the design of your projectile in terms of the freezing process seemed to be geared to getting it to survive the gun environment without its changing shape. If you designed it to survive that gun environment, and if you keep coming up with some freezing process to do that, won't you also optimize the amount of damage that it will do to the tiles when it ultimately hits them? Isn't that an unrealistic simulation?

Mr. DeWolfe: Definitely. One of our problems is that we are now shooting hard ice. The ice that condenses on the tank is not necessarily solid ice. It is some sort of condensed frost. So the tests are, in themselves, extremely conservative. Unfortunately, we haven't come up with a method of first building condensed frost, of the size and mass that we need, and then finding a way of firing it without getting a snow storm out the end of the gun.

Mr. Scavuzzo (University of Akron): I would like to carry that same thought further by saying that I was thinking the same thing. But, how can you get the relative velocities as high as 500 feet per second in the take-off time when you have all that vibration and the ice breaking loose? Would you get that much velocity?

Mr. DeWolfe: The air stream velocity is such during the first minute or minute and a half of flight that we are in the range of 700 feet per second on the vehicle; the ice breaks loose, and it is accelerated from the tip of the tank back toward the vehicle. Yes, it has gone far enough toward the back end of the vehicle so that it is travelling at these velocities, and we are fairly confident of that. In fact, there is a bit of a dispute between our organization and the Johnson Space Center. They feel that we are using too large a projectile and too slow a velocity. They feel the velocities should be on the range of 1,500 feet per second. We do not agree with that, but it is quite possible to get this sort of velocity.

Mr. Scavuzzo: Have you thought about shielding the portions that do build up with frost in such a way that the ice couldn't impact the vehicle? Wouldn't that eliminate one of your problems?

Mr. DeWolfe: Unfortunately, ideas like that have come up. So far, they have been too heavy to consider. There are many ground support systems that are under consideration now. Currently at Vandenburg, the system that is in favor is one with four jet engines which will burn hydrogen and oxygen and are mounted horizontally at the pad. They blow hot air up across the stack all during the pre-launch phase after tanking, to keep the ice from forming. There are quite a few people who, realizing that the product of a hydrogen-oxygen engine is water, do not quite believe they can get it warm enough to keep from forming ice.

PROCEDURES FOR SHOCK TESTING ON NAVY CLASS H.I. SHOCK MACHINES

by Edward W. Clements
Naval Research Laboratory
Washington, D.C.

Combat worthiness of Navy shipboard systems and equipment is in large part due to tests conducted on the Navy Class HI (High Impact) Shock Machines for Lightweight and Mediumweight Equipments. These machines are often referred to be the abbreviated names of Lightweight Shock Machine (LWSM) and Mediumweight Shock Machine (MWSM). The validity of tests performed on these machines depends on their being operated properly. The rules and guides for their proper operation, however, are scattered throughout the literature of the field, and some seem not to be documented at all. This paper discusses the general rules to be followed and the guides to be observed to achieve consistent, valid tests of Navy equipment by use of the LWSM and MWSM.

INTRODUCTION

Prior to World War II, most explosive damage to naval vessels was caused by contact explosions, which caused severe local damage but had little effect some distance away. When large, noncontact weapons were encountered early in World War II, it was found that the shock environment they produced affected the entire ship, or a sizable portion of it, and damage was widespread. While some work in the field of shipboard shock had been in progress since 1917, the need for shipboard equipment and systems to withstand the effects of this UNDEX shock spurred a greatly accelerated program. Foreseeing the development of even larger weapons and more severe shock environments which would pervade the entire ship, the Navy set a goal that all vital shipboard equipment should withstand what is designated High Impact Shock. The Navy Class H.I. (High Impact) Shock Machines for Lightweight and Mediumweight Equipment (LWSM and MWSM, respectively) were developed to help achieve this goal. They provide tools for research into shock and shock-related phenomena and test standards for accepting equipment for use aboard Navy ships.

The shock environment produced by the H.I. machines is a function of both how they are configured structurally and how they are operated. Configuration and operating procedures were developed and adjusted to satisfy the dual requirements for realism and consistency. Damage similarity served as the criterion for meeting these requirements, since at that time little measurement capability existed to allow shock environments to be quantified and compared. When built and operated as specified, the H.I. machines would cause essentially the same kind and extent of damage to the test item as was observed in service. Consistency, perhaps even more essential than realism in an acceptance test machine, entailed having a test performed on any one H.I. machine produce much the same kind and extent of damage as any other machine of the class. As the data base of measured shock environmental parameters has accumulated from ship tests and machine calibrations, it has tended to corroborate the inferences from damage statistics.

The standards for configuration of the H.I. machines are references (1) and (2), and that for operating procedures is reference (3). These documents are inseparable in that both configuration and operation must be as specified in order for the test environment to be correct. The standards for configuration and operation are to be adjusted to some extent depending on the weight and geometry of the test item. These standards are defined in

the notes and dimensions of references (1) and (2), and in the text, figures and notes of reference (3). Some of these standards are not explicity defined, but are implied. In all, a fairly diligent search of references (1) - (3), together with some interpretation, is needed to determine the standards of configuration and operation appropriate for testing a given item. The purpose of this paper is to review these standards, calling attention to some which are sometimes overlooked. The major concern will be with Type A testing, tests of a "principal unit" or system, since this is the preferred type of test according to reference 3. Types B and C testing differ by requiring special fixtures, while retaining the same standards for operation.

LIGHTWEIGHT SHOCK MACHINE (LWSM)

The current weight limitation on the LWSM is to be interpreted as a requirement that the total weight attached to the anvil-plate shall not exceed 550 lb. This places a limit to the weight of the test item at around 350 lb.

Control of the configuration of the LWSM comes mainly from requiring use of one of the array of standard fixtures illustrated in references 1 and 3. In general, bulkhead mounted items are to use the 4-A plate (note that spacers are required between the item and the 4-A plate), and deck-mounted items are to use one of the 4-C shelf-plates. There are three sizes of these: the one to be used is the smallest which will accomodate the item. The remaining adjustable facet of configuration is the travel of the anvil-plate. The spring assemblies are to be set so that the clearance between stops of the forward springs for Back and Edge blows is $1\frac{1}{2}$ inches; this clearance may be measured directly. The stops of the springs for Top blows are enclosed within the spring housing, and clearance is adjusted by a nut beneath the assembly. When this clearance is set at its proper value of $1\frac{1}{2}$ inches, the overall height of the spring assembly is 9 1/8 inches, and the distance between the outer sleeve of the assembly and its base plate is 1 13/16 inches.

The remaining standards are not adjustable, but must be checked. Other checks of conformance of configuration could be regarded as part of maintenance. Welds in the anvil-plate assembly must be free from cracks. Those around the anvil-pads and the bottom rollers are particularly susceptible to cracking, and must be checked regularly. The anvil-pads themselves must be replaced when they become excessively deformed. As a rule of thumb, a dent deeper than about $\frac{1}{2}$ in. would be excessive. Spring assemblies should be inspected for deformation or breakage. As the spring assemblies for Top blows are enclosed, they are most easily checked by their height. When supporting the weight of the bare anvil-plate alone, they should have a total height of about 9 1/8 inches. Lowering the vertical hammer until it rests on the top anvil-pad should not shorten this height. If only one of the Top springs is acting, the height may decrease by about $\frac{1}{2}$ inch. The pivot bearings of the swinging hammer should be lubricated occassionally, as should the guide tracks for the vertical hammer. Finally, the top and bottom anvil-plate guide rollers for Edge blows should turn freely.

Controls on operation mostly follow automatically from the above criteria for configuration and maintenance. About the only additional precautions are to ensure that all fasteners are properly tightened, that spring clearances are set to $1\frac{1}{2}$ in., and that the hammer which is not in use is secured so that it does not contact its anvil-pad.

MEDIUMWEIGHT SHOCK MACHINE (MWSM)

The MWSM was designed to extend the capability to perform the type of testing done with the LWSM to larger and heavier items. Its current weight limit is a total of 7400 lb attached to the anvil-table, implying a practical weight limit of 5000 - 6000 lb for the test item.

The MWSM is intrinsically a uniaxial machine, since its anvil-table moves only in the vertical direction. Testing in two or perhaps three axes are still required, however. Reference 3 specifies a fundamental standard mounting arrangement, described as "for deck-mounted equipment." This arrangement consists of a pair of base-rails which are bolted to the anvil-table, and a set of mounting channels which are clamped tightly to them so as to span the gap between, and to which the test item is fastened using its normal shipboard mounting system. The purpose of this arrangement is to introduce a closely controlled flexibility into the configuration - control is achieved by specifying the number of channels according to the weight and dimension of the test item. Note particularly that the item is to be disposed so that the shorter of its horizontal mounting dimensions lies along the length of the channels. If the item's mounting geometry is such that it cannot be fitted to this arrangement, then an auxiliary structure may be interposed to serve as a mounting interface to meet the requirement that all of the items mounting fasteners shall be utilized. In particular, if the item has a circular or irregular hole pattern, it may be fastened to a plate which in turn is bolted to the mounting channels. The plate, however, may be no larger than necessary. If it must be so large that its mounting dimension along the channels exceeds the maximum permissible value of 44 in., then it should be separated from the channels by spacer blocks to bring its effective mounting dimension into the permissible range. It is

generally good practice to include spacers whenever a plate interface is used.

Bulkhead mounted items must be attached to a fixture providing a vertical surface which is itself fastened to the channels. No such fixture is at present specified in reference 3, although one will be in MIL-S-901D. Bulkhead supported items are attached to both the channels and a similar fixture. In both cases, balancing the test array will often result in the bulkhead fixture's being adjacent to or even overlapping one of the base rails, essentially short-circuiting the flexibility of the channels. Here again the use of spacer blocks is a necessity.

Testing along the horizontal axes of the test item may be accomplished in several ways. Reference 3 permits the item to be rotated 90°, which may be done by using a bracket or box structure bolted to the channels which supports the item by its normal mounting system and still allows the test array to be balanced. Reference 3 also allows rotation of 30°, and specifies three mounting arrangements for doing so. Two of these substitute for the base rails and retain the mounting channel arrangement. One rotates the mounting channels about an axis parallel to their length, the other about an axis parallel to their width. The third arrangement substitutes a 30° corner bracket and special base rails for the normal arrangement of base rails and mounting channels. This fixture inclines both of the item's horizontal axes, and can be used for bulkhead-mounted equipment.

An essential step in preparing for a shock test on the MWSM is balancing the test array. The center of gravity of the entire array - anvil-table, fixtures, test item, etc. - must be aligned on the axis of percussion. This is accomplished by statically balancing the array on the balancing stands illustrated in reference 2. Each axis is balanced separately by moving the test item along the mounting channels or the test item and mounting channels along the base rails before mounting bolts and clamps are tightened. It is not acceptable to rely on calculated positioning to provide adequate balancing. Failure to balance the test array will often result in an invalid test, as excessive rotation will cause impact, or even binding, of the anvil-table hold-down bolts producing unintended and unpredictable sidewise loadings, and possibly bending the hold-down bolts. Some rotation is inevitable, both because static balance does not ensure dynamic balance and because the hammer impact is not central on the anvil face for the 3 inch travel setting. It must, however, be minimized.

As a last check before commencing the test, the anvil-table should be raised to the $1\frac{1}{2}$ inch travel position, the hammer height set to the zero mark, and the hammer released. Contact between hammer and anvil face should be clearly audible, but the anvil-table should not move. This check verifies that the brakes are not dragging and that the hammer height pointer is set properly.

Relatively little maintenance is required for the MWSM. Welds and webs in the anvil-table structure should be inspected for cracks, which should be repaired promptly if found. The mounting channels may bend slightly with extended use, and should be straightened as necessary. The various bolted connection should be checked for tightness, and the required stress of 50ksi in the hold-down bolts verified. The ability of the brakes to stop the hammer from an $5\frac{1}{2}$ foot drop before it strikes the anvil should be checked occasionally.

ACKNOWLEDGEMENTS

This material was compiled with the support of the Naval Sea Systems Command, Code 55X.

REFERENCES

1. BuShips Dwg. 10-T-2145-L-13, "Class HI (High Impact) Shock Machine for Lightweight Equipment."

2. BuShips Dwg N0807-655947-6, "Class H.I. (High Impact) Shock Machine for Mediumweight Equipment."

3. MIL-S-901C "Military Specification Shock Tests, H.I. (High Impact); Shipboard Machinery, Equipment and Systems, Requirements for" 15 January 1963, with "Submarine Shock Requirements Appendix," December 1973.

EQUIVALENT NUCLEAR YIELD AND PRESSURE BY THE RESPONSE SPECTRUM FIT METHOD

J. R. Bruce and H. E. Lindberg
SRI International
Menlo Park, California

A new method for assigning an equivalent nuclear yield and range to the pressure-time history measured in simulating experiments is presented. The method is based on the linear response spectrum. Equivalent nuclear event parameters are selected so that the response spectrum of the nuclear event best fits that of the measured data over a preselected frequency range. The advantage of the method is that the user has a direct method of quantitatively evaluating the quality of the fit relative to the structure being tested, and the user can be assured that, for the given range of frequencies and therefore for the given test structure, the nuclear weapon parameters obtained by the method give the best possible fit to the measured data. The method is also used to show that for the tests analyzed, the "scatter" in yield and range for several pulse measurements in the same test is more properly interpreted as a family of attack parameters that all give essentially the same response spectrum and are all closely represented by the experimental pulses.

INTRODUCTION

In simulating airblast effects from nuclear weapons, there are inevitable differences between the simulated pressure-time history and the pressure-time history from idealized nuclear events. Two techniques used to simulate high pressure nuclear blast effects are the High Explosive Simulation Technique (HEST) and Dynamic Airblast Simulators (DABS). The HEST produces a pressure loading by detonation of a thin layer of explosive sandwiched between the loaded surface and a sand berm that provides inertial confinement. The DABS is a large inertially confined shock tube which extends over the surface to be loaded. An explosive charge is detonated at one end of the tube to generate an intense air shock, which then propagates past or reflects from the loaded surfaces. Both of these techniques produce pressure-time histories that are similar to, but not exactly like ideal nuclear airblasts.

Figure 1 compares typical HEST and DABS data to corresponding ideal nuclear pressure-time histories,* highlighting some of the differences.[1,2] HEST data typically shows pressure oscillations in the early portion of the record. These oscillations result from shock reflections within the relatively thin HEST cavity and are commonly one to two orders of magnitude higher in frequency than a characteristic frequency based on the duration of the pulse. These oscillations make it difficult to determine an equivalent peak pressure for the HEST pulse. In the example in Figure 1, for instance, the peak of the oscillation is close to twice the peak that would be obtained if a smooth curve were drawn through the early portion of the record.

DABS data typically show little or none of the early time oscillation observed in HEST data. However, typical DABS data often do not follow the smooth exponential shape of the ideal nuclear airblast. In the example shown in Figure 1, the early portion of the DABS record is more triangular in shape than the nuclear pulse and discontinuities are apparent at 20 ms and 40 ms. These discontinuities can be caused either by the passage of the contact surface which separate the shocked air from the explosion products or by a shock reflection

*The parameters for these ideal nuclear pressure-time histories were selected by using the response spectrum fitting method described in this paper.

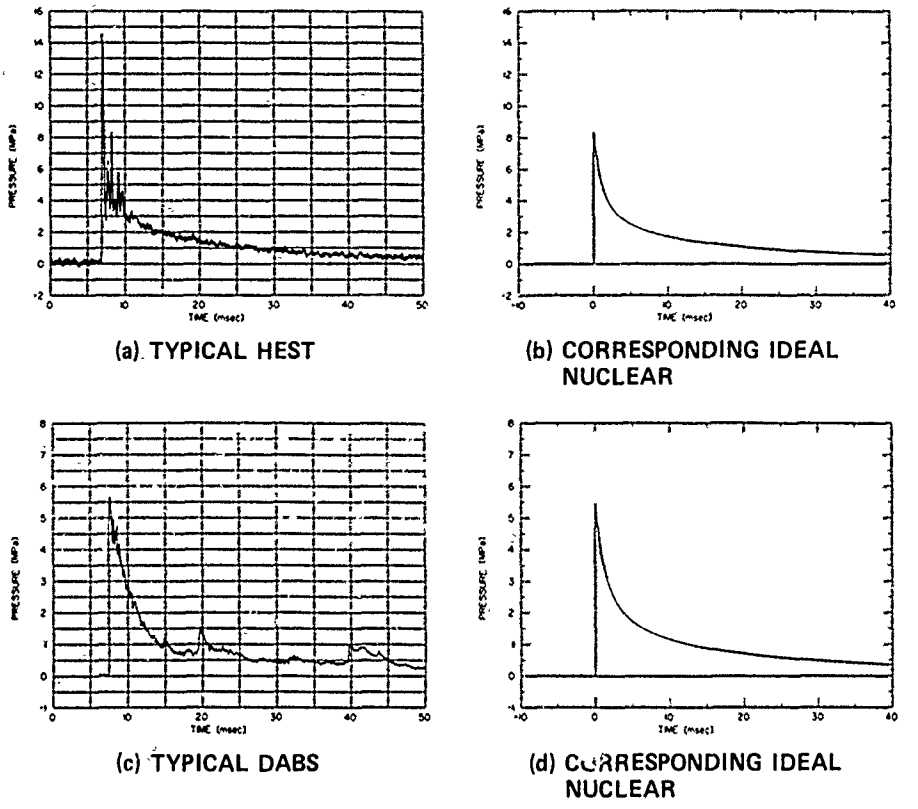

FIGURE 1 COMPARISON OF TYPICAL HEST AND DABS PRESSURE-TIME HISTORIES WITH IDEAL NUCLEAR AIRBLAST HISTORIES

from some obstacle in the DABS shock tube.

The differences between HEST and DABS pulses and ideal nuclear airblast pulses complicate the process of relating the blast simulation loading and resulting structural response to the loading and response that would be experienced in a nuclear event. Current methods estimate equivalent nuclear weapon parameters (i.e., peak pressure P_o and yield W or range R and W) by achieving a best fit between the ideal nuclear and measured pressure-time histories or between their impulse-time histories. This paper presents a method in which nuclear parameters are estimated from simulation pressure-time records by matching displacement response spectra over a preselected frequency range.

The advantage of this approach over pulse fitting approaches is that it assures that, if the response frequencies of a given test structure can be grouped within a known frequency range, the nuclear weapon parameters can be selected to give a best fit to the measured data for the given test structure. Additionally, a posttest comparison of the nuclear spectrum and the data spectrum gives a quantitative measure of the quality of the fit, something missing from current best fit methods.

DESCRIPTION OF THE METHOD

As mentioned above, our approach is based on the linear response spectrum. Equivalent nuclear event parameters are selected so that the response spectrum of the nuclear event best fits that of the measured data over a preselected frequency range. The linear response spectrum has not previously been used as a fitting method because of the computational difficulty in calculating spectra for many combinations of W and R when searching for the combination that best matches the data spectrum over the selected frequency range. Our approach greatly reduces this computational effort by using the scaling relationships given by the self-similar simplification of the nuclear airblast.[3]

In the self-similar simplification, the nuclear explosion is idealized as a

sudden release of a finite energy in a small volume of gas, giving in the limit an infinite energy density at a mathematical point. As the gas expands away from the point of energy release, it drives an intense spherical shock into the surrounding undisturbed gas.

If we confine our attention to the early motion, the energy per unit volume within the blast is so large compared with the ambient energy density that the ambient energy can be neglected. Stated another way, near the explosion, the shock pressure is so much greater than the ambient pressure that the ambient pressure can be neglected. Under these conditions, the ambient gas is described by its density alone and dimensionless parameter groups can be formed with no characteristic length. Consequently, with no length as a basis of comparison, the blast wave at any instant is identical to the blast wave at any other instant except for scale changes as the sphere expands--the wave is self-similar. Thus, in the self-similar approximation, there is only one normalized pressure-time history for all combinations of yield and range.

Figure 2 gives normalized pressure-time histories, impulse-time histories and response spectra from the self-similar theory and comparisons with the same quantities calculated with nuclear airblast theory for peak pressures of 2.00 MPa and 75.3 MPa.[1,2] Pressure has been normalized to the peak pressure P_o and time has been normalized to the time of arrival of the shock, t_a. The response spectrum is a plot of the peak response of a linear, single-degree-of-freedom, spring-mass system as a function of its frequency. The vertical scale is the peak displacement x. In order to generalize the displacement for pressure loads, it is given in most plots here as the product kx/A in units of pressure, where k is the spring constant and A is the projected area of the structure. In Figure 2 the vertical scale has been made dimensionless by dividing by P_o.

As we will show below, the similarity of the time histories and response spectra in Figure 2 allows us to apply the self-similar scaling relationships to the nuclear blast wave pulse and to represent a wide range of nuclear blast wave pulses with a small family of "universal" nuclear blast wave pulses. We found that ten pulses cover all weapon yields over a range of peak pressures from 2 to 75 MPa to an accuracy better than 2% in all quantities.

To date we have used a graphical approach to determine the best fit. (In the future, the process could be automated with the best fit determined by the method of least squares.) The approach is outlined in Figure 3 using a record from a high explosive test performed at the Air Force Weapons Laboratory.[6] First, the response spectrum for the measured data was calculated and plotted on log-log axes. Second, a normalized response spectrum for a nuclear airblast was selected from the family of 10 previously calculated spectra. It is desirable to select a nuclear spectrum with a peak pressure P_o near the peak pressure of the data; however, this selection is not critical because all normalized spectra near this value of P_o are essentially the same. It is this fact, which arises because the nuclear pulse closely follows the self-similar pulse in shape, that allows us to maintain a high accuracy using a small family of "universal" spectra. A P_o of 3.5 MPa was chosen here after a quick visual check of the data.

Figure 3(a) shows the two spectra, that of the measured data and that of the 3.5-MPa normalized spectra, overlaid as if both were in real units of MPa and Hz. In this position, the normalized ideal nuclear spectrum represents a spectrum from a nuclear airblast with a P_o = 1 MPa and a time of shock arrival t_a = 1 s.

The third step in our approach is to shift the two spectra relative to each other, as shown in Figure 3(b), to obtain the best visual fit to the data spectrum over the frequency range of interest to the test structure. (A two-decade range from 4 to 400 Hz was arbitrarily chosen in this example. In practice, the range would be chosen after consideration of the response modes of the test structure.) We can make this shift because on log-log axes the nuclear response spectra for any combinations W and R are essentially the same shape as any other, as long as the peak pressure is not drastically changed. Again, this arises because all nuclear pulse in this pressure range closely follow the single self-similar pulse in shape.

Once the fit is visually determined, we observe in Figure 3(b) that the ideal nuclear spectrum was shifted by a factor of 30 in frequency and by a factor of 3 in pressure from the normalized position shown in Figure 2(a), which represented a P_o = 1 MPa and t_a = 1 s blast. Thus, values of P_o = 3 MPa and t_a = 1/30 s represent the position shown for the ideal nuclear spectra in Figure 2(b). Finally, we determine the values of yield W and R corresponding to the best fit by using

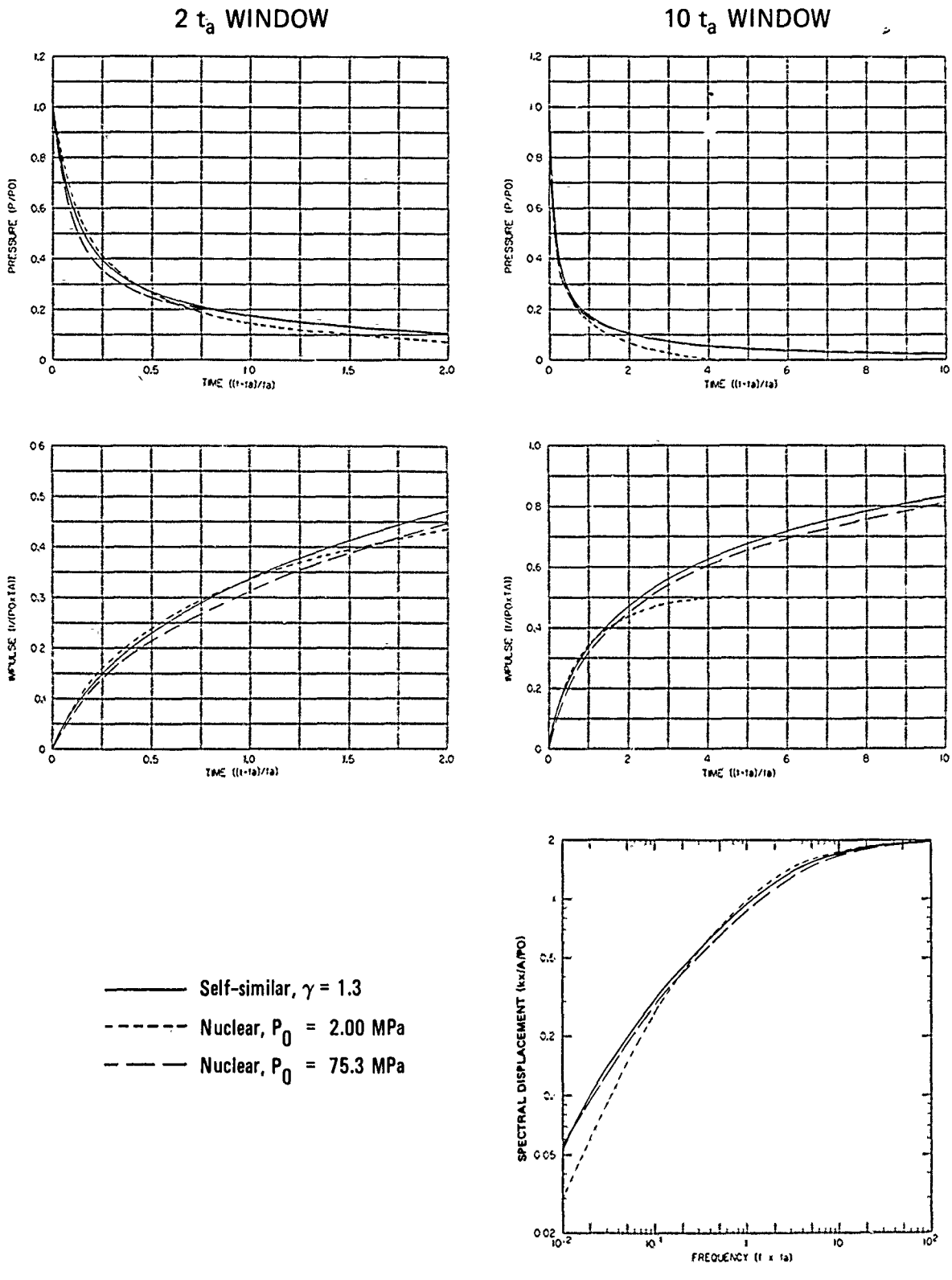

FIGURE 2 COMPARISON OF SELF-SIMILAR AND IDEAL NUCLEAR AIR BLASTS FOR P_0 = 2.00 MPa AND 75.3 MPa

(a) TEST DATA SPECTRUM OVERLAID WITH SPECTRUM FROM NORMALIZED NUCLEAR AIRBLAST FOR P_0 = 3.5 MPa

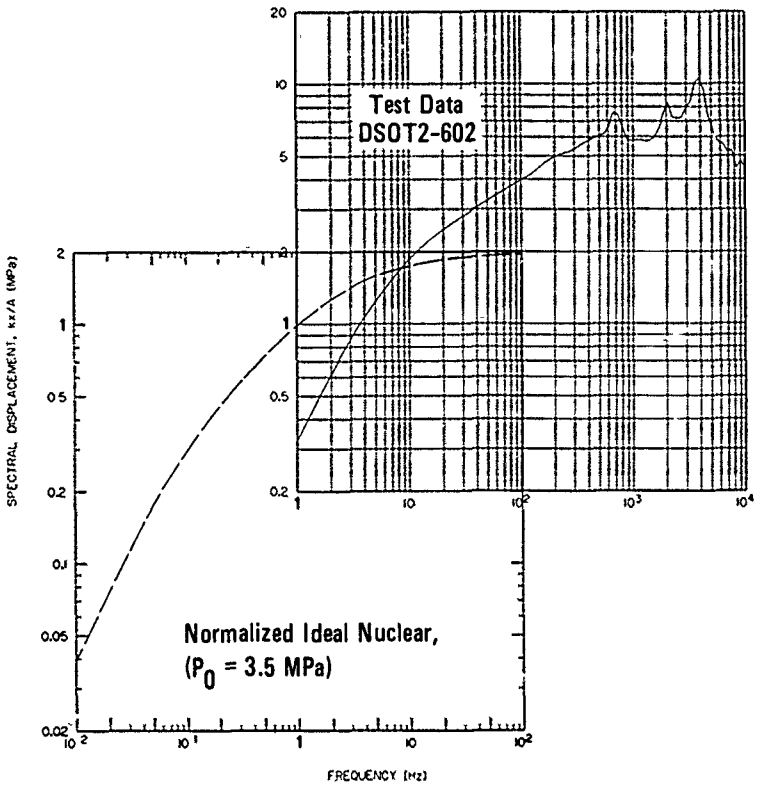

(b) BEST FIT OCCURS WITH A 3-MPa SHIFT IN RESPONSE AND A 30-Hz SHIFT IN FREQUENCY FROM THE NORMALIZED POSITION, GIVING P_0 = 3 MPa, t_a = 1/30 s FOR THE IDEAL NUCLEAR AIRBLAST

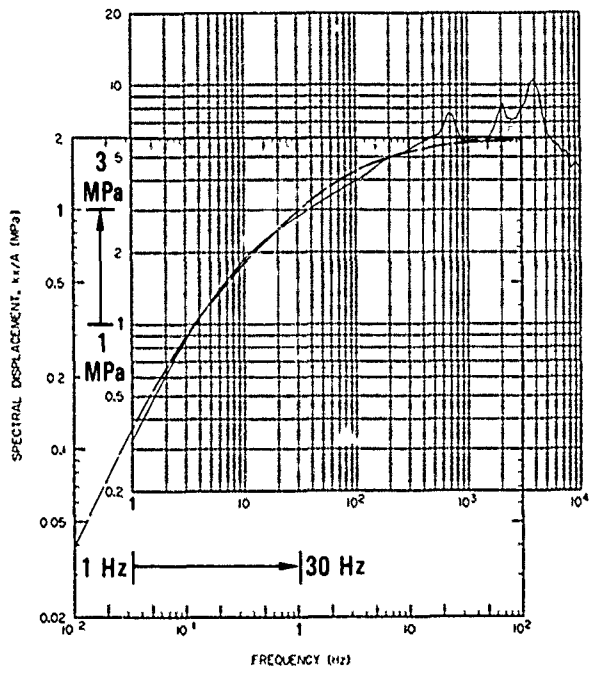

JA-1191-21A

FIGURE 3 DIAGRAM OF RESPONSE SPECTRUM FIT (RESFIT) TECHNIQUE
(Note: In this example we are using a 3.5-MPa nuclear spectra to determine a best fit at 3.0 MPa.)

the self-similar scaling relationship between W, R and P_o, t_a. The development of these relationships is beyond the scope of this paper. However, they are given below and their development is described in References 4 and 5.

Both W and R can be written as functions of P_o and t_a within the unknown constants, k_W and k_R as follows:

$$W = k_W \, t_a^3 \, P_o^{5/2} \tag{1}$$

$$R = k_R \, t_a \, P_o^{1/2} \tag{2}$$

Therefore, if W_1 and R_1 are known for a single combination of P_{o1} and t_{a1}, Eqs. (1) and (2) can be used to calculate W_2 and R_2 for a given P_{o2} and t_{a2} as follows:

$$\frac{W_2}{W_1} = \left(\frac{t_{a2}}{t_{a1}}\right)^3 \left(\frac{P_{o2}}{P_{o1}}\right)^{5/2} \tag{3}$$

$$\frac{R_2}{R_1} = \frac{t_{a2}}{t_{a1}} \left(\frac{P_{o2}}{P_{o1}}\right)^{1/2} \tag{4}$$

One combination of W_1, R_1, P_{o1}, and t_{a1} which is known is the values used to calculate the normalized ideal nuclear spectrum used for the initial fit (chosen from our family of 10). As we mentioned above, the pressure-time history used calculate this spectra had a peak pressure before normalizing of 3.5 MPa. It also had values of t_{a1} = 63.1 ms, W_1 = 100 kT and range R_1 = 277 m. Using these values for W_1, R_1, t_{a1}, P_{o1} in Eqs. (3) and (4), we find W_2 = 10.0 kT and R_2 = 135 m for P_{o2} = 3.0 MPa and t_{a2} = 1/30 s. Thus a yield of 10.0 kT at a range 135 m is the best fit to the measured data for a system with primary modes of response in the 4 to 400 Hz band.

It is important to note the sensitivity of yield W to variations in either P_o or t_a indicated by Eq. (3). Yield varies as t_a^3 and as $P_o^{2.5}$. Therefore, small variations in the fit can lead to much larger variations in W. Stated differently, response within a given frequency range would be essentially the same for the entire variation in W. Later, we will discuss this point in more detail.

EXAMPLE OF BEST FIT OBTAINED WITH METHOD

Figure 4 shows an example of a best fit made with the response spectra method, which we named RESFIT. The left side of the figure shows a comparison of the pressure-time history, the impulse-time history and the response spectrum of the measured data (solid line) with those of the nuclear airblast obtained using RESFIT (dotted line). The right side of the figure makes the same comparison for the measured data and the ideal nuclear airblast obtained using the Air Force Weapons Laboratory's BRNUFT code.[7,8] (BRNUFT makes a fit to the measured impulse-time history.)

The response spectrum fit was made over a two-decade frequency range from 4 to 400 Hz. The BRNUFT fit was made over the first 20 ms of impulse. A 20-ms window gives a best response spectrum fit at frequencies near 1/0.020 or 50 Hz. Because of 50 Hz is central to the 4 to 400 Hz frequency range used in RESFIT, the fit parameters for the two methods were considered to be as compatible as possible.

The record shown in Figure 4 deviates significantly from the exponential decay of the nuclear waveform. As a result, the spread in P_o and W determined by each method is large. Comparison of the shape of the test data spectrum with that of the ideal nuclear spectrum makes it apparent that a good fit over the entire four-decade frequency range shown is not possible. However, RESFIT was able to provide a good fit over the prescribed 4 to 400 Hz frequency range.

This control over the frequency range to be fit is a key advantage of the RESFIT technique. The lack of control on the frequency range by BRNUFT, along with the sensitivity of the fit parameters P_o and W to small changes in the fit, are major reasons for the large variation of P_o and W often obtained by users of BRNUFT for similar records from the same test. RESFIT, by providing control on the frequency range of emphasis, reduces the variation in P_o and W, and more importantly, ensures that the fit is the best possible for a given test structure. Furthermore, a quantitative description of the errors in structure response introduced by simulation inaccuracy is also obtained.

SENSITIVITY OF THE FIT PARAMETERS

Figure 5 shows nuclear peak pressure-yield combinations for 6 gage records taken from a HEST test performed at AFWL.[6] All 6 gages should theoretically

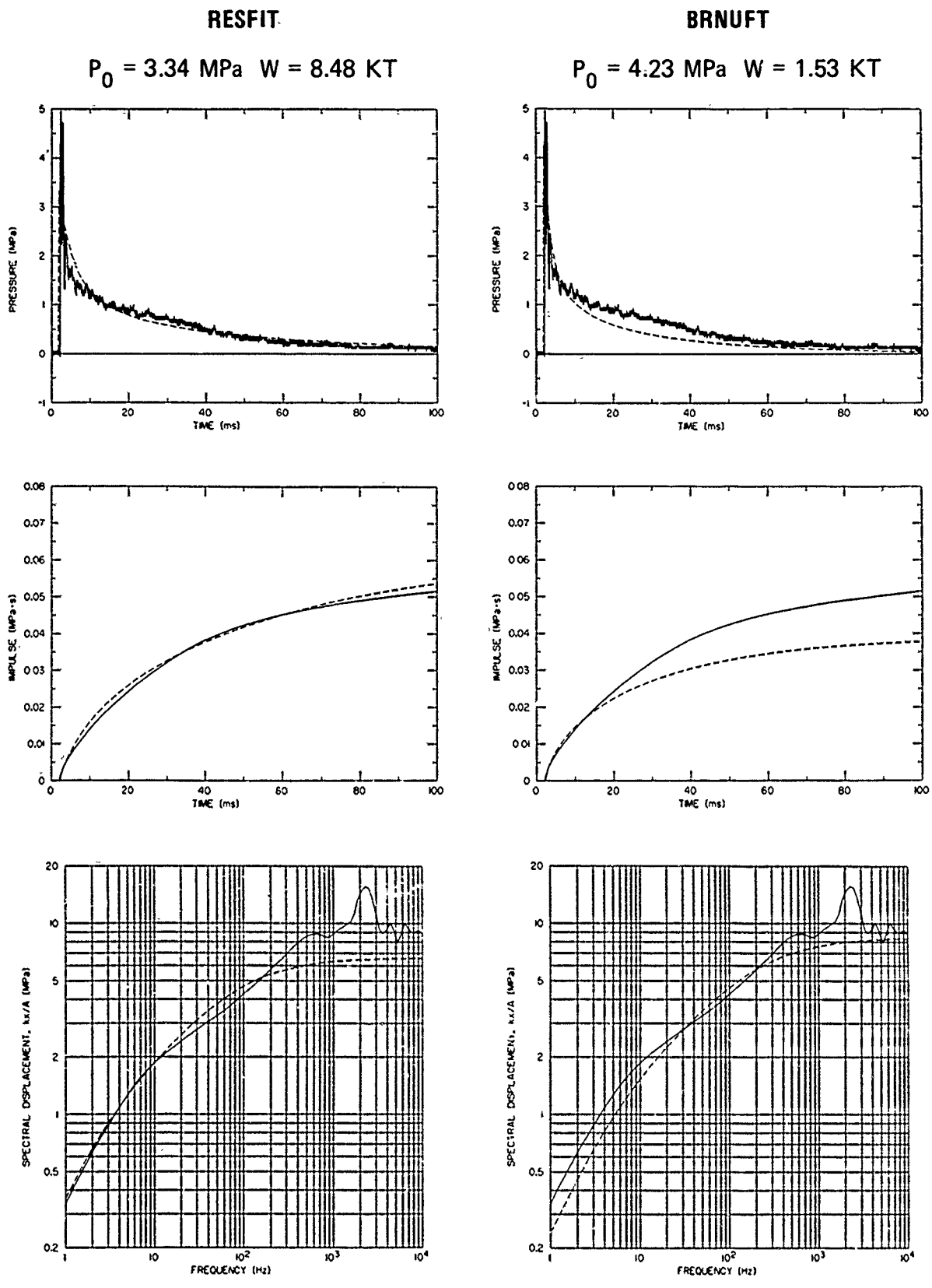

JA-1191-8

FIGURE 4 RESFIT/BRNUFT COMPARISON (DSOT-2-607)

have seen the same environment. The solid circles represent the values of P_o and W determined by RESFIT and the hollow circles represent values determined by BRNUFT. The three-digit numbers are the page designation. The RESFIT values scatter in peak pressure by a factor of 1.8 and in yield by a factor of 8. The BRNUFT values scatter in peak pressure by a factor of 2.4 and in yield by a factor of 22. While RESFIT eliminates some of the inconsistency observed with BRNUFT, we observe that there is still considerable scatter in the parameters of P_o and W for similarly located gages in the same test. However, the RESFIT method gives us the tool to properly interpret this scatter, as described below.

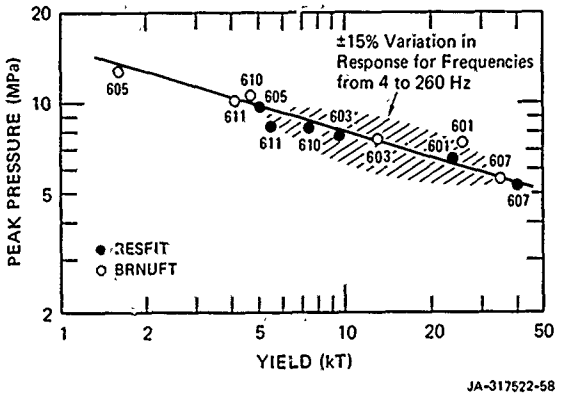

FIGURE 5 NUCLEAR PEAK PRESSURE-YIELD COMBINATIONS FOUND BY RESFIT AND BRNUFT FOR 6 GAGES IN HEST TEST DSOT5

We first observed that all the points on Figure 5 lie within 15% of a line drawn through the data at a slope of -1/3.5, and most of the points are within 5% of this line. The two RESFIT points farthest from each other are from gages 605 and 607, and have peak pressure-yield combinations 9.7 MPa, 5.1 kT and 5.4 MPa, 41 kT. To see the effect on structural response of the wide spread between these extreme fits, we calculated the response spectra for the two corresponding nuclear pulses. These are given in Figure 6. The two spectra differ most at very low and very high frequencies. For intermediate frequencies, representative of test structures of interest, the difference in response in the two spectra are quite modest. The curve cross at 30 Hz and differ by less than ±10% for frequencies from 8 Hz to 120 Hz. If accuracy is relaxed to 15%, this frequency band becomes 4 Hz to 260 Hz. Thus, for test structures with dominant frequencies within these bands, the wide spread in peak pressure-yield combinations of the nuclear fits nevertheless results in essentially the same structural response.

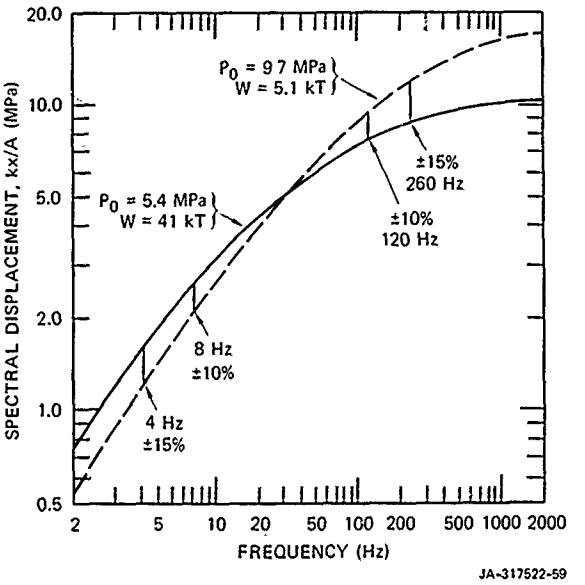

FIGURE 6 RESPONSE SPECTRA FOR IDEAL NUCLEAR PULSES AT THE EXTREMES IN PEAK PRESSURE AND YIELD FOUND USING RESFIT

This shows that one can interpret a region in the peak pressure-yield plane as assembly of attack conditions that give essentially the same response for a broad range of structures. For example, the high-explosive simulation test considered here gives a response that would be produced by all attack combinations within the hatched region in Figure 2. It is inappropriate to interpret this range as an error in simulation of a specific attack condition of interest.

The shape and orientation of the hatched region in Figure 5 can be deduced from the response spectrum curve for a ideal nuclear pulse with a peak pressure in the region, and the self-similar scaling relationships. These relations show, for example, that the two spectra curves in Figure 6 have the same shape and are simply shifted vertically by the pressure ratio of 9.7 MPa/5.4 MPa = 1.80 and horizontally by the ratio of the characteristic time, t_a, of the two nuclear pulses. We can rewrite Eq. (3) as

$$\frac{t_{a2}}{t_{a1}} = \left(\frac{W_2}{W_1}\right)^{1/3} \left(\frac{P_{o1}}{P_{o2}}\right)^{5/6} \qquad (5)$$

which for the example in Figure 6 is

$$\frac{t_{a2}}{t_{a1}} = \left(\frac{41\ kT}{5.1\ kT}\right)^{1/3}\left(\frac{9.7\ MPa}{5.4\ MPa}\right)^{5/6} = 3.26$$

The angle of the shift of response spectra is therefore $\phi = \tan^{-1}$ (2 log 1.80/ log 3.26) = 45°. The 2 appears because the frequency log scale in Figure 6 is compressed by 2 compared with the displacement log scale.

This is the shift angle for all points on the response spectrum curve, and in particular is the shift angle for the point of intersection after the shift. Small shifts are therefore tangent to the response spectrum at the point of intersection because points before and after the shift lie on nearby points of the same curve. Therefore, in this region the shift in response spectrum has little effect on the resulting curve because the shift is along the curve. As a result, response to the two nuclear pulses is very nearly the same for frequencies in a broad band about the intersection point.

When the curve shift relationship

$$\left(\frac{P_{o2}}{P_{o1}}\right) = \left(\frac{t_{a1}}{t_{a2}}\right)^{\frac{\tan\phi}{2}} \qquad (6)$$

is combined with the self-similar scaling relationship in Eq. (5), we obtain a relationship between peak pressure and yield for the two curves:

$$\frac{W_2}{W_1} = \left(\frac{P_{o1}}{P_{o2}}\right)^{\left(\frac{6}{\tan\phi} - \frac{5}{2}\right)} \qquad (7)$$

For the example in Figure 2, ϕ = 45° and

$$\frac{W_2}{W_1} = \left(\frac{P_{o1}}{P_{o2}}\right)^{3.50}$$

This defines the slope -1/3.5 of the line in Figure 1 connecting the two attack conditions for the Brode pulses used to calculate the response spectra in Figure 2.

We have shown that for nuclear pulses along this sloped line, the response spectra differ by no more than ±15% for frequencies from 4 to 260 Hz. Also, at a fixed yield, the characteristic time of a Brode pulse changes only as peak pressure to the 5/6 power [Eq. (5)]. Thus, with pulse duration nearly constant along vertical lines in Figure 2, response varies directly as peak pressure in this direction. A shaded ellipse is therefore drawn with height ±15% around the sloped line to encompass attack conditions that give the same response to within ±15%.

CONCLUSIONS

We observed that RESFIT eliminates some of the inconsistency observed with current best fit methods, such as BRNUFT, by allowing control of the frequency range over which the fit is made. While there is still scatter in the parameters of W and R obtained with RESFIT for similarly located gages in the same test, primarily because of the sensitivity of the parameters, it is less than that obtained with BRNUFT. However, the primary advantage with RESFIT is that the user has a direct method of quantitatively evaluating the quality of the fit relative to the structure being tested, and the user can be assured that, for the given range of frequencies and therefore for the given test structure, the nuclear weapon parameters obtained by RESFIT give the best possible fit to the measured data. The method can also be used to show that for the tests analyzed, the "scatter" in W and R is more properly interpreted as a family of attack parameters that all give essentially the same response spectrum and are all closely represented by the experimental pulse. A similar approach can be used for nonlinear structure response (e.g., yielding structures) if response is dominated by a single collapse mode; that is, if the structure can be represented as a one-degree-of-freedom system.

ACKNOWLEDGMENT

This work is part of a program performed for the Defense Nuclear Agency (DNA) under Contract DNA001-80-C-0059. The technical monitor was Major M. E. Furbee.

The authors wish to thank Mr. J. D. Renick of the Air Force Weapons Laboratory for his consultation and assistance in obtaining the BRNUFT code and a digital tape of representative HEST and DABS data.

REFERENCES

1. Brode H. L., "Height of Burst Effects at High Overpressure," Defense Atomic Support Agency (DASA) Report 2506, July 1970.

2. Brode, H. L., "Improvements and Corrections to DASA2506," R&D Associates, 30 November 1978.

3. Sedov, L. I., Similarity and Dimensional Methods in Mechanics, Academic Press, New York, N.Y., 1959, pp. 146-260.

4. Lindberg, H. E., "Simulation of Transient Surface Loads Using Plane, Cylindrical, and Spherical Blast Waves," Proceedings of the Conference on Military Applications of Blast Simulators (July 1967), Volume 2, pp. 397-440.

5. Bruce, J. R. and Lindberg, H. E., "Interpretation of Airblast Simulation Tests, Volume 2: Equivalent Nuclear Yield and Pressure by the Impulse Fit and Response Spectrum Fit Method," SRI International Draft Final Report, PYU-1191, January 1982.

6. Shih, P. Y. et al., "Dynamic Side-On Trench Test 5 (DSOT-5)," Civil Engineering Research Facility Interim Technical Report, University of New Mexico, December 1978.

7. Renick, J. D., "Some Consideration in the Design of a Dynamic Airblast Simulator," Air Force Weapons Laboratory Internal Technical Memorandum, 1978.

8. Renick, J. D., "Dynamic Airblast Simulator Design Manual," Air Force Weapons Laboratory Internal Technical Report, November 1978.